DEMONSTRATING PREDICTIVE CONFIDENCE FOR A PARADIGM DISSOLVER MODEL USING METHODS FOR EVALUATING HIGHER ORDER MOMENTS: A "CASE STUDY" FOR NUCLEAR NONPROLIFERATION

Zur Erlangung des akademischen Grades

Doktor der Ingenieurwissenschaften

der Fakultat für Maschinenbau

Karlsruher Institut für Technologie (KIT)

genehmigte

Dissertation

von

James J. Peltz

Tag der mündlichen Prüfung: 5.12.2016

Hauptreferent: o. Prof. Dr. rer. nat. Dr. h. c. mult. D. G. Cacuci

Korreferent: Prof. Dr.-Ing. Carsten Proppe

Korreferent: Prof. Dr. Christopher Pain, Imperial College London

Acknowledgements

Abstract

Through an exhaustive process of verification, validation and uncertainty quantification, this dissertation performs *sensitivity analysis, uncertainty quantification up to 3rd-order* (including covariance and skewness), and *forward and inverse predictive modeling* for a dissolver model of interest to nonproliferation activities regarding aqueous reprocessing of spent nuclear fuel. This dissolver model comprises sixteen nonlinear differential equations, which include 1291 model parameters characterizing the underlying physical and chemical processes. The original results presented in this dissertation highlight the effects of uncertainties which necessarily characterize measurements and computations, and the reduction in the predicted uncertainties by combining optimally the experimental and computational information.

The uncertainties in the dissolver model parameters are propagated to compute uncertainties in the model responses by using first-order sensitivities (i.e., functional derivatives) of the respective responses to the model parameters. The first-order sensitivities to all model parameters of the time-dependent acid concentrations are computed by applying the adjoint sensitivity analysis method for nonlinear systems with function-valued responses originally conceived by Cacuci (1981a). Furthermore, this work also develops a reduced-order surrogate dissolver model, and extends Cacuci's original adjoint technique to enable the computation of second-order sensitivities. As shown in this work, the second-order sensitivities are essential for computing the skewness (i.e., third-order moment) of the response distribution, highlighting the latter's asymmetrical (non-Gaussian) features.

The response sensitivities also serve as the weighting functions for combining experimental and computational information for the dissolver model using the comprehensive *predictive modeling* methodology originally developed by Cacuci and Ionescu-Bujor (2010b). The only experimental information available in the open literature for this dissolver model are the measurements performed by Lewis and Weber (1980) of the nitric acid in the compartment furthest away from the inlet. Using this experimental information with the forward and inverse predictive modeling formalism is shown to yield optimal predictions throughout the entire dissolver, reducing everywhere the uncertainties in these predicted results. This stems

from the fact that the predictive modeling methodology combines and transmits information simultaneously over the entire phase-space, comprising all time steps and spatial locations. Another remarkable original result obtained in this dissertation is the innovative use of the predictive modeling framework of Cacuci and Ionescu-Bujor (2010b) in an *inverse prediction* mode for inferring unknown model parameters (specifically: the time-dependent inlet boundary condition) from measurements of the acid concentration in the compartment furthest from the inlet. This is particularly useful in applications where inferences on a target of interest can only be made from indirect measurements.

In summary, this dissertation presents an efficient mathematical model for a dissolver of spent nuclear fuel of interest to international nuclear safeguards and nonproliferation, and demonstrates the procedure for rigorous uncertainty quantification and validation of this model. The dissertation also introduces an innovative adjoint procedure for computing second-order response sensitivities to model parameters, and highlights the latter's essential role for computing non-Gaussian features of the distributions of model responses of interest. The methodology demonstrated in this dissertation will serve as a role model for rigorous forward and inverse predictive modeling of other nuclear facilities of interest to international nuclear safeguards and nonproliferation, aiming at optimizing predictions for "signatures" and "causes" of interest while reducing drastically the accompanying uncertainties, thus enabling more accurate risk-informed decision processes.

Abstract

Mithilfe eines gründlichen Prozesses aus Prüfung, Validierung und Unsicherheitsquantifizierung wird in dieser Dissertation eine *Sensitivitätsanalyse, eine Unsicherheitsquantifizierung bis zur 3. Stufe* (einschließlich Kovarianz und Schiefe) sowie eine vorwärtsgerichtete und umgekehrte *prädiktive Modellierung* für ein Dissolvermodell durchgeführt, das für die Nichtweiterverbreitung im Hinblick auf die wässrige Aufbereitung von abgebranntem Kernbrennstoff von Interesse ist. Dieses Dissolvermodell beinhaltet sechzehn nichtlineare Differentialgleichungen, welche 1291 Modellparameter enthalten, die die zugrundeliegenden physikalischen und chemischen Prozesse beschreiben. Die Ergebnisse, welche in dieser Dissertation vorgestellt werden, unterstreichen die Effekte von Unsicherheiten, die notwendigerweise Messungen und Berechnungen prägen sowie die Reduktion der vorhergesagten Unsicherheiten durch optimale Kombination der empirischen und berechneten Informationen.

Die Unsicherheiten in den Parametern des Dissolvermodells werden übertragen, um Unsicherheiten in den modellierten Reaktionen zu errechnen, indem Sensitivitäten erster Ordnung (d. h. funktionale Derivate) der entsprechenden Reaktionen auf die Modellparameter angewandt werden. Die Sensitivitäten erster Ordnung aller Modellparameter der zeitabhängigen Säurekonzentrationen werden berechnet, indem die zugehörige Sensitivitätsanalysemethode für nichtlineare Systeme mit funktionsbewerteten Reaktionen, ursprünglich von Cacuci entwickelt (1981a), angewandt wird. Weiterhin entwickelt diese Arbeit auch ein reduziertes Ersatzdissolvermodell und erweitert die originale zugehörige Technik von Cacuci um die Berechnung von Sensitivitäten zweiter Stufe zu ermöglichen. Wie in dieser Arbeit gezeigt wird, sind Sensitivitäten zweiter Ordnung wesentlich für die Berechnung der Schiefe (d. h. des Moments dritter Stufe) der Reaktionsverteilung, was die asymmetrischen (nicht gaußverteilten) Eigenschaften der Letzteren unterstreicht.

Die Reaktionssensitivitäten dienen auch als Gewichtungsfunktionen zur Kombination von empirischen und berechneten Informationen für das Dissolvermodell unter Einsatz der umfassenden *prädiktiven Modellierungs*methodik, welche ursprünglich von Cacuci und Ionescu-Bujor (2010b) entwickelt wurde. Die einzigen empirischen Informationen aus der verfügbaren Literatur für dieses Dissolvermodell sind die Messungen von Lewis und Weber (1980) zur Salpetersäure im Fach, welches am weitesten vom Zulauf entfernt ist. Der Einsatz dieser empirischen Informationen und des Formalismus der vorwärtsgerichteten und umgekehrten prädiktiven Modellierung zeigt sich als Mittel zur optimalen Vorhersage innerhalb des gesamten Dissolvers mit einer umfassenden Reduktion der Unsicherheiten in diesen vorhergesagten Ergebnissen. Dies ist der Tatsache geschuldet, dass die prädiktive Modellierungsmethodik Informationen gleichzeitig über den gesamten Phasenraum, einschließlich aller Zeitschritte und Orte, kombiniert und überträgt. Ein weiteres bemerkenswertes Ergebnis dieser Dissertation ist der innovative Einsatz des prädiktiven Modellierungsrahmens von Cacuci und Ionescu-Bujor (2010b) in einem Modus der *umgekehrten Vorhersage* zur Ableitung von unbekannten Modellparametern (besonders: die zeitabhängige Zulaufrandbedingung) aus Messungen der Säurekonzentration in dem Fach, welches sich am weitesten entfernt vom Zulauf befindet. Dies ist besonders nützlich bei Anwendungen, bei welchen Rückschlüsse auf ein bestimmtes Ziel nur durch indirekte Messungen gezogen werden können.

Zusammenfassend präsentiert diese Dissertation ein effizientes mathematisches Modell für einen Dissolver für abgebrannten Kernbrennstoff, welcher für internationale atomare Sicherheit und Nichtweiterverbreitung von Interesse ist und zeigt die Vorgehensweise für strenge Unsicherheitsquantifizierung und Validierung dieses Modells. Die Dissertation stellt außerdem einen innovativen zugehörigen Prozess zur Berechnung von Reaktionssensitivitäten zweiter Stufe der Modellparameter vor und zeigt die wesentliche Rolle des Letzteren für die Berechnung nicht gaußverteilter Eigenschaften der Verteilungen modellierter Reaktionen auf. Die in dieser Dissertation vorgestellte Methodik wird als Vorbild für strenge vorwärtsgerichtete und umgekehrte prädiktive Modellierung anderer nuklearer Einrichtungen dienen, welche für die atomare Sicherheit und Nichtweiterverbreitung von Interesse sind. Das Ziel ist die Optimierung von Vorhersagen für "Signaturen" und "Ursachen", bei gleichzeitiger drastischer Reduktion der Unsicherheiten und ein damit einhergehender, genauer risikoinformierter Entscheidungsprozess.

Table of Contents

List of Figures

List of Tables

Nomenclature

1st-LFSS	First Level Forward Sensitivity System
ASAM	Adjoint Sensitivity Analysis Methodology
FAST	Fast Fourier Amplitude Test
FSAM	Forward Sensitivity Analysis Methodology
FSAP	Forward Sensitivity Analysis Procedure
HDMRs	high-dimensional model representations
IAEA	International Atomic Energy Agency
NRC	Nuclear Regulatory Commission
OECD	Organisation for Economic Co-operation and Development's
PM_CMPS	Predictive Modeling of Coupled Multi-Physics Systems
PUREX	Plutonium and Uranium Recovery by EXtraction aqueous separation process
UREX	URanium EXtraction aqueous separation process
VVUQ	Verification, Validation, and Uncertainty Quantification
VCE	Variance of the Conditional Expectation

1. INTRODUCTION

The basic motivation for pursuing research and development in support of nuclear nonproliferation and international nuclear safeguards is to make informed decisions on a target of interest where the ability to collect *accurate* data are limited for numerous physical and even political reasons. The concept holds for exploring any system using measurements and theory, and the goal of trying to understand a target source through some observed quanta of information; yet is further complicated by the constraints posed by real world targets outside a controlled laboratory. These efforts can be a great expense in terms of time, human capital, resource costs, etc., when accuracy for decision-making is desired, since extracting "best estimate" values for model parameters and predicted results (responses), together with "best estimate" uncertainties requires reasoning from incomplete, error-afflicted, and occasionally discrepant information, Cacuci and Ionescu-Bujor (2010b). Therefore, the effort to identify and quantify these uncertainties is generally only demanded of and afforded to, situations such as reactor licensing, or specific programs such as the U.S. Stockpile Stewardship Program National Research Council of the National Academies (2012b) where high consequences for failing identify the full risks in using this information would be dire.

On one hand, results from measurements inevitably reflect the influence of experimental errors, imperfect instruments, or imperfectly known calibration standards; and, on the other, results from computational models are subject to uncertainties stemming from imperfectly known model parameters, correlations, boundary conditions, and imperfectly known physical processes or problem geometry. Therefore, if one is going to use physical or simulated data for decision making, then the quantitative uncertainties accompanying these measurements and computations are essential to understanding *how well* the available information answers specific questions regarding the domain of interest, and the level of risk presented in what is not known.

The National Research Council of the National Academies (2012a) reports on both probabilistic and deterministic methods regarding understanding the reliability of complex models and is a useful summary for the nomenclature used throughout this work. However, it should be noted these definitions accompany most relevant comprehensive studies on

verification, validation, and uncertainty quantification (VVUQ) such as Cacuci and Ionescu-Bujor (2010b) which is strongly referenced throughout this body of work. Moreover, this dissertation does not claim credit for the definitions on VVUQ, and favors loose definitions of them since they are merely used to establish a common frame of reference for discussing the methods and the results that follow, rather than precisely defining or defending their technical boundaries.

Discrepancies between experimental and computational results provide the basic motivation for performing quantitative model verification, validation. Quantification of these discrepancies leads to code qualification and predictive modeling. C*ode verification* documents if the underlying mathematical models are being solved correctly. C*ode qualification* is the activity of then assessing the documented results of these activities for how well this information covers the domain of interest against a defined performance or safety specification. Validation and qualification activities require both physical and analytical benchmarking to account systematically for how well these combined data arrive at the right answer for the right reasons. Ganapol (2008), and Oberkampf and Smith (2014) articulate the motivation and provide useful examples for semi analytical benchmarks and describe the difficulties involving measurements and the contextual information needed from sensors and models to perform such an analysis for neutron transport and computational fluid dynamics, respectively. Overall though, there are numerous examples in the literature including the work of Cacuci referenced throughout this dissertation as well as that sponsored by Organisation for Economic Co-operation and Development's (OECD) Nuclear Energy Agency which are available on their website.

The results of this work rely significantly on the general mathematical framework developed by Cacuci and Ionescu-Bujor (2010b), for best estimate model calibration and predictive estimation and add another illustrative application in the area of nuclear safeguards similar to the companion paper Patruzzi et.al., (2010) for a thermal hydraulic benchmark experiment. Central to the framework are the response sensitivities to the model parameters and the adjoint sensitivity analysis procedure. These "sensitivities" support a wide range of valuable efforts related to model validation allowing for:

(i)   understanding the system by identifying and ranking the importance of model parameters in influencing the response under consideration;

(ii)   determining the effects of parameter variations on the system's behavior;

(iii)   improving the system design, possibly reducing conservatism and redundancy;

(iv)   prioritizing possible improvements for the system under consideration;

(v)   quantifying uncertainties in responses due to quantified parameter uncertainties; and;

(vi)   performing "predictive modeling", including data assimilation and model calibration, for the purpose of obtaining best-estimate predicted results with reduced predicted uncertainties as demonstrated by Cacuci (2015).

This dissertation shows the power of *predictive modeling* that is realized from exercising the VVUQ process; the rigor necessary to fully describe *and* quantify errors needed to support decision making; and, the rigor needed to understand the full risk of using any data beyond the boundaries where they were collected and used in calibration. Predictive modeling itself starts with the identification and characterization of uncertainties from all steps in the sequence of modeling and simulation processes that leads to a computational model prediction including: (a) data error or uncertainty (e.g., input data such as cross sections, model parameters such as reaction-rate coefficients, initial conditions, boundary conditions, and forcing functions such as external loading); (b) numerical discretization error; and (c) uncertainty in (e.g., lack of knowledge of) the processes being modeled. *The result of the predictive modeling analysis is a probabilistic description of possible future outcomes based on all recognized errors and uncertainties.* These results are usually assumed to be Gaussian for the purposes of assigning confidence intervals so this work also intends to discuss the potential risks associated with making decisions without the full description of errors.

1.1. Statement of Thesis:

The original work proposed in this dissertation will creatively use the general *forward and inverse predictive modeling methodology* of Cacuci and Ionescu-Bujor (2010b) to perform *sensitivity analysis, uncertainty quantification up to 3rd-order* (including covariance and skewness), and *forward and inverse predictive modeling* for a deterministic chemio-physio

spent fuel dissolver model relevant to aqueous reprocessing. Furthermore, this work plans to develop a reduced-order surrogate dissolver model, and shows evidence for extending Cacuci's original adjoint technique to enable the computation of second-order sensitivities which are essential for computing skewness (i.e., third-order moment) that characterize asymmetrical (non-Gaussian) features of the true response distribution. This work will also show how the predictive modeling framework of Cacuci and Ionescu-Bujor (2010b) can be used in an inverse prediction mode and infer unknown model parameters (specifically: the time-dependent inlet boundary condition) from measured data, and how this methodology would be particularly useful when inferences on a target of interest can only be made from indirect measurements such as the case of international nuclear safeguards.

All computations in this paper were performed by using Maple™, and ROOT - An Object Oriented Data Analysis Framework was used for all analyses and figures. This work essentially proposes a comprehensive study of quantifying uncertainties for a deterministic model in the application of nuclear nonproliferation, much like the self-contained applications of Petruzzi et.al., (2010), M.C. Badea et al (2012), and by Cacuci and Arslan (2014) in nuclear engineering, but with the addition of computing higher order response sensitivities needed to quantify non-Gaussian features of computed responses needed for assigning accurate Gaussian confidence intervals used for decision making. This work will also demonstrate improved computational efficiency with Adjoint Sensitivity Analysis Methodology for Operator-Type Responses (Cacuci, 1981.b) and discuss the rigor of the results as they apply to dissolver model's verification, validation and uncertainty quantification. A review of international safeguards policy, operations related to a nuclear fuel reprocessing facility, and the merits and shortcomings of numerous VVUQ were conducted to enable a discussion about how the work overall *could be* used to support decision making in these areas as well as how this work and its results will advance the current state of practice.

1.2.A Mechanical Dissolver, International Safeguards, and Background

The work in this dissertation focuses on a paradigm dissolver model. A dissolver is a likely component of any aqueous reprocessing facility and therefore a useful "case study" for a discussion of the VVUQ methods that would be needed for informed decision-making for the International Atomic Energy Agency (IAEA). Woolf. et.al, (2014), states, "The IAEA was created to assist nations in their peaceful programs and to safeguard nuclear materials from these peaceful programs to ensure they are not diverted to nuclear weapons uses." This report also indicates that the safeguards system relies on data collection, review, and periodic inspections at declared facilities. It is not inconceivable then, for inspectors to collect reliable information from any component where fissile material could be lost or diverted such as a dissolver. Figure 1, from Jubin (2009), depicts an aqueous reprocessing block diagram and the major chemical and mechanical processes used by a nuclear fuel reprocessing facility.
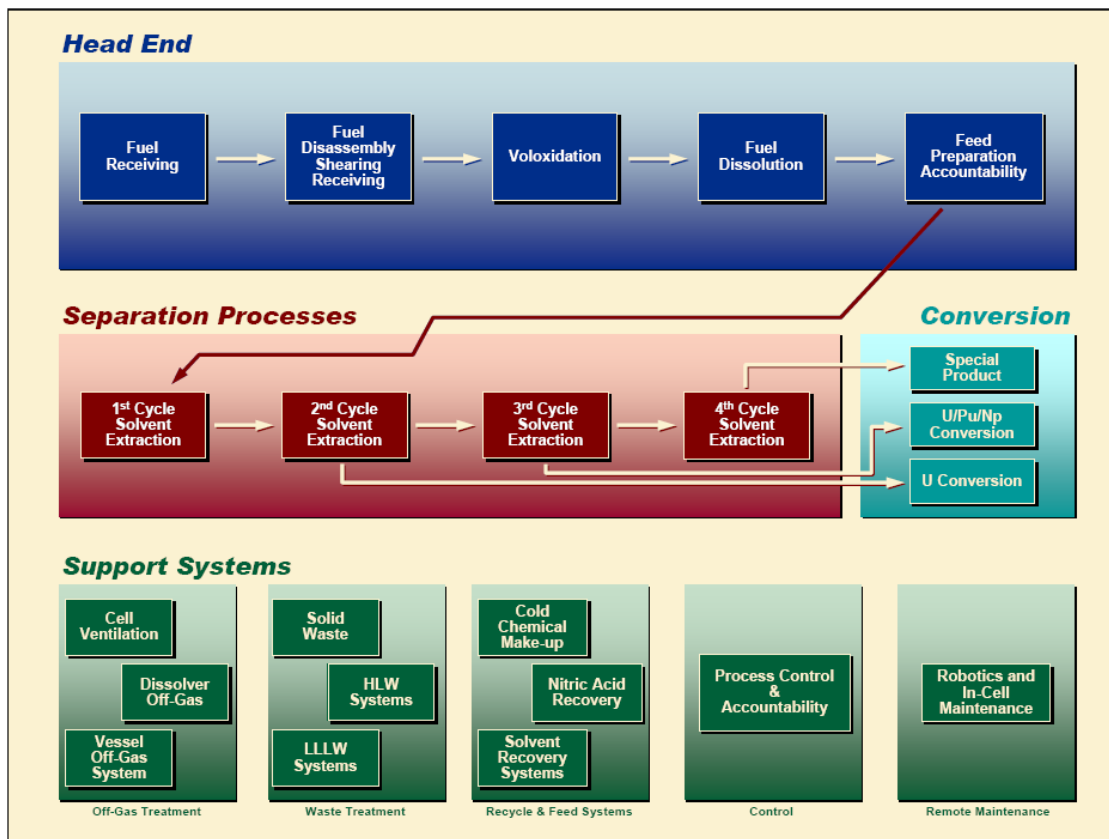
Figure 1 Aqueous Reprocessing Diagram

Numerous flowsheets for chemical separation processes have been developed historically for numerous purposes CRS (2008), and Paulenova (2008) but most utilized the PUREX and UREX flowsheets all which pose risks since they separate plutonium and other actinide elements. These flowsheets not only pose risks for material diversion but are also subject to material holdup, other losses which need accounting for safeguards purposes Burr (2013).

The numerous boxes presented in this figure are all candidates for monitoring where operator declarations and material inventories would be negotiated for inspection and verified with the host operator's declaration. Monitoring, directly or indirectly, is fundamental to establishing international nuclear safeguards agreements, and measurements made to inform any agreed procedure would likely be compared with theoretical computations since historic data from the candidate country would be lacking or not readily shared with an independent inspector. The lack of information, varied expertise in understanding, asymmetry of information from scientists, inspectors, and facility operators are all the more reason to pursue increasing levels of rigor demonstrated in this dissertation.

(1) How to account accurately for material holdup from previous reprocessing activities, and (2) How to assess the degree to which surrogate aqueous reprocessing facilities are compareable surrogates (where measurements and models were calibrated) would be two technical questions that would need to be assessed. These assessments would likely include the use of sensors, inspectors, and subject matter experts to collect data and compare them with the design information and operational envelop declarations by the facility operators and as such, would abe ffected with the aforementioned errors. These errors would certainly need to be characterized and quantified in order to have confidence in the correct assessment. Another major technical issue (3) is how to establish a baseline that would allow for comparing activities from one facility to another. Without a detailed understanding of the exact parameters needed for these comparisons and the sheer number of measurements needed to establish this baseline physically, computational models would be used and need to be assessed for their contributions of error. It's hard to conceive a solution to begin answering these type of questions without a discussion of the uncertainties that would need to be understood.

The works of Garcia et al (2011), Sadasivan and DePaoli (2011) and Cipiti and McDaniel (2011) represent important steps towards modeling an integrated facility so that facilities could be monitored holistically, but these efforts too suffered numerous challenges to accessing data with sufficient descriptions on the contextual information needed to understand the measurements for modeling purposes. A large body of literature exists on performance and methods for assessing the reliability of these models (Oberkampf, 2003; NRC, 2012; Nelson et al, 2010) to improve the understanding of processes and systems (e.g., optimizing material separation, unit operations, etc.), diagnostics (e.g., radiation detectors, calorimeters, radiation imagers, etc.), and the emissions and waste streams, but end with moderate success highlighting the poor contextual details regarding using historical data the measurements and models (e.g., systematic errors of the sensor, sensor response, data analysis software, source codes, parameter minimization, boundary conditions) of which are missing, yet essential to quantifying any uncertainties.

Although the efforts referenced above consider model validation, none of them quantify the impact of uncertainties in model parameters to the level of rigor that will be demonstrated in this work. Furthermore, none of the previously mentioned works attempted to combine measurements with computations, including the respective uncertainties, in order to obtain optimal predictions with reduced predicted uncertainties. This dissertation demonstrates that the judicious combination of computational and experimental information, including the respective computational and experimental uncertainties, produces optimally predicted mean values, with reduced uncertainties for typical quantities that characterize a paradigm dissolver producing chemical feed stock within an aqueous nuclear fuel separations facility. This work also indicates the path for performing similarly rigorous predictive modeling of other tools of interest to any topic where a high degree of confidence is needed.

The dissolver physically resembles a rotating drum, comprising of eight active compartments in which the solids and liquids flow in opposite directions, and includes a ninth compartment used for rinsing. This work will highlight that assimilating even a single experimental measurement, for the purpose of obtaining calibrated model parameters with reduced calibrated standard deviations and best-estimate predicted responses will result in reduced predicted standard deviations than what was measured or originally computed. Moreover, the

2nd-order responses sensitivities to the model parameters are calculated for quantifying the skewness of the response distribution which in practice is generally assumed to be Gaussian.

The analysis concentrates on the flow of liquids, which are most relevant to material separation. Using the original work of Lewis and Weber (1980), *Chapter 3* of this work presents the development of *a new mathematical model* for describing the time-evolution of the nitric acid concentrations and volumetric mass flow rates within the dissolver. This new model comprises sixteen spatially dependent state functions and 1291 model parameters. The most important response for the dissolver model is the time-dependent nitric acid in the compartment furthest away from the inlet, where measurements (unique in the open literature) were performed by Lewis and Weber (1980), over a period of 10.5 hours.

The sensitivities (i.e., first-order functional derivatives) of the time-dependent nitric acid concentrations to the 1291 model parameters are computed in *Chapter 4* of this work by using the *adjoint sensitivity analysis method for nonlinear systems* conceived by Cacuci (1981a, 1981b). The starting point for the efficient computation of these sensitivities is the development of the *adjoint dissolver model*. The relative importance of the most important sensitivities in contributing to the uncertainties in the computed model responses were quantified and analyzed against the physics modeled. Using the sensitivities of the acid concentrations, the uncertainties in the model parameters are propagated in *Chapter 5* of this work to quantify the uncertainties they induce in the computed responses. The predictive modeling formalism is subsequently used to combine the computational results with the experimental information measured in the compartment furthest from the inlet, and then used to predict optimal values and uncertainties throughout the dissolver. The results in *Chapter 5* show that even though the experimental data pertains solely to the compartment furthest from the inlet (where the data was measured), the predictive modeling procedure actually improves the predictions and reduces the predicted uncertainties not only in the compartment in which the data was actually measured, but also throughout the entire dissolver including the compartment furthest from the measurements. This is because information is transmitted simultaneously over the entire phase-space, comprising all time steps and spatial locations.

Many measurement problems, particularly in nonproliferation activities, are "*inverse*" to the "forward" problem in that they *seek to determine the properties of the medium, and/or the size of the medium on its boundaries, or the properties of the source, from measurements of quantities that depend on the unknown state-variables*. The methods for solving inverse problems can be "explicit" or "implicit". The (historically older) explicit methods attempt to manipulate the forward model in conjunction with measurements in order to estimate explicitly the unknown source and/or other unknown characteristics of the medium. On the other hand, implicit methods combine measurements with repeated solutions of the direct problem obtained with different values of the unknowns, iterating until an "a priori" selected functional, usually representing the user-defined "goodness of fit" between measurements and direct computations, is reduced to a value deemed to be "acceptable" by the user. All of these methods have underscored the fundamental characteristics of inverse problems, namely that they are ill-posed (admitting non-unique solutions) and/or ill-conditioned, unstable to small errors or perturbations that are inherently affecting both the model parameters and the experimental measurements. Using an inverse neutron diffusion problem, Cacuci (2014) has highlighted how the amplification of "noise" renders naïve solutions completely useless.

In the nuclear engineering literature, inverse problems have been addressed only in the area of *time-independent neutron and radiation transport*. Time-independent inverse radiative transfer problems were reviewed by McCormick (1992), while examples of inverse source problems for time-independent neutron transport have been provided by Sanchez and McCormick (2008). More recently, Jarman et al (2011) addressed the "source identification problem" by using a Bayesian approach in conjunction with numerical adjoint transport computations to localize radiological sources; however, they only accounted for counting statistics, completely disregarding experimental and modeling uncertainties. On the other hand, Bledsoe et al (2011a, 2011b) used the "differential evolution method" and the "Levenberg-Marquardt method" (Levenberg-Marquardt,1944, 1963), respectively, to solve inverse transport problems by minimizing an "a priori" chosen chi-square-type functional to estimate the "differences between measured and computed quantities of interest", but also neglecting all uncertainties stemming from the underlying cross sections and material properties, which were supposed to be perfectly well known. Hykes and Azmy (2015)

presented a Bayesian approach to solve the inverse problems of mapping the spectral and spatial distributions of radioactive sources using a limited number of detectors when the system's geometry and material composition are known and fixed. All of the methods mentioned above "regularize" the solution of the inverse problems in a more or less ad-hoc implicit manner, without clearly showing the effects of the respective implicit regularizations. The fundamental difficulties associated with inverse problems affect profoundly the numerical methods for solving them, particularly in the presence of errors (including numerical ones). Therefore, all methods for solving inverse problems are not the same: different methods do produce different results.

Inverse time-dependent problems seem to have yet to be addressed in nuclear engineering activities. This work will address such an inverse problem in the context of the dissolver model analyzed in the previous Chapters, by considering that a time-dependent boundary condition (specifically: the time-dependent inlet acid concentration) is unknown and is to be determined from the available measurements. In *Chapter 6* of this work, the application of the methodology of Cacuci and Ionescu-Bujor (2010b) in the *inverse* mode is shown to predict within an "a priori" chosen error criterion the actual time-dependent boundary condition *without needing to invoke ad-hoc procedures or needing to introduce arbitrary parameters* to "regularize" the inverse problem at hand, as the currently popular procedures, e.g., the methods due to Tichonov (1963), Levenberg-Marquardt (1944, 1963), and/or Tarantola (2005) must do. This is because the forward and inverse predicting modeling methodology of Cacuci and Ionescu-Bujor (2010b) uses the maximum entropy principle to combine the model's uncertainties and sensitivities to construct intrinsically the inverse problem's regularizing metric.

Chapter 7, computes the exact 2nd-order sensitivities of the acid concentration in the surrogate dissolver model using adjoint operators; however, only the mean values and the standard deviations are available for the full dissolver's model parameters which in turn assume an *uncorrelated and normally distributed* for the dissolver model's input parameters. Based on this information the non-Gaussian features of the acid concentrations in the full dissolver model are quantified. These results highlight large skewness in the distributions of

several parameters and the implications of smaller than the expected values of these responses resulting from a heavily negatively skewed (by a factor of about 5) distribution for the nitric acid concentration over the transient event.

The concluding remarks presented in *Chapter 8* of this work underscore the importance of this work in presenting the *objective resolution* (i.e., resolution in the absence of user-defined subjective "adjustment" of arbitrary "regularization parameters") of a time-dependent inverse "case study" of potential importance to diversion activities associated with proliferation and international safeguards. Aspects pertaining to the *verification* of the numerical solution of the equations underlying the adjoint dissolver model are briefly presented in Appendix A, while Appendix B presents an abbreviated "*user's manual*" for the software module which has been produced as part of this dissertation for applications of the forward and inverse predictive modeling of Cacuci and Ionescu-Bujor (2010b) to *any* physical system.

Using the dissolver model as a "case study", the results obtained in this work demonstrate a modern path for establishing confidence in computational tools in an efficient, accurate, and manner. In particular, these results enable the evaluation of the subject dissolver model's potential for generating source terms for other components, downstream from the dissolver, within an aqueous nuclear reprocessing facility in supporting material accountability studies for safeguard applications. Furthermore, the methodology used in this work also indicates where to reduce uncertainties (e.g., by increasing the amount of measured data, by increasing model fidelity, exploring missing physics, etc.), should a higher level of confidence be desired. This work does not argue for all problems or modeling efforts to require such rigor, but rather that the appropriate level of rigor be instituted to assess what's "good enough" for the intended application, and to extend the value of any measured data and models beyond the individual researcher who collected or developed them. Finally, this work's conclusions highlight the need for an extensible general method for computing mixed 2nd-order sensitivities for quantifying non-Gaussian features for correlated parameters which are likely for most real world targets of interest as future work.

2. SURROGATE DISSOLVER MODEL AND A COMPARISON OF SENSITIVITY ANALYSIS METHODS FOR PROBABILISTIC AND DETERMINISTIC MODELING

This chapter uses a surrogate model, constructed from the spent nuclear fuel dissolver model, to illustrate the methods and the motivation underlying the various direction of research. The surrogate model enables the analytical illustration of the underlying mathematical concepts, underscoring both the original methodological and conceptual novelties as well as the major new results produced by this work without the numerous terms that would be generated from the dissolver model itself.

Section 2.1 then presents a brief but critical review of the most popular statistical and deterministic methods for sensitivity analysis and quantification of model response uncertainties that are induced by uncertainties in the model parameters. It concludes with a discussion on why the "*adjoint sensitivity analysis method for operator-valued responses*" originally introduced by Cacuci (1981.b) was selected as the method for computing the acid concentration response sensitivities to parameters of the dissolver model essential to the rest of the work considered in the subsequent sections. Section 2.2 actually develops the surrogate model, which is used without loss of generality to again, illustrate the novel concepts and results reported in this work. Section 2.3 demonstrates the application of the "*adjoint sensitivity analysis method for operator-valued responses*" to compute efficiently the 1st-order sensitivities of the surrogate model's response to the surrogate model's parameters. Section 2.4 applies the predictive modeling methodology developed by Cacuci and Ionescu-Bujor (2010b) to the surrogate model, both in the *forward and inverse predictive modes*, demonstrating mathematically the reasons for which this methodology actually reduces the predicted uncertainties (in this case: standard deviations) for the optimally predicted best-estimate nominal response and parameter values. Extending the concepts presented in Section 2.3, Section 2.5 *proposes a new adjoint-based methodology* for computing efficiently 2nd-order sensitivities of responses to model parameters. As will also be shown in this section,

such 2nd-order sensitivities are needed for quantifying the non-Gaussian features (i.e., *skewness* and consequent asymmetries, long and/or short tails) of the unknown response distribution as a function of the model parameters. Finally, Section 2.6 concludes showing the correspondences between the surrogate model and the actual dissolver model that will be analyzed in Chapters 3-7.

2.1. Statistical Versus Deterministic Methods for Sensitivity and Uncertainty Analysis

This section presents a brief yet critical review of the most popular statistical methods used for uncertainty and sensitivity analysis, and compares them with deterministic methods, particularly with the adjoint method for nonlinear systems with operator-valued responses introduced by Cacuci (1981.b), highlighting the respective strengths and weakness of the various methods. Since the notation used by Cacuci (1981.b) is optimal for describing his method, it will also be used in this Chapter, to highlight the features that will be used and expanded in subsequent chapters of this dissertation.

In general, physical systems and/or results of indirect experimental measurements are modeled using the following mathematical concepts:

(a) Nonlinear equations that relate the system's independent variables and parameters to the system's state (i.e., dependent) variables;

(b) Probability distributions, moments thereof, inequality and/or equality constraints that define the range of variations of the system's parameters;

(c) One or several *quantities of interest*, called system *responses* (or objective functions, or indices of performance), which are computed using the mathematical model.

Mathematically, a physical system conforming to the above description is represented by means of N_u coupled *nonlinear* operator equations of the form

$$\mathbf{N}\big[\boldsymbol{\alpha}(\mathbf{x}), \mathbf{u}(\mathbf{x})\big] = \mathbf{Q}\big[\boldsymbol{\alpha}(\mathbf{x})\big], \quad \mathbf{x} \in \Omega_x. \tag{2.1}$$

It is convenient to consider that all vectors in this work are *column vectors*. Transposition is indicated by a dagger $(\dagger)$ superscript. The quantities appearing in Eq. (2.1) are defined as follows:

1. $\mathbf{x} \triangleq \left(x_1, \ldots, x_{J_x} \right)$ denotes the J_x-dimensional phase-space position vector for the primary system; the symbol "$\triangleq$" will be used to denote "is defined as" or "is by definition;" note that $\mathbf{x} \in \Omega_x \subset \mathbb{R}^{J_x}$, where Ω_x is a subset of the J_x-dimensional real vector space $\mathbb{R}^{J_x}$;

2. $\mathbf{u}(\mathbf{x}) \triangleq \left[u_1(\mathbf{x}), \ldots, u_{N_u}(\mathbf{x}) \right]$ denotes a N_u-dimensional column vector whose components are the system's dependent (i.e., state) variables; $\mathbf{u}(\mathbf{x}) \in \mathbf{E}_u$, where $\mathbf{E}_u$ is a normed linear space over the scalar field $\mathbf{F}$ of real numbers;

3. $\boldsymbol{\alpha}(\mathbf{x}) \triangleq \left[\alpha_1(\mathbf{x}), \ldots, \alpha_{N_\alpha}(\mathbf{x}) \right]$ denotes a N_α-dimensional column vector whose components are the system's parameters; $\boldsymbol{\alpha} \in \mathbf{E}_\alpha$, where $\mathbf{E}_\alpha$ is also a normed linear space;

4. $\mathbf{Q}\left[\boldsymbol{\alpha}(\mathbf{x}) \right] \triangleq \left[Q_1(\boldsymbol{\alpha}), \ldots, Q_{N_u}(\boldsymbol{\alpha}) \right]$ denotes a N_u-dimensional column vector whose components represent inhomogeneous source terms that are functions of $\boldsymbol{\alpha}(\mathbf{x})$; $\mathbf{Q} \in \mathbf{E}_Q$, where $\mathbf{E}_Q$ is also a normed linear space;

5. $\mathbf{N}\left[\boldsymbol{\alpha}(\mathbf{x}), \mathbf{u}(\mathbf{x}) \right] \triangleq \left[N_1(\boldsymbol{\alpha}, \mathbf{u}), \ldots, N_{N_u}(\boldsymbol{\alpha}, \mathbf{u}) \right]$ denotes a N_u-component column vector whose components are *operators* (including differential, difference, integral, distributions, and/or infinite matrices) acting *nonlinearly* on $\mathbf{u}$ and $\boldsymbol{\alpha}$;

6. All of the equalities in this work are considered to hold in the weak ("distributional") sense, since the right-sides ("sources") of the various equations, including Eq. (2.1) may contain distributions ("generalized functions/functionals"), particularly Dirac-distributions and derivatives and/or integrals thereof.

In view of the definitions given above, $\mathbf{N}(\mathbf{\alpha}, \mathbf{u})$ represents the mapping $\mathbf{N}:\mathbf{D} \subset \mathbf{E} \rightarrow \mathbf{E}_Q$, where $\mathbf{D} = \mathbf{D}_u \oplus \mathbf{D}_\alpha$, $\mathbf{D}_u \subset \mathbf{E}_u$, $\mathbf{D}_\alpha \subset \mathbf{E}_\alpha$, and $\mathbf{E} = \mathbf{E}_u \oplus \mathbf{E}_\alpha$. Note that an arbitrary element $\mathbf{e} \in \mathbf{E}$ is of the form $\mathbf{e} = (\mathbf{\alpha}, \mathbf{u})$. If differential operators appear in Eq. (2.1), then a corresponding set of boundary and/or initial conditions (which are essential to define the domain of $\mathbf{D}$) must also be given; these boundary and/or initial conditions are represented in operator form as

$$\left[\mathbf{B}(\mathbf{\alpha}, \mathbf{u}) - \mathbf{C}(\mathbf{\alpha}) \right]_{\partial\Omega_x} = \mathbf{0}, \quad \mathbf{x} \in \partial\Omega_x, \tag{2.2}$$

where $\partial\Omega_x$ denotes the boundary of Ω_x, the operator $\mathbf{B}(\mathbf{\alpha}, \mathbf{u})$ acts nonlinearly on both $\mathbf{u}$ and on the model parameters $\mathbf{\alpha}$, while $\mathbf{C}(\mathbf{\alpha})$ denotes an operator that acts nonlinearly on $\mathbf{\alpha}$.

The vector-valued function $\mathbf{u}(\mathbf{x})$ is considered to be the unique nontrivial solution of the physical problem described by Eqs. (2.1) and (2.2). The system response (i.e., result of interest), associated with the problem modeled by Eqs. (2.1) and (2.2) will be denoted as $\mathbf{R}(\mathbf{u}, \mathbf{\alpha})$, and will generally be a phase-space dependent function-valued operator that acts on the system's state function $\mathbf{u}$ and parameters $\mathbf{\alpha}$. Most generally, such a response can be represented in operator form as

$$\mathbf{R}(\mathbf{u}, \mathbf{\alpha}):\mathbf{D}_R \subset \mathbf{E} \rightarrow \mathbf{E}_R, \tag{2.3}$$

where $\mathbf{E}_R$ denotes another normed vector space. The nominal solution of Eqs. (1) and (2) is denoted as $\mathbf{u}^0(\mathbf{x})$, and is obtained by solving these equations at the nominal parameter values $\mathbf{\alpha}^0(\mathbf{x})$, i.e.,

$$\mathbf{N}\left[\mathbf{\alpha}^0(\mathbf{x}), \mathbf{u}^0(\mathbf{x}) \right] = \mathbf{Q}\left[\mathbf{\alpha}^0(\mathbf{x}) \right], \quad \mathbf{x} \in \Omega_x, \tag{2.4}$$

$$\left[\mathbf{B}(\mathbf{\alpha}^0, \mathbf{u}^0) - \mathbf{C}(\mathbf{\alpha}^0) \right]_{\partial\Omega_x} = \mathbf{0}, \quad \mathbf{x} \in \partial\Omega_x. \tag{2.5}$$

Equations (2.4) and (2.5) represent the "*base-case*" or *nominal* state of the physical system. The *nominal solution*, $\mathbf{u}^0(\mathbf{x})$, of these equations is subsequently used to compute the *nominal value* $R(\mathbf{e}^0)$, $\mathbf{e}^0 \equiv (\boldsymbol{\alpha}^0, \mathbf{u}^0)$, of the response $R(\mathbf{e})$. Throughout this work, the superscript "0" will be used to denote "nominal values." An important particular case of responses is scalar valued "quantities of interest," such scalar-valued will be called *functionals* of $(\boldsymbol{\alpha}, \mathbf{u})$, and will be generally represented in operator form as

$$R(\boldsymbol{\alpha}, \mathbf{u}): \mathbf{D}_R \subset \mathbf{E} \to \mathbf{F}, \tag{2.6}$$

where $\mathbf{F}$ denotes the field of real scalars.

The model parameters are considered to be imprecisely known quantities, so their actual values may differ from their nominal values by quantities denoted as $\delta\alpha_i(\mathbf{x}) \triangleq \alpha_i(\mathbf{x}) - \alpha_i^0(\mathbf{x})$, $i = 1, ..., N_\alpha$. Large-scale models of complex physical systems usually involve two distinct sources of uncertainties, namely: (a) *stochastic uncertainty*, which arises because the system under investigation can behave in many different ways, and (b) *subjective or epistemic uncertainty*, which arise from the inability to specify an exact value for a parameter that is assumed to have a constant value in the respective investigation. A typical example of such a complex system is a nuclear power reactor plant; in a typical risk analysis of a nuclear power plant, stochastic uncertainty arises due to the many hypothetical accident scenarios which are considered in the respective risk analysis, while epistemic uncertainties arise because of the many uncertain parameters that underlie the estimation of the probabilities and consequences of the respective hypothetical accident scenarios. Usually, the effects of stochastic uncertainties are propagated by using importance sampling, while the effects of subjective uncertainties are propagated by using Latin Hypercube sampling. In particular, event trees, if available, are used in conjunction with importance-sampling to propagate stochastic uncertainties. This concept has been amply illustrated in two large risk assessment studies, namely the reassessment of risk associated with US commercial nuclear power plants, carried out under the auspices of the US Nuclear Regulatory Commission (NUREG-1150, 1990-91), and the Compliance Certification

Application for the Waste Isolation Power Plant (US Department of Energy, 1996, Helton et al., 1998).

Since the model parameters $\boldsymbol{\alpha}(\mathbf{x})$ and the state functions $\mathbf{u}(\mathbf{x})$ are related to each other through Eqs. (2.1) and (2.2), it follows that the vector of "parameter variations" $\delta\boldsymbol{\alpha} \triangleq \left(\delta\alpha_1,\ldots,\delta\alpha_{N_\alpha}\right) \in \mathbf{E}_\alpha$ will cause corresponding variations $\delta\mathbf{u} \triangleq \left(\delta u_1,\ldots,\delta u_{K_u}\right) \in \mathbf{E}_u$ in the state functions around the nominal solution $\mathbf{u}^0(\mathbf{x})$. All of these variations will cause variations in the response around the nominal response value $\mathbf{R}(\mathbf{e}^0)$. *Sensitivity analysis* aims at quantifying the response variations, $\mathbf{R}(\mathbf{e}^0 + \mathbf{h})$, that are induced in the response $R(\mathbf{e}^0)$ by variations $\mathbf{h} \triangleq (\delta\boldsymbol{\alpha}, \delta\mathbf{u}) \in \mathbf{E} = \mathbf{E}_\alpha \oplus \mathbf{E}_u$ in the model's state functions and parameters in a neighborhood around the nominal values $\mathbf{e}^0 = \left(\boldsymbol{\alpha}^0, \mathbf{u}^0\right) \in \mathbf{E}$.

Sensitivities of model response to model parameters are needed in many activities, including:

(i)   understanding the system by identifying and ranking the importance of model parameters in influencing the response under consideration; as illustrated for the dissolver model in Chapter 3;

(ii)   quantifying uncertainties in responses due to quantified parameter uncertainties; as illustrated in Chapters 4, 5 and 7, and demonstrated with the method of "propagation of uncertainties";

(iii)   performing *forward* "predictive modeling", including data assimilation and model calibration, for the purpose of obtaining best-estimate predicted results with reduced predicted uncertainties; as demonstrated for this work in Chapter 5;

(iv)   performing *inverse* "predictive modeling", as illustrated in Chapter 6;

(v)   determining the effects of parameter variations on the system's behavior, for system optimization;

(vi)   improving the system design, possibly reducing conservatism and redundancy;

(vii)   prioritizing possible improvements for the system under consideration.

Section 2.1.1 below presents a brief review of the most popular statistical methods for sensitivity analysis and quantification of model response uncertainties that are induced by uncertainties in the model parameters. Following this brief review of statistical methods, Section 2.1.2 presents the basic concepts underlying the "adjoint sensitivity analysis method for operator-valued responses" originally introduced by Cacuci (1981.b). For the reasons discussed in Section 2.1.3, this adjoint method will be applied for the computation of 1st-order sensitivities acid concentration response to parameters of the dissolver model considered throughout the rest of the chapters considered in this work.

2.1.1 Statistical Methods for Uncertainty and Sensitivity Analysis

The currently popular statistical methods for uncertainty and sensitivity analysis are broadly categorized as follows: (A) sampling-based methods, (B) variance-based methods, and (C) spectral methods. All of these methods essentially consider that the response is an implicit functional (i.e., a scalar-valued function) of scalar model parameters $\boldsymbol{\alpha} \equiv (\alpha_1, ..., \alpha_{N_\alpha})$; therefore, the response will be simply denoted as $R(\boldsymbol{\alpha})$. If the uncertainty associated with the parameters $\boldsymbol{\alpha}$ were known unambiguously, then the uncertainty in the response $R(\boldsymbol{\alpha})$ could also be assessed unambiguously. In practice, the uncertainty in $\boldsymbol{\alpha}$ can be characterized by assigning a distribution of plausible values

$$D_1, D_2, ..., D_I, \tag{2.7}$$

to each component α_i of $\boldsymbol{\alpha}$. Correlations and other restrictions can also be considered to affect the parameters α_i. Uncertainties characterized by distributions of the form shown in Eq. (2.7) are often called *epistemic* or *subjective uncertainties*, and characterize a degree of belief regarding the location of the appropriate value of each α_i. In turn, these subjective uncertainties for the parameters α_i lead to subjective uncertainties for the response $R(\boldsymbol{\alpha})$, which reflect a corresponding degree of belief regarding the location of the appropriate response values as the outcome of analyzing the model under consideration.

The definition of the distributions D_i is the most important aspect of characterizing subjective uncertainties. Consequently, the characterization of subjective uncertainty has been widely studied (see, e. g., Berger, 1985; Hora and Iman, 1989, Bonano and Apostolakis, 1989). Two of the largest examples of analyses which use formal expert review processes to assign subjective uncertainties to input parameters are the US Nuclear Regulatory Commission's reassessment of the risks from commercial nuclear reactor power stations (US NRC 1990-1991), and the assessment of seismic risk in the Eastern USA (EPRI, 1989). Although formal statistical procedures can be occasionally used for constructing subjective distributions, practical experience has shown that it is more useful to rely on *expert opinion*s for specifying selected quantile (minimum, median, maximum, etc.) values, rather than specify a particular type of distribution (e.g., normal, beta, etc.,) and its associated parameters. Respective experts are more likely to be able to justify the selection of specific quantile values rather than the selection of a particular form of distribution with specific parameters. When distributions from several expert opinions are combined, it is practically very difficult to assign weights to the respective opinions, as discussed by Clement and Winkler (1999).

A. *Sampling-Based Methods*

These methods are based on a sample

$$\mathbf{\alpha}_\kappa = \left[\alpha_{k1}, \alpha_{k2}, \ldots, \alpha_{kI}\right], \quad k = 1, 2, \ldots, n_S, \tag{2.8}$$

of size n_S taken from the possible values of $\mathbf{\alpha}$ as characterized by the distributions in Eq. (2.7). The response evaluations corresponding to the sample $\mathbf{\alpha}_k$ defined in Eq. (2.8) can be represented in vector form as

$$\mathbf{R}(\mathbf{\alpha}_\kappa) = \left[R_1(\mathbf{\alpha}_\kappa), R_2(\mathbf{\alpha}_\kappa), \ldots, R_J(\mathbf{\alpha}_\kappa)\right], \quad k = 1, 2, \ldots, n_S, \tag{2.9}$$

where the subscript *J* denotes the number of components of $\mathbf{R}(\mathbf{\alpha}_\kappa)$. The pairs

$$\left[\mathbf{\alpha}_\kappa, \mathbf{R}(\mathbf{\alpha}_\kappa)\right], \quad k = 1, 2, \ldots, n_S, \tag{2.10}$$

represent a *mapping* of the uncertain "inputs" $\boldsymbol{\alpha}_k$ to the corresponding uncertain "outputs" $\mathbf{R}(\boldsymbol{\alpha}_\kappa)$ which are obtained from the "sampling-based uncertainty analysis". The "*sampling-based sensitivity analysis*" consists of quantifying the effects of the elements of $\boldsymbol{\alpha}$ on the elements of $R(\boldsymbol{\alpha})$ by performing regression analysis, partial correlation, analyzing scatter plots, etc., of the mapping represented by Eq. (2.10).

The widest used sampling procedures are: random sampling, importance sampling, and Latin Hypercube sampling; the salient features of these procedures will be summarized briefly in the following. Thus, *random sampling* involves selection of the observations

$$\boldsymbol{\alpha}_\kappa = [\alpha_{k1}, \alpha_{k2}, \ldots, \alpha_{kI}], \quad k = 1, 2, \ldots, n_{RS}, \tag{2.11}$$

where n_{RS} represents the sample size from a region S. A point from a specific region of S occurs as dictated by the probability of occurrence of the respective region. Although each sample point is selected independently of all other sample points, there is no guarantee that points will be sampled from any given sub-region of S. Furthermore, if sampled values fall closely together, the sampling of S is quite inefficient. The *importance sampling* procedure has been designed to address and alleviate these shortcomings, by dividing S exhaustively into several non-overlapping sub-regions, called *strata,* S_i, $i = 1, 2, \ldots, n_S$, which are defined on the basis of how important the parameters ($\boldsymbol{\alpha}_\kappa \in \mathsf{S}_i$) that are contained in the strata are to the final outcome of the analysis. Importance sampling aims at ensuring *full coverage of specified regions* in the sample space, so that parameters which have low occurrence probabilities but high consequences are included in the analysis.

The *Latin Hypercube sampling* procedure (see, e.g., McKay et al., 1979) further extends the idea of fully covering the range of each parameter by dividing the range of each parameter α_i into n_{LH} intervals of equal probability, and randomly selecting one value from each interval. The n_{LH} values thus obtained for the first parameter, α_1, are then randomly paired, without replacement, with the n_{LH} values obtained for α_2. In turn, these *pairs* are combined randomly, without replacement, with the n_{LH} values for α_3 to form n_{LH} *triples*. This process is continued until a set of n_{LH} *I-tuples* are obtained, of the form

$$\boldsymbol{\alpha}_{\kappa} = \left[\alpha_{k1}, \alpha_{k2}, \ldots, \alpha_{kI}\right], \quad k = 1, 2, \ldots, n_{LH}, \tag{2.12}$$

which is called a *Latin Hypercube sample*. However, this method is suited only for uncorrelated parameters. If the parameters are correlated, then the respective correlation structure must be incorporated into the sample; otherwise the ensuing uncertainty/sensitivity analysis is destined to yield false results. To incorporate parameter correlations into the sample, Iman and Conover (1982) proposed a restricted pairing technique for generating Latin Hypercubes based on rank-correlations (i.e., correlations between rank-transformed parameters) rather than sample correlations (i.e., correlations between the original, untransformed, parameters).

Once the sample has been generated, its elements must be used to perform model recalculations, which then generate the responses $\mathbf{R}(\boldsymbol{\alpha}_{\kappa})$ described by Eq. (2.9). *These model recalculations can become the most expensive computational part of the entire statistical uncertainty and sensitivity analysis* and, if the model is complex, the model recalculations severely limit the sample size and the other aspects of the overall analysis.

In the context of sampling-based methods, *statistical sensitivity analysis* (as opposed to *deterministic* sensitivity analysis) involves the exploration of mapping given in Eq. (2.10) to assess the effects of *some but not all of* the individual components of $\boldsymbol{\alpha}$ on the response $R(\boldsymbol{\alpha})$. This exploration includes examination of scatter plots, regression and stepwise regression analysis, correlation and partial correlation analysis, rank transformation, identification of non-monotonic patterns, and identification of non-random patterns. The starting point of statistical sensitivity analysis is the generation of scatter plots, which are obtained by plotting the points

$$\left[\alpha_{kj}, R_2(\boldsymbol{\alpha}_{\kappa})\right], \quad \left(k = 1, \ldots, n_S\right), \tag{2.13}$$

for each element α_j of $\boldsymbol{\alpha}$ for $\left(j = 1, \ldots, I\right)$. The resulting I scatter plots are then examined to find possible relations between the response $R(\boldsymbol{\alpha})$ and the elements α_j of $\boldsymbol{\alpha}$.

A more formal analysis of the parameter-to-response mapping depicted by Eq. (2.13) is to perform *linear* regression analysis on a model for which the predicted *responses, $R_{predicted}$*, is a linear function of the input parameters, α_j, of the form

$$R_{predicted} = b_0 + \sum_{j=1}^{I} b_j \alpha_j . \tag{2.14}$$

The calculated *responses, R_k*, are also formally expressed in terms of the *actual* parameter values, α_{kj}, used in the analysis, by means of a *linear* relationship of the form

$$R_k = b_0 + \sum_{j=1}^{I} b_j \alpha_{kj} + \varepsilon_k, \quad k = 1,\ldots M, \tag{2.15}$$

where *M* denotes the actual number of calculations and where

$$\varepsilon \equiv R_k - R_{predicted}, \tag{2.16}$$

denotes the error between the calculated and predicted value of the corresponding element of the response. The regression analysis then commences by assuming that the unknown regression coefficients b_j can be determined by minimizing the sums $\sum_k \left(R_k - R_{predicted}\right)^2 \triangleq \sum_k \varepsilon^2$ of the squared errors. The regression coefficients b_j can be used, along with other indicators computed during the regression analysis, to assess the importance of the individual parameters α_j with respect to the uncertainty in the response components. A measure of the extent to which the regressions model can match the observed data is provided by the so called *coefficient of multiple determination*, C^2, defined by the following ratio:

$$C^2 \equiv S_{reg} / S_{tot}, \tag{2.17}$$

where the quantities S_{reg} and S_{tot} are defined by means of the sums

$$S_{reg} \triangleq \sum_{k=1}^{M} \left(R_{k,est} - R_{ave}\right)^2, \quad S_{tot} \triangleq \sum_{k=1}^{M} \left(R_k - R_{ave}\right)^2, \tag{2.18}$$

and where $R_{k,est}$ denotes the estimate of R_k obtained from the regression model, while R_{ave} denotes the mean of the R_k's. A value of C^2 close to unity indicates that the regression model accounts well for most of the uncertainties in the R_k's; conversely, a value of C^2 close to zero indicates that the regression model accounts poorly for the uncertainties in the R_k's.

It is important to note that *if the parameters* are not independent but *are statistically correlated*, then the magnitudes and even the signs of the regression coefficients b_j associated with the respective parameters may be erroneous, and therefore indicate incorrectly the effects of these parameters on the response. *Correlated variables introduce unstable regression coefficients*, b_j, in that the values of b_j become sensitive to the specific variables introduced into the regression model. In such situations, the regression coefficients of a regression model that includes *all* of the parameters are likely to give misleading indications of parameter importance. If several input parameters are suspected (or known) to be highly correlated, it is usually recommended to transform the respective parameters so as to remove the correlations or, if this is not possible, to analyze the full model by using a sequence of regression models with all but one of the parameters removed, in turn. Furthermore, if the regression model is used in an attempt to match the predictions associated with individual sample parameters rather than to match the trend displayed by the collective sample, then over-fitting of data may arise when parameters are arbitrarily forced into the regression model. Note also that the regression relationship in Eq. (2.14) is a linear representation of the impact of parameters on the response, which will perform poorly when the relationships between the parameters and the response are nonlinear. In such cases, the *rank transformation* may be used to improve the construction of the respective regression model. The regression analysis is then performed by using the ranks as input/output parameters, as replacements for the actual parameter/response values. This replacement has the effect of replacing the *linearized* parameter/response relationships by rank-transformed *monotonic* input/output relationships in an otherwise conventional regression analysis. In practice, a regression analysis using the rank-transformed (instead of raw) data may yield better results, but only as long as the relationships between parameters and responses are

monotonically nonlinear. Otherwise, the rank-transformation does not improve significantly the quality of the results produced by regression analysis.

B. *Variance -Based Methods*

In contrast to the sampling-based methods discussed in the previous subsection, the variance-based methods do *not* make the "a priori" assumption that the input model parameters are linearly related to the model's response. The variance-based methods are based on the relation between *the marginal probability distribution, $p_R(R)$*, of *R*, and the *conditional probability distribution, $p_{R|\alpha}(R|\alpha)$, of R conditioned on an input parameter α* , which can be written in the following form:

$$p_R(R) = \int p_{R|\alpha}(R|\alpha)p_\alpha(\alpha)d\alpha \ . \tag{2.19}$$

The above relation can be intuitively *interpreted that an input parameter α is important if fixing its value would reduce significantly the conditional prediction variance relative to the marginal prediction variance.* This interpretation indicates that various conditional variance ratios may be used as indicators of importance. Variance-based methods usually assume that the model simulating the system under investigation is of the form

$$R = E(R|\mathbf{\alpha}) + \mathbf{\epsilon}, \tag{2.20}$$

where $\mathbf{\alpha}$ represents, as before, the set of *I* model parameters, and $\mathbf{\epsilon}$ represents a vector of errors with the properties that $E(\mathbf{\epsilon}) = 0$ and $Var\left[E(R|\mathbf{\alpha}), \mathbf{\epsilon}\right] = known$. As noted in Eq. (2.14), the standard regression analysis assumes that the expectation $E(R|\mathbf{\alpha})$ is a linear function of the model parameters, of the form $\sum_{k=1}^{M}\alpha_k b_k$, where the quantities b_k are the regression coefficients determined by least-square fitting. By contrast, there are *no assumptions* in Eq. (2.20) regarding the specific mathematical form of the conditional expectation $E(R|\mathbf{\alpha})$. Replacing Eq. (2.20) in Eq. (2.19) yields the following form for the prediction variance, $Var(R)$, of R :

$$Var(R) = Var_{\alpha}\left[E(R \mid \alpha)\right] + E_{\alpha}\left(Var[R \mid \alpha]\right), \tag{2.21}$$

where

$$E(R \mid \alpha) \equiv \int p_{R\mid\alpha}(R) R dR, \tag{2.22}$$

$$Var_{\alpha}\left[E(R \mid \alpha)\right] \equiv \int \left[E(R \mid \alpha) - E(R)\right]^2 p_{\alpha}(\alpha) d\alpha, \tag{2.23}$$

$$E_{\alpha}\left(Var[R \mid \alpha]\right) \equiv \int \left[R - E(R \mid \alpha)\right]^2 \left[p_{R\mid\alpha}(R) dR\right] p_{\alpha}(\alpha) d\alpha. \tag{2.24}$$

The quantity $Var_{\alpha}\left[E(R \mid \alpha)\right]$ is the *variance of the conditional expectation* (*VCE*) of R conditioned on α; this quantity is a suitable measure of the importance of α since it indicates how the constituents parts of $Var(R)$, given by Eq. (2.21), relate to α. More specifically, $Var_{\alpha}\left[E(R \mid \alpha)\right]$ measures the total variation in R in the sense that, as α varies, the variation in R would match the variation in $E(R \mid \alpha)$, if the second term in Eq. (2.21), namely $E_{\alpha}\left(Var[R \mid \alpha]\right)$, were small. In fact, the term $E_{\alpha}\left(Var[R \mid \alpha]\right)$ is a residual term that measures the remaining variability in R due to other unobserved inputs or other unknown sources of variation when α is fixed. The ratio

$$\eta^2 = \frac{Var_{\alpha}\left[E(R \mid \alpha)\right]}{Var(R)}, \tag{2.25}$$

is called the *correlation ratio* and represents a measure of the magnitude of the *VCE* relative to the prediction variance $Var(R)$ (see, e.g., McKay, 1995).

Another variance-based method is "Sobol's Method" (1993) which uses a particular case of Kolmogorov's decomposition theorem. Kolmogorov's theorem states that any multivariate function, $f(x_1, ..., x_n)$, defined on the unit cube $[0,1]^n$ can be written as a linear superposition of univariate functions $h_j(x_i)$, of the form

$$f(x_1,...,x_n) = \sum_{j=1}^{2n+1} g\left[a_1 h_j(x_1) + a_2 h_j(x_2) + ... + a_n h_j(x_n)\right], \tag{2.26}$$

where the functions $h_j(x_i)$ are continuous, albeit highly non-smooth. Considering a response, $R(\boldsymbol{\alpha})$, which is a function of the vector of model parameters $\boldsymbol{\alpha} \triangleq (\alpha_1,...,\alpha_n)$ where each parameters varies between zero and one, [i.e., $\boldsymbol{\alpha}$ defined on the unit cube $[0,1]^n$], Sobol's decomposition method [see, e.g., Sobol (1993), Saltelli et al., (2000)] takes on the following particular form of Eq. (2.26):

$$R(\boldsymbol{\alpha}) \equiv R(\alpha_1,...,\alpha_n) = R_0 + \sum_{i=1}^{n} R_i(\alpha_i) + \sum_{1\le i<j\le n} R_{ij}(\alpha_i,\alpha_j) + ... + R_{12...n}(\alpha_1,\alpha_2,...,\alpha_n), \tag{2.27}$$

where

(i) R_0 is a constant, i.e., $R_0 \equiv \displaystyle\int_{[0,1]^n} R(\boldsymbol{\alpha})\, d\boldsymbol{\alpha} = \text{constant}$,

(ii)   the summands are orthogonal, i.e.,

$$\int_{[0,1]^n} f_{i_1 i_2 ... i_n}(\boldsymbol{\alpha}) f_{j_1 j_2 ... j_m}(\boldsymbol{\alpha})\, d\boldsymbol{\alpha} = 0, \quad \text{if } (i_1, i_2,...,i_n) \ne (j_1, j_2,...,j_m);$$

(iii)   the integrals of any summand over any of its own variables is zero, i.e.,

$$\int_0^1 f_{i_1 i_2 ... i_n}(\alpha_{i_1}, \alpha_{i_2},...,\alpha_{i_n})\, d\alpha_{i_m} = 0, \quad \text{if } 1 \le m \le n.$$

By squaring Eq. (2.27) and integrating the resulting expression over the unit cube $[0,1]^n$, the following relation is obtained for the total variance, denoted as D, of $R(\boldsymbol{\alpha})$:

$$D \equiv \int_{[0,1]^n} R^2(\boldsymbol{\alpha})\, d\boldsymbol{\alpha} - R_0^2 = \sum_{i=1}^{n} D_i + \sum_{1\le i<j\le n} D_{ij} + ... + D_{12...n}, \tag{2.28}$$

where the partial variances of $R(\boldsymbol{\alpha})$ are defined as follows:

$$D_{i_1 i_2 ... i_m} \equiv \int_0^1 ... \int_0^1 R_{i_1 i_2 ... i_m}(\alpha_{i_1}, \alpha_{i_2},...,\alpha_{i_m})\, d\alpha_{i_1}...d\alpha_{i_m}, \quad \text{for } 1 \le i_1 < ... < i_m \le n, \ m = 1,...,n. \tag{2.29}$$

Finally, the sensitivity indices are defined as

$$S_{i_1 i_2 \ldots i_m} \equiv D_{i_1 i_2 \ldots i_m} / D, \quad for \quad 1 \le i_1 < \ldots < i_m \le n, \quad m = 1, \ldots, n. \qquad (2.30)$$

In view of the above definitions, the first-order sensitivity index, S_i, for the parameter α_i indicates the fractional contribution of α_i to the variance D of $R(\boldsymbol{\alpha})$. The second-order sensitivity index, $S_{ij}, (i \ne j)$, measures the part of the variation in $R(\boldsymbol{\alpha})$ due to α_i and α_j that cannot be explained by the sum of the individual effects of α_i and α_j; and so on. Note also that Eqs. (2.29) and (2.30) imply that

$$\sum_{i=1}^{n} S_i + \sum_{1 \le i < j \le n}^{n} S_{ij} + \ldots + S_{12 \ldots n} = 1. \qquad (2.31)$$

Attempting to reduce the number of model evaluations inherent to Sobol's method, Rabitz et.al., (1999) introduced the so-called *high-dimensional model representations* (*HDMRs*), which aim at identifying relationships between sets of inputs (e.g., parameters) and outputs (responses). HDMRs express the model output as a finite additive sum of correlated functions with increasing numbers of input variables up to the total number of inputs, in the same spirit as Sobol's expansion shown in Eq. (2.27). The resultant HDMR expansion is subsequently used as a *reduced-order surrogate model* that depends on fewer parameters and, more importantly, fewer coupled parameters (interactions among parameters). The two commonly used expansions, are called ANOVA-HDMR and Cut-HDMR, respectively. ANOVA-HDMR requires computationally expensive numerical integrations of the model over the entire parameter space, while Cut-HDMR requires response-function evaluations along the so-called cut lines or hyperplanes with respect to pre-selected reference points in the domain of the inputs. Although Cut-HDMR is computationally less expensive, it is also less accurate and its accuracy depends strongly on the choice of the reference point; constructing a second-order Cut-HDMR expansion can still be computationally expensive. Hu et al (2014) have improved the efficiency of the second-order Cut-HDMR by first using a screening algorithm (based on the so-called "New Morris Method") to pre-screen the parameter (input) space for significant inputs and interactions while eliminating parameters that were deemed

insignificant, and subsequently applied the Cut-HDMR expansion in the reduced parameter space.

C. *Spectral Methods*

The spectral uncertainty quantification methods (see, e.g., Le Maître and Kino, 2010) use a set of independent random variables, often called the *germ*, and denoted here as $\mathbf{\omega} \equiv (\omega_1, \omega_1, ...)$, to express the imprecisely known model parameters $\mathbf{\alpha} \equiv (\alpha_1, ..., \alpha_n)$ as

$$\mathbf{\alpha} \equiv \mathbf{\alpha}(\mathbf{\omega}), \tag{2.32}$$

and subsequently to compute the statistics of the response distribution $R\big[\mathbf{\alpha}(\mathbf{\omega})\big]$ in terms of the germ $\mathbf{\omega} \equiv (\omega_1, \omega_1, ...)$. Some methods explicitly expand the response $R\big[\mathbf{\alpha}(\mathbf{\omega})\big]$ in an infinite spectral series of the form

$$R\big[\mathbf{\alpha}(\mathbf{\omega})\big] = \sum_{k=1}^{\infty} r_k \Psi_k(\mathbf{\omega}), \tag{2.33}$$

where the quantities $\Psi_k(\mathbf{\omega})$ are suitably selected functionals of the germ $\mathbf{\omega} \equiv (\omega_1, \omega_1, ...)$, while the quantities r_k are deterministic ("spectral") coefficients. Once available, the series development in Eq. (2.33) is used to determine the statistics of $R\big[\mathbf{\alpha}(\mathbf{\omega})\big]$, either analytically or via sampling of the germ $\mathbf{\omega} \equiv (\omega_1, \omega_1, ...)$.

The principle underlying the use of Eq. (2.32) for computing the variance of a response $R\big[\mathbf{\alpha}(\mathbf{\omega})\big]$ can be conveniently illustrated using the so-called "*Fast Fourier Amplitude Test*" (*FAST*), originally been proposed by Cukier et al. (1973), and then extended Cukier and others. This procedure uses the following Fourier transformation of the parameters α_i:

$$\alpha_i = F_i \sin(\omega_i z), \quad i = 1, ..., n, \tag{2.34}$$

where $\{\omega_i\}$ is a set of integer frequencies, while $z \in (-\pi, \pi)$ is a scalar variable. The response $R\big[\mathbf{\alpha}(\mathbf{\omega})\big]$ is thus considered to be a function of $z \in (-\pi, \pi)$.

The expectation, $E(R)$, of the response $R[\boldsymbol{\alpha}(\boldsymbol{\omega})]$ can be formally obtained by integrating Eq. (2.35) over $z \in (-\pi, \pi)$, to obtain

$$E(R) = \frac{1}{2\pi} \int_{-\pi}^{\pi} R\left[F_1 \sin(\omega_1 z), F_2 \sin(\omega_2 z), \dots, F_n \sin(\omega_n z)\right] dz. \tag{2.35}$$

The variance, $Var(R)$, of the response R can be approximately obtained as follows

$$Var(R) \cong 2\sum_{j=1}^{\infty} \left(A_j^2 + B_j^2\right), \tag{2.36}$$

where

$$A_j \equiv \frac{1}{2\pi} \int_{-\pi}^{\pi} R\left[F_1 \sin(\omega_1 z), F_2 \sin(\omega_2 z), \dots, F_n \sin(\omega_n z)\right] \cos(jz) dz \tag{2.37}$$

$$B_j \equiv \frac{1}{2\pi} \int_{-\pi}^{\pi} R\left[F_1 \sin(\omega_1 z), F_2 \sin(\omega_2 z), \dots, F_n \sin(\omega_n z)\right] \sin(jz) dz \tag{2.38}$$

The transformation given by Eq. (2.34) should provide, for each parameter α_i, a uniformly distributed sample in the unit n-dimensional cube. As $z \in (-\pi, \pi)$ varies for a given transformation, all parameters change simultaneously, but their respective ranges of uncertainty is systematically and exhaustively explored (i.e., the search curve is space-filling) if and only if the set of frequencies $\{\omega_i\}$ is incommensurate (i.e., if none of the frequencies ω_i may be obtained as a linear combination, with integer coefficients, of the remaining frequencies). The 1st-order sensitivity indices are computed by evaluating the coefficients A_j and B_j for the fundamental frequencies $\{\omega_i\}$ and their higher harmonics $p\omega_i$ ($p = 1, 2, \dots$). If the frequencies $\{\omega_i\}$ are integer, the contribution to the total variance $Var(R)$ coming from the variance D_i corresponding to parameter α_i is approximately obtained as

$$D_i \cong 2\sum_{p=1}^{M} \left(A_{p\omega_i}^2 + B_{p\omega_i}^2\right), \tag{2.39}$$

where M is the maximum harmonic taken into consideration (usually $M \leq 6$). The ratio of the partial variance D_i to the total variance $Var(R)$ provides the so-called *first-order sensitivity index*. The minimum sample size required to compute D_i is $(2M\omega_{max} + 1)$, where ω_{max} is the maximum frequency in the set $\{\omega_i\}$ (see, e.g., Saltelli at al., 2000). Furthermore, the frequencies that do not belong to the set $\{p_1\omega_1, p_2\omega_2, ..., p_n\omega_n\}$ for $(p_i = 1, 2, ...)$ and any $(i = 1, 2, ..., n)$ contain information about the residual variance $[Var(R) - D_i]$ that is not accounted for by the first-order indices.

On the other hand, the expansion expressed by Eq. (2.33) can be constructed using various methods, selected based on the nature of the components of $\boldsymbol{\alpha} \equiv (\alpha_1, ..., \alpha_n)$. The *germ* $\boldsymbol{\omega} \equiv (\omega_1, \omega_1, ...)$ that parameterizes the random data follows a probability law that is not necessarily the same as that of the random data itself, particularly when parametrization of the data involves nonlinear functionals. One of the oldest methods used to achieve the expansion expressed by Eq. (2.33) is the Karhunen-Loève decomposition of a second-order random process based on the spectral decomposition of its autocorrelation function, where the deterministic functions are fixed by the form of the autocorrelation kernel, while the joint probability law of $\boldsymbol{\omega} \equiv (\omega_1, \omega_1, ...)$ remains unknown in the absence of information other than the second-order properties of the process (specifically, one can only ascertain that the random variables have zero mean, unit variance, and are mutually orthogonal). More general methods for achieving the expansion in Eq. (2.33) are the so-called "*polynomial chaos*" decompositions which employ various orthogonal polynomials: Hermite; Laguerre; the Jacobi family of polynomials (including, in particular, the Legendre polynomials), or piecewise polynomial functions.

The numerical methods used for computing the statistics of the response distribution $R[\boldsymbol{\alpha}(\boldsymbol{\omega})]$, using either Eq. (2.32) or Eq. (2.33) can be grouped into two broad categories, namely "*intrusive methods*" and "*non-intrusive methods*." The fundamental concept behind "non-intrusive" uncertainty propagation methods essentially consists in the (repeated) application of a deterministic solver in order to determine the unknown expansion coefficients appearing in the spectral expansion of the solution. This approach is called

non-intrusive, because (existing or legacy) deterministic solvers can be immediately applied without modification for obtaining the spectral coefficients in Eq. (2.33).

On the other hand, when analytical methods are not available, the original solvers need to be modified *intrusively* to obtain the solution of the system of equations governing the spectral coefficients, r_k. Intrusive methods require adaptation of deterministic solvers, using basis function expansions in the appropriate function spaces, to construct discrete parametrizations of both the random data and the model solutions. Using these discretized representations, a weighted residual formalism of Galerkin-type is used to define the so-called "spectral problem," which governs the behavior of the unknown solution coefficients r_k. After solving this "spectral problem", the spectral coefficients thus determined ("intrusively") are used in the "polynomial chaos" representation given in Eq. (2.33) to quantify statistical properties of the response

2.1.2 Deterministic Methods for Uncertainty and Sensitivity Analysis

Denoting the unknown multivariate parameter distribution function as $p(\boldsymbol{\alpha})$, and considering that $p(\boldsymbol{\alpha})$ is defined on a domain D_α, it is possible to write *formally* the expressions of the mean values, covariance and variances of the parameter distribution, using their customary definitions, as follows:

(i)   the expected (or mean) value of a model parameter α_i, denoted as α_i^0, is defined as

$$\alpha_i^0 \triangleq \int_{D_\alpha} \alpha_i p(\boldsymbol{\alpha}) d\boldsymbol{\alpha} ; \tag{2.40}$$

(ii)   the *covariance,* $\mathrm{cov}(\alpha_i, \alpha_j)$, of two parameters, α_i and α_j, is defined as

$$\mathrm{cov}(\alpha_i, \alpha_j) \triangleq \int_{D_\alpha} \left(\alpha_i - \alpha_i^0 \right)\left(\alpha_j - \alpha_j^0 \right) p(\boldsymbol{\alpha}) d\boldsymbol{\alpha}, \quad i, j = 1, \ldots, N_\alpha; \tag{2.41}$$

(iii)   the *variance,* $\text{var}(\alpha_i)$, of a parameter α_i is defined as

$$\text{var}(\alpha_i) \triangleq \int_{D_\alpha} \left(\alpha_i - \alpha_i^0\right)^2 p(\boldsymbol{\alpha}) d\boldsymbol{\alpha}, \quad i = 1,\ldots,N_\alpha;$$ (2.42)

(iv)   the *standard deviation*, σ_i, of α_i is defined as $\sigma_i \triangleq \sqrt{\text{var}(\alpha_i)}$;

(v)   the correlation, ρ_{ij}, between two parameters α_i and α_j is defined as

$$\rho_{ij} \triangleq \text{cov}(\alpha_i,\alpha_j)\big/\left(\sigma_i\sigma_j\right); \quad i,j = 1,\ldots,N_\alpha;$$ (2.43)

(vi)   higher-order moments and correlations are defined by generalizing the definition in Eq. (2.41); thus, the 3rd-order moment, μ_3^{ijk}, of the multivariate parameter distribution function $p(\boldsymbol{\alpha})$, and the 3rd-order parameter correlation, t_{ijk}, respectively, are defined as follows:

$$\mu_3^{ijk} \triangleq \int_{D_\alpha} \left(\alpha_i - \alpha_i^0\right)\left(\alpha_j - \alpha_j^0\right)\left(\alpha_k - \alpha_k^0\right) p(\boldsymbol{\alpha}) d\boldsymbol{\alpha} \triangleq t_{ijk}\sigma_i\sigma_j\sigma_k, \quad i,j,k = 1,\ldots,N_\alpha;$$ (2.44)

(i)   the 4th-order moment, μ_4^{ijkl}, of the multivariate parameter distribution function $p(\boldsymbol{\alpha})$, and the 4th-order parameter correlation, q_{ijkl}, respectively, are defined as follows:

$$\mu_4^{ijkl} \triangleq \int_{D_\alpha} \left(\alpha_i - \alpha_i^0\right)\left(\alpha_j - \alpha_j^0\right)\left(\alpha_k - \alpha_k^0\right)\left(\alpha_l - \alpha_l^0\right) p(\boldsymbol{\alpha}) d\boldsymbol{\alpha}$$
$$\triangleq q_{ijkl}\sigma_i\sigma_j\sigma_k\sigma_l, \quad i,j,k,l = 1,\ldots,N_\alpha.$$ (2.45)

Similarly, for a vector-valued response of the form $\mathbf{r}(\boldsymbol{\alpha}) = \left[r_1(\boldsymbol{\alpha}),\ldots,r_{N_r}(\boldsymbol{\alpha})\right]$ distributed according to a (generally unknown) distribution $p(\mathbf{r})$ defined on a domain D_r, the first three moments of response distribution $p(\mathbf{r})$ are defined analogously, namely:

(i)   the expected value, denoted as $E(R_k)$, of a response $R_k(\boldsymbol{\alpha})$, is defined as

$$E(R_k) \triangleq \int_{D_r} R_k(\boldsymbol{\alpha}) p(\mathbf{r}) d\mathbf{r}, \quad k = 1,\ldots,N_r;$$ (2.46)

(ii)   the *covariance*, $\text{cov}(R_k, R_l)$, of two responses, $R_k(\boldsymbol{\alpha})$ and $R_l(\boldsymbol{\alpha})$, is defined as

$$\text{cov}(R_k, R_l) \triangleq \int_{D_r} \left[R_k - E(R_k) \right]\left[R_l - E(R_l) \right] p(\mathbf{r}) d\mathbf{r}, \quad k,l = 1,\ldots,N_r; \qquad (2.47)$$

(iii)   the *variance*, $\text{var}(R_k)$, of a response R_k is defined as

$$\text{var}(R_k) \triangleq \int_{D_r} \left[R_k - E(R_k) \right]^2 p(\mathbf{r}) d\mathbf{r}, \quad k = 1,\ldots,N_r; \qquad (2.48)$$

(iv)   the third-order moment (triple correlation), $\mu_3(R_k, R_l, R_m)$, of three responses, R_k, R_l, and R_m, is defined as

$$\mu_3(R_k, R_l, R_m) \triangleq \int_{D_r} \left[R_k - E(R_k) \right]\left[R_l - E(R_l) \right]\left[R_m - E(R_m) \right] p(\mathbf{r}) d\mathbf{r}, \quad k,l,m = 1,\ldots,N_r.$$

$$(2.49)$$

It is known that the uncertainties in a response $R_k(\boldsymbol{\alpha})$ that stem from uncertainties in the parameters $\boldsymbol{\alpha}$ can be computed by using the "propagation of errors" or "propagation of moments" method [see, e.g., Cacuci (2003)]. This method relies on expanding formally the response $r_k(\boldsymbol{\alpha})$ in a Taylor series around the mean parameter values $\boldsymbol{\alpha}^0$, constructing appropriate products of such Taylor series, and integrating formally these products over the unknown parameter distribution function $p(\boldsymbol{\alpha})$, to obtain response correlations. Assuming that only 1st- and 2nd-order response derivatives with respect to parameters are available, the Taylor-series of a response $R_k(\boldsymbol{\alpha})$ around the mean values $\boldsymbol{\alpha}^0 \equiv \left(\alpha_1^0,\ldots,\alpha_{N_\alpha}^0 \right)$ is:

$$R_k(\boldsymbol{\alpha}) = R_k(\boldsymbol{\alpha}^0) + \sum_{i=1}^{N_\alpha} \left\{ \frac{\partial R_k}{\partial \alpha_i} \right\}_{\boldsymbol{\alpha}^0} (\alpha_i - \alpha_i^0) + \frac{1}{2} \sum_{i,j=1}^{N_\alpha} \left\{ \frac{\partial^2 R_k}{\partial \alpha_i \partial \alpha_j} \right\}_{\boldsymbol{\alpha}^0} (\alpha_i - \alpha_i^0)(\alpha_j - \alpha_j^0), \quad (2.50)$$

where $R_k(\boldsymbol{\alpha}^0)$ denotes the computed nominal value of the response. Using Eq. (2.50) in Eqs. (2.46), (2.47), and (2.49) yields the following expressions, up to the 3rd-order response derivatives:

$$E(r_k) = R_k(\boldsymbol{\alpha}^0) + \frac{1}{2} \sum_{i,j=1}^{N_\alpha} \left\{ \frac{\partial^2 R_k}{\partial \alpha_i \partial \alpha_j} \right\}_{\boldsymbol{\alpha}^0} \mathrm{cov}(\alpha_i, \alpha_j). \tag{2.51}$$

$$cov(R_k, R_\ell) \equiv \left\langle \left[R_k - E(R_k) \right] \left[R_\ell - E(R_\ell) \right] \right\rangle = \sum_{i=1}^{N_\alpha} \sum_{j=1}^{N_\alpha} \left(\frac{\partial R_k}{\partial \alpha_i} \frac{\partial R_\ell}{\partial \alpha_j} \right) \rho_{ij} \sigma_i \sigma_j$$

$$+ \frac{1}{2} \sum_{i=1}^{N_\alpha} \sum_{j=1}^{N_\alpha} \sum_{\mu=1}^{N_\alpha} \left(\frac{\partial^2 R_k}{\partial \alpha_i \partial \alpha_j} \frac{\partial R_\ell}{\partial \alpha_\mu} + \frac{\partial R_k}{\partial \alpha_i} \frac{\partial^2 R_l}{\partial \alpha_j \partial \alpha_\mu} \right) t_{ij\mu} \sigma_i \sigma_j \sigma_\mu$$

$$+ \frac{1}{4} \sum_{i=1}^{N_\alpha} \sum_{j=1}^{N_\alpha} \sum_{\mu=1}^{N_\alpha} \sum_{\nu=1}^{N_\alpha} \left(\frac{\partial^2 R_k}{\partial \alpha_i \partial \alpha_j} \right) \left(\frac{\partial^2 R_\ell}{\partial \alpha_\mu \partial \alpha_\nu} \right) \left(q_{ij\mu\nu} - \rho_{ij} \rho_{\mu\nu} \right) \sigma_i \sigma_j \sigma_\mu \sigma_\nu \tag{2.52}$$

$$+ \frac{1}{6} \sum_{i=1}^{N_\alpha} \sum_{j=1}^{N_\alpha} \sum_{\mu=1}^{N_\alpha} \sum_{\nu=1}^{N_\alpha} \left(\frac{\partial R_k}{\partial \alpha_i} \frac{\partial^3 R_l}{\partial \alpha_j \partial \alpha_\mu \partial \alpha_\nu} + \frac{\partial R_l}{\partial \alpha_i} \frac{\partial^3 R_k}{\partial \alpha_j \partial \alpha_\mu \partial \alpha_\nu} \right) q_{ij\mu\nu} \sigma_i \sigma_j \sigma_\mu \sigma_\nu.$$

$$\mu_3(R_k, R_l, R_m) \equiv \left\langle \left[R_k - E(R_k) \right] \left[R_l - E(R_l) \right] \left[R_m - E(R_m) \right] \right\rangle$$

$$= \sum_{i=1}^{N_\alpha} \sum_{j=1}^{N_\alpha} \sum_{\mu=1}^{N_\alpha} \frac{\partial R_k}{\partial \alpha_i} \frac{\partial R_l}{\partial \alpha_j} \frac{\partial R_m}{\partial \alpha_\mu} t_{ij\mu} \sigma_i \sigma_j \sigma_\mu$$

$$+ \frac{1}{2} \sum_{i=1}^{N_\alpha} \sum_{j=1}^{N_\alpha} \sum_{\mu=1}^{N_\alpha} \sum_{\nu=1}^{N_\alpha} \frac{\partial R_k}{\partial \alpha_i} \frac{\partial R_l}{\partial \alpha_j} \frac{\partial^2 R_m}{\partial \alpha_\mu \partial \alpha_\nu} \left(q_{ij\mu\nu} - \rho_{ij} \rho_{\mu\nu} \right) \sigma_i \sigma_j \sigma_\mu \sigma_\nu \tag{2.53}$$

$$+ \frac{1}{2} \sum_{i=1}^{N_\alpha} \sum_{j=1}^{N_\alpha} \sum_{\mu=1}^{N_\alpha} \sum_{\nu=1}^{N_\alpha} \frac{\partial R_k}{\partial \alpha_i} \frac{\partial^2 R_l}{\partial \alpha_j \partial \alpha_\mu} \frac{\partial R_m}{\partial \alpha_\nu} \left(q_{ij\mu\nu} - \rho_{iv} \rho_{j\mu} \right) \sigma_i \sigma_j \sigma_\mu \sigma_\nu$$

$$+ \frac{1}{2} \sum_{i=1}^{N_\alpha} \sum_{j=1}^{N_\alpha} \sum_{\mu=1}^{N_\alpha} \sum_{\nu=1}^{N_\alpha} \frac{\partial^2 R_k}{\partial \alpha_i \partial \alpha_j} \frac{\partial R_l}{\partial \alpha_\mu} \frac{\partial R_m}{\partial \alpha_\nu} \left(q_{ij\mu\nu} - \rho_{ij} \rho_{\mu\nu} \right) \sigma_i \sigma_j \sigma_\mu \sigma_\nu;$$

The corresponding statistics for a single response, $R_k(\boldsymbol{\alpha})$, are obtained by setting $k = l = m$ in Eqs. (2.51) - (2.53). It is evident from Eqs. (2.51) - (2.53) that the statistics (expectation value, covariance and 3rd-order moments) of the response distribution can be computed after obtaining all of the first-, second-, and (possibly) third-order response sensitivities to the model parameters.

The most efficient method for computing exactly the 1st-order sensitivities of a model's scalar-valued nonlinear response, $R(\mathbf{e})$, with respect to the model's parameters is the *first-order adjoint sensitivity analysis methodology* formulated and developed by Cacuci (1981.a). For such a response, Cacuci (1981.a) showed that the most general definition of the 1st-order sensitivity of an scalar-valued model response $R(\mathbf{e})$ to variations $\mathbf{h} \triangleq (\delta\boldsymbol{\alpha}, \delta\mathbf{u})$ in the model parameters and state functions in a neighborhood around $\mathbf{e}^0 = (\boldsymbol{\alpha}^0, \mathbf{u}^0) \in \mathbf{E}$ is given by the 1st-order Gateaux- (G-) differential (also called "G-variation"), which will be denoted as $\delta R(\mathbf{e}^0; \mathbf{h})$ and is defined as

$$\delta R(\mathbf{e}^0; \mathbf{h}) \triangleq \left\{ \frac{d}{d\varepsilon} \left[R(\mathbf{e}^0 + \varepsilon\mathbf{h}) \right] \right\}_{\varepsilon=0} \triangleq \lim_{\varepsilon \to 0} \frac{R(\mathbf{e}^0 + \varepsilon\mathbf{h}) - R(\mathbf{e}^0)}{\varepsilon} \tag{2.54}$$

for an arbitrary scalar $\varepsilon \in \mathbf{F}$, and all (i.e., arbitrary) vectors $\mathbf{h} \in \mathbf{E} = \mathbf{E}_\alpha \times \mathbf{E}_u$ in a neighborhood $(\mathbf{e}^0 + \varepsilon\mathbf{h})$ around $\mathbf{e}^0 = (\boldsymbol{\alpha}^0, \mathbf{u}^0) \in \mathbf{E}$. However, the existence of the G-differential $\delta R(\mathbf{e}^0; \mathbf{h})$ does not guarantee its numerical computability. Numerical methods require that $\delta R(\mathbf{e}^0; \mathbf{h})$ be linear in $\mathbf{h} \triangleq (\delta\boldsymbol{\alpha}, \delta\mathbf{u})$ in a neighborhood $(\mathbf{e}^0 + \varepsilon\mathbf{h})$ around $\mathbf{e}^0 = (\mathbf{u}^0, \boldsymbol{\alpha}^0) \in \mathbf{E}$. In this case, $\delta R(\mathbf{e}^0; \mathbf{h})$ can be written in the form

$$\delta R(\mathbf{e}^0; \mathbf{h}) = \left\{ \frac{\partial R(\boldsymbol{\alpha}, \mathbf{u})}{\partial \mathbf{u}} \right\}_{(\boldsymbol{\alpha}^0, \mathbf{u}^0)} \delta\mathbf{u} + \left\{ \frac{\partial R(\boldsymbol{\alpha}, \mathbf{u})}{\partial \boldsymbol{\alpha}} \right\}_{(\boldsymbol{\alpha}^0, \mathbf{u}^0)} \delta\boldsymbol{\alpha}, \quad \mathbf{x} \in \partial\Omega_x, \tag{2.55}$$

where $\partial R(\boldsymbol{\alpha}, \mathbf{u}) / \partial \mathbf{u}$ and $\partial R(\boldsymbol{\alpha}, \mathbf{u}) / \partial \boldsymbol{\alpha}$ denote the *partial G-derivatives* of $R(\mathbf{e})$ with respect to $\mathbf{u}$ and $\boldsymbol{\alpha}$. The necessary and sufficient conditions for the G-differential $\delta R(\mathbf{e}^0; \mathbf{h})$ of a nonlinear operator $R(\mathbf{e})$ to be linear in $\mathbf{h}$ in a neighborhood $(\mathbf{e}^0 + \varepsilon\mathbf{h})$ around

$\mathbf{e}^0 = \left(\boldsymbol{\alpha}^0, \mathbf{u}^0 \right) \in \mathbf{E}$, and thus admit G-derivatives, have been given by Cacuci (1981.a, 1981.b). In nonlinear responses of interest for the dissolver model developed and analyzed in this work will be shown to fulfill the requirements needed for Eq. (2.55) to hold. It is convenient to refer to the quantities $\left[\partial R(\boldsymbol{\alpha}, \mathbf{u})/\partial \boldsymbol{\alpha} \right] \delta \boldsymbol{\alpha}$ and $\left[\partial R(\boldsymbol{\alpha}, \mathbf{u})/\partial \mathbf{u} \right] \delta \mathbf{u}$ as the "*direct effect term*" and the "*indirect effect term,*" respectively, because the *direct effect term* $\left[\partial R(\boldsymbol{\alpha}, \mathbf{u})/\partial \boldsymbol{\alpha} \right] \delta \boldsymbol{\alpha}$ can be evaluated immediately while the *indirect effect term* $\left[\partial R(\boldsymbol{\alpha}, \mathbf{u})/\partial \mathbf{u} \right] \delta \mathbf{u}$ can be quantified only after determining $\delta \mathbf{u}$ as function of $\delta \boldsymbol{\alpha}$, since the system's state vector $\mathbf{u}$ and parameters $\boldsymbol{\alpha}$ are related to each other through Eqs. (1) and (2).

The relationship between $\delta \mathbf{u}$ and $\delta \boldsymbol{\alpha}$ is determined by taking the G-differentials at $\mathbf{e}^0$ of Eqs. (2.1) and (2.2), which yields:

$$\mathbf{F}_{11}^{(1)} \left(\boldsymbol{\alpha}^0, \mathbf{u}^0 \right) \delta \mathbf{u} = \mathbf{Q}^{(1)} \left(\boldsymbol{\alpha}^0, \mathbf{u}^0; \delta \boldsymbol{\alpha} \right), \quad \mathbf{x} \in \Omega_x, \tag{2.56}$$

$$\mathbf{B}_F^{(1)} \left(\boldsymbol{\alpha}^0, \mathbf{u}^0; \delta \boldsymbol{\alpha}, \delta \mathbf{u} \right) = \mathbf{0}, \quad \mathbf{x} \in \partial \Omega_x, \tag{2.57}$$

where the superscript "(1)" indicates "*1ˢᵗ-Level*," the letter "F" (used as "operator" and "subscript") indicates "*Forward*", the letter "B" indicates "*boundary and/or initial conditions,*" and where the following definitions were used:

$$\mathbf{F}_{11}^{(1)} \left(\boldsymbol{\alpha}, \mathbf{u} \right) \triangleq \left\{ \frac{\partial \mathbf{N}(\boldsymbol{\alpha}, \mathbf{u})}{\partial \mathbf{u}} \right\}; \quad \mathbf{Q}^{(1)} \left(\boldsymbol{\alpha}, \mathbf{u}; \delta \boldsymbol{\alpha} \right) \triangleq \frac{\partial \left[\mathbf{Q}(\boldsymbol{\alpha}) - \mathbf{N}(\boldsymbol{\alpha}, \mathbf{u}) \right]}{\partial \boldsymbol{\alpha}} \delta \boldsymbol{\alpha}; \quad \mathbf{x} \in \Omega_x, \tag{2.58}$$

$$\mathbf{B}_F^{(1)} \left(\boldsymbol{\alpha}^0, \mathbf{u}^0; \delta \boldsymbol{\alpha}, \delta \mathbf{u} \right) \triangleq \left\{ \frac{\partial \mathbf{B}(\boldsymbol{\alpha}, \mathbf{u})}{\partial \mathbf{u}} \right\}_{\left(\boldsymbol{\alpha}^0, \mathbf{u}^0 \right)} \delta \mathbf{u} + \left\{ \frac{\partial \left[\mathbf{C}(\boldsymbol{\alpha}) - \mathbf{B}(\boldsymbol{\alpha}, \mathbf{u}) \right]}{\partial \boldsymbol{\alpha}} \right\}_{\left(\boldsymbol{\alpha}^0, \mathbf{u}^0 \right)} \delta \boldsymbol{\alpha}, \quad \mathbf{x} \in \partial \Omega_x.$$

$$\tag{2.59}$$

The partial G-derivatives $\partial \mathbf{N}(\boldsymbol{\alpha}, \mathbf{u})/\partial \mathbf{u}$ and $\partial \mathbf{N}(\boldsymbol{\alpha}, \mathbf{u})/\partial \boldsymbol{\alpha}$ appearing in Eq. (2.58) are matrices of the form

$$\frac{\partial \mathbf{N}(\boldsymbol{\alpha},\mathbf{u})}{\partial \mathbf{u}} \triangleq \begin{pmatrix} \dfrac{\partial N_1(\boldsymbol{\alpha},\mathbf{u})}{\partial u_1} & \cdots & \dfrac{\partial N_1(\boldsymbol{\alpha},\mathbf{u})}{\partial u_{N_u}} \\ \vdots & \ddots & \vdots \\ \dfrac{\partial N_{N_u}(\boldsymbol{\alpha},\mathbf{u})}{\partial u_1} & \cdots & \dfrac{\partial N_{N_u}(\boldsymbol{\alpha},\mathbf{u})}{\partial u_{N_u}} \end{pmatrix}, \quad \frac{\partial \mathbf{N}(\boldsymbol{\alpha},\mathbf{u})}{\partial \boldsymbol{\alpha}} \triangleq \begin{pmatrix} \dfrac{\partial N_1(\boldsymbol{\alpha},\mathbf{u})}{\partial \alpha_1} & \cdots & \dfrac{\partial N_1(\boldsymbol{\alpha},\mathbf{u})}{\partial \alpha_{N_\alpha}} \\ \vdots & \ddots & \vdots \\ \dfrac{\partial N_{N_u}(\boldsymbol{\alpha},\mathbf{u})}{\partial \alpha_1} & \cdots & \dfrac{\partial N_{N_u}(\boldsymbol{\alpha},\mathbf{u})}{\partial \alpha_{N_\alpha}} \end{pmatrix}.$$

$$(2.60)$$

The other partial G-derivatives which appear in Eqs. (2.58) and (2.59) are also matrices, with structures similar to those defined above in Eq. (2.60).

The system comprising Eqs. (2.56) and (2.57) represents the "*1st-Level Forward Sensitivity System*" (*1st-LFSS*). For a given vector of parameter variations $\delta\boldsymbol{\alpha}$ in a neighborhood around $\boldsymbol{\alpha}^0$, the *1st-LFSS* needs to be solved to obtain $\delta\mathbf{u}$ as a function of $\delta\boldsymbol{\alpha}$. In turn, the relationship between $\delta\mathbf{u}$ and $\delta\boldsymbol{\alpha}$ would lead to the elimination of the appearance of $\delta\mathbf{u}$ in Eq. (2.55). Consequently, Eq. (2.55) would be expressed in the form

$$\delta R\left(\boldsymbol{\alpha}^0,\mathbf{u}^0;\delta\boldsymbol{\alpha}\right) = \sum_{i_1=1}^{N_\alpha} R_{i_1}^{(1)} \delta\alpha_{i_1}, \qquad (2.61)$$

where the quantities $R_{i_1}^{(1)}$ are independent of the parameter variations $\delta\alpha_{i_1}$ [although they may depend on $\boldsymbol{\alpha}^0$, $\mathbf{u}^0$, and/or other known quantities], and represent *the 1st-order partial sensitivities (1st-order partial G-derivatives) of the response $R(\mathbf{e})$ with respect to each of the model parameters α_i, evaluated at the nominal values $\mathbf{e}^0$*. The partial sensitivities $R_{i_1}^{(1)}$ of the response $R(\mathbf{e})$ with respect to each of the model parameters $\delta\alpha_{i_1}$, evaluated at the nominal values $\mathbf{e}^0 = \left(\boldsymbol{\alpha}^0,\mathbf{u}^0\right)$, are obtained by successively setting $\left(\delta\alpha_i = 1, \ \delta\alpha_j = 0 \ for \ j \neq i, \ i = 1,\ldots,N_\alpha\right)$ in the expression of $\delta R(\mathbf{e}^0;\mathbf{h})$ given in Eq. (9). *Computing the (total) response sensitivity $\delta R(\mathbf{e}^0;\mathbf{h})$ by using the ($\delta\boldsymbol{\alpha}$-dependent) solution $\delta\mathbf{u}$ of the 1st-LFSS is called the Forward Sensitivity Analysis Methodology (FSAM).* From the standpoint of computational costs and effort, the *FSAM* requires $O(N_\alpha)$ large-scale forward computations and is advantageous only when the number N_r of responses of interest

exceeds the number of system parameters and/or parameter variations of interest. This is rarely the case in practice, however, since most problems of practical interest are characterized by many parameters (i.e., $\boldsymbol{\alpha}$ has many components) and comparatively few responses. In such situations, it is not economical to employ the *FSAM* since it becomes prohibitively expensive to solve repeatedly the $\delta\boldsymbol{\alpha}$-dependent *$1^{st}$-LFSS* in order to determine $\delta\mathbf{u}$ for all possible variations $\delta\boldsymbol{\alpha}$ in the model parameters.

In most practical situations, the number of model parameters exceeds significantly the number of functional responses of interest, i.e., $N_r \ll N_\alpha$. In such cases, *the Adjoint Sensitivity Analysis Methodology* (*ASAM*) developed by Cacuci (1981.b) *is the most efficient method for computing exactly the first-order sensitiviti*es *since it requires only a single large-scale computation for each scalar-valued response* $R(\mathbf{e})$. The implementation of the *ASAM* requires the introduction of adjoint operators, which can be practically introduced by requiring the spaces $\mathbf{E}_u$ and $\mathbf{E}_Q$ to be inner-product (Hilbert) spaces, denoted as $\mathbf{H}_u(\Omega_x)$ and $\mathbf{H}_Q(\Omega_x)$, respectively. The elements of $\mathbf{H}_u(\Omega_x)$ and $\mathbf{H}_Q(\Omega_x)$ are, as before, vector-valued functions defined on the open set $\Omega_x \subset \mathbb{R}^{J_x}$, with smooth boundary $\partial\Omega_x$. On $\mathbf{H}_u(\Omega_x)$, the inner product of two vectors $\mathbf{u}^{(a)} \in \mathbf{H}_u$ and $\mathbf{u}^{(b)} \in \mathbf{H}_u$ will be denoted as $\langle \mathbf{u}^{(a)}, \mathbf{u}^{(b)} \rangle_u$. Typically, the inner product $\langle \mathbf{u}^{(a)}, \mathbf{u}^{(b)} \rangle_u$ is defined as

$$\langle \mathbf{u}^{(a)}, \mathbf{u}^{(b)} \rangle_u \triangleq \int_{\Omega_x} \mathbf{u}^{(a)}(\mathbf{x}) \cdot \mathbf{u}^{(b)}(\mathbf{x}) \, d\mathbf{x}. \qquad (2.62)$$

The inner product on $\mathbf{H}_Q(\Omega_x)$ of two vectors $\mathbf{Q}^{(a)} \in \mathbf{H}_Q$ and $\mathbf{Q}^{(b)} \in \mathbf{H}_Q$ will be denoted as $\langle \mathbf{Q}^{(a)}, \mathbf{Q}^{(b)} \rangle_Q$, and has the same form as shown in Eq. (2.62). In particular, the Riesz representation theorem ensures that the "indirect effect term" $\left[\partial R(\boldsymbol{\alpha}, \mathbf{u}) / \partial \mathbf{u} \right] \delta\mathbf{u}$ can be written in the following inner product form:

$$\left[\partial R(\boldsymbol{\alpha}, \mathbf{u}) / \partial \mathbf{u} \right] \delta\mathbf{u} = \langle \partial R(\boldsymbol{\alpha}, \mathbf{u}) / \partial \mathbf{u}, \, \delta\mathbf{u} \rangle_u, \quad \delta\mathbf{u} \in \mathbf{H}_u. \qquad (2.63)$$

The goal of the ASAM is to compute the above "indirect effect term" exactly and efficiently without needing to compute explicitly the variations $\delta\mathbf{u}$. This goal is accomplished by constructing the "*1ˢᵗ-Level Adjoint Sensitivity System (1ˢᵗ-LASS)*," which commence by considering a vector $\boldsymbol{\psi}^{(1)}(\mathbf{x}) \equiv \left[\psi_1^{(1)}(\mathbf{x}),\ldots,\psi_{N_u}^{(1)}(\mathbf{x})\right] \in \mathbf{H}_Q$ that satisfies the following relationship:

$$\left\langle \boldsymbol{\psi}^{(1)}, \mathbf{F}_{11}^{(1)}\left(\boldsymbol{\alpha}^0,\mathbf{u}^0\right)\delta\mathbf{u} \right\rangle_Q = \left\langle \mathbf{A}_{11}^{(1)}\left(\boldsymbol{\alpha}^0,\mathbf{u}^0\right)\boldsymbol{\psi}^{(1)}, \delta\mathbf{u} \right\rangle_u + \left\{ P^{(1)}\left(\boldsymbol{\alpha}^0,\mathbf{u}^0;\boldsymbol{\psi}^{(1)};\delta\mathbf{u}\right) \right\}_{\partial\Omega_x}, \qquad (2.64)$$

where $\mathbf{A}_{11}^{(1)}\left(\boldsymbol{\alpha},\mathbf{u}\right) \triangleq \left[\mathbf{F}_{11}^{(1)}\left(\boldsymbol{\alpha},\mathbf{u}\right)\right]^*$ denotes <u>*the adjoint operator*</u> of $\mathbf{F}_{11}^{(1)}\left(\boldsymbol{\alpha},\mathbf{u}\right) \triangleq \partial\mathbf{N}\left(\boldsymbol{\alpha},\mathbf{u}\right)/\partial\mathbf{u}$. In this work, the symbol $\left[\ \right]^*$ will be used to indicate "adjoint" of the quantity within the respective brackets. The quantity $\left\{ P^{(1)}\left(\boldsymbol{\alpha},\mathbf{u};\boldsymbol{\psi}^{(1)};\delta\mathbf{u}\right) \right\}_{\partial\Omega_x}$ in Eq. (2.64) denotes the *associated bilinear form* evaluated on the domain's boundary $\partial\Omega_x$. In certain situations, it might be computationally advantageous to include certain boundary components of $\left\{ P^{(1)}\left(\boldsymbol{\alpha},\mathbf{u};\boldsymbol{\psi}^{(1)};\delta\mathbf{u}\right) \right\}_{\partial\Omega_x}$ into the components of $\mathbf{A}_{11}^{(1)}\left(\boldsymbol{\alpha},\mathbf{u}\right)$. An important intermediate step in the construction of the adjoint operator $\mathbf{A}_{11}^{(1)}\left(\boldsymbol{\alpha},\mathbf{u}\right) \triangleq \left[\mathbf{F}_{11}^{(1)}\left(\boldsymbol{\alpha},\mathbf{u}\right)\right]^*$ is the construction of the *formal adjoint operator,* $\mathbf{A}_{11}^{(1,form)}\left(\boldsymbol{\alpha},\mathbf{u}\right)$, of $\mathbf{F}_{11}^{(1)}\left(\boldsymbol{\alpha},\mathbf{u}\right)$, which is defined as the $N_u \times N_u$ matrix obtained by transposing the formal adjoint of the components of the $N_u \times N_u$ matrix $\partial\mathbf{N}\left(\boldsymbol{\alpha},\mathbf{u}\right)/\partial\mathbf{u}$ in Eq. (2.60). The *formal adjoint,* $\mathbf{A}_{11}^{(1,form)}\left(\boldsymbol{\alpha},\mathbf{u}\right)$, will usually differ from "<u>the adjoint</u>" operator $\mathbf{A}_{11}^{(1)}\left(\boldsymbol{\alpha},\mathbf{u}\right) \triangleq \left[\mathbf{F}_{11}^{(1)}\left(\boldsymbol{\alpha},\mathbf{u}\right)\right]^*$.

The domain of $\mathbf{A}_{11}^{(1)}\left(\boldsymbol{\alpha},\mathbf{u}\right)$ is determined next by selecting appropriate *adjoint boundary and/or initial conditions*, which will be denoted in operator form as:

$$\mathbf{B}_A^{(1)}\left(\boldsymbol{\alpha}^0,\mathbf{u}^0;\boldsymbol{\psi}^{(1)}\right) = \mathbf{0}, \ \ \mathbf{x} \in \partial\Omega_x. \qquad (2.65)$$

The above boundary conditions for $\mathbf{A}_{11}^{(1)}\left(\boldsymbol{\alpha},\mathbf{u}\right)$ are usually inhomogeneous in $\boldsymbol{\psi}^{(1)}$, i.e., $\mathbf{B}_A^{(1)}\left(\boldsymbol{\alpha}^0,\mathbf{u}^0;\mathbf{0}\right) \neq \mathbf{0}$; they are obtained by requiring that:

(a) Eq. (2.65) must be independent of *unknown* values of $\delta\mathbf{u}$ and $\delta\boldsymbol{\alpha}$;

(b) The substitution of the forward and adjoint boundary and/or initial conditions represented by Eqs. (2.57) and (2.65), respectively, into the expression of $\left\{P^{(1)}\left(\boldsymbol{\alpha},\mathbf{u};\boldsymbol{\psi}^{(1)};\delta\mathbf{u}\right)\right\}_{\partial\Omega_x}$ must cause all terms containing unknown values of $\delta\mathbf{u}$ to vanish.

Constructing the adjoint initial and/or boundary conditions for $\mathbf{A}_{11}^{(1)}\left(\boldsymbol{\alpha},\mathbf{u}\right)$ as described above, and implementing them together with the forward adjoint boundary and/or initial conditions [represented by Eqs. (2.57)] into Eq. (2.64) reduces the bilinear concomitant $\left\{P^{(1)}\left(\boldsymbol{\alpha},\mathbf{u};\boldsymbol{\psi}^{(1)};\delta\mathbf{u}\right)\right\}_{\partial\Omega_x}$ to a quantity that will contain boundary terms involving only <u>known values</u> of $\delta\boldsymbol{\alpha}$, $\boldsymbol{\alpha}^0$, $\mathbf{u}^0$, and $\boldsymbol{\psi}^{(1)}$; this quantity will be denoted by $\hat{P}^{(1)}\left(\boldsymbol{\alpha},\mathbf{u};\boldsymbol{\psi}^{(1)};\delta\boldsymbol{\alpha}\right)$. In general, $\hat{P}^{(1)}\left(\boldsymbol{\alpha},\mathbf{u};\boldsymbol{\psi}^{(1)};\delta\boldsymbol{\alpha}\right)$ does not automatically vanish as a result of the operations discussed in the foregoing. In certain cases, though, $\hat{P}^{(1)}\left(\boldsymbol{\alpha},\mathbf{u};\boldsymbol{\psi}^{(1)};\delta\boldsymbol{\alpha}\right)$ may vanish automatically or it may be forced to vanish by considering appropriately constructed extensions of $\mathbf{A}_{11}^{(1,form)}\left(\boldsymbol{\alpha},\mathbf{u}\right)$; however, such extensions are seldom needed in practice.

Implementing the forward and adjoint boundary and/or initial conditions, cf. (2.57) and (2.65) into Eq. (2.64) will transform the later into the form

$$\left\langle \mathbf{A}_{11}^{(1)}\left(\boldsymbol{\alpha}^0,\mathbf{u}^0\right)\boldsymbol{\psi}^{(1)},\delta\mathbf{u}\right\rangle_u = \left\langle \boldsymbol{\psi}^{(1)},\mathbf{F}_{11}^{(1)}\left(\boldsymbol{\alpha}^0,\mathbf{u}^0\right)\delta\mathbf{u}\right\rangle_Q - \hat{P}^{(1)}\left(\boldsymbol{\alpha}^0,\mathbf{u}^0;\boldsymbol{\psi}^{(1)};\delta\boldsymbol{\alpha}\right). \qquad (2.66)$$

The quantity $\mathbf{F}_{11}^{(1)}\left(\boldsymbol{\alpha}^0,\mathbf{u}^0\right)\delta\mathbf{u}$ in the first term on the right-side of Eq. (2.66) is now replaced by the right-side of Eq. (2.56) to obtain

$$\left\langle \mathbf{A}_{11}^{(1)}\left(\boldsymbol{\alpha}^0,\mathbf{u}^0\right)\boldsymbol{\psi}^{(1)},\delta\mathbf{u}\right\rangle_u = \left\langle \boldsymbol{\psi}^{(1)},\mathbf{Q}^{(1)}\left(\boldsymbol{\alpha}^0,\mathbf{u}^0;\delta\boldsymbol{\alpha}\right)\right\rangle_Q - \hat{P}^{(1)}\left(\boldsymbol{\alpha}^0,\mathbf{u}^0;\boldsymbol{\psi}^{(1)};\delta\boldsymbol{\alpha}\right). \qquad (2.67)$$

The definition of the function $\boldsymbol{\psi}^{(1)}$ will now be completed by requiring that the left-side of Eq. (2.67) and the right-side of Eq. (2.63) represent the same functional, namely the "*indirect effect term*" $\left[\partial R\left(\boldsymbol{\alpha},\mathbf{u}\right)/\partial\mathbf{u}\right]\delta\mathbf{u}$. Imposing this requirement yields the following relationship:

$$\left\langle \mathbf{A}_{11}^{(1)}\left(\boldsymbol{\alpha}^{0},\mathbf{u}^{0}\right)\boldsymbol{\psi}^{(1)},\delta\mathbf{u}\right\rangle_{u}=\left\langle \partial R\left(\boldsymbol{\alpha}^{0},\mathbf{u}^{0}\right)\middle/\partial\mathbf{u}\,,\,\delta\mathbf{u}\right\rangle_{u},\quad \delta\mathbf{u}\in\mathbf{H}_{u}, \tag{2.68}$$

which implies that the adjoint function $\boldsymbol{\psi}^{(1)}$ is the *weak solution* (in the sense of distributions) of the equation

$$\mathbf{A}_{11}^{(1)}\left(\boldsymbol{\alpha}^{0},\mathbf{u}^{0}\right)\boldsymbol{\psi}^{(1)}\left(\mathbf{x}\right)=\left\{\frac{\partial R\left(\boldsymbol{\alpha},\mathbf{u}\right)}{\partial\mathbf{u}}\right\}_{\left(\boldsymbol{\alpha}^{0},\mathbf{u}^{0}\right)},\quad \mathbf{x}\in\Omega_{x}. \tag{2.69}$$

Of course, the adjoint function $\boldsymbol{\psi}^{(1)}$ must also satisfy the adjoint boundary conditions represented by Eq. (2.65).

The results obtained in Eqs. (2.64), (2.67) and (2.68) are now replaced in Eq. (2.55) to obtain:

$$\delta R\left(\mathbf{e}^{0};\mathbf{h}\right)=\left\{\frac{\partial R\left(\boldsymbol{\alpha},\mathbf{u}\right)}{\partial\boldsymbol{\alpha}}\right\}_{\left(\boldsymbol{\alpha}^{0},\mathbf{u}^{0}\right)}\delta\boldsymbol{\alpha}+\left\langle\boldsymbol{\psi}^{(1)},\mathbf{Q}^{(1)}\left(\boldsymbol{\alpha}^{0},\mathbf{u}^{0};\delta\boldsymbol{\alpha}\right)\right\rangle_{Q}-\hat{P}^{(1)}\left(\boldsymbol{\alpha}^{0},\mathbf{u}^{0};\boldsymbol{\psi}^{(1)};\delta\boldsymbol{\alpha}\right)$$
$$=\delta R\left(\boldsymbol{\alpha}^{0},\mathbf{u}^{0};\boldsymbol{\psi}^{(1)};\delta\boldsymbol{\alpha}\right)=\sum_{i_{1}=1}^{N_{\alpha}}R_{i_{1}}^{(1)}\left(\boldsymbol{\alpha}^{0},\mathbf{u}^{0};\boldsymbol{\psi}^{(1)}\right)\delta\alpha_{i_{1}}.$$

$$\tag{2.70}$$

The last equality on the right-side of Eq. (2.70) is obtained in view of Eq. (2.61) and indicates that the desired elimination of all unknown values of $\delta\mathbf{u}$ from the expression of total first-order differential $\delta R\left(\boldsymbol{\alpha}^{0},\mathbf{u}^{0};\boldsymbol{\psi}^{(1)};\delta\boldsymbol{\alpha}\right)$ of $R\left(\mathbf{e}\right)$ at $\mathbf{e}^{0}$ has been accomplished. Instead of depending on $\delta\mathbf{u}$, the 1st-order response differential, $\delta R\left(\boldsymbol{\alpha}^{0},\mathbf{u}^{0};\boldsymbol{\psi}^{(1)};\delta\boldsymbol{\alpha}\right)$, and the 1st-order response derivatives, $R_{i_{1}}^{(1)}\left(\boldsymbol{\alpha}^{0},\mathbf{u}^{0};\boldsymbol{\psi}^{(1)}\right)$, with respect to the model parameter now depend on the adjoint function $\boldsymbol{\psi}^{(1)}\in\mathbf{H}_{Q}$. The explicit expressions of the *1st-order partial G-derivatives, $R_{i_{1}}^{(1)}\left(\boldsymbol{\alpha}^{0};\mathbf{u}^{0};\boldsymbol{\psi}^{(1)}\right)$,* of the response $R\left(\mathbf{e}\right)$ with respect to each of the model parameters α_{i}, evaluated at $\boldsymbol{\alpha}^{0},\mathbf{u}^{0},\boldsymbol{\psi}^{(1)}$, are as follows:

$$R_{i_1}^{(1)}\left(\boldsymbol{\alpha},\mathbf{u};\boldsymbol{\psi}^{(1)}\right) \triangleq \frac{\partial R(\boldsymbol{\alpha},\mathbf{u})}{\partial \alpha_{i_1}} - \frac{\partial \hat{P}^{(1)}\left(\boldsymbol{\alpha},\mathbf{u};\boldsymbol{\psi}^{(1)}\right)}{\partial \alpha_{i_1}}$$
$$+ \int_{\Omega_x} \boldsymbol{\psi}^{(1)}(\mathbf{x}) \bullet \left\{ \frac{\partial \left[\mathbf{Q}(\boldsymbol{\alpha}) - \mathbf{N}(\boldsymbol{\alpha},\mathbf{u}) \right]}{\partial \alpha_{i_1}} \right\} d\mathbf{x}, \quad i_1 = 1,\ldots,N_\alpha. \tag{2.71}$$

As indicated by Eqs. (2.70) and (2.71), *the total 1st-order response variation* $DR\left(\boldsymbol{\alpha}^0,\mathbf{u}^0;\boldsymbol{\psi}^{(1)};\delta\boldsymbol{\alpha}\right)$ *can be computed after solving Eqs.* (2.69) *and* (2.65) ***only once*** *to obtain the adjoint function* $\boldsymbol{\psi}^{(1)} \in \mathbf{H}_\psi^{(1)}(\Omega_x)$. *Equations* (2.69) *and* (2.65) *will be called the 1st-Level Adjoint Sensitivity System (1st-LASS), and its solution,* $\boldsymbol{\psi}^{(1)} \in \mathbf{H}_\psi^{(1)}(\Omega_x)$*, will be called the* 1st-level adjoint function. It is very important to note that the *1st-LASS* is independent of the variation $\delta\mathbf{u}$ in the original state functions $\mathbf{u}$. Once the adjoint function $\boldsymbol{\psi}^{(1)} \in \mathbf{H}_\psi^{(1)}(\Omega_x)$ has been obtained, the individual sensitivities of the response $R(\mathbf{e})$ with respect to each of the model parameters α_i, evaluated at the nominal values $\mathbf{e}^0 = \left(\boldsymbol{\alpha}^0,\mathbf{u}^0\right)$, are obtained by means of the simple integrations, as shown in Eq. (2.71), over the definition domain (Ω_x) of the system's independent variables.

Cacuci (1981.b) has also provided the *adjoint sensitivity analysis methodology for computing the 1st-order sensitivities of function-valued operator responses,* $\mathbf{R}(\mathbf{e})$*,* as opposed to the scalar-valued response considered in the foregoing. In such a case, $\mathbf{R}(\mathbf{e})$ can be represented by the spectral (generalized Fourier) expansion

$$\mathbf{R}\left(\mathbf{e}^0\right) = \sum_{n\in N} \left\langle \mathbf{R}\left(\mathbf{e}^0\right), \boldsymbol{\varphi}_n(\mathbf{x}) \right\rangle_R \boldsymbol{\varphi}_n(\mathbf{x}), \tag{2.72}$$

where the set $\{\boldsymbol{\varphi}_n(\mathbf{x})\}$, $n\in N$, is an orthonormal basis for the Hilbert space $\mathbf{H}_R(\Omega_R)$; the index set N may be finite or infinite. The first-order G-derivative of Eq. (2.72) yields

$$\delta R\left(\boldsymbol{\alpha}^{0},\mathbf{u}^{0};\delta\mathbf{u};\delta\boldsymbol{\alpha}\right)\triangleq\left\{\frac{d}{d\varepsilon}\Big[\mathbf{R}\big(\mathbf{e}^{0}+\varepsilon\mathbf{h}\big)\Big]\right\}_{\varepsilon=0}$$

$$=\left\{\frac{\partial\mathbf{R}\left(\boldsymbol{\alpha},\mathbf{u}\right)}{\partial\boldsymbol{\alpha}}\right\}_{\left(\boldsymbol{\alpha}^{0},\mathbf{u}^{0}\right)}\delta\boldsymbol{\alpha}+\left\{\frac{\partial\mathbf{R}\left(\boldsymbol{\alpha},\mathbf{u}\right)}{\partial\mathbf{u}}\right\}_{\left(\boldsymbol{\alpha}^{0},\mathbf{u}^{0}\right)}\delta\mathbf{u}=\left\{\frac{\partial\mathbf{R}\left(\boldsymbol{\alpha},\mathbf{u}\right)}{\partial\boldsymbol{\alpha}}\right\}_{\left(\boldsymbol{\alpha}^{0},\mathbf{u}^{0}\right)}\delta\boldsymbol{\alpha}+\sum_{n\in N}\left\langle\frac{\partial\mathbf{R}}{\partial\mathbf{u}}\delta\mathbf{u},\boldsymbol{\varphi}_{n}\right\rangle_{R}\boldsymbol{\varphi}_{n}.$$

(2.73)

As noted in Eq. (2.73) above, the "*direct effect term*," $\left\{\partial\mathbf{R}\left(\boldsymbol{\alpha},\mathbf{u}\right)/\partial\boldsymbol{\alpha}\right\}_{\left(\boldsymbol{\alpha}^{0},\mathbf{u}^{0}\right)}\delta\boldsymbol{\alpha}$, can be

computed directly when applying to the response $\mathbf{R}\left(\mathbf{e}\right)$ the definition of the G-differential,

without needing to evaluate its spectral expansion. Furthermore, each of the *generalized*

Fourier coefficients $\left\langle\left\{\partial\mathbf{R}\left(\boldsymbol{\alpha},\mathbf{u}\right)/\partial\mathbf{u}\right\}_{\left(\boldsymbol{\alpha}^{0},\mathbf{u}^{0}\right)}\delta\mathbf{u},\boldsymbol{\varphi}_{n}\right\rangle_{R}$ will be considered, in turn, to provide a

source term for the adjoint sensitivity system, just as has been done for the functional

$\left[\partial R\left(\boldsymbol{\alpha},\mathbf{u}\right)/\partial\mathbf{u}\right]\delta\mathbf{u}=\left\langle\partial R\left(\boldsymbol{\alpha},\mathbf{u}\right)/\partial\mathbf{u},\ \delta\mathbf{u}\right\rangle_{u}$ that was defined in Eq. (2.63). Repeating the

mathematical derivations from Eq. (2.63) to Eq. (2.70) yields the following result for

computing the 1$^{\text{st}}$-order totals differential $\delta\mathbf{R}\left(\boldsymbol{\alpha}^{0},\mathbf{u}^{0};\boldsymbol{\psi}_{1}^{(1)}\left(\mathbf{x}\right),...,\boldsymbol{\psi}_{N}^{(1)}\left(\mathbf{x}\right);\delta\boldsymbol{\alpha}\right)$ of function-

valued operator response $\mathbf{R}\left(\boldsymbol{\alpha},\mathbf{u}\right)$:

$$\delta\mathbf{R}\left(\boldsymbol{\alpha}^{0},\mathbf{u}^{0};\boldsymbol{\psi}_{1}^{(1)}\left(\mathbf{x}\right),...,\boldsymbol{\psi}_{N}^{(1)}\left(\mathbf{x}\right);\delta\boldsymbol{\alpha}\right)=\left\{\frac{\partial\mathbf{R}\left(\boldsymbol{\alpha},\mathbf{u}\right)}{\partial\boldsymbol{\alpha}}\right\}_{\left(\boldsymbol{\alpha}^{0},\mathbf{u}^{0}\right)}\delta\boldsymbol{\alpha}+$$

$$\sum_{n\in N}\left\{\left\langle\boldsymbol{\psi}_{n}^{(1)}\left(\mathbf{x}\right),\ \mathbf{Q}_{\alpha}'\left(\mathbf{e}^{0}\right)\mathbf{h}_{\alpha}-\mathbf{N}_{\alpha}'\left(\mathbf{e}^{0}\right)\mathbf{h}_{\alpha}\right\rangle_{Q}-\hat{P}\left(\mathbf{h}_{\alpha},\boldsymbol{\psi}_{n}^{(1)}\left(\mathbf{x}\right);\boldsymbol{\alpha}^{0}\right)\right\}\boldsymbol{\varphi}_{n},$$

(2.74)

where each adjoint function $\boldsymbol{\psi}_{n}^{(1)}\left(\mathbf{x}\right)$, $n\in N$, is the solution of the following *1$^{\text{st}}$-Level Adjoint*

Sensitivity System (1$^{\text{st}}$-LASS):

$$\mathbf{A}_{11}^{(1)}\left(\boldsymbol{\alpha}^{0},\mathbf{u}^{0}\right)\boldsymbol{\psi}_{n}^{(1)}\left(\mathbf{x}\right)=\left\{\frac{\partial\mathbf{R}\left(\boldsymbol{\alpha},\mathbf{u}\right)}{\partial\mathbf{u}}\right\}_{\left(\boldsymbol{\alpha}^{0},\mathbf{u}^{0}\right)}\boldsymbol{\varphi}_{n}\left(\mathbf{x}\right),\quad\mathbf{x}\in\Omega_{x},\ \ n\in N,\qquad(2.75)$$

$$\mathbf{B}_{A}^{(1)}\left(\boldsymbol{\alpha}^{0},\mathbf{u}^{0};\boldsymbol{\psi}_{n}^{(1)}\left(\mathbf{x}\right)\right)=\mathbf{0},\ \ \mathbf{x}\in\partial\Omega_{x}.\qquad(2.76)$$

As Eqs. (2.75) and (2.76) indicate, the adjoint system must be solved anew, with a different source on the right-side of Eq. (2.75), for each $n \in N$. From the foregoing considerations, it is evident that *the orthonormal basis* $\left\{ \boldsymbol{\varphi}_n(\mathbf{x}) \right\}$, $n \in N$, *must be chosen such as to minimize an "a priori" user-selected error criterion, to ensure that the spectral expansion in Eq.* (2.72) *represents the known nominal value of* $\mathbf{R}(\boldsymbol{\alpha}, \mathbf{u})$ *within the selected error criterion with a minimal number, N, of terms in the expansion.* The selection of this error criterion and of the basis $\left\{ \boldsymbol{\varphi}_n \right\}$, $n \in N$, are clearly problem-dependent issues but the procedures and considerations for performing this selection (e.g., using classical Fourier expansion, orthogonal and/or chaos polynomials, wavelets, collocation, pseudo-spectral methods, etc.) are well-known.

2.1.3 Discussion

The presentations of the major statistical methods in Sub-Section 2.1.1, and the presentation of the adjoint sensitivity analysis methodology in Sub-Section 2.1.2 have highlighted the following fundamental distinctions between these two groups of methods:

(i)   In contrast to statistical methods, deterministic methods aim at calculating *exactly* the local sensitivities (derivatives) of the response to the model parameters, rather than infer a sensitivity measure from statistical indicators. The adjoint sensitivity analysis methodology (ASAM) can only be applied if the original model can be accessed in order to develop the adjoint sensitivity model; thus, this methodology is intrinsically intrusive. If this adjoint model is developed simultaneously with the original model, then the adjoint model requires very little additional resources to develop. If, however, the adjoint model is developed posteriori, considerable skills may be required for its successful implementation and use. However, once the adjoint model is available, the computation of response sensitivities using the ASAM is by far more efficient computationally than using any other method, deterministic or statistical.

(ii)   If a model cannot be accessed intrusively, then the only path to performing sensitivity and uncertainty analysis is by using non-intrusive statistical methods. Statistical methods commence with the "uncertainty analysis" stage, and only subsequently proceeds to the "sensitivity-analysis" stage, which is the exact reverse of the conceptual path underlying the methods of deterministic sensitivity and uncertainty analysis. Statistical methods can only infer a sensitivity measure from statistical indicators, but cannot compute exactly response sensitivities. The relative advantages and disadvantages of the various statistical methods, when compared among themselves, will be summarized in the remainder of this subsection.

Statistical uncertainty and sensitivity analysis methods aim at assessing the contributions of uncertainties in parameters in contributing to the overall uncertainty of the model response (output). The relative magnitude of this uncertainty contribution is assigned a measure of the statistical sensitivity of the response uncertainty to the respective parameter, and this measure is also used to rank the importance of the respective parameter. Without any "a priori" assumption regarding the relationship between the parameters and the response, the construction of a full-space uncertainty analysis requires $O(s^I)$ computations, where s denotes the number of sample values for each parameter and I denotes the number of parameters. If a local polynomial regression is used, Stone (1982) has shown that the rate of convergence is $s_N = N^{-p/(2p+I)}$, where N denotes the number of sample points, p denotes the degree of smoothness of the function representing the response in terms of the parameters, and I denotes the number of parameters. This relation indicates that the parameters-response mapping (function) can be approximated to a resolution of s^{-1} with $O(s^{I/p})$ sample points. The *FAST* method appears to be the most efficient of the statistical methods, needing $I(8\omega_i + 1)N_r$ computations for each frequency, where N_r denotes the number of replicates. For example, if the response is a function of 8 parameters, and if the sample size is 64, then Sobol's method requires 1088 model evaluations, while the *FAST* method requires 520 model evaluations, if the sample size

increases to 1024, then Sobol's method requires 17 408 model evaluations, while the *FAST* method requires 8200 model evaluations. These examples underscore the fact that the number of model evaluations becomes rapidly impractical for realistic large-scale models comprising many parameters.

Since random sampling is easy to implement, and provides unbiased estimates for the means, variances, and distribution functions, it is the preferred technique in practice, if large samples are available. However, a sufficiently "large sample", for producing meaningful results by random sampling, cannot be generated for complex models and/or for estimating extremely high quantiles (e.g., the 0.99999 quantile), with many parameters, since the computation of the required sample becomes prohibitively expensive and computationally impractical. In such cases, the random sampling method of choice becomes the stratified sampling method. The main difficulty for implementing stratified sampling lies with defining the strata and for calculating the probabilities for the respective strata, unless considerable "a priori" knowledge is already available for this purpose. For example, the fault and event trees used in risk assessment studies of nuclear power plants and other complex engineering facilities can be used as algorithms for defining stratified sampling procedures. Latin Hypercube sampling is used when very high quantiles need not be estimated, but the large number of calculations needed for generating the "large sample" required for random sampling still remain unpractical. This is often the case in practice when assessing the effects of subjective uncertainty in medium-sized problems (e.g., ca. 30 parameters), and a 0.9 to 0.95 quantile is adequate for indicating the location of a likely outcome. For such problems, random sampling is still unfeasible computationally, but the unbiased means and distribution functions provided by the full stratification (i.e., each parameter is treated equally) of the Latin Hypercube sampling makes it the preferred alternative over the importance sampling, where the unequal strata probabilities produce results that are difficult to interpret (particularly for subsequent sensitivity analysis). In this sense, Latin Hypercube sampling provides a compromise importance sampling when *"a priori"* knowledge of the relationships between the sampled parameters and predicted responses is not available. For example, the method devised by McKay (1995) for evaluating η^2, defined in Eq. (2.25), is based on a Latin Hypercube sampling of size *m* with *r* replicates, and is computationally very expensive, requiring $rm \times (I+1)$ model evaluations, where *I* represents the number of parameters in $\boldsymbol{\alpha}$.

As has been discussed in the foregoing, sampling-based uncertainty and sensitivity analysis is performed in order to ascertain if model predictions fall within some region of concern (uncertainty in model responses due to uncertainties in model parameters) and to identify the dominant parameters in contributing to the response uncertainty (statistical sensitivity analysis). As a by-product, sampling-based uncertainty and sensitivity analysis also provides an indication of the proper operation of the model under investigation. However, the results of sampling-based uncertainty and sensitivity analysis depend entirely on the distributions assigned to the sampled parameters, so the proper assignment of these distributions is essential to avoid producing spurious results.

It is customary to display the estimated expected value and the estimated variance of the response (as estimated from the sample size). However, these quantities may not be the most useful indicators about the response because information is always lost in the calculations of means and variances. In particular, the mean and variance are less useful for summarizing information about the distribution of subjective uncertainties; by comparison, quantiles associated with the respective distribution provide a more meaningful locator for the quantity under consideration. Distribution functions (e.g., cumulative and/or complementary distribution functions, density functions) provide the complete information that can be extracted from the sample under consideration.

Currently, a general "fool-proof" statistical method for analyzing correctly mathematical models of physical processes involving highly correlated parameters does not seem to exist, so that particular care must be used when interpreting regression results for such models.

2.2. Development of a Surrogate Dissolver Model

The spent nuclear fuel dissolver model developed in Chapter 3, and analyzed in subsequent Chapters of this work, comprises 16 coupled nonlinear first-order equations that describe the time-evolution of the volumetric mass concentration of nitric acid of the liquid phase. The dissolver model also comprises 1291 imprecisely known scalar model parameters, for which only the nominal values and the corresponding standard deviations are known; these parameters are considered to be all uncorrelated. A simple surrogate model that can be used without loss of generality to illustrate the novel concepts and results reported in this work

can be constructed by considering (see Chapter 3) the evolution of the volumetric mass concentration of nitric acid of the liquid phase, in units of $[g/L]$, denoted as $\rho_a^{(8)}(t)$, in the compartment closest to the dissolver's inlet (i.e., compartment #8). The evolution equation for $\rho_a^{(8)}(t)$ has the following form [see Eqs. (3.11) and (3.14) in Chapter 3]:

$$\frac{d}{dt}\left[\rho_a^{(8)}(t)\right] + \frac{f^{(in)}(t)}{V^{(8)}(t)}\rho_a^{(8)}(t) = \frac{f^{(in)}(t)}{V^{(8)}(t)}\rho_a^{in}(t), \ \ 0 < t \le t_f. \tag{2.77}$$

$$\rho_a^{(8)}(0) = 0.0, \quad at \ t = 0, \tag{2.78}$$

where: (i) $V^{(8)}(t)$ denotes the volume of the liquid phase, in units of liters $[L]$, in compartment #8; (ii) $f^{(in)}(t)$ denotes the inflow volumetric flow rate of the liquid mixture, in units of liter/hour $[L/h]$; (iii) $\rho_a^{(in)}(t)$ denotes the time-dependent variation of the inlet mass flow rate of nitric acid solution, which evolves in time as depicted in Figure 3.4. As shown in Chapter 3, the inflow volumetric flow rate, $f^{(in)}(t)$, is computed from Eq. (3.9), namely

$$f^{(in)}(t) = \dot{m}^{(in)}(t)\left[63a\rho_a^{(in)}(t) + b\right]^{-1}, \tag{2.79}$$

where a and b are imprecisely known parameters with nominal values and standard deviations given in Table 3.1, and where $\dot{m}^{(in)}(t)$ denotes the inlet nitric mass concentration, in units of gram/hour $[g/h]$, which evolves in time as depicted in Figure 3.3.

Both $\dot{m}^{(in)}(t)$ and $\rho_a^{(in)}(t)$ are piecewise-constant in time, as depicted in Figures 3.3 and 3.4, respectively. On the other hand, $V^{(8)}(t)$ is a state function of the dissolver model, and is thus determined as part of the model's solution; in principle, therefore, $V^{(8)}(t)$ depends on all 1291 scalar parameters comprised within the dissolver model. Consider that a measurement were made in compartment #8 at a time $t = t_1$, shortly after the initiation of the transient, such that the quantity $f^{(in)}(t)/V^{(8)}(t)$, which depends on all of the model parameters, can

essentially be considered to be time independent, i.e., $f^{(in)}(t)/V^{(8)}(t) \cong \sum_{i=1}^{N_\alpha} w_i \beta_i$, where N_α

is a large number (of order 10^3) denoting the total number of model parameters, denoted here as β_i, and the quantities w_i represent known "weighting factors" that are not subject to uncertainties. Furthermore, the quantity $\rho_a^{in}(t)$ is also constant in time (see Figure 3.4), remaining at a value $\rho_a^{in}(t) = \rho_{a,A}^{in}$ during the short initial time interval $t \in (0, t_1)$. Dropping, for notational simplicity, the various superscripts and subscripts in Eqs. (2.77) and (2.78), it follows that, for an initial time interval $t \in (0, t_1)$, the evolution of the acid density in compartment #8, which shall simply be denoted as $\rho(t)$, would be governed by the following evolution equation derived from Eqs. (2.77) and (2.78):

$$\frac{d\rho(t)}{dt} + \rho(t) \sum_{i=1}^{N_\alpha} w_i \beta_i = \rho_{a,A}^{in} \sum_{i=1}^{N_\alpha} w_i \beta_i, \ \ 0 < t \le t_1, \tag{2.80}$$

$$\rho(0) = 0, \ \ t = 0. \tag{2.81}$$

The response of interest for the above model would be the measurement of $\rho(t)$ at time $t = t_1$. Such a measurement can be represented mathematically by the following functional:

$$\rho(t_1) = \int_0^{t_1} \rho(t) \delta(t - t_1) dt, \tag{2.82}$$

where $\delta(t - t_1)$ denotes the well-known Dirac-delta (impulse) functional.

The parameters in Eq. (2.80) could be determined by applying the tools of *reduced order modeling* to the full dissolver model (developed in Chapter 3). Such tools range from relatively simple regression "fitting" of the results produced by Eq. (2.80) to the corresponding results for compartment #8 produced by the full model, to the "polynomial chaos" methods of spectral decomposition of the full model, using (most likely) Legendre polynomials in time, since the time interval of interest is finite. In fact, Legendre polynomials in time will be used in Chapter 4, Section 4.2, for performing sensitivity analysis of spectral

representations of function-valued (in this case: time-dependent) acid concentration responses in various dissolver compartments. However, since the full dissolver model (to be developed in Chapter 3) will be used in this work, the actual numerical values, and needed number of, model parameters β_i will not be determined here. Therefore, the model for the acid concentration in the dissolver's compartment #8, represented by Eqs. (2.80) and (2.81) will be called the *surrogate dissolver model*, and will be used in the remainder of this Chapter for illustrating the structure of, and novel results in, the body of this work, to be described in Chapters 3 through 7. The solution of Eqs. (2.80) and (2.81) can be readily obtained by using the general "integrating factor" method for solving linear first-order ordinary differential equations (see appendix A), which yields

$$\rho(t) = \rho_{a,A}^{in} \left[1 - \exp\left(-t \sum_{i=1}^{N_\alpha} w_i \beta_i \right) \right].\qquad(2.83)$$

2.3. First-Order Adjoint Sensitivity and Uncertainty Analysis of the Surrogate Dissolver Model

Since Eqs. (2.80) - (2.81) describe a mathematically well-defined surrogate model, either intrusive or non-intrusive methods could, in principle, be applied for performing sensitivity and uncertainty analysis of the response of interest, $\rho(t_1)$. However, the large number $N_\alpha = O(10^3)$ of model parameters precludes, ab initio, the use of any statistical method for performing sensitivity and uncertainty analysis, since the ensuing computational costs would be prohibitive. The ASAM will therefore be used to compute the first-order sensitivities, which will then be used in with Eqs. (2.51) – (2.51) to compute the first-order contributions to the expectation value $E[\rho(t_1)]$, and variance, $Var[\rho(t_1)]$, of $\rho(t_1)$. Thus, applying the definition of the G-derivative given in Eq. (2.54) to the response $\rho(t_1)$ defined in Eq. (2.82)

yields the following expression for the total sensitivity $\delta\rho(t_1)$ of $\rho(t_1)$ to variations in the model parameters β_i and $\rho_{a,A}^{in}$:

$$\delta\rho(t_1) \triangleq \left\{ \frac{d}{d\varepsilon} \int_0^{t_1} \left[\rho(t) + \varepsilon\delta\rho(t)\right]\delta(t-t_1)dt \right\}_{\varepsilon=0} = \int_0^{t_1} \delta\rho(t)\delta(t-t_1)dt. \quad (2.84)$$

Note that there is no "direct effect term" in Eq. (2.83), since the response $\rho(t_1)$ does not depend explicitly on any parameters; this response depends *implicitly* on all of the model parameters. The variation $\delta\rho(t)$ in the state function $\rho(t)$ depends on the variations in the model parameters as generally represented by the *1ˢᵗ-LFSS*, defined by Eqs. (2.56) and (2.57). The *1ˢᵗ-LFSS* corresponding to Eqs. (2.80) and (2.81) is obtained by taking the G-differential of these equations, which yields:

$$\mathbf{F}_{11}^{(1)}\left(\boldsymbol{\alpha}^0, \mathbf{u}^0\right)\delta\mathbf{u} = \mathbf{Q}^{(1)}\left(\boldsymbol{\alpha}^0, \mathbf{u}^0; \delta\boldsymbol{\alpha}\right), \quad \mathbf{x} \in \Omega_x,$$

$$\rightarrow \frac{d}{d\varepsilon}\left\{ \frac{d\left[\rho^0(t) + \varepsilon\delta\rho(t)\right]}{dt} + \left[\rho^0(t) + \varepsilon\delta\rho(t)\right]\sum_{i=1}^{N_\alpha} w_i\left(\beta_i^0 + \varepsilon\delta\beta_i\right)\right. \quad (2.85)$$

$$\left. - \left(\rho_{a,A}^{in,0} + \varepsilon\delta\rho_{a,A}^{in}\right)\sum_{i=1}^{N_\alpha} w_i\left(\beta_i^0 + \varepsilon\delta\beta_i\right)\right\}_{\varepsilon=0}, 0 < t \le t_1,$$

$$\mathbf{B}_F^{(1)}\left(\boldsymbol{\alpha}^0, \mathbf{u}^0; \delta\boldsymbol{\alpha}, \delta\mathbf{u}\right) = \mathbf{0}, \quad \mathbf{x} \in \partial\Omega_x,$$
$$\rightarrow \frac{d}{d\varepsilon}\left\{\rho^0(t) + \varepsilon\delta\rho(t)\right\}_{\varepsilon=0} = 0, \quad t = 0. \quad (2.86)$$

Performing the differentiation with respect to ε in Eqs. (2.84) and (2.85), and setting $\varepsilon = 0$ in the resulting expressions yields the following specific *1ˢᵗ-LFSS for the surrogate dissolver model:*

$$\frac{d\left[\delta\rho(t)\right]}{dt} + \delta\rho(t)\sum_{i=1}^{N_\alpha} w_i\beta_i^0 = \left[\rho_{a,A}^{in,0} - \rho^0(t)\right]\sum_{i=1}^{N_\alpha} w_i\delta\beta_i + \delta\rho_{a,A}^{in}\sum_{i=1}^{N_\alpha} w_i\beta_i^0, \quad 0 < t \le t_1, \quad (2.87)$$

$$\delta\rho(0) = 0, \quad t = 0. \quad (2.88)$$

In principle, the 1st-LFSS could be solved $N_\alpha = O(10^3)$ times to obtain the sensitivities of $\rho(t_1)$ to every model parameter, but such a procedure would be prohibitively expensive computationally. Therefore, the ASAM will be applied by developing the 1st-Level Adjoint Sensitivity System (1st-LASS), cf. Eqs. (2.69) and (2.65). For the surrogate dissolver model, the Hilbert spaces $\mathbf{H}_u(\Omega_x)$ and $\mathbf{H}_Q(\Omega_x)$ will be identical, consisting of all square-integrable functions $\rho(t)$, and endowed with the inner product, $\langle \rho_1(t), \rho_2(t) \rangle$, between two (square-integrable) functions, $\rho_1(t)$ and $\rho_2(t)$ defined as

$$\langle \rho_1(t), \rho_2(t) \rangle \triangleq \int_0^{t_1} \rho_1(t) \rho_2(t) dt. \tag{2.89}$$

In view of the above definition of the inner product, the "indirect effect term" in Eq. (2.84) indicates that the Dirac-functional actually corresponds to the quantity $\left[\partial R(\boldsymbol{\alpha}, \mathbf{u}) / \partial \mathbf{u} \right] \delta \mathbf{u}$, cf. Eq. (2.63), namely:

$$\left[\partial R(\boldsymbol{\alpha}, \mathbf{u}) / \partial \mathbf{u} \right] \delta \mathbf{u} \rightarrow \delta(t - t_1). \tag{2.90}$$

The 1st-LASS is constructed by following the principles presented in Eq. (2.64) et seq. For the surrogate dissolver model, these principles require the introduction of a square-integrable function $\psi^{(1)}(t) \in \mathbf{H}_Q$, which is used to construct the inner product with Eq. (2.87), just as was generally done in Eq. (2.64), namely:

$$\int_0^{t_1} \psi^{(1)}(t) \left[\frac{d\left[\delta\rho(t) \right]}{dt} + \delta\rho(t) \sum_{i=1}^{N_\alpha} w_i \beta_i^0 \right] dt = \int_0^{t_1} \psi^{(1)}(t) \left\{ \left[\rho_{a,A}^{in,0} - \rho^0(t) \right] \sum_{i=1}^{N_\alpha} w_i \delta\beta_i + \delta\rho_{a,A}^{in} \sum_{i=1}^{N_\alpha} w_i \beta_i^0 \right\} dt. \tag{2.91}$$

The adjoint operator corresponding to $\mathbf{A}_{11}^{(1)}(\boldsymbol{\alpha}, \mathbf{u})$ in Eq. (2.64) is obtained by integrating the left-side of Eq. (2.91) by parts, so as to transfer the differential operation from $\delta\rho(t)$ onto $\psi^{(1)}(t)$. Performing these operations yields:

$$\int_0^{t_1} \psi^{(1)}(t) \left[\frac{d[\delta\rho(t)]}{dt} + \delta\rho(t) \sum_{i=1}^{N_\alpha} w_i \beta_i^0 \right] dt = \int_0^{t_1} \delta\rho(t) \left[-\frac{d\psi^{(1)}(t)}{dt} + \psi^{(1)}(t) \sum_{i=1}^{N_\alpha} w_i \beta_i^0 \right] dt$$

$$+ \psi^{(1)}(t_1) \delta\rho(t_1) - \psi^{(1)}(0) \delta\rho(0).$$

$$(2.92)$$

Comparison of Eqs. (2.91) with Eq. (2.64) reveals correspondences between the general theory and the particular surrogate dissolver model:

$$\mathbf{A}_{11}^{(1)}(\boldsymbol{\alpha}^0, \mathbf{u}^0) \to \left[-\frac{d\psi^{(1)}(t)}{dt} + \psi^{(1)}(t) \sum_{i=1}^{N_\alpha} w_i \beta_i^0 \right], \tag{2.93}$$

$$\left\{ P^{(1)}(\boldsymbol{\alpha}^0, \mathbf{u}^0; \boldsymbol{\psi}^{(1)}; \delta\mathbf{u}) \right\}_{\partial\Omega_x} \to \psi^{(1)}(t_1) \delta\rho(t_1) - \psi^{(1)}(0) \delta\rho(0). \tag{2.94}$$

The "boundary conditions" for the (adjoint) function $\psi^{(1)}(t)$, corresponding to the general ones represented by Eq. (2.65), are determined by requiring that they be independent of unknown variations in the forward function. In view of Eqs. (2.94) and (2.88), this requirement can be fulfilled by requiring that $\psi^{(1)}(t_1) = 0$, which implies that

$$\mathbf{B}_A^{(1)}(\boldsymbol{\alpha}^0, \mathbf{u}^0; \boldsymbol{\psi}^{(1)}) = \mathbf{0}, \ \mathbf{x} \in \partial\Omega_x \to \psi^{(1)}(t_1) = 0. \tag{2.95}$$

The selection of the above boundary condition implies that the bilinear concomitant $\left\{ P^{(1)}(\boldsymbol{\alpha}^0, \mathbf{u}^0; \boldsymbol{\psi}^{(1)}; \delta\mathbf{u}) \right\}_{\partial\Omega_x}$ vanishes in the case of the surrogate dissolver model.

Collecting the results in Eqs. (2.84), (2.90), (2.92) - (2.95) yields the following expression for the *1ˢᵗ-LASS* satisfied by the adjoint function $\psi^{(1)}(t)$:

$$-\frac{d\psi^{(1)}(t)}{dt} + \psi^{(1)}(t) \sum_{i=1}^{N_\alpha} w_i \beta_i^0 = \delta(t - t_1), \ 0 < t \le t_1, \tag{2.96}$$

$$\psi^{(1)}(t_1) = 0, \tag{2.97}$$

as well as the following expressions for the total sensitivity $\delta\rho(t_1)$ of $\rho(t_1)$ with respect to variations in the model parameters β_i and $\rho_{a,A}^{in}$:

$$\int_0^{t_1} \psi^{(1)}(t)\left\{ \left[\rho_{a,A}^{in,0} - \rho^0(t) \right] \sum_{i=1}^{N_\alpha} w_i \delta\beta_i + \delta\rho_{a,A}^{in} \sum_{i=1}^{N_\alpha} w_i \beta_i^0 \right\} dt = \int_0^{t_1} \delta\rho(t)\delta(t-t_1)dt = \delta\rho(t_1).$$

(2.98)

The partial sensitivities of $\rho(t_1)$ with respect to variations the model parameters β_i and $\rho_{a,A}^{in}$ are obtained from Eq. (2.98), and their expressions are as follows:

$$\frac{\partial\rho(t_1)}{\partial\beta_i} = w_i \int_0^{t_1} \psi^{(1)}(t)\left[\rho_{a,A}^{in,0} - \rho^0(t) \right] dt, \quad i=1,...,N_\alpha,$$

(2.99)

$$\frac{\partial\rho(t_1)}{\partial\rho_{a,A}^{in}} = \left(\sum_{i=1}^{N_\alpha} w_i \beta_i^0 \right) \int_0^{t_1} \psi^{(1)}(t)dt.$$

(2.100)

It is evident from Eqs. (2.99) and (2.100) that the sensitivities of the acid concentration response $\rho(t_1)$ can be computed by fast quadrature once the adjoint function $\psi^{(1)}(t)$ has been obtained by solving the *1st-LASS,* i.e., Eqs. (2.96) and (2.97). Notably, the *1st-LASS* needs to be solved once only, since the *1st-LASS* does not depend on any variations in the model parameters or state functions. The explicit solution of the *1st-LASS* is readily obtained by using the integrating factor method (see Appendix A) in the form

$$\psi^{(1)}(t) = \left[1 - H(t-t_1) \right] \exp\left[(t-t_1) \sum_{i=1}^{N_\alpha} w_i \beta_i \right],$$

(2.101)

where $H(t_1 - t)$ is the customary Heaviside unit step-functional, defined as

$$H(t-t_1) \triangleq \begin{cases} 1, & t \geq t_1 \\ 0, & t < t_1 \end{cases}$$

(2.102)

Inserting the results in Eqs. (2.102) and (2.83) into Eqs. (2.99) and (2.100), respectively, yields the following explicit expressions for the 1st-order sensitivities of the response $\rho(t_1)$:

$$\frac{\partial \rho(t_1)}{\partial \beta_i} = \rho_{a,A}^{in,0} t_1 w_i \exp\left(-t_1 \sum_{i=1}^{N_\alpha} w_i \beta_i\right), \quad i = 1, ..., N_\alpha,$$ (2.103)

$$\frac{\partial \rho(t_1)}{\partial \rho_{a,A}^{in}} = \left[1 - \exp\left(-t_1 \sum_{i=1}^{N_\alpha} w_i \beta_i\right)\right].$$ (2.104)

The correctness of the above expressions can be readily verified by computing the 1st-order sensitivities directly from the forward solution presented in Eq. (2.83). In this particular case, the sensitivities of the surrogate dissolver model response $\rho(t_1)$ can be obtained analytically and exactly from Eq. (2.83). For large-scale systems, however, the forward solution would not be available analytically in a closed form [such as given in Eq. (2.83)], so the sensitivities obtained by the ASAM can only be verified to 1st-order in the parameter variations $\delta\beta_i$ by using forward computations, with altered parameter values $\left(\beta_i^0 + \delta\beta_i\right)$, in conjunction with 1st-order difference formulas of the form

$$\frac{\partial \rho(t_1; \beta_i^0)}{\partial \beta_i} \cong \frac{\rho(t_1; \beta_i^0 + \delta\beta_i) - \rho(t_1; \beta_i^0)}{\delta\beta_i}.$$ (2.105)

If only the 1st-order sensitivities are available for the single *computed* response, denoted as $\rho^{comp}(t_1)$, then Eqs. (2.51) through (2.53) reduce to the following expressions:

$$\left\{E\left[\rho^{comp}(t_1)\right]\right\}_1 = \rho(t_1; \beta_i^0),$$ (2.106)

$$\left\{Var\left[\rho^{comp}(t_1)\right]\right\}_1 = \left[\frac{\partial \rho(t_1)}{\partial \rho_{a,A}^{in}}\right]^2 Var\left(\rho_{a,A}^{in}\right) + 2\sum_{i=1}^{N_\alpha}\left(\frac{\partial \rho(t_1)}{\partial \rho_{a,A}^{in}} \frac{\partial \rho(t_1)}{\partial \beta_i}\right) cov\left(\rho_{a,A}^{in}, \beta_i\right)$$
$$+ \sum_{i=1}^{N_\alpha}\sum_{j=1}^{N_\alpha}\left(\frac{\partial \rho(t_1)}{\partial \beta_i} \frac{\partial \rho(t_1)}{\partial \beta_j}\right) cov\left(\beta_i, \beta_j\right)$$
$$= \sum_{i=1}^{N_\alpha+1}\sum_{j=1}^{N_\alpha+1} \frac{\partial \rho(t_1)}{\partial \alpha_i} \frac{\partial \rho(t_1)}{\partial \alpha_j} cov\left(\alpha_i, \alpha_j\right), \quad \alpha_{N_\alpha+1} \triangleq \rho_{a,A}^{in};$$

(2.107)

$$\left\{\mu_3\left[\rho^{comp}\left(t_1\right)\right]\right\}_1 = \sum_{i=1}^{N_\alpha+1}\sum_{j=1}^{N_\alpha+1}\sum_{\mu=1}^{N_\alpha+1}\frac{\partial\rho\left(t_1\right)}{\partial\alpha_i}\frac{\partial\rho\left(t_1\right)}{\partial\alpha_j}\frac{\partial\rho\left(t_1\right)}{\partial\alpha_\mu}t_{ij\mu}\sigma_i\sigma_j\sigma_\mu; \quad \alpha_{N_\alpha+1}\triangleq\rho_{a,A}^{in}.$$

(2.108)

Recall also that the *skewness*, $\gamma_1\left[\rho\left(t_1\right)\right]$, of the response $\rho\left(t_1\right)$ is generally defined as

$$\gamma_1\left[\rho\left(t_1\right)\right]\triangleq\frac{\mu_3\left[\rho\left(t_1\right)\right]}{\left\{var\left[\rho\left(t_1\right)\right]\right\}^{3/2}}.$$

(2.109)

Recall that the *skewness* of a distribution quantifies the departure of the subject distribution from symmetry. Symmetric univariate distributions are characterized by $\gamma_1\left(r_k\right)=0$. If $\gamma_1\left[\rho\left(t_1\right)\right]<0$, then the respective response distribution is skewed towards the left of the mean $E\left[\rho\left(t_1\right)\right]$, favoring lower values of r_k relative to $E\left[\rho\left(t_1\right)\right]$. On the other hand, if $\gamma_1\left[\rho\left(t_1\right)\right]>0$, then the respective response distribution is skewed towards the right of the mean $E\left[\rho\left(t_1\right)\right]$, favoring higher values of r_k relative to $E\left[\rho\left(t_1\right)\right]$.

The *subscript "1"* is used for the quantities $\left\{E\left[\rho^{comp}\left(t_1\right)\right]\right\}_1$, $\left\{Var\left[\rho^{comp}\left(t_1\right)\right]\right\}_1$ and $\left\{\mu_3\left[\rho^{comp}\left(t_1\right)\right]\right\}_1$ defined by the expressions in Eqs. (2.106) - (2.108), respectively, to indicate that these quantities are approximations that *include only the 1st-order response sensitivities*, of the exact expressions for the expectation, variance and 3rd-order moment of the exact (but unavailable) response distribution function. Thus, when only *1st-order response sensitivities are available*, the expressions in Eqs. (2.106) - (2.108) point to the following conclusions:

(i)   If the second- and higher-order sensitivities are unavailable, then the expectation value of the response is the same as the computed value of the response.

(ii)   It the triple-correlations, $t_{ij\mu}$, for the parameters are unavailable, then the third-order response moment, $\mu_3\left[\rho(t_1)\right]$, cannot be computed; hence, it would not be possible to assess the asymmetries in the resulting response distribution.

(iii)   If the second- and higher-order sensitivities are unavailable, and the distribution of the parameters is normal or symmetric with respect to its mean, then $t_{ij\mu} = 0$ and the response distribution would appear to be symmetric. Consequently, for normal or symmetric parameter distributions, any asymmetries in the response distribution could only be assessed if the second-order sensitivities were available, as indicated by Eq. (2.53).

In Chapter 4 of this work (in the sequel), the responses of interest will be measurements of the nitric acid concentration taken at 635 instances in time, over the duration of the transient event under consideration. If each response were to be considered separately, then 635 adjoint systems would need to be solved to determine the 1st-order sensitivities of each of these responses to the 1291 model parameters. Even though 635 adjoint computations would still be fewer computations than 1291 forward computations [which would be needed if the 1st-order sensitivities were to be computed using the finite-difference formula given in Eq. (2.105)], 635 adjoint computations is not insignificant. In Chapter 4 (where the sensitivity analysis of the full dissolver model will be performed) the ASAM applied in this Section for computing the sensitivities obtained in Eqs. (2.103) and (2.104) is extended by using spectral expansions based on Legendre Polynomials and is shown as a nearly 20 factor improvement with less than 0.1% loss of accuracy.

2.4. Forward and Inverse Predictive Modeling: Data Assimilation, Model Calibration, Optimal Best-Estimate Predictions with Reduced Uncertainties using the Surrogate Dissolver Model

Cacuci (2014) has recently formulated a "*Predictive Modeling of Coupled Multi-Physics Systems (PM_CMPS)*" methodology, which unifies the concepts underlying forward and inverse modeling of coupled multi-physics systems in the presence of uncertainties. This

work builds upon and extends the work of Cacuci and Ionescu-Bujor (2010b) on predictive modeling for a single multi-physics system in the presence of experimental and computational uncertainties. The forward and inverse predictive modeling methodology of Cacuci and Ionescu-Bujor (2010b) is applied in Chapters 5 and 6 to the full dissolver model, which comprises 1291 model parameters and 635 measured responses. Although the surrogate dissolver model comprises, in principle, just as many parameters as the full dissolver model, its single response, $\rho(t)$, measured just once, at $t = t_1$, allows the mathematical framework of Cacuci and Ionescu-Bujor (2010b) to take on a simpler form for which the following information is "a priori" known:

(i) the nominal (mean) value of the measurement, denoted as $\rho^{meas}(t_1)$, and the measurement's variance, denoted as $Var\left[\rho^{meas}(t_1)\right]$;

(ii) the parameter mean values, denoted as α_i^0, and the parameter covariance, denoted as $\mathrm{cov}(\alpha_i, \alpha_j)$, of the $(N_\alpha + 1)$ imprecisely known system (model) parameters, $\alpha_i \triangleq \beta_i$, $i = 1,...,N_\alpha$, and $\alpha_{N_\alpha+1} \triangleq \rho_{a,A}^{in}$;

(iii) the response sensitivities, $\partial\rho(t_1)/\partial\alpha_i$, computed using the ASAM, with expressions given in Eqs. (2.103) and (2.104);

(iv) the expected value, $E\left[\rho^{comp}(t_1)\right]$, of the computed response, given by Eq. (2.106);

(v) the variance, $Var\left[\rho^{comp}(t_1)\right]$, of the computed response $\rho^{comp}(t_1)$, given by Eq. (2.107), which can be written in the form $Var\left[\rho^{comp}(t_1)\right] = \mathbf{S}_{r\alpha}\mathbf{C}_{\alpha\alpha}\mathbf{S}_{r\alpha}^{\dagger}$, where $\mathbf{C}_{\alpha\alpha}$ represents the parameter covariance matrix, and $\mathbf{S}_{r\alpha}$ represents the row-vector of sensitivities $\left[\partial\rho(t_1)/\partial\alpha_1,...,\partial\rho(t_1)/\partial\alpha_{N_\alpha+1}\right]$;

(vi) the response $\rho(t)$ is uncorrelated with the model parameters α_i.

Application of the methodology of Cacuci and Ionescu-Bujor (2010b) to the surrogate dissolver model yields the following results:

1. "Model calibration", yielding the following optimally predicted "best-estimate" nominal values, $\boldsymbol{\alpha}^{pred}$, for the "calibrated" model parameters:

$$\boldsymbol{\alpha}^{pred} = \boldsymbol{\alpha}^0 - \mathbf{C}_{\alpha\alpha}\mathbf{S}_{r\alpha}^\dagger \left\{ Var\left[\rho^{comp}(t_1)\right] + Var\left[\rho^{meas}(t_1)\right]\right\}^{-1}\left[\rho^{comp}(t_1) - \rho^{meas}(t_1)\right],$$

or, in component form, for each $i = 1,...,N_\alpha + 1$,

$$\alpha_i^{pred} = \alpha_i^0 - \frac{\left[\rho^{comp}(t_1) - \rho^{meas}(t_1)\right]}{Var\left[\rho^{comp}(t_1)\right] + Var\left[\rho^{meas}(t_1)\right]} \sum_{j=1}^{N_\alpha+1} \frac{\partial\rho(t_1)}{\partial\alpha_j} cov\left(\alpha_i,\alpha_j\right); \qquad (2.110)$$

As Eq. (2.110) indicates, the calibrated parameter value α_i^{pred} may become larger or smaller than the original mean (nominal) parameter value α_i^0 depending on the sign of the second term on the right-side of this equation. If the parameters are uncorrelated, Eq. (2.110) takes on the simpler form

$$\alpha_i^{pred} = \alpha_i^0 - \frac{\left[\rho^{comp}(t_1) - \rho^{meas}(t_1)\right]}{Var\left[\rho^{comp}(t_1)\right] + Var\left[\rho^{meas}(t_1)\right]} \frac{\partial\rho(t_1)}{\partial\alpha_i} Var\left(\alpha_i\right); \qquad (2.110)$$

2. Predicted covariance matrices, denoted as $\mathbf{C}_{\alpha\alpha}^{pred}$, for the predicted nominal parameter values:

$$\mathbf{C}_{\alpha\alpha}^{pred} = \mathbf{C}_{\alpha\alpha} - \frac{\left(\mathbf{C}_{\alpha\alpha}\mathbf{S}_{r\alpha}^\dagger\right)\left(\mathbf{C}_{\alpha\alpha}\mathbf{S}_{r\alpha}^\dagger\right)^\dagger}{Var\left[\rho^{comp}(t_1)\right] + Var\left[\rho^{meas}(t_1)\right]},$$

which implies that

$$\mathbf{C}_{\alpha\alpha}^{pred} - \mathbf{C}_{\alpha\alpha} = -\frac{\sum_{j=1}^{N_\alpha+1}\left[\partial\rho(t_1)/\partial\alpha_i\right]^2\left(\mathbf{C}_{\alpha\alpha}\right)^2}{Var\left[\rho^{comp}(t_1)\right] + Var\left[\rho^{meas}(t_1)\right]}; \qquad (2.111)$$

Since the right-side of Eq. (2.111) represents a *negative-definite matrix*, it follows that the diagonal elements in this equation obey the inequality

$$Var\left(\alpha_i^{pred}\right) - Var\left(\alpha_i\right) < 0. \qquad (2.112)$$

The above inequality is equivalent to the inequality

$$Std.Dev.\left(\alpha_i^{pred}\right) < Std.Dev\left(\alpha_i\right), \qquad (2.113)$$

77

which indicates that *the predicted "uncertainties" in the predicted ("calibrated")*
parameters are smaller than (i.e., are reduced) the original "uncertainties" in the
model parameters.

3. Optimally predicted "best-estimate" nominal values, denoted as $\rho^{pred}(t_1)$, for the
   model responses, given by the expression:

$$\rho^{pred}(t_1) = \rho^{meas}(t_1) + \frac{Var\left[\rho^{meas}(t_1)\right]\left[\rho^{comp}(t_1) - \rho^{meas}(t_1)\right]}{Var\left[\rho^{comp}(t_1)\right] + Var\left[\rho^{meas}(t_1)\right]}; \tag{2.114}$$

The above expression can be recast in the form

$$\rho^{pred}(t_1) - \rho^{meas}(t_1) = x\left[\rho^{comp}(t_1) - \rho^{meas}(t_1)\right], \tag{2.115}$$

with

$$0 \le x \triangleq \frac{Var\left[\rho^{meas}(t_1)\right]}{Var\left[\rho^{comp}(t_1)\right] + Var\left[\rho^{meas}(t_1)\right]} \le 1; \tag{2.116}$$

As Eqs. (2.115) and (2.116) indicate, if the measurement is performed with perfect accuracy,
then $Var\left[\rho^{meas}(t_1)\right] = 0$ and, consequently, $\rho^{pred}(t_1) = \rho^{meas}(t_1)$. In other words, the
predicted values for the responses coincide when there is no variance in measured values,
since the model's uncertain parameters are calibrated with the measured values This yields
similar results when the computation is assumed to be perfect since $Var\left[\rho^{comp}(t_1)\right] = 0$ and
$\rho^{pred}(t_1) = \rho^{comp}(t_1)$. Meaning the experimental measurements would have no effect on the
predictions since imperfect measurements could not possibly improve a "perfect" model's
predictions. Finally, if both the computation and the experiment are affected by uncertainties,
then Eqs. (2.115) and (2.116) indicate that the predicted response value falls, as would be
expected, between the computed and measured response values, i.e.,

$$\rho^{meas}(t_1) \le \rho^{pred}(t_1) \le \rho^{comp}(t_1), \tag{2.117}$$

The above argument has tacitly assumed that both the computed and measured responses
have positive nominal values; for responses that have negative nominal values, the above
argument is repeated using the responses' absolute values, leading to the same general
conclusion.

4. Predicted variances/covariance for the predicted responses values, which is obtained from the expression:

$$Var\left[\rho^{pred}(t_1)\right] = Var\left[\rho^{meas}(t_1)\right] - \frac{\left\{Var\left[\rho^{meas}(t_1)\right]\right\}^2}{Var\left[\rho^{comp}(t_1)\right] + Var\left[\rho^{meas}(t_1)\right]}; \qquad (2.118)$$

The above expression can be used show that

$$Var\left[\rho^{pred}(t_1)\right] - Var\left[\rho^{meas}(t_1)\right] < 0, \quad Var\left[\rho^{pred}(t_1)\right] - Var\left[\rho^{comp}(t_1)\right] < 0, \qquad (2.119)$$

which indicates that the predicted standard deviation will be smaller that both the measured and the computed response standard deviations, respectively; in this sense, the uncertainties in the predicted response will reduce by comparison to the uncertainties for both the computed and the measured response.

5. Predicted correlations, $\mathbf{C}_{\alpha r}^{pred}$, between the predicted model parameters and responses:

$$\mathbf{C}_{\alpha r}^{pred} = \left(\mathbf{C}_{\alpha\alpha}\mathbf{S}_{r\alpha}^{\dagger}\right)\frac{Var\left[\rho^{meas}(t_1)\right]}{Var\left[\rho^{comp}(t_1)\right] + Var\left[\rho^{meas}(t_1)\right]}, \qquad (2.120)$$

or, in component form, for each $i = 1,...,N_\alpha + 1$,

$$Corr\left[\alpha_i^{pred}, \rho^{pred}(t_1)\right] = \frac{Var\left[\rho^{meas}(t_1)\right]}{Var\left[\rho^{comp}(t_1)\right] + Var\left[\rho^{meas}(t_1)\right]}\sum_{j=1}^{N_\alpha+1}\frac{\partial\rho(t_1)}{\partial\alpha_j}\mathrm{cov}\left(\alpha_i,\alpha_j\right);$$

$$(2.121)$$

As indicated by the expressions in Eqs. (2.120) or (2.121), even if the response is "a priori" uncorrelated with the model parameters [i.e., $Corr\left[\alpha_i,\rho(t_1)\right] = 0$], an imperfect measurement [i.e., $Var\left[\rho^{meas}(t_1)\right] \neq 0$] will introduce non-zero posterior correlations [i.e., $Corr\left[\alpha_i^{pred},\rho^{pred}(t_1)\right] \neq 0$] between the predicted calibrated parameter values and the predicted "best-estimate" response. Only if the measurement(s) were perfect would initially uncorrelated response-parameters remain uncorrelated after the measurements, in which case the predicted responses would also coincide with the measured ones as was discussed in item 3, above.

6. The methodology of Cacuci and Ionescu-Bujor (2010a) also provides the consistency indicator

$$\chi^2 \triangleq \frac{\left[\rho^{comp}(t_1) - \rho^{meas}(t_1)\right]^2}{Var\left[\rho^{comp}(t_1)\right] + Var\left[\rho^{meas}(t_1)\right]}, \qquad (2.122)$$

For a single measurement, the above consistency indicator is helpful to identify possibly inconsistent data such as when the "distance" between the measurement and computation is larger than the sum of the respective standard deviations of the computed and measured responses, i.e., when $\left|\rho^{comp}(t_1) - \rho^{meas}(t_1)\right| > Std.Dev.\left[\rho^{meas}(t_1)\right] + Std.Dev.\left[\rho^{comp}(t_1)\right]$ due to unrecognized errors. Cacuci and Ionescu-Bujor (2010a) addressed such situations, but this is not the case for the spent fuel dissolver model developed and studied in the remainder of this work.

In the "inverse predictive modeling" mode, the methodology of Cacuci and Ionescu-Bujor (2010b) would use measurements in order to identify unknown parameters α_i. For the surrogate dissolver model, the "inverse predictive mode" would use Eq. (2.110) iteratively, starting the iteration using an "initial estimate", $\left(\alpha_i^0\right)^{estimated}$, instead of the (known –in the forward mode) nominal value α_i^0. In other words, in the "inverse predictive mode", Eq. (2.110) would be replaced, for the initial iteration, by the equation

$$\alpha_i^{pred} = \left(\alpha_i^0\right)^{estimated} - \frac{\left[\rho^{comp}(t_1) - \rho^{meas}(t_1)\right]}{Var\left[\rho^{comp}(t_1)\right] + Var\left[\rho^{meas}(t_1)\right]} \sum_{j=1}^{N_\alpha+1} \frac{\partial \rho(t_1)}{\partial \alpha_j} cov\left(\alpha_i, \alpha_j\right); \qquad (2.123)$$

Subsequently, all of the quantities in Eqs. (2.110) through (2.122) would be computed repeatedly, using the newly computed "predicted values" to replace the corresponding values obtained in the previous iteration, until the computed values would agree with the corresponding measured values, within an "a priori" user-selected error criterion.

2.5. Correspondences between the Surrogate and the Dissolver Models: Highlighting the Novel Results Produced within this Work

The purpose of this sub-section is to establish correspondences between simpler surrogate dissolver which models the time-dependent behavior of the nitric acid concentration in the full dissolver's compartment #8, at the dissolver's inlet with the full model of the time-dependent behavior of the volumetric mass density of the liquid phase, and the volumetric mass concentration of nitric acid which comprises 16 nonlinear time-dependent differential equations, including 1291 model parameters, and describe the time-variation of the dissolver's state variables in the dissolver's 8 compartments. The surrogate was used to emphasize the methods over handling the sheer numbers of terms that would document both the method and the results, especially for the higher order response sensitivities.

Section 2.3 presented the application of the Adjoint Sensitivity Analysis Method (ASAM) developed by Cacuci (1981.a) to the surrogate, and the ASAM is applied again in Chapter 4 to the full dissolver model to obtain the sensitivities of the nitric acid concentrations in all of the dissolver's compartments to the model parameters. The use of Legendre Polynomials for computing spectral expansions of the responses reduce drastically, by a factor of almost 20, the number of adjoint computations with a loss of accuracy of less than 0.1%.

The application of the predictive modeling methodology of Cacuci and Ionescu-Bujor (2010b) to the surrogate dissolver model illustrated in Section 2.4 shows assimilating even a single consistent experimental measurement results in calibrated model parameters with reduced standard deviations and best-estimate predicted responses that are smaller than either the measured or original computations. In Chapter 5, the predictive modeling methodology of Cacuci and Ionescu-Bujor (2010b) is applied in the *forward* mode to the full dissolver model, with a drastic reduction of the standard deviations of the predicted acid concentration responses and calibrated model parameters, respectively. The model developed in Chapter 3, the sensitivity analysis presented in Chapter 4, and the forward predictive modeling results presented in Chapter 5 are all original, as underscored by their recent publication in the oldest and still highest-impact world-leading nuclear engineering journal:

81

1. James J. Peltz and Dan G. Cacuci "Predictive Modeling Applied to a Paradigm Spent Fuel Dissolver Model: I. Adjoint Sensitivity Analysis," *Nucl. Sci. Eng*., **183**, 305-331. dx.doi.org/10.13182/NSE15-98.

2. James J. Peltz, Dan G. Cacuci, Aurelian F. Badea, and Madalina C. Badea, "Predictive Modeling Applied to a Paradigm Spent Fuel Dissolver Model: II. Uncertainty Quantification and Reduction," *Nucl. Sci. Eng*., **183**, 332-346. dx.doi.org/10.13182/NSE15-99.

The application of the methodology of Cacuci and Ionescu-Bujor (2010b) for *inverse predictive modeling*, e.g., for determining a parameter of the surrogate dissolver model from an experimental measurement is illustrated in Section 2.4. In Chapter 6 of this work, the *inverse predictive modeling* of the dissolver's time-dependent *inlet* acid concentration results mathematically in a boundary condition for the dissolver model by considering measurements of the nitric acid concentration response in the compartment furthest from the inlet boundary. All of the results reported in Chapter 6 are original, as underscored by the acceptance for their publication in the journal article below:

3. J. J. Peltz and D. G. Cacuci, "Inverse Predictive Modeling of a Spent Fuel Dissolver Model," *Nucl. Sci. Eng*, accepted, April 2016.

The following conclusions were highlighted in Section 2.3:

(i)   If the second- and higher-order sensitivities are unavailable, then the expectation value of the response is the same as the computed value of the response.

(ii)   It the triple-correlations, $t_{ij\mu}$, for the parameters are unavailable, then the third-order response moment, $\mu_3\left[\rho(t_1)\right]$, cannot be computed; hence, it would not be possible to assess the asymmetries in the resulting response distribution.

(iii)   If the second- and higher-order sensitivities are unavailable, and the distribution of the parameters is normal or symmetric with respect to its mean, then $t_{ij\mu} = 0$ and the response distribution would appear to be symmetric. Consequently, for

normal or symmetric parameter distributions any asymmetries in the response distribution could only be assessed if the 2nd-order sensitivities were available.

Clearly, the quantification of non-Gaussian features of responses necessitates the computation of the 2nd-order responses sensitivities to the model parameters. Section 7.1 presents *a new method, using adjoint operators*, for computing most efficiently the exact 2nd-order sensitivities of the acid concentration in the surrogate dissolver model. This new adjoint method extends the 1st-order ASAM, and enables the computations of all of the 2nd-order response sensitivities exactly and efficiently, requiring at most $(N_\alpha + 1)$ adjoint computations, as opposed to $(N_\alpha + 1)(N_\alpha + 2)/2$ forward computations that are require if the 2nd-order sensitivities are computed using finite-difference formulas. It will also be shown in Chapter 7 that the *2nd-order sensitivities have the following impacts on the moments of the response distribution:*

(a) They cause the "expected value of the response" to differ from the "computed nominal value of the response";

(b) They contribute to the response variances and covariance; however, since the contributions involving the second-order sensitivities are multiplied by the fourth power of the parameters' standard deviations, the total of these contributions is expected to be relatively smaller than the contributions stemming from the first-order response sensitivities;

(c) They provide the leading contributions to the third-order moment, $\left[\mu_3 (r_k) \right]^{UG}$, and – hence-- skewness a response that depends on *uncorrelated and normally distributed* parameters.

In the case of the full dissolver model developed and analyzed in this work, Gaussian-based confidence intervals would be very misleading for the times into the transient behavior of the acid concentration in the dissolver, particularly around the middle of the transient (around 3.5 to 4.5 hours after the initiation of the transient) and towards the last third of the transient (after 6 to 7.5 hours) that lasts for 10.5 hours, since the response skewness becomes large and

negative over these times. Different procedures, based on chi-squared (with few degrees of freedom) or other asymmetric distributions would need to be used for establishing confidence intervals at these particularly important times. The results presented in Chapter 7 emphasize the importance of quantifying, as exactly as possible, 1st-order, but also the 2nd-order sensitivities of responses with respect to all of the model parameters if this information were going to be used for decisions which demanded a high degree of confidence. In the absence of the 2nd-order sensitivities, non-linear features, such as asymmetries could not be identified in the response distributions. *The material presented in Chapter 7 is entirely new, and will be submitted for publication after the deposition of this work.*

Finally, it should be mentioned that the accuracy of the adjoint functions computed using the ASAM for the full dissolver model has been verified by forward computations; the results of these "solution verification" computations are presented in Appendix A. Finally, Appendix B presents the description of the forward and inverse predictive modeling software module that was developed to obtain all of the numerical results presented in this work.

3. MATHEMATICAL MODELING OF A ROTARY DISSOLVER START-UP

The "case study" investigated in this dissertation is a modification by Peltz and Cacuci (2015) of the model of a rotary dissolver of used nuclear fuel originally developed by Lewis and Weber (1980). This model is depicted in Figures 3.1 and 3.2. The liquid flows through the dissolver's eight compartments labeled using the superscript $k = 1,...,8$. Compartment #9 exists but is used for rinsing, and thus is not relevant to this work.
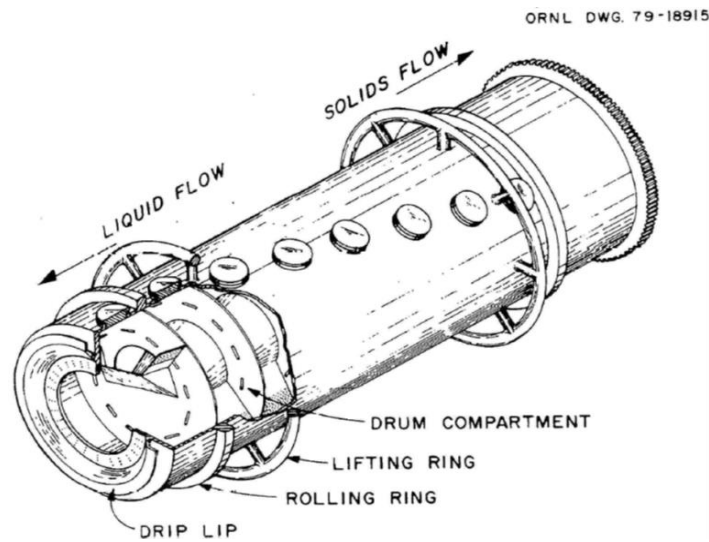
Figure 3.1 Cutaway view of the rotary dissolver drum [after Lewis and Webber, 1980]
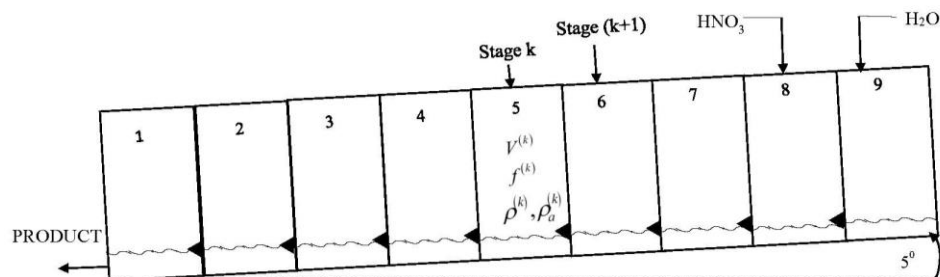
Figure 3.2 Liquid flow diagram for the compartmented rotary dissolver [after Lewis and Weber, 1980]

The start-up conditions for the dissolver involve a non-ideal mixture of nitric acid and water at ambient conditions. The temporal and spatial variation of the physico-chemical processes occurring within the dissolver were modeled mathematically by Lewis and Weber (1980) by means of nonlinear coupled first-order time-dependent differential equations describing: (A) mass conservation of a non-ideal mixture of nitric acid and water at ambient conditions; (B) resistance to fluid flowing through the compartments; and (C) an equation of state, as follows:

(A) The equations modeling conservation of mass:

Total mass: $\dfrac{d}{dt}\left[\rho^{(k)}V^{(k)}\right] = -\rho^{(k)}(t)f^{(k)}(t) + \rho^{(k+1)}(t)f^{(k+1)}(t), \;\; k = 1,...,7, \;\; 0 < t \le t_f,$ (3.1)

Acid mass: $\dfrac{d}{dt}\left[\rho_a^{(k)}V^{(k)}\right] = -\rho_a^{(k)}(t)f^{(k)}(t) + \rho_a^{(k+1)}(t)f^{(k+1)}(t), \;\; k = 1,...,7, \;\; 0 < t \le t_f,$ (3.2)

Total mass in compart. 8: $\dfrac{d}{dt}\left[\rho^{(8)}V^{(8)}\right] = -\rho^{(8)}(t)f^{(8)}(t) + \dot{m}^{(in)}(t), \; 0 < t \le t_f,$ (3.3)

Acid mass in compart. 8: $\dfrac{d}{dt}\left[\rho_a^{(8)}V^{(8)}\right] = -\rho_a^{(8)}(t)f^{(8)}(t) + \rho_a^{in}(t)f^{(in)}(t), \; 0 < t \le t_f,$ (3.4)

The quantities appearing in the above equations are defined as follows: (i) the index $k = 1,...,8$ denotes the respective dissolver compartment; (ii) $V^{(k)}(t)$ denotes the volume of the liquid phase, in units of liters $[L]$; (iii) $\rho^{(k)}(t)$ denotes the volumetric mass density of the liquid phase, in units of gram/liter $[g/L]$; (iv) $\rho_a^{(k)}(t)$ denotes the volumetric mass concentration of nitric acid of the liquid phase, in units of $[g/L]$ in the solution; (v) $f^{(k)}(t)$ denotes the volumetric flow rate of the liquid mixture, in units of liter/hour $[L/h]$; and (vi) $\dot{m}^{(in)}(t)$ denotes the liquid solution mass rate inflow in units of gram/hour $[g/h]$.

(B) Resistance to fluid flow through the compartments:

$\dfrac{d}{dt}\left[V^{(k)}(t)\right] = -C\left(V^{(k)}\right) + f^{(k+1)}(t), \;\; k = 1,...,7, \;\; 0 < t \le t_f,$ (3.5)

86

$$\frac{d}{dt}\left[V^{(8)}(t)\right] = -C\left(V^{(8)}\right) + f^{(in)}(t), \ \ 0 < t \le t_f, \tag{3.6}$$

where

$$C\left(V^{(k)}\right) = \begin{cases} \left(\dfrac{V^{(k)} - V_0}{G}\right)^p \ [\text{L/h}], & \text{if } \ V^{(k)}(t) - V_0 > 0, \ \ k = 1,...,8, \\ 0, & \text{otherwise.} \end{cases} \tag{3.7}$$

In the above relation, the scalar quantities G, V_0 and p are experimentally determined parameters, with nominal (mean) values and estimated relative standard deviations presented in Table 3.1. Note that due to counter-flow conditions in the dissolver, the flow-inlet parameters $\dot{m}^{(in)}(t)$, $\rho_a^{(in)}(t)$, and $f^{(in)}(t)$ appear in compartment $k = 8$ [cf. Eqs. (3.3), (3.4) and (3.6)], rather than in compartment $k = 1$.

(C) An *Equation of state,* is needed to complete Eqs. (3.1) - (3.7), in order to obtain a well-posed mathematical model. For the rotary dissolver considered here, the equation of state takes on the linear form

$$\rho^{(k)}(t) = 63a\rho_a^{(k)}(t) + b, \ \ k = 1,...,8. \tag{3.8}$$

where a and b are experimentally determined scalar parameters with nominal (mean) values and estimated relative standard deviations also presented in Table 3.1. The time-dependent variations of the inlet mass flow rate of solution, $\dot{m}^{(in)}(t)$, and inlet nitric mass concentration, $\rho_a^{(in)}(t)$, are presented in Figures 3.3 and 3.4, respectively. The estimated relative standard deviations of $\rho_a^{(in)}(t)$ and $\dot{m}^{(in)}(t)$ are based on "expert opinion" following a search of the relevant literature, and are presented in Table 3.1.

Table 3.1 Nominal (mean) values and corresponding standard deviations for model parameters

Para-Meter	$\rho_a^{(in)}(t)$	$\dot{m}^{(in)}(t)$	a	b	V_0	p	G
Nominal value	See Fig. 3.4	See Fig. 3.3	0.48916	1001.2 $[g/L]$	4.8 $[L]$	2.7	0.201941 $[L]$
Standard deviation	20%	10%	10%	10%	10%	10%	10%

Figure 3.3 depicts the time variation of the solution's inlet mass flow rate, and Figure 3.4 depicts the time variation of the nitric acid concentration. The time-dependent nominal value of the inflow volumetric flow rate, $f^{(in)}(t)$, is obtained from the following expression:

$$f^{(in)}(t) = \dot{m}^{(in)}(t)\big/\rho^{(k)}(t) = \dot{m}^{(in)}(t)\left[63a\rho_a^{(in)}(t)+b\right]^{-1},$$
(3.9)

which uses the equation of state, the inflow mass rate from Figure 3.3, and the time dependent nitric acid mass concentration data from Figure 3.4. In particular, the initial nominal value of $f^{(in)}(t)$ is $f^{(in)}(0) = 36.79 \times 10^3 / 1001.2$ at $t = 0$.
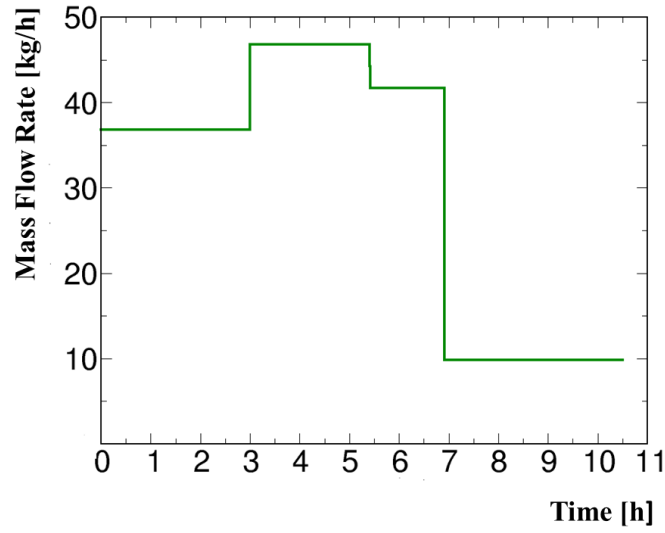
Figure 3.3 Time variation of the inlet mass flow rate, $\dot{m}^{(in)}(t)/1000\,[\mathrm{kg/h}]$
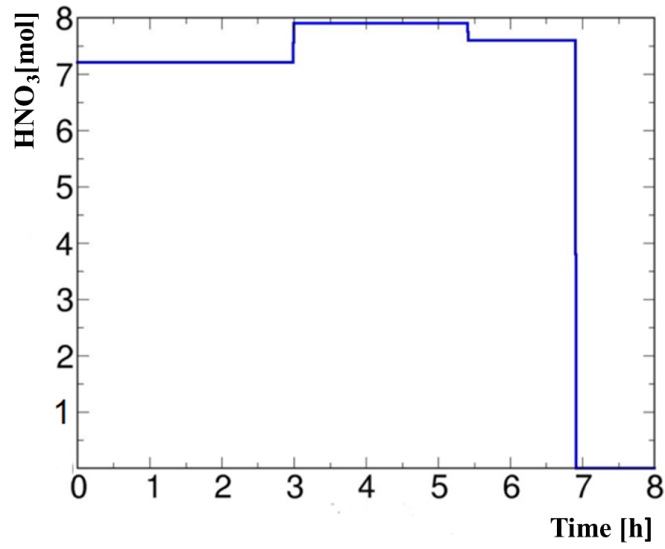
Figure 3.4 Time variation of the inlet nitric acid mass concentration $\rho_a^{(in)}(t)/63\,[\mathrm{mol}]$

Using the equation of state (3.8), the volumetric mass density of the liquid phase, $\rho^{(k)}(t)$, algebraically simplifies Eqs. (3.1) - (3.6), as follows:

$$V^{(k)}(t)\frac{d}{dt}\left[\rho_a^{(k)}\right]+\left[\rho_a^{(k)}(t)-\rho_a^{(k+1)}(t)\right]C\left[V^{(k+1)}(t)\right]=0,\ k=1,...,7,\ 0<t\le t_f,\ (3.10)$$

$$V^{(8)}(t)\frac{d}{dt}\left[\rho_a^{(8)}\right]+\rho_a^{(8)}(t)f^{(in)}(t)=\rho_a^{in}(t)f^{(in)}(t), \ 0<t\leq t_f. \tag{3.11}$$

$$\frac{d}{dt}\left[V^{(k)}(t)\right]=-C\left[V^{(k)}(t)\right]+C\left[V^{(k+1)}(t)\right], \ k=1,...,7, \ 0<t\leq t_f, \tag{3.12}$$

$$\frac{d}{dt}\left[V^{(8)}(t)\right]=-C\left[V^{(8)}(t)\right]+f^{(in)}(t), \ 0<t\leq t_f. \tag{3.13}$$

The initial conditions for Eqs. (3.10) through (3.13) are as follows:

$$\rho_a^{(k)}(0)=\rho_{a0}^{(k)}=0.0, \ V^{(k)}(0)=V_0^{(k)}, \quad k=1,...,8. \tag{3.14}$$

The compatibility condition for a fully developed initial flow implies that $\frac{d}{dt}V^{(k)}(0)=0, \ k=1,...,8$; in turn, this condition implies that

$$V_0^{(k)}\equiv G\left[f^{(in)}(0)\right]^{1/p}+V_0, \quad k=1,...,8. \tag{3.15}$$

The nitric acid concentration in compartment 1, $\rho_a^{(1)}(t)$, has been measured (Lewis and Weber, 1980) at 635 instances in time over a period of 10.5 hours. The nominal values of these measurements are denoted as $\rho_{a,meas}^{(1)}(t_i)$, and are depicted using blue circles in Figure 3.6. Notably, these experimental results are unique in the open literature for a rotary dissolver. The relative standard deviation of each of these measurements has been estimated to be 5%.

For the subsequent developments in this work, it is convenient consider the model's state functions and parameters to be the components of two vectors, respectively, defined as follows:

$$\mathbf{u}(t)\equiv\left[\rho_a^{(1)}(t),...,\rho_a^{(8)}(t),V^{(1)}(t),...,V^{(8)}(t)\right] \tag{3.16}$$

$$\begin{aligned}\boldsymbol{\alpha}(t)\equiv(\alpha_1,...,\alpha_{1291})\equiv&\left[\rho_a^{(in)}(t_1),...,\rho_a^{(in)}(t_{635}),\dot{m}^{(in)}(t_1),...,\dot{m}^{(in)}(t_{635}),\right.\\&\left.\rho_a^{(1)}(0),...,\rho_a^{(8)}(0),V^{(1)}(0),...,V^{(8)}(0),a,b,V_0,p,G\right].\end{aligned} \tag{3.17}$$

It is also convenient to denote the *nominal values* of the model's state functions and parameters by using the superscript "0":

$$\mathbf{u}^0(t) \triangleq \left[\rho_{a,nom}^{(1)}(t),...,\rho_{a,nom}^{(8)}(t),V_{nom}^{(1)}(t),...,V_{nom}^{(8)}(t) \right] \tag{3.18}$$

$$\begin{aligned}
\boldsymbol{\alpha}^0(t) &\triangleq \left(\alpha_1^0,...,\alpha_{1291}^0 \right) \triangleq \left[\rho_{a,nom}^{(in)}(t_1),...,\rho_{a,nom}^{(in)}(t_{635}),\dot{m}_{nom}^{(in)}(t_1),...,\dot{m}_{nom}^{(in)}(t_{635}), \right. \\
&\left. \rho_{a,nom}^{(1)}(0),...,\rho_{a,nom}^{(8)}(0),V_{nom}^{(1)}(0),...,V_{nom}^{(8)}(0),a^0,b^0,V_0^0,p^0,G^0 \right].
\end{aligned} \tag{3.19}$$

Solving Eqs. (3.10) – (3.15) using *nominal values for the model's parameters* [as listed in Table 3.1] yields the time-dependent evolution of *the computed nominal value of the nitric acid concentration*. In particular, the computed nominal values for $\rho_{a,nom}^{(1)}(t)$, $\rho_{a,nom}^{(4)}$, and $\rho_{a,nom}^{(7)}$, of the time-dependent acid concentrations in compartments #1, #4, and #7, respectively, are depicted in Figure 3.5. The time evolutions of these concentrations are similar to each other although time-delayed as expected, and also similar to the time variation, depicted in Figure 3.4, of the inlet nitric acid mass concentration, $\rho_a^{(in)}(t)$. Figure 3.6 depicts the time-evolution of the normalized nominal values of the computed response of the nitric acid concentration, $\rho_{a,nom}^{(1)}(t)\,[\text{mol/L}]$ (red-colored graph), together with the corresponding normalized measurements (Lewis and Weber, 1980), denoted as $\rho_{a,meas}^{(1)}(t_i)$ and depicted using blue circles. The agreement between the computed and experimentally measured values is remarkable.
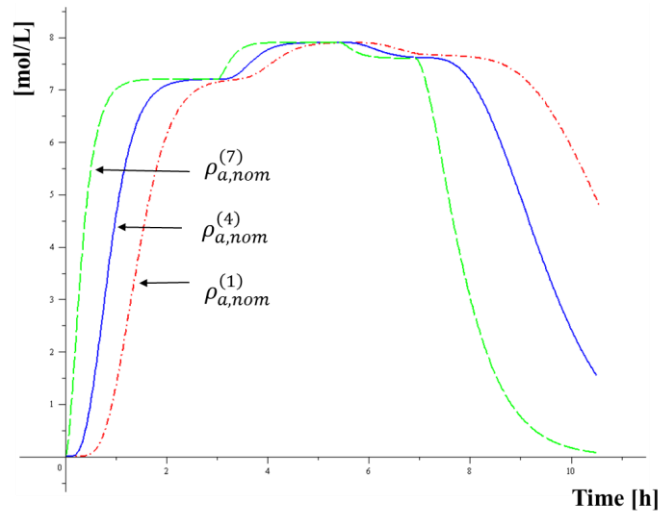
Figure 3.5 Time-evolution of the nominal values of the computed nitric acid concentrations in $[\text{mol/L}]$, for $\rho_{a,nom}^{(1)}$, $\rho_{a,nom}^{(4)}$, $\rho_{a,nom}^{(7)}$, in compartments #1, #4, and #7, respectively
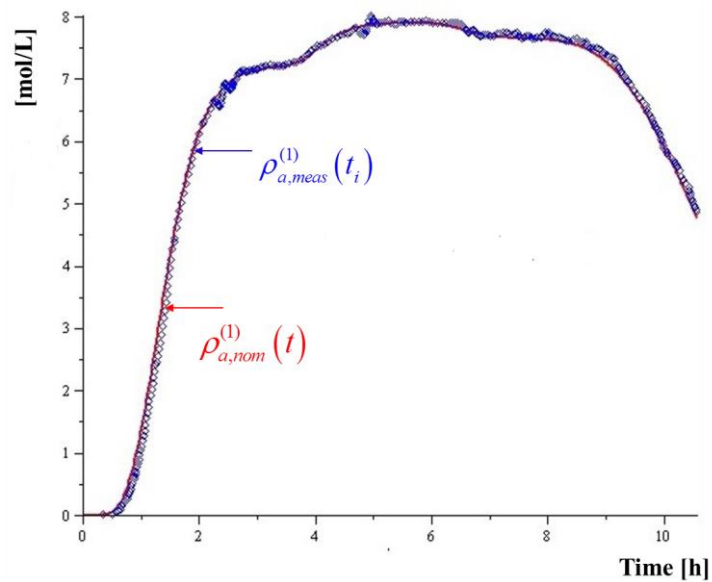
Figure 3.6 Red graph: time-evolution of the nominal values of the computed response of the nitric acid concentration $[\text{mol/L}]$, $\rho_{a,nom}^{(1)}(t)$. Blue circles: experimentally measured nominal values, $\rho_{a,meas}^{(1)}(t_i)$, of the nitric acid concentration $[\text{mol/L}]$, over a period of 10.5 hours (Lewis and Weber, 1980)

92

4. ADJOINT SENSITIVITY ANALYSIS OF TIME-DEPENDENT ACID CONCENTRATIONS IN THE DISSOLVER MODEL

The equations underlying the dissolver model considered in this work, cf. Eqs. (3.10) – (3.14), comprise sixteen state variables, namely $\left[\rho_a^{(1)}(t),...,\rho_a^{(8)}(t),V^{(1)}(t),...,V^{(8)}(t) \right]$. They also comprise 1291 model parameters, as follows:

(i) The 5 scalar parameters a,b,V_0,p,G, which appear in the correlations characterizing the fluid's equation of state, and have nominal values and standard deviations as presented in Table 3.1;

(ii) The 8 initial values, denoted as $\rho_a^{(1)}(0),...,\rho_a^{(8)}(0)$, of the acid volumetric mass concentration of nitric acid of the liquid phase in compartments #1 through #8;

(iii) The 8 initial values, denoted as $V^{(1)}(0),...,V^{(8)}(0)$, of the volumes of the liquid phase in compartments #1 through #8;

(iv) The inlet mass flow rate of solution at 635 time instances, denoted as $\dot{m}^{(in)}(t_1),...,\dot{m}^{(in)}(t_{635})$ and depicted in Figure 3.3;

(v) The acid volumetric mass concentration of nitric acid of the liquid phase at 635 time instances, denoted as $\rho_a^{(in)}(t_1),...,\rho_a^{(in)}(t_{635})$ and depicted in Figure 3.4.

4.1. Mathematical Derivation of the Adjoint Sensitivity Analysis System for Scalar-Valued Responses

In sensitivity analysis, it is customary to refer to the results of interest as "*system responses*" or "*model responses*". The *sensitivity analysis* of system responses entails *the computation and analysis of the functional derivatives* of these responses with respect to all of the model parameters; these functional derivatives are called "response *sensitivities*." The sensitivities

can subsequently be used for quantifying the uncertainties caused in the responses by parameter uncertainties, and for reducing such uncertainties by combining computational and experimental information. For the sensitivity analysis of the dissolver model, it is convenient to consider that the (yet unspecified) variations in the model parameters are components of the $N_\alpha = 1291$-component vector $\mathbf{h}_\alpha(t)$ defined as follows:

$$
\begin{aligned}
\mathbf{h}_\alpha(t) &\triangleq (h_1,...,h_{1291}) \triangleq \Big[\Delta\rho_a^{(in)}(t_1),...,\Delta\rho_a^{(in)}(t_{635}), \Delta\dot{m}^{(in)}(t_1),...,\Delta\dot{m}^{(in)}(t_{635}), \\
&\quad \Delta\rho_a^{(1)}(0),...,\Delta\rho_a^{(8)}(0), \Delta V^{(1)}(0),...,\Delta V^{(8)}(0), \Delta a, \Delta b, \Delta V_0, \Delta p, \Delta G \Big].
\end{aligned}
\tag{4.1}
$$

Variations $\mathbf{h}_\alpha(t)$ in the model parameters will cause variations in the state functions; these variations will be considered to be the components of the vector $\mathbf{h}_u(t)$ defined below:

$$
\mathbf{h}_u(t) \triangleq \Big[\mathbf{h}_\rho(t), \mathbf{h}_V(t) \Big], \ \mathbf{h}_\rho(t) \triangleq \Big[\Delta\rho_a^{(1)}(t),...,\Delta\rho_a^{(8)}(t) \Big], \ \mathbf{h}_V(t) \triangleq \Big[\Delta V^{(1)}(t),...,\Delta V^{(8)}(t) \Big].
\tag{4.2}
$$

Altogether, the variations in the model's parameters and state functions will cause variations in the model responses of interest. A general representation of a *scalar-valued response* associated with the dissolver model, such as a measurement of a dissolver's state-function, is achieved by the following integral form

$$
R(\mathbf{u},\boldsymbol{\alpha}) = \int_0^{t_f} F(\mathbf{u},\boldsymbol{\alpha})\, dt,
\tag{4.3}
$$

where $F(\mathbf{u},\boldsymbol{\alpha})$ is some function of the model's state variables $\mathbf{u}(t)$ and parameters $\boldsymbol{\alpha}(t)$. As shown be Cacuci (1981.a, 1981.b), the most general definition of the (first-order) sensitivity of an operator-valued quantity of interest, denoted as $R(\mathbf{u},\boldsymbol{\alpha})$, to variations $(\mathbf{h}_u, \mathbf{h}_\alpha)$ in the model's state functions and parameters is given by the Gâteaux- (G)-differential $\delta R(\mathbf{u}^0, \boldsymbol{\alpha}^0; \mathbf{h}_u, \mathbf{h}_\alpha)$ of the response $R(\mathbf{u},\boldsymbol{\alpha})$ at $(\mathbf{u}^0, \boldsymbol{\alpha}^0)$ with "increments" or "variations" $(\mathbf{h}_u, \mathbf{h}_\alpha)$; the 1$^{\text{st}}$-order G-differential $\delta R(\mathbf{u}^0, \boldsymbol{\alpha}^0; \mathbf{h}_u, \mathbf{h}_\alpha)$ is defined as follows:

$$\delta R\left(\mathbf{u}^{0},\boldsymbol{\alpha}^{0};\mathbf{h}_{u},\mathbf{h}_{\alpha}\right) \triangleq \left\{\frac{d}{d\varepsilon}\left[R\left(\mathbf{u}^{0}+\varepsilon\mathbf{h}_{u};\boldsymbol{\alpha}^{0}+\varepsilon\mathbf{h}_{\alpha}\right)\right]\right\}_{\varepsilon=0}$$

$$= \int_{0}^{t_{f}}\left\{\left[\frac{\partial F\left(\mathbf{u},\boldsymbol{\alpha}\right)}{\partial \mathbf{u}}\right]_{\left(\mathbf{u}^{0},\boldsymbol{\alpha}^{0}\right)}\mathbf{h}_{u}+\left[\frac{\partial F\left(\mathbf{u},\boldsymbol{\alpha}\right)}{\partial \boldsymbol{\alpha}}\right]_{\left(\mathbf{u}^{0},\boldsymbol{\alpha}^{0}\right)}\mathbf{h}_{\alpha}\right\}dt$$

$$= \sum_{k=1}^{8}\int_{0}^{t_{f}}\left\{\left[\frac{\partial F\left(\mathbf{u},\boldsymbol{\alpha}\right)}{\partial \rho_{a}^{(k)}\left(t\right)}\right]_{\left(\mathbf{u}^{0},\boldsymbol{\alpha}^{0}\right)}\Delta\rho_{a}^{(k)}\left(t\right)+\left[\frac{\partial F\left(\mathbf{u},\boldsymbol{\alpha}\right)}{\partial V^{(k)}\left(t\right)}\right]_{\left(\mathbf{u}^{0},\boldsymbol{\alpha}^{0}\right)}\Delta V^{(k)}\left(t\right)\right\}dt \tag{4.4}$$

$$+ \sum_{i=1}^{N_{\alpha}=1291}\int_{0}^{t_{f}}\left\{\left[\frac{\partial F\left(\mathbf{u},\boldsymbol{\alpha}\right)}{\partial \alpha_{i}\left(t\right)}\right]_{\left(\mathbf{u}^{0},\boldsymbol{\alpha}^{0}\right)}h_{i}\right\}dt.$$

The sensitivity $\delta R\left(\mathbf{u}^{0},\boldsymbol{\alpha}^{0};\mathbf{h}_{u},\mathbf{h}_{\alpha}\right)$ is also an operator, defined on the same domain and with the same range as $R\left(\mathbf{u},\boldsymbol{\alpha}\right)$. Since the system's state vector $\mathbf{u}(t)$ and parameters $\boldsymbol{\alpha}(t)$ are related to each other through Eqs. (2.10) - (2.14), it follows that the vectors of variations $\mathbf{h}_{u}(t)$ and $\mathbf{h}_{\alpha}(t)$ are also related to each other. Therefore, the sensitivity $\delta R\left(\mathbf{u}^{0},\boldsymbol{\alpha}^{0};\mathbf{h}_{u},\mathbf{h}_{\alpha}\right)$ of a quantity of interest can be evaluated only after determining the vector of variations $\mathbf{h}_{u}(t)$ in terms of the vector of parameter variations $\mathbf{h}_{\alpha}(t)$. The first-order relationship between $\mathbf{h}_{u}(t)$ and $\mathbf{h}_{\alpha}(t)$ is determined by taking the G-differentials of Eqs. (2.10) - (2.14). Performing these operations yields the following systems of differential equations:

$$V_{nom}^{(k)}\left(t\right)\frac{d\left[\Delta\rho_{a}^{(k)}\left(t\right)\right]}{dt}+C\left[V_{nom}^{(k+1)}\left(t\right)\right]\left[\Delta\rho_{a}^{(k)}\left(t\right)\right]-C\left[V_{nom}^{(k+1)}\left(t\right)\right]\left[\Delta\rho_{a}^{(k+1)}\left(t\right)\right]$$

$$+\left[\frac{d\rho_{a}^{(k)}\left(t\right)}{dt}\right]_{nom}\left[\Delta V^{(k)}\left(t\right)\right]+\left[\rho_{a,nom}^{(k)}\left(t\right)-\rho_{a,nom}^{(k+1)}\left(t\right)\right]\left[\frac{dC\left[V^{(k+1)}\left(t\right)\right]}{dV^{(k+1)}\left(t\right)}\right]_{nom}\left[\Delta V^{(k+1)}\left(t\right)\right] \tag{4.5}$$

$$= q_{\rho}^{(k)}\left(t\right),\quad k=1,...,7,\ 0<t\le t_{f};$$

$$V_{nom}^{(8)}\left(t\right)\frac{d\left[\Delta\rho_{a}^{(8)}\left(t\right)\right]}{dt}+f_{nom}^{(in)}\left(t\right)\left[\Delta\rho_{a}^{(8)}\left(t\right)\right]$$

$$+\left[\frac{d\rho_{a}^{(8)}\left(t\right)}{dt}\right]_{nom}\left[\Delta V^{(8)}\left(t\right)\right]=q_{\rho}^{(8)}\left(t\right),\ 0<t\le t_{f}; \tag{4.6}$$

95

$$\frac{d\left[\Delta V^{(k)}(t)\right]}{dt} + \left[\frac{dC\left[V^{(k)}(t)\right]}{dV^{(k)}(t)}\right]_{nom} \left[\Delta V^{(k)}(t)\right]$$

$$-\left[\frac{dC\left[V^{(k+1)}(t)\right]}{dV^{(k+1)}(t)}\right]_{nom} \left[\Delta V^{(k+1)}(t)\right] = q_V^{(k)}(t), \quad k=1,...,7, \ 0 < t \le t_f; \tag{4.7}$$

$$\frac{d\left[\Delta V^{(8)}(t)\right]}{dt} + \left[\frac{dC\left[V^{(8)}(t)\right]}{dV^{(8)}(t)}\right]_{nom} \left[\Delta V^{(8)}(t)\right] = q_V^{(8)}(t), \ 0 < t \le t_f, \tag{4.8}$$

$$\Delta \rho_a^{(k)}(0) = \Delta \rho_{a0}^{(k)}, \quad k=1,...,8,$$

$$\Delta V^{(k)}(0) \triangleq \Delta V_0^{(k)} \triangleq (\Delta G)\left[f_{nom}^{(in)}(0)\right]^{1/p} + \Delta\left(f^{(in)}(0)\right)\frac{G_{nom}}{p_{nom}}\left[f_{nom}^{(in)}(0)\right]^{(1-p_{nom})/p_{nom}} \tag{4.9}$$

$$+(\Delta p)G_{nom}\left[f_{nom}^{(in)}(0)\right]^{1/p_{nom}} \ln\left[f_{nom}^{(in)}(0)\right] + \Delta V_0, \quad k=1,...,8.$$

where the source terms on the right-sides of the above equations are defined as follows:

$$q_\rho^{(k)}(t) \triangleq \left[\rho_{a,nom}^{(k+1)}(t) - \rho_{a,nom}^{(k)}(t)\right]\left\{\left[\partial C\left(V^{(k+1)}\right)\middle/\partial V_0\right]_{nom}\Delta V_0\right.$$

$$\left.+\left[\partial C\left(V^{(k+1)}\right)\middle/\partial G\right]_{nom}\Delta G + \left[\partial C\left(V^{(k+1)}\right)\middle/\partial p\right]_{nom}\Delta p\right\}, \quad k=1,...,7, \tag{4.10}$$

$$q_\rho^{(8)}(t) \triangleq \left[\rho_{a,nom}^{(in)}(t) - \rho_{a,nom}^{(8)}(t)\right]\Delta f^{(in)}(t) + f_{nom}^{(in)}(t)\left[\Delta \rho_a^{(in)}(t)\right], \tag{4.11}$$

$$q_V^{(k)}(t) \triangleq -\left[\partial C\left(V^{(k)}\right)\middle/\partial V_0\right]_{nom}\Delta V_0 - \left[\partial C\left(V^{(k)}\right)\middle/\partial G\right]_{nom}\Delta G$$

$$-\left[\partial C\left(V^{(k)}\right)\middle/\partial p\right]_{nom}\Delta p + \left[\partial C\left(V^{(k+1)}\right)\middle/\partial V_0\right]_{nom}\Delta V_0 \tag{4.12}$$

$$+\left[\partial C\left(V^{(k+1)}\right)\middle/\partial G\right]_{nom}\Delta G + \left[\partial C\left(V^{(k+1)}\right)\middle/\partial p\right]_{nom}\Delta p, \quad k=1,...,7,$$

$$q_V^{(8)}(t) \triangleq -\left[\partial C\left(V^{(8)}\right)\middle/\partial V_0\right]_{nom}\Delta V_0 - \left[\partial C\left(V^{(8)}\right)\middle/\partial G\right]_{nom}\Delta G$$

$$-\left[\partial C\left(V^{(8)}\right)\middle/\partial p\right]_{nom}\Delta p + \Delta f^{(in)}(t), \tag{4.13}$$

with

$$\Delta f^{(in)}(t) \triangleq \frac{\Delta \dot{m}^{(in)}(t)}{63 a_{nom} \rho_{a,nom}^{(in)}(t) + b_{nom}} - \frac{\dot{m}_{nom}^{(in)}(t)\left\{(\Delta a)63\rho_{a,nom}^{(in)}(t) + 63 a_{nom}\left[\Delta \rho_a^{(in)}(t)\right] + \Delta b_{nom}\right\}}{\left[63 a_{nom}\rho_{a,nom}^{(in)}(t) + b_{nom}\right]^2}.$$

(4.14)

Note also the following relations:

$$\frac{\partial C\left[V^{(k)}(t)\right]}{\partial V_0} = \begin{cases} -\dfrac{p}{G}\left[\dfrac{V^{(k)}(t) - V_0}{G}\right]^{p-1}, & \text{if } V^{(k)}(t) - V_0 > 0, \ k = 1,...,8, \\ 0, & \text{otherwise.} \end{cases}$$

(4.15)

$$\frac{\partial C\left[V^{(k)}(t)\right]}{\partial G} = \begin{cases} -\dfrac{p}{G}\left[\dfrac{V^{(k)}(t) - V_0}{G}\right]^{p}, & \text{if } V^{(k)}(t) - V_0 > 0, \ k = 1,...,8, \\ 0, & \text{otherwise.} \end{cases}$$

(4.16)

$$\frac{\partial C\left[V^{(k)}(t)\right]}{\partial p} = \begin{cases} \left[\dfrac{V^{(k)}(t) - V_0}{G}\right]^{p} \ln\left[\dfrac{V^{(k)}(t) - V_0}{G}\right], & \text{if } V^{(k)}(t) - V_0 > 0, \ k = 1,...,8, \\ 0, & \text{otherwise.} \end{cases}$$

(4.17)

Equations (4.5) - (4.9) are called (Cacuci, 1981.a, 1981.b) the *forward sensitivity system*. Evidently, the response sensitivity $\delta R\left(\mathbf{u}^0, \boldsymbol{\alpha}^0; \mathbf{h}_u, \mathbf{h}_\alpha\right)$ can be computed after solving the forward sensitivity system given in Eqs. (3.5) - (3.9) *repeatedly*, for every possible parameter variation contained in the vector $\mathbf{h}_\alpha(t)$, cf. Eq. (4.2). This procedure is called (Cacuci, 1981.a, 1981.b) the *Forward Sensitivity Analysis Procedure* (*FSAP*). For a model comprising N_α model parameters, the *FSAP* requires at least N_α large-scale computations.

Particularly important scalar-valued responses for the dissolver model are the measured and/or computed nitric acid concentration in a compartment k at a time-instance t_i. Such measurements can be represented in the form

$$\rho_a^{(k)}(t_i) = \int_0^{t_f} \rho_a^{(k)}(t_i)\delta(t - t_i)dt,$$

(4.18)

97

where $\delta(t-t_i)$ represents the customary Dirac-delta functional. The sensitivity of such a response is given by the G-derivative of Eq. (3.18), which is readily obtained as

$$\delta\rho_a^{(k)}(t_i) = \int_0^{t_f} \Delta\rho_a^{(k)}(t)\delta(t-t_i)dt, \quad i=1,...,I. \tag{4.19}$$

It is evident that using the *FSAP* to compute the sensitivity $\delta\rho_a^{(k)}(t_i)$ expressed in Eq. (4.19) would require solving Eqs. (4.5) - (4.9) at least $N_\alpha = 1291$ times in order to account for the variations in all of the model parameters. Thus, for the dissolver model under consideration, as for most practical situations, the number of model parameters exceeds significantly the number of functional responses of interest. In such cases, *The Adjoint Sensitivity Analysis Methodology (ASAM)* introduced by Cacuci's (1981a, 1981b) *is known to be the most efficient method for computing exactly the first-order sensitivities since it requires only a single large-scale computation for each response of interest*.

In preparation for applying the ASAM to the dissolver model, the forward sensitivity equations [cf., Eqs. (4.5) through (4.9)] are written in matrix form as

$$\begin{bmatrix} \mathbf{N}_{11} & \mathbf{N}_{12} \\ \mathbf{0} & \mathbf{N}_{22} \end{bmatrix} \begin{bmatrix} \mathbf{h}_\rho(t) \\ \mathbf{h}_V(t) \end{bmatrix} = \begin{bmatrix} \mathbf{q}_\rho(t) \\ \mathbf{q}_V(t) \end{bmatrix}, \tag{4.20}$$

where

$$\mathbf{q}_\rho(t) \triangleq \left[q_\rho^{(1)}(t),...,q_\rho^{(8)}(t) \right], \quad \mathbf{q}_V(t) \triangleq \left[q_V^{(1)}(t),...,q_V^{(8)}(t) \right], \tag{4.21}$$

$$\mathbf{N}_{11}(t) \triangleq \begin{bmatrix} a_{11}^{11} & a_{12}^{11} & 0 & . & 0 & 0 \\ 0 & a_{22}^{11} & a_{23}^{11} & . & 0 & 0 \\ . & . & . & . & . & . \\ 0 & 0 & 0 & . & a_{77}^{11} & a_{78}^{11} \\ 0 & 0 & 0 & . & 0 & a_{88}^{11} \end{bmatrix}, \tag{4.22}$$

$$\mathbf{N}_{12}(t) \triangleq \begin{bmatrix} a_{11}^{12} & a_{12}^{12} & 0 & . & 0 & 0 \\ 0 & a_{22}^{12} & a_{23}^{12} & . & 0 & 0 \\ . & . & . & . & . & . \\ 0 & 0 & 0 & . & a_{77}^{12} & a_{78}^{12} \\ 0 & 0 & 0 & . & 0 & a_{88}^{12} \end{bmatrix}, \tag{4.23}$$

$$\mathbf{N}_{22}(t) \triangleq \begin{bmatrix} a_{11}^{22} & a_{12}^{22} & 0 & . & 0 & 0 \\ 0 & a_{22}^{22} & a_{23}^{22} & . & 0 & 0 \\ . & . & . & . & . & . \\ 0 & 0 & 0 & . & a_{77}^{22} & a_{78}^{22} \\ 0 & 0 & 0 & . & 0 & a_{88}^{22} \end{bmatrix}, \tag{4.24}$$

$$a_{ii}^{11}(t) \triangleq V_{nom}^{(i)}(t) \frac{d[*]}{dt} + C\left[V_{nom}^{(i+1)}(t)\right], \ i=1,...,7; \tag{4.25}$$

$$a_{88}^{11}(t) \triangleq V_{nom}^{(8)}(t) \frac{d[*]}{dt} + f_{nom}^{(in)}(t); \tag{4.26}$$

$$a_{i,i+1}^{11}(t) \triangleq -C\left[V_{nom}^{(i+1)}(t)\right], \ i=1,...,7; \tag{4.27}$$

$$a_{ii}^{12}(t) \triangleq \frac{d\rho_{a,nom}^{(i)}(t)}{dt}, \ i=1,...,8; \tag{4.28}$$

$$a_{i,i+1}^{12}(t) \triangleq \left[\rho_{a,nom}^{(i)}(t) - \rho_{a,nom}^{(i+1)}(t)\right]\left[\frac{dC\left(V^{(i+1)}\right)}{dV^{(i+1)}}\right]_{nom}, \ i=1,...,7; \tag{4.29}$$

$$a_{ii}^{22}(t) \triangleq \frac{d[*]}{dt} + \left[\frac{dC\left(V^{(i)}\right)}{dV^{(i)}}\right]_{nom}, \ i=1,...,8; \tag{4.30}$$

$$a_{i,i+1}^{22}(t) \triangleq -\left[\frac{dC\left(V^{(i+1)}\right)}{dV^{(i+1)}}\right]_{nom}, \ i=1,...,7; \tag{4.31}$$

Next, consider two square-integrable vector-valued functions of the form $\mathbf{f}(t) \triangleq \left[\mathbf{f}_\rho(t), \mathbf{f}_V(t)\right]$, and $\mathbf{g}(t) \triangleq \left[\mathbf{g}_\rho(t), \mathbf{g}_V(t)\right]$, and introduce an *inner product* defined as

$$\langle \mathbf{f}(t), \mathbf{g}(t) \rangle \triangleq \int_0^{t_f} \left[\mathbf{f}_\rho(t) \mathbf{g}_\rho(t) + \mathbf{f}_V(t) \mathbf{g}_V(t) \right] dt = \sum_{j=1}^{8} \int_0^{t_f} \left[f_\rho^{(i)}(t) g_\rho^{(i)}(t) + f_V^{(i)}(t) g_V^{(i)}(t) \right] dt.$$

(4.32)

Taking the inner product of Eq. (4.20) with a yet undefined vector $\boldsymbol{\psi}(t)$ of the form

$$\boldsymbol{\psi}(t) \triangleq \left[\boldsymbol{\psi}_\rho(t), \boldsymbol{\psi}_V(t) \right], \ \boldsymbol{\psi}_\rho(t) \triangleq \left[\psi_\rho^{(1)}(t), ..., \psi_\rho^{(8)}(t) \right], \ \boldsymbol{\psi}_V(t) \triangleq \left[\psi_V^{(1)}(t), ..., \psi_V^{(8)}(t) \right],$$

(4.33)

yields

$$\left\langle \left[\boldsymbol{\psi}_\rho(t), \boldsymbol{\psi}_V(t) \right] \begin{bmatrix} \mathbf{N}_{11}(t) & \mathbf{N}_{12}(t) \\ \mathbf{0} & \mathbf{N}_{22}(t) \end{bmatrix} \begin{bmatrix} \mathbf{h}_\rho(t) \\ \mathbf{h}_V(t) \end{bmatrix} \right\rangle = \left\langle \left[\boldsymbol{\psi}_\rho(t), \boldsymbol{\psi}_V(t) \right] \begin{bmatrix} \mathbf{q}_\rho(t) \\ \mathbf{q}_V(t) \end{bmatrix} \right\rangle$$

$$= \left\langle \left[\mathbf{h}_\rho(t), \mathbf{h}_V(t) \right] \begin{bmatrix} \mathbf{N}_{11}^*(t) & \mathbf{0} \\ \mathbf{N}_{21}^*(t) & \mathbf{N}_{22}^*(t) \end{bmatrix} \begin{bmatrix} \boldsymbol{\psi}_\rho(t) \\ \boldsymbol{\psi}_V(t) \end{bmatrix} \right\rangle,$$

(4.34)

where

$$\mathbf{N}_{11}^*(t) \triangleq \begin{bmatrix} b_{11}^{11} & 0 & 0 & . & 0 & 0 \\ b_{21}^{11} & b_{22}^{11} & 0 & . & 0 & 0 \\ . & . & . & . & . & . \\ 0 & 0 & 0 & . & b_{77}^{11} & 0 \\ 0 & 0 & 0 & . & b_{87}^{11} & b_{88}^{11} \end{bmatrix},$$

(4.35)

$$\mathbf{N}_{21}^*(t) \triangleq \begin{bmatrix} b_{11}^{21} & 0 & 0 & . & 0 & 0 \\ b_{21}^{21} & b_{22}^{21} & 0 & . & 0 & 0 \\ . & . & . & . & . & . \\ 0 & 0 & 0 & . & b_{77}^{21} & 0 \\ 0 & 0 & 0 & . & b_{87}^{21} & b_{88}^{21} \end{bmatrix},$$

(4.36)

$$\mathbf{N}_{22}^*(t) \triangleq \begin{bmatrix} b_{11}^{22} & 0 & 0 & . & 0 & 0 \\ b_{21}^{22} & b_{22}^{22} & 0 & . & 0 & 0 \\ . & . & . & . & . & . \\ 0 & 0 & 0 & . & b_{77}^{22} & 0 \\ 0 & 0 & 0 & . & b_{87}^{22} & b_{88}^{22} \end{bmatrix},$$

(4.37)

where the components $b_{ij}^{kl} \triangleq \left[a_{ji}^{lk} \right]^*$ are the transposed formal adjoints of the quantities a_{ij}^{kl}, i.e.,

100

$$b_{ii}^{11}(t) \triangleq -\frac{d\left[V_{nom}^{(i)}(t)*\right]}{dt} - \frac{\partial V_{nom}^{(i)}}{\partial t} + C\left[V_{nom}^{(i+1)}(t)\right], \ i = 1,...,7; \tag{4.38}$$

$$b_{88}^{11}(t) \triangleq -\frac{d\left[V_{nom}^{(8)}(t)*\right]}{dt} - \frac{\partial V_{nom}^{(i)}}{\partial t} + f_{nom}^{(in)}(t); \tag{4.39}$$

$$b_{i+1,i}^{11}(t) \triangleq -C\left[V_{nom}^{(i+1)}(t)\right], \ i = 1,...,7; \tag{4.40}$$

$$b_{ii}^{21}(t) \triangleq \frac{d\rho_{a,nom}^{(i)}(t)}{dt}, \ i = 1,...,8; \tag{4.41}$$

$$b_{i+1,i}^{21}(t) \triangleq \left[\rho_{a,nom}^{(i)}(t) - \rho_{a,nom}^{(i+1)}(t)\right]\left[\frac{dC\left(V^{(i+1)}\right)}{dV^{(i+1)}}\right]_{nom}, \ i = 1,...,7; \tag{4.42}$$

$$b_{ii}^{22}(t) \triangleq -\frac{d[*]}{dt} + \left[\frac{dC\left(V^{(i)}\right)}{dV^{(i)}}\right]_{nom}, \ i = 1,...,8; \tag{4.43}$$

$$b_{i+1,i}^{22}(t) \triangleq -\left[\frac{dC\left(V^{(i+1)}\right)}{dV^{(i+1)}}\right]_{nom}, \ i = 1,...,7. \tag{4.44}$$

The function $\psi(t) \triangleq \left[\psi_\rho(t), \psi_V(t)\right]$ will now be defined to be the solution of the following system

$$\begin{bmatrix} \mathbf{N}_{11}^*(t) & \mathbf{0} \\ \mathbf{N}_{21}^*(t) & \mathbf{N}_{22}^*(t) \end{bmatrix}\begin{bmatrix} \psi_\rho(t) \\ \psi_V(t) \end{bmatrix} = \begin{bmatrix} \partial F(\mathbf{u},\boldsymbol{\alpha})/\partial \boldsymbol{\rho}_a \\ \partial F(\mathbf{u},\boldsymbol{\alpha})/\partial \mathbf{V} \end{bmatrix}, \tag{4.45}$$

where

$$\frac{\partial F(\mathbf{u},\boldsymbol{\alpha})}{\partial \boldsymbol{\rho}_a} \triangleq \left[\frac{\partial F(\mathbf{u},\boldsymbol{\alpha})}{\partial \rho_a^{(1)}(t)},...,\frac{\partial F(\mathbf{u},\boldsymbol{\alpha})}{\partial \rho_a^{(8)}(t)}\right]^\dagger, \quad \frac{\partial F(\mathbf{u},\boldsymbol{\alpha})}{\partial \mathbf{V}} \triangleq \left[\frac{\partial F(\mathbf{u},\boldsymbol{\alpha})}{\partial V^{(1)}(t)},...,\frac{\partial F(\mathbf{u},\boldsymbol{\alpha})}{\partial V^{(8)}(t)}\right]^\dagger. \tag{4.46}$$

In component form, Eq. (4.45) has the form

$$-\frac{d\left[V_{nom}^{(1)}(t)\psi_{\rho}^{(1)}(t)\right]}{dt}+C\left[V_{nom}^{(2)}(t)\right]\psi_{\rho}^{(1)}(t)=\frac{\partial F(\mathbf{u},\boldsymbol{\alpha})}{\partial\rho_a^{(1)}(t)}\triangleq w_{\rho}^{(1)}(t),\tag{4.47}$$

$$-\frac{d\left[V_{nom}^{(k)}(t)\psi_{\rho}^{(k)}(t)\right]}{dt}+C\left[V_{nom}^{(k+1)}(t)\right]\psi_{\rho}^{(k)}(t)$$
$$-C\left[V_{nom}^{(k)}(t)\right]\psi_{\rho}^{(k-1)}(t)=\frac{\partial F(\mathbf{u},\boldsymbol{\alpha})}{\partial\rho_a^{(k)}(t)}\triangleq w_{\rho}^{(k)}(t),\quad k=2,...,7;\tag{4.48}$$

$$-\frac{d\left[V_{nom}^{(8)}(t)\psi_{\rho}^{(8)}(t)\right]}{dt}+f_{nom}^{(in)}(t)\psi_{\rho}^{(8)}(t)-C\left[V_{nom}^{(8)}(t)\right]\psi_{\rho}^{(7)}(t)=\frac{\partial F(\mathbf{u},\boldsymbol{\alpha})}{\partial\rho_a^{(8)}(t)}\triangleq w_{\rho}^{(8)}(t),\tag{4.49}$$

$$-\frac{d\left[\psi_V^{(1)}(t)\right]}{dt}+\left[\frac{dC\left[V^{(1)}(t)\right]}{dV^{(1)}(t)}\right]_{nom}\psi_V^{(1)}(t)+\left[\frac{d\rho_{a,nom}^{(1)}(t)}{dt}\right]\psi_{\rho}^{(1)}(t)=\frac{\partial F(\mathbf{u},\boldsymbol{\alpha})}{\partial V^{(1)}(t)}\triangleq w_V^{(1)}(t),\tag{4.50}$$

$$-\frac{d\left[\psi_V^{(k)}(t)\right]}{dt}+\left[\frac{dC\left[V^{(k)}(t)\right]}{dV^{(k)}(t)}\right]_{nom}\psi_V^{(k)}(t)-\left[\frac{dC\left[V^{(k)}(t)\right]}{dV^{(k)}(t)}\right]_{nom}\psi_V^{(k-1)}(t)$$
$$+\left[\frac{d\rho_{a,nom}^{(k)}(t)}{dt}\right]\psi_{\rho}^{(k)}(t)+\left[\rho_{a,nom}^{(k-1)}(t)-\rho_{a,nom}^{(k)}(t)\right]\left[\frac{dC\left[V^{(k)}(t)\right]}{dV^{(k)}(t)}\right]_{nom}\psi_{\rho}^{(k-1)}(t)\tag{4.51}$$
$$=\frac{\partial F(\mathbf{u},\boldsymbol{\alpha})}{\partial V^{(k)}(t)}\triangleq w_V^{(k)}(t),\quad k=2,...,8;$$

subject to the "final-time" values

$$\psi_{\rho}^{(k)}(t_f)=0,\quad \psi_V^{(k)}(t_f)=0,\quad k=1,...,8.\tag{4.52}$$

Equations (4.47) - (4.52) comprise the *Adjoint Sensitivity System* (*ASS*), and the vector $\boldsymbol{\psi}(t)\triangleq\left[\boldsymbol{\psi}_{\rho}(t),\boldsymbol{\psi}_V(t)\right]$ is called the *adjoint function*. Using now Eqs. (4.20), (4.33) and (4.45) into Eq. (4.4) yields the following expression for the response sensitivities in terms of the adjoint function $\boldsymbol{\psi}(t)\triangleq\left[\boldsymbol{\psi}_{\rho}(t),\boldsymbol{\psi}_V(t)\right]$:

$$\delta R\left(\mathbf{u}^0, \boldsymbol{\alpha}^0; \boldsymbol{\psi}, \mathbf{h}_\alpha\right) = \sum_{k=1}^{8} \int_0^{t_f} \psi_\rho^{(k)}(t) q_\rho^{(k)}(t) dt + \sum_{k=1}^{8} \int_0^{t_f} \psi_V^{(k)}(t) q_V^{(k)}(t) dt$$

$$+ \sum_{k=1}^{8} \left\{ \psi_\rho^{(k)}(0) V_{nom}^{(k)}(0) \left[\Delta \rho_{a0}^{(k)} \right] + \psi_V^{(k)}(0) \left[\Delta V_0^{(k)} \right] \right\}. \tag{4.53}$$

As the above equation indicates, the sensitivities $\delta R\left(\mathbf{u}^0, \boldsymbol{\alpha}^0; \boldsymbol{\psi}, \mathbf{h}_\alpha\right)$ to all system parameters can be computed after the corresponding adjoint functions $\boldsymbol{\psi} \triangleq \left[\boldsymbol{\psi}_\rho, \boldsymbol{\psi}_V \right]$ have been computed by solving *once* the adjoint sensitivity system defined in Eqs. (4.47) - (4.52). For subsequent mathematical simplifications, it is convenient to introduce the following definitions:

$$D_\rho^{(k)} \left[\rho_a^{(k+1)}(t), \rho_a^{(k)}(t), V^{(k+1)}(t), V^{(k)}(t), p, G, V_0 \right] \triangleq \frac{d\rho_a^{(k)}(t)}{dt}$$

$$= \frac{\rho_a^{(k+1)}(t) - \rho_{a,nom}^{(k)}(t)}{V^{(k)}(t)} C\left[V^{(k+1)}(t) \right], \ k = 1, ..., 7; \tag{4.54}$$

$$D_\rho^{(8)} \left[\rho_a^{(8)}(t), V^{(8)}(t), \rho_a^{(in)}(t), f^{in}(t) \right] \triangleq \frac{d\rho_a^{(8)}(t)}{dt} = \frac{\rho_a^{(in)}(t) - \rho_a^{(8)}(t)}{V^{(8)}(t)} f^{in}(t), \tag{4.55}$$

$$D_V^{(k)} \left[V^{(k)}(t), p, G, V_0 \right] \triangleq \left[\frac{dC\left[V^{(k)}(t) \right]}{dV^{(k)}(t)} \right]_{nom}$$

$$= \begin{cases} \dfrac{p}{G} \left[\dfrac{V^{(k)}(t) - V_0}{G} \right]^{p-1}, & if \ V^{(k)}(t) - V_0 > 0, \ k = 1, ..., 8, \\ 0, & otherwise. \end{cases} \tag{4.56}$$

It will be convenient to use the following "short-hand" notations for the quantities defined in Eqs. (4.53) - (4.56)

$$D_\rho^{(k)} \left[\rho_a^{(k+1)}(t), \rho_a^{(k)}(t), V^{(k+1)}(t), V^{(k)}(t), p, G, V_0 \right] \triangleq D_\rho^{(k)}(t), \ k = 1, ..., 7; \tag{4.57}$$

$$D_\rho^{(8)} \left[\rho_a^{(8)}(t), V^{(8)}(t), \rho_a^{(in)}(t), f^{in}(t) \right] \triangleq D_\rho^{(8)}(t),$$

$$D_V^{(k)} \left[V^{(k)}(t), p, G, V_0 \right] \triangleq D_V^{(k)}(t), \ k = 1, ..., 8. \tag{4.58}$$

The *ASS* defined in Eqs. (4.47) - (4.52) can now be further simplified by using the definitions introduced in Eqs. (4.54) – (4.56) and the shorthand notation given in Eq. (4.57) and (4.58), together with the original forward model, namely Eqs. (3.10) - (3.14), to obtain the following form of the *ASS*:

$$-V_{nom}^{(1)}(t)\frac{d\psi_{\rho}^{(1)}(t)}{dt} + C\left[V_{nom}^{(1)}(t)\right]\psi_{\rho}^{(1)}(t) = w_{\rho}^{(1)}(t), \ 0 < t < t_f, \tag{4.59}$$

$$-V_{nom}^{(k)}(t)\frac{d\psi_{\rho}^{(k)}(t)}{dt} + C\left[V_{nom}^{(k)}(t)\right]\left[\psi_{\rho}^{(k)}(t) - \psi_{\rho}^{(k-1)}(t)\right] = w_{\rho}^{(k)}(t), \ 0 < t < t_f, \ k = 2,...,8; \tag{4.60}$$

$$-\frac{d\psi_{V}^{(1)}(t)}{dt} + D_{V}^{(1)}(t)\psi_{V}^{(1)}(t) + D_{\rho}^{(1)}(t)\psi_{\rho}^{(1)}(t) = w_{V}^{(1)}(t), \ 0 < t < t_f, \tag{4.61}$$

$$-\frac{d\psi_{V}^{(k)}(t)}{dt} + D_{V}^{(k)}(t)\left[\psi_{V}^{(k)}(t) - \psi_{V}^{(k-1)}(t)\right] + D_{\rho}^{(k)}(t)\psi_{\rho}^{(k)}(t)$$
$$+ \left[\rho_{a,nom}^{(k-1)}(t) - \rho_{a,nom}^{(k)}(t)\right]D_{V}^{(k)}(t)\psi_{\rho}^{(k-1)}(t) = w_{V}^{(k)}(t), \ k = 2,...,8, \ 0 < t < t_f. \tag{4.62}$$

The "final-time" conditions in Eq. (4.52) clearly indicate that the adjoint sensitivity system is a final-time problem rather than an initial-value problem. It is useful to convert the adjoint sensitivity system from a "final-time" problem to an "initial-condition problem" accustomed by solvers of ordinary differential equations. This can be accomplished by changing the independent variable t to another independent variable, τ, defined as follows:

$$\tau \triangleq t_f - t. \tag{4.63}$$

Introducing the above change of independent variable into Eqs. (4.59) – (4.62) transforms them into the following "***computationally-suitable***" form of the ***adjoint sensitivity system:***

$$V_{nom}^{(1)}(t_f - \tau)\frac{d\psi_{\rho}^{(1)}(\tau)}{d\tau} + C\left[V_{nom}^{(1)}(t_f - \tau)\right]\psi_{\rho}^{(1)}(\tau) = w_{\rho}^{(1)}(t_f - \tau), \ 0 < \tau < t_f, \tag{4.64}$$

$$V_{nom}^{(k)}\left(t_f - \tau\right)\frac{d\psi_{\rho}^{(k)}(\tau)}{d\tau} + C\left[V_{nom}^{(k)}\left(t_f - \tau\right)\right]\left[\psi_{\rho}^{(k)}(\tau) - \psi_{\rho}^{(k-1)}(\tau)\right]$$

$$= w_{\rho}^{(k)}\left(t_f - \tau\right),\ 0 < \tau < t_f,\ k = 2,...,8; \tag{4.65}$$

$$\frac{d\psi_{V}^{(1)}(\tau)}{d\tau} + D_{V}^{(1)}\left(t_f - \tau\right)\psi_{V}^{(1)}(\tau) + D_{\rho}^{(1)}\left(t_f - \tau\right)\psi_{\rho}^{(1)}(\tau) = w_{V}^{(1)}\left(t_f - \tau\right),\ 0 < \tau < t_f, \tag{4.66}$$

$$\frac{d\psi_{V}^{(k)}(\tau)}{d\tau} + D_{V}^{(k)}\left(t_f - \tau\right)\left[\psi_{V}^{(k)}(\tau) - \psi_{V}^{(k-1)}(\tau)\right] + D_{\rho}^{(k)}\left(t_f - \tau\right)\psi_{\rho}^{(k)}(\tau)$$

$$+\left[\rho_{a,nom}^{(k-1)}\left(t_f - \tau\right) - \rho_{a,nom}^{(k)}\left(t_f - \tau\right)\right]D_{V}^{(k)}\left(t_f - \tau\right)\psi_{\rho}^{(k-1)}(\tau) = w_{V}^{(k)}\left(t_f - \tau\right),\ k = 2,...,8,\ 0 < \tau < t_f. \tag{4.67}$$

The initial conditions for Eqs. (4.64) – (4.67) are

$$\psi_{\rho}^{(k)}\left(\tau = 0\right) = 0,\ \ \psi_{V}^{(k)}\left(\tau = 0\right) = 0,\ \ k = 1,...,8. \tag{4.68}$$

In particular, to compute the sensitivity $\delta\rho_a^{(k)}\left(t_i\right)$, given in Eq. (4.19), of the measured and/or computed nitric acid concentration in a compartment k at a time-instance t_i, a comparison of Eq. (4.19) with the general from given in Eq. (4.4) indicates that the source terms for the right-sides of the adjoint sensitivity system, cf. Eqs. (4.64) - (4.67), are as follows:

$$w_{\rho}^{(k)}(t) = \delta\left(t - t_j\right),\ w_{\rho}^{(j)}(t) = 0,\ \ 1 \le j \ne k \le 8;\ w_{V}^{(1)}(t) = ... = w_{V}^{(8)}(t) = 0. \tag{4.69}$$

4.2. Mathematical Derivation of the Adjoint Sensitivity Analysis System for Function-Valued Responses

Particularly important response of interest for the dissolver model are the time-dependent nitric acid concentrations, $\rho_a^{(k)}(t)$, in compartments $k = 1,...,8$ for the entire duration of 10.5 hours of the transient event under consideration. The sensitivity of such a response to variations in the model parameters is given by the expression

$$\delta R\left(\mathbf{e}^0;\mathbf{h}\right) \triangleq \frac{d}{d\varepsilon}\left[\rho_{a,nom}^{(k)}\left(t\right)+\varepsilon\Delta\rho_a^{(k)}\left(t\right)\right]_{\varepsilon=0}=\Delta\rho_a^{(k)}\left(t\right),\ \ k=1,...,8. \tag{4.70}$$

As the above expression indicates, the sensitivity $\Delta\rho_a^{(k)}\left(t\right)$ is a time-dependent function, rather than a scalar-valued functional, as was the sensitivity $\delta\rho_a^{(k)}\left(t_i\right)$, given by Eq. (4.19), of the measured and/or computed nitric acid concentration in a compartment k at a time-instance t_i. Function-valued response sensitivities, such as $\Delta\rho_a^{(k)}\left(t\right)$, are computed efficiently using the *Adjoint Sensitivity Analysis Methodology for Operator-Type Responses* (Cacuci, 1981.b), which entails *the spectral representation of the respective function-valued response*. As an illustration of the application of this methodology (Cacuci, 1981.b), consider the time-dependent nitric acid concentration response, $\Delta\rho_a^{(k)}\left(t\right)$, in compartment #1. The Legendre polynomials will be chosen to serve as the orthonormal basis for the spectral representation of $\rho_a^{(1)}\left(t\right)$. Recall that the Nth-order spectral expansion, $f_N\left(x\right)$, of a function $f\left(x\right),\ x\in\left[-1,1\right]$, using Legendre polynomials, $P_n\left(x\right)$, is defined as

$$f_N\left(x\right)=\sum_{n=0}^{N}a_nP_n\left(x\right), \tag{4.71}$$

where $P_n\left(x\right)$ denotes the Legendre polynomial of order n, and where the coefficients a_n are defined as

$$a_n \equiv \frac{2n+1}{2}\int_{-1}^{1}f\left(x\right)P_n\left(x\right)dx,\ \ n=0,1,...,N. \tag{4.72}$$

The Legendre polynomials satisfy several well-known recursion relationships; the relationship below can be conveniently used for the numerical computations, to avoid undue accumulation and magnification of round-off errors:

$$P_{n+1}\left(x\right)=2xP_n\left(x\right)-P_{n-1}\left(x\right)-\frac{xP_n\left(x\right)-P_{n-1}\left(x\right)}{n+1}. \tag{4.73}$$

Recall also that the Legendre polynomials satisfy the orthogonality relation

106

$$\int_{-1}^{1} P_n(x) P_n(x) dx = \frac{2}{2n+1} \delta_{mn} \tag{4.74}$$

where δ_{mn} represents the Kronecker delta functional, defined as $\delta_{mn} = 1, \; m = n$ and $\delta_{mn} = 0, \; m \neq n$.

Since the time-dependent response of interest, namely the nitric acid concentration in the first compartment, $\rho_a^{(1)}(t)$, is defined over the time interval $t \in [0, t_f]$, it follows that the interval $x \in [-1, 1]$ must be shifted to the interval $t \in [0, t_f]$ in order to obtain the corresponding spectral expansion for $\rho_a^{(1)}(t)$. The correspondence between the independent variables $t \in [0, t_f]$ and $x \in [-1, 1]$ is provided by the relationships

$$t = (x+1) t_f / 2, \quad x = (2t/t_f - 1). \tag{4.75}$$

Denoting the Nth-order spectral expansion $\rho_a^{(1)}(t)$ by $\rho_{a,S}^{(1)}(t)$, where the subscript "S" indicates "spectral," it follows that from Eqs. (4.71), (4.72), (4.74) and (4.75) that

$$\rho_{a,S}^{(1)}(t) = \sum_{n=0}^{N} a_n P_n(2t/t_f - 1), \quad 0 < t \leq t_f, \tag{4.76}$$

with

$$a_n = \frac{2n+1}{t_f} \int_{0}^{t_f} \rho_{a,S}^{(1)}(t) \, P_n(2t/t_f - 1) dt, \quad n = 0, 1, ..., N. \tag{4.77}$$

For the shifted Legendre polynomials $P_n(2t/t_f - 1)$, the "orthogonality relation" expressed by Eq. (4.74) takes on the following form:

$$\int_{0}^{t_f} P_n(2t/t_f - 1) P_n(2t/t_f - 1) dt = \frac{\delta_{mn}}{2n+1}. \tag{4.78}$$

Using the shifted polynomials $P_n\left(2t/t_f - 1\right)$, the nitric acid concentration $\rho_a^{(1)}(t)$ depicted in Figure 3.5 is approximated by $\rho_{a,S}^{(1)}(t)$ within a maximum global error of less than 0.01%, by using $N = 16$ in the spectral expansion in Eq. (4.76). The results of the approximation are depicted in Figure 4.1, and show similarly accurate computations of the response sensitivities as will be shown after establishing the corresponding adjoint sensitivity system presented later in the chapter.
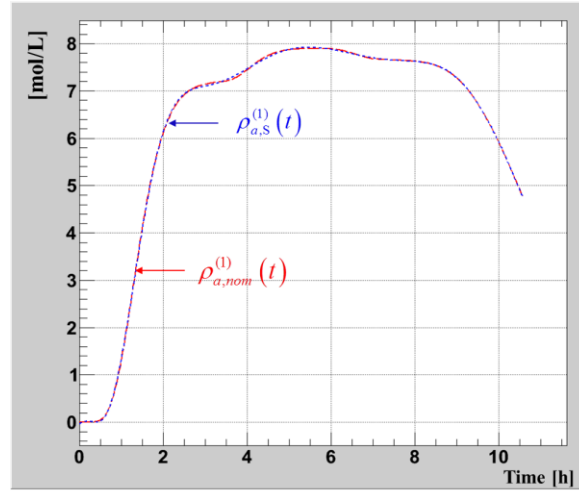
Figure 4.1 Time-dependent behavior of the exact nominal value of the nitric acid concentration $\left[\text{mol/L}\right]$ in compartment #1, $\rho_{a,nom}^{(1)}(t)$, reproduced from Figure 3.5, and its spectral representation, $\rho_{a,S}^{(1)}(t)$, using the first 17 Legendre polynomials ($N = 16$)

For the particular case of the response $\rho_{a,S}^{(1)}(t)$ defined in Eq. (4.76), Eq. (4.70) takes on the following particular form for the sensitivity $\delta\rho_{a,S}^{(1)}(t)$ of $\rho_{a,S}^{(1)}(t)$:

$$\delta\rho_{a,S}^{(1)}(t) = \sum_{n=0}^{N}\left[\int_0^{t_f}\Delta\rho_{a,S}^{(1)}(t)\left[\frac{2n+1}{t_f}P_n\left(2t/t_f - 1\right)\right]dt\right]P_n\left(2t/t_f - 1\right), \quad (4.79)$$

Comparing the right-side of the above expression with the right-most side of Eq. (4.4) and keeping in mind Eqs. (4.64)- (4.68), it follows that the sources for the adjoint system are $\left[(2n+1)/t_f\right]P_n\left(2t/t_f - 1\right)$ for the equation involving the adjoint function $\psi_{\rho,n}^{(1)}(t)$,

$n = 0, 1, ..., N = 16$, and are zero for the other equations. Consequently, the corresponding adjoint sensitivity system becomes

➢ *For each $n = 0, 1, ..., N = 16$, solve:*

$$V_{nom}^{(1)}\left(t_f - \tau\right)\frac{d\psi_{\rho,n}^{(1)}(\tau)}{d\tau} + C\left[V_{nom}^{(1)}\left(t_f - \tau\right)\right]\psi_{\rho,n}^{(1)}(\tau) = \frac{2n+1}{t_f}P_n\left(1 - 2\tau/t_f\right), \; 0 < \tau < t_f, \quad (4.80)$$

$$V_{nom}^{(k)}\left(t_f - \tau\right)\frac{d\psi_{\rho,n}^{(k)}(\tau)}{d\tau} + C\left[V_{nom}^{(k)}\left(t_f - \tau\right)\right]\left[\psi_{\rho,n}^{(k)}(\tau) - \psi_{\rho,n}^{(k-1)}(\tau)\right] = 0, \; k = 2,...,8; \; 0 < \tau < t_f,$$

$$\tag{4.81}$$

$$\frac{dy_{V,n}^{(1)}(t)}{dt} + D_V^{(1)}\left(t_f - t\right)y_{V,n}^{(1)}(t) + D_r^{(1)}\left(t_f - t\right)y_{r,n}^{(1)}(t) = 0, \; 0 < t < t_f, \tag{4.82}$$

$$\frac{dy_{V,n}^{(k)}(t)}{dt} + D_V^{(k)}\left(t_f - t\right)\acute{\text{ê}}y_{V,n}^{(k)}(t) - y_{V,n}^{(k-1)}(t)\grave{\text{ù}} + D_r^{(k)}\left(t_f - t\right)y_{r,n}^{(k)}(t)$$

$$+ \acute{\text{ê}}r_{a,nom}^{(k-1)}\left(t_f - t\right) - r_{a,nom}^{(k)}\left(t_f - t\right)\grave{\text{ù}}D_V^{(k)}\left(t_f - t\right)y_{r,n}^{(k-1)}(t) = 0, \; k = 2,...,8, \; 0 < t < t_f, \tag{4.83}$$

subject to the initial conditions

$$\psi_{\rho,n}^{(k)}(\tau = 0) = 0, \; \psi_{V,n}^{(k)}(\tau = 0) = 0, \; k = 1,...,8. \tag{4.84}$$

Furthermore, it follows that the general expression of the response sensitivities represented by Eq. (4.53) takes on the following particular for form for computing the sensitivities $\delta\rho_{a,S}^{(1)}(t)$:

$$\delta\rho_{a,S}^{(1)}(t) = \sum_{n=0}^{N=16} \delta a_n\left(\mathbf{h}_\alpha, \mathbf{\psi}; \mathbf{\alpha}^0\right)P_n\left(2t/t_f - 1\right), \tag{4.85}$$

where

$$\delta a_n\left(\mathbf{h}_\alpha, \mathbf{\psi}; \mathbf{\alpha}^0\right) = \sum_{k=1}^{8}\int_0^{t_f}\psi_{\rho,n}^{(k)}(t)q_\rho^{(k)}(t)dt + \sum_{k=1}^{8}\int_0^{t_f}\psi_{V,n}^{(k)}(t)q_V^{(k)}(t)dt$$

$$+ \sum_{k=1}^{8}\left\{\psi_{\rho,n}^{(k)}(0)V_{nom}^{(k)}(0)\left[\Delta\rho_{a0}^{(k)}\right] + \psi_{V,n}^{(k)}(0)\left[\Delta V_0^{(k)}\right]\right\}, \; n = 0, 1, ..., N = 16. \tag{4.86}$$

The sensitivities of the nitric acid concentration in the other compartments have been similarly computed by using the above-mentioned "*adjoint sensitivity analysis methodology for operator-type responses*" developed by in conjunction with spectral expansions in Legendre Polynomials. In addition to the results obtained above for the nitric acid concentrations in compartment #1, we will also illustrate the significant computational advantages of applying this methodology (Cacuci, 1981.b) by considering the nitric acid concentrations in compartment #4, in the middle of the dissolver, and in compartment #7, which is closest to the dissolver's inlet. Following the same procedure as for compartment #1, the time-dependent acid concentration in compartment #4, $\rho_{a,nom}^{(4)}(t)$, can be approximated within a maximum error of less than 0.01% by its *finite spectral representation*, $\rho_{a,S}^{(4)}(t)$, using 21 Legendre polynomials. Similarly, the time-dependent acid concentration in compartment #7, $\rho_{a,nom}^{(7)}(t)$, can be approximated within a maximum error of less than 0.01% by its *finite spectral representation*, $\rho_{a,S}^{(7)}(t)$, using 29 Legendre polynomials. The exact values of $\rho_{a,S}^{(4)}(t)$ and $\rho_{a,S}^{(7)}(t)$, reproduced from Figure 3.5, and their corresponding finite spectral representations are shown in Figures 4.2 and 4.3, respectively.
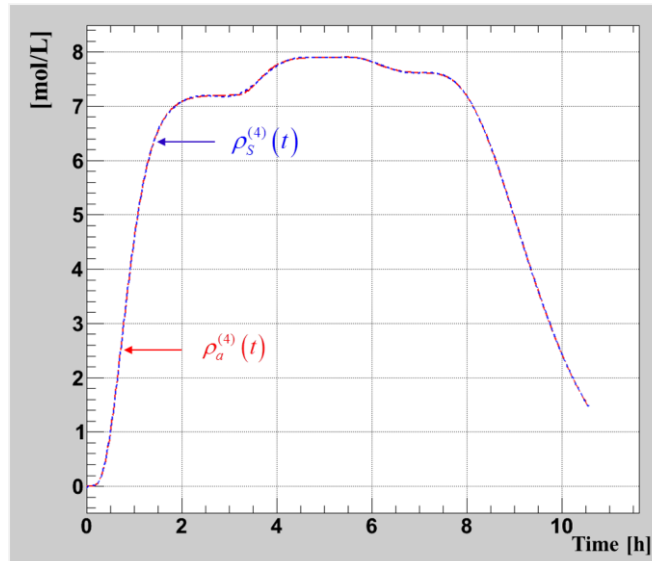
Figure 4.2 Time-dependent behavior of the exact nominal value of the nitric acid concentration $[\text{mol/L}]$ in compartment #4, $\rho_{a,nom}^{(4)}(t)$, reproduced from Figure 3.5, and its spectral representation, $\rho_{a,S}^{(4)}(t)$, using the first 21 Legendre polynomials ($N = 20$).
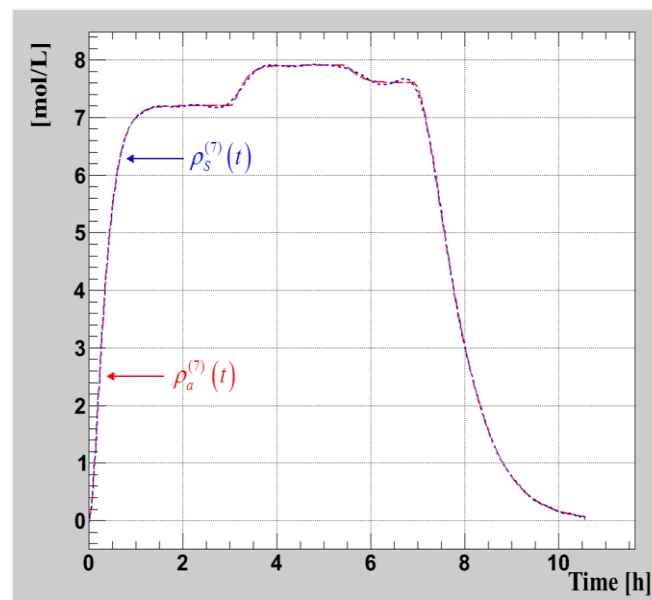
Figure 4.3 Time-dependent behavior of the exact nominal value of the nitric acid concentration $[\text{mol/L}]$, in compartment #7, $\rho_{a,nom}^{(7)}(t_i)$, reproduced from Figure 3.5, and its spectral representation, $\rho_{a,S}^{(7)}(t)$, using the first 29 Legendre polynomials ($N = 28$)

111

The adjoint sensitivity system for computing the sensitivities $\delta\rho_{a,S}^{(4)}(t)$ of $\rho_{a,S}^{(4)}(t)$ becomes

➤ *For each $n = 0,1,...,N = 20$, solve:*

$$V_{nom}^{(1)}(t_f - \tau)\frac{d\psi_{\rho,n}^{(1)}(\tau)}{d\tau} + C\left[V_{nom}^{(1)}(t_f - \tau)\right]\psi_{\rho,n}^{(1)}(\tau) = 0, \ 0 < \tau < t_f, \tag{4.87}$$

$$V_{nom}^{(k)}(t_f - \tau)\frac{d\psi_{\rho,n}^{(k)}(\tau)}{d\tau} + C\left[V_{nom}^{(k)}(t_f - \tau)\right]\left[\psi_{\rho,n}^{(k)}(\tau) - \psi_{\rho,n}^{(k-1)}(\tau)\right] = 0,$$

$$\text{for } k = 2,3,5,6,7,8; \ 0 < \tau < t_f, \tag{4.88}$$

$$V_{nom}^{(k)}(t_f - \tau)\frac{d\psi_{\rho,n}^{(k)}(\tau)}{d\tau} + C\left[V_{nom}^{(k)}(t_f - \tau)\right]\left[\psi_{\rho,n}^{(k)}(\tau) - \psi_{\rho,n}^{(k-1)}(\tau)\right]$$

$$= \frac{2n+1}{t_f}P_n\left(1 - 2\tau/t_f\right), \ k = 4; \ 0 < \tau < t_f, \tag{4.89}$$

$$\frac{dy_{V,n}^{(1)}(t)}{dt} + D_V^{(1)}(t_f - t)y_{V,n}^{(1)}(t) + D_r^{(1)}(t_f - t)y_{r,n}^{(1)}(t) = 0, \ 0 < t < t_f, \tag{4.90}$$

$$\frac{dy_{V,n}^{(k)}(t)}{dt} + D_V^{(k)}(t_f - t)\left[\hat{y}_{V,n}^{(k)}(t) - y_{V,n}^{(k-1)}(t)\right] + D_r^{(k)}(t_f - t)y_{r,n}^{(k)}(t)$$

$$+ \left[r_{a,nom}^{(k-1)}(t_f - t) - r_{a,nom}^{(k)}(t_f - t)\right]D_V^{(k)}(t_f - t)y_{r,n}^{(k-1)}(t) = 0, \ k = 2,...,8, \ 0 < t < t_f, \tag{4.91}$$

subject to the initial conditions

$$\psi_{\rho,n}^{(k)}(\tau = 0) = 0, \ \ \psi_{V,n}^{(k)}(\tau = 0) = 0, \ \ k = 1,...,8. \tag{4.92}$$

The sensitivities $\delta\rho_{a,S}^{(4)}(t)$ of $\rho_{a,S}^{(4)}(t)$ are computed by using the following summation:

$$\delta\rho_{a,S}^{(4)}(t) = \sum_{n=0}^{N=20} \delta a_n\left(\mathbf{h}_\alpha, \boldsymbol{\psi}; \boldsymbol{\alpha}^0\right)P_n\left(2t/t_f - 1\right), \tag{4.93}$$

where the expression of $\delta a_n\left(\mathbf{h}_\alpha, \boldsymbol{\psi}; \boldsymbol{\alpha}^0\right)$ remains *formally* the same as shown in Eq. (4.86), except that the adjoint functions $\psi_{\rho,n}^{(k)}(t)$ and $\psi_{V,n}^{(k)}(t)$ are now the solutions of Eqs. (4.87) through (4.92).

The sensitivities of $\rho_{a,S}^{(7)}(t)$ for compartment (#7) are computed similarly, except that the summation formula becomes

$$D\rho_{a,S}^{(7)}(t) = \sum_{n=0}^{N=28} Da_n\left(\mathbf{h}_\alpha, \mathbf{\psi}; \mathbf{\alpha}^0\right) P_n\left(2t/t_f - 1\right), \tag{4.94}$$

where the expression of $Da_n\left(\mathbf{h}_\alpha, \mathbf{\psi}; \mathbf{\alpha}^0\right)$ remains *formally* the same as shown in Eq. (4.86), except that the adjoint functions $\psi_{\rho,n}^{(k)}(t)$ and $\psi_{V,n}^{(k)}(t)$ are now the solutions of the adjoint sensitivity system given below:

➤ *For each $n = 0,1,...,N = 28$, solve:*

$$V_{nom}^{(1)}\left(t_f - \tau\right)\frac{d\psi_{\rho,n}^{(1)}(\tau)}{d\tau} + C\left[V_{nom}^{(1)}\left(t_f - \tau\right)\right]\psi_{\rho,n}^{(1)}(\tau) = 0, \ 0 < \tau < t_f, \tag{4.95}$$

$$V_{nom}^{(k)}\left(t_f - \tau\right)\frac{d\psi_{\rho,n}^{(k)}(\tau)}{d\tau} + C\left[V_{nom}^{(k)}\left(t_f - \tau\right)\right]\left[\psi_{\rho,n}^{(k)}(\tau) - \psi_{\rho,n}^{(k-1)}(\tau)\right] = 0,$$
$$for \quad k = 2,3,4,5,6,8; \ 0 < \tau < t_f, \tag{4.96}$$

$$V_{nom}^{(k)}\left(t_f - \tau\right)\frac{d\psi_{\rho,n}^{(k)}(\tau)}{d\tau} + C\left[V_{nom}^{(k)}\left(t_f - \tau\right)\right]\left[\psi_{\rho,n}^{(k)}(\tau) - \psi_{\rho,n}^{(k-1)}(\tau)\right]$$
$$= \frac{2n+1}{t_f}P_n\left(1 - 2\tau/t_f\right), \quad k = 7; \ 0 < \tau < t_f, \tag{4.97}$$

$$\frac{dy_{V,n}^{(1)}(t)}{dt} + D_V^{(1)}\left(t_f - t\right)y_{V,n}^{(1)}(t) + D_r^{(1)}\left(t_f - t\right)y_{r,n}^{(1)}(t) = 0, \ 0 < t < t_f, \tag{4.98}$$

$$\frac{dy_{V,n}^{(k)}(t)}{dt} + D_V^{(k)}\left(t_f - t\right)\left[y_{V,n}^{(k)}(t) - y_{V,n}^{(k-1)}(t)\right] + D_r^{(k)}\left(t_f - t\right)y_{r,n}^{(k)}(t)$$
$$+ \left[r_{a,nom}^{(k-1)}\left(t_f - t\right) - r_{a,nom}^{(k)}\left(t_f - t\right)\right]D_V^{(k)}\left(t_f - t\right)y_{r,n}^{(k-1)}(t) = 0, \ k = 2,...,8, \ 0 < t < t_f, \tag{4.99}$$

subject to the initial conditions

$$\psi_{\rho,n}^{(k)}(\tau = 0) = 0, \ \psi_{V,n}^{(k)}(\tau = 0) = 0, \ k = 1,...,8. \tag{4.100}$$

The explicit expressions of the various sensitivities are obtained by introducing Eqs. (4.10) through (4.14) into Eq. (4.86) and collecting like terms. For example, the 1st-order

113

sensitivities of $\rho_{a,S}^{(1)}(t)$ with respect to the model parameters V_0, b, a, G, p have the following expressions:

$$S_{1,n}^{(1)}(\mathbf{u}, \boldsymbol{\psi}; \boldsymbol{\alpha}) \triangleq \frac{\partial a_n(\mathbf{u}, \boldsymbol{\psi}; \boldsymbol{\alpha})}{\partial a}$$
$$= -\int_0^{t_f} \left\{ \psi_{\rho,n}^{(8)}(t) \left[\rho_a^{(in)}(t) - \rho_a^{(8)}(t) \right] + \psi_{V,n}^{(8)}(t) \right\} \frac{\dot{m}^{(in)}(t) \left[63 \rho_a^{(in)}(t) \right]}{\left[63 a \rho_a^{(in)}(t) + b \right]^2} dt \qquad (4.101)$$

$$S_{2,n}^{(1)}(\mathbf{u}, \boldsymbol{\psi}; \boldsymbol{\alpha}) \triangleq \frac{\partial a_n(\mathbf{u}, \boldsymbol{\psi}; \boldsymbol{\alpha})}{\partial b}$$
$$= -\int_0^{t_f} \left\{ \psi_{\rho,n}^{(8)}(t) \left[\rho_a^{(in)}(t) - \rho_a^{(8)}(t) \right] + \psi_{V,n}^{(8)}(t) \right\} \frac{\dot{m}^{(in)}(t)}{\left[63 a \rho_a^{(in)}(t) + b \right]^2} dt \qquad (4.102)$$

$$S_{3,n}^{(1)}(\mathbf{u}, \boldsymbol{\psi}; \boldsymbol{\alpha}) \triangleq \frac{\partial a_n(\mathbf{u}, \boldsymbol{\psi}; \boldsymbol{\alpha})}{\partial V_0} = \sum_{k=1}^{7} \int_0^{t_f} \psi_{\rho,n}^{(k)}(t) \left[\rho_a^{(k+1)}(t) - \rho_a^{(k)}(t) \right] \frac{\partial C\left(V^{(k+1)}\right)}{\partial V_0} dt$$
$$+ \sum_{k=1}^{7} \int_0^{t_f} \psi_{V,n}^{(k)}(t) \frac{\partial \left[C\left(V^{(k+1)}\right) - C\left(V^{(k)}\right) \right]}{\partial V_0} dt - \int_0^{t_f} \psi_{V,n}^{(8)}(t) \frac{\partial C\left(V^{(8)}\right)}{\partial V_0} dt, \qquad (4.103)$$

$$S_{4,n}^{(1)}(\mathbf{u}, \boldsymbol{\psi}; \boldsymbol{\alpha}) \triangleq \frac{\partial a_n(\mathbf{u}, \boldsymbol{\psi}; \boldsymbol{\alpha})}{\partial G} = \sum_{k=1}^{7} \int_0^{t_f} \psi_{\rho,n}^{(k)}(t) \left[\rho_a^{(k+1)}(t) - \rho_a^{(k)}(t) \right] \frac{\partial C\left(V^{(k+1)}\right)}{\partial G} dt$$
$$+ \sum_{k=1}^{7} \int_0^{t_f} \psi_{V,n}^{(k)}(t) \frac{\partial \left[C\left(V^{(k+1)}\right) - C\left(V^{(k)}\right) \right]}{\partial G} dt - \int_0^{t_f} \psi_{V,n}^{(8)}(t) \frac{\partial C\left(V^{(8)}\right)}{\partial G} dt, \qquad (4.104)$$

$$S_{5,n}^{(1)}(\mathbf{u}, \boldsymbol{\psi}; \boldsymbol{\alpha}) \triangleq \frac{\partial a_n(\mathbf{u}, \boldsymbol{\psi}; \boldsymbol{\alpha})}{\partial p} = \sum_{k=1}^{7} \int_0^{t_f} \psi_{\rho,n}^{(k)}(t) \left[\rho_a^{(k+1)}(t) - \rho_a^{(k)}(t) \right] \frac{\partial C\left(V^{(k+1)}\right)}{\partial p} dt$$
$$+ \sum_{k=1}^{7} \int_0^{t_f} \psi_{V,n}^{(k)}(t) \frac{\partial \left[C\left(V^{(k+1)}\right) - C\left(V^{(k)}\right) \right]}{\partial p} dt - \int_0^{t_f} \psi_{V,n}^{(8)}(t) \frac{\partial C\left(V^{(8)}\right)}{\partial G} dt, \qquad (4.105)$$

4.3. Sensitivity Analysis Results

The absolute and, respectively, relative sensitivities of the nitric acid concentrations $\rho_{a,nom}^{(1)}(t_i)$, $\rho_{a,nom}^{(4)}(t_i)$, and $\rho_{a,nom}^{(7)}(t_i)$ computed at a time instance t_i to the scalar parameter a are presented in Figures 4.4 and 4.5. The main features of these sensitivities are as follows:

(i)   the sensitivities of the responses to each of these parameters are quite localized temporally;

(ii)   all of these sensitivities are negative, meaning that an increase in the magnitude of each of the respective parameters will induce a decrease in the magnitude respective response;

(iii)   after reaching a minimum (or maximum in absolute value), all of these sensitivities decay quickly to zero for the remaining duration of the transient;

(iv)   the earliest (in time) impact of the respective sensitivity is on the compartment (#7) closest to the inlet; the impact of the sensitivity/disturbance propagates in time towards the last compartment; and,

(v)   the largest impact of the each of these sensitivities is on the compartment (#1) furthest from the inlet.

To enable the comparison of the respective relative sensitivities, the respective normalizations were normalized, arbitrarily but consistently, to be the acid concentration after 60 minutes into the transient.
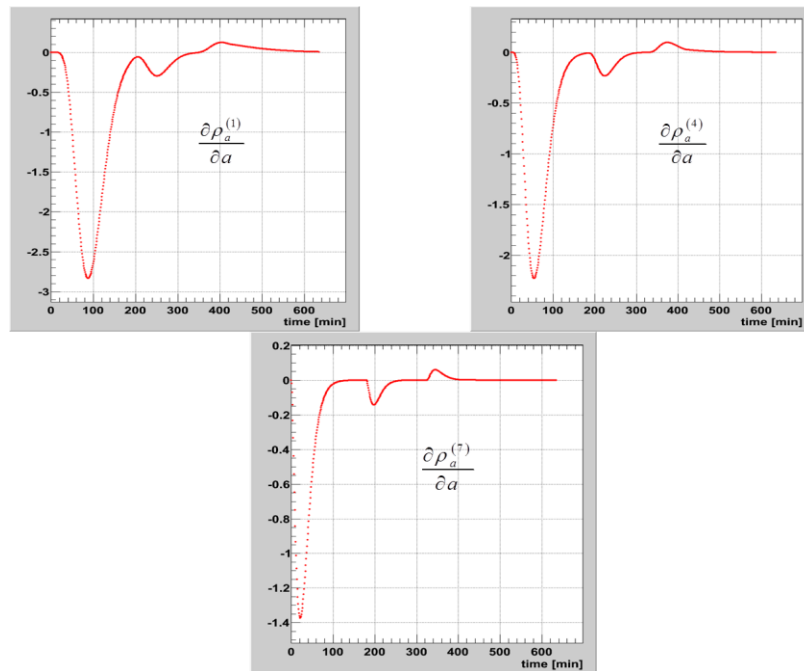
Figure 4.4 Absolute sensitivities of $\rho_{a,nom}^{(1)}\left(t_i\right), \rho_{a,nom}^{(4)}\left(t_i\right)$, and, $\rho_{a,nom}^{(7)}\left(t_i\right)$ to the scalar parameter a.
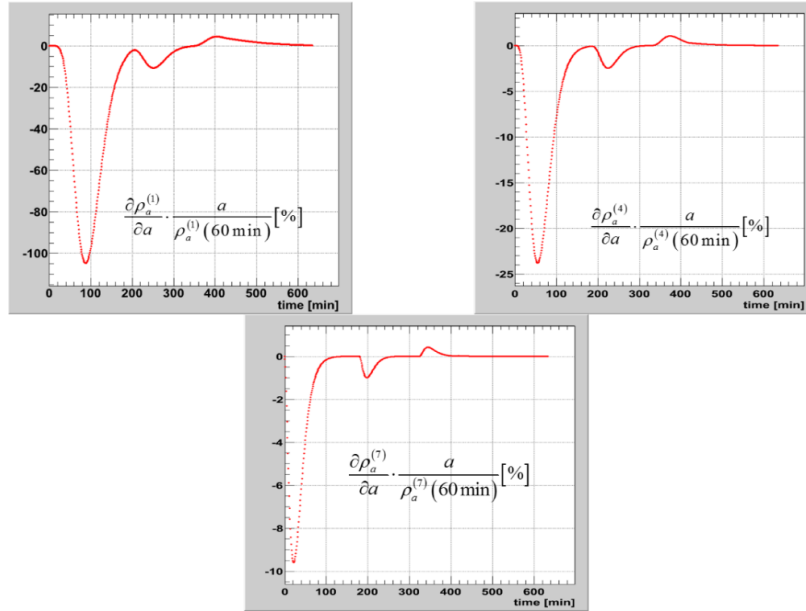
Figure 4.5 Relative sensitivities of $\rho_{a,nom}^{(1)}\left(t_i\right), \rho_{a,nom}^{(4)}\left(t_i\right)$, and, $\rho_{a,nom}^{(7)}\left(t_i\right)$ to the scalar parameter a.

The absolute and, respectively, relative sensitivities of $\rho_{a,nom}^{(1)}\left(t_i\right)$, $\rho_{a,nom}^{(4)}\left(t_i\right)$, and $\rho_{a,nom}^{(7)}\left(t_i\right)$ to the scalar parameters V_0, b, and G are presented in Figures 4.6 through 4.11. The response sensitivities to these parameters show similar features, as follows:

(i)   In time, the sensitivities of the responses to each of these parameters undergo first a minimum having large negative values, then display a plateau around zero, followed by a rise to a maximum; this maximum decays towards zero in the first compartment, but does not "have sufficient time" to do the same in the last compartment, remaining there with a high value at the end of the transient;

(ii)   The earliest (in time) impact of the respective sensitivity is on the compartment (#7) closest to the inlet; the impact of the sensitivity/disturbance propagates in time towards the last compartment;

(iii)   The largest impact, in absolute value, of the each of these sensitivities is on the compartment (#1) furthest from the inlet;

(iv)   As before the respective normalizations were chosen, arbitrarily but consistently, to be the acid concentration 60 minutes into the transient. Comparing the various relative sensitivities reveals that their magnitudes are largest for the parameters

116

V_0 and b, and smaller for G, indicating that the impact of comparable uncertainties in V_0 and b will have a higher impact on the response uncertainties than those for G.
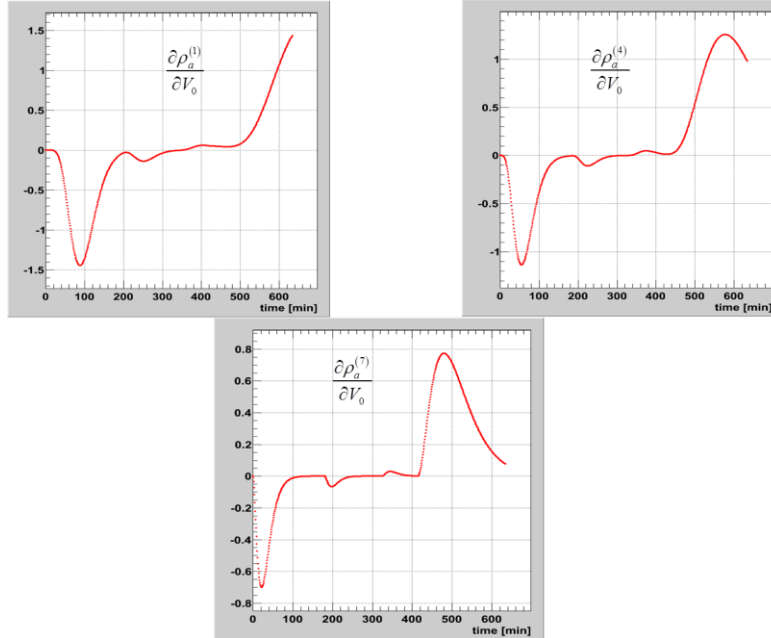
Figure 4.6 Absolute sensitivities, in units of $\left[\text{mol/L}^2\right]$, of $\rho_{a,nom}^{(1)}\left(t_i\right)$, $\rho_{a,nom}^{(4)}\left(t_i\right)$, and $\rho_{a,nom}^{(7)}\left(t_i\right)$, to the scalar parameter V_0.
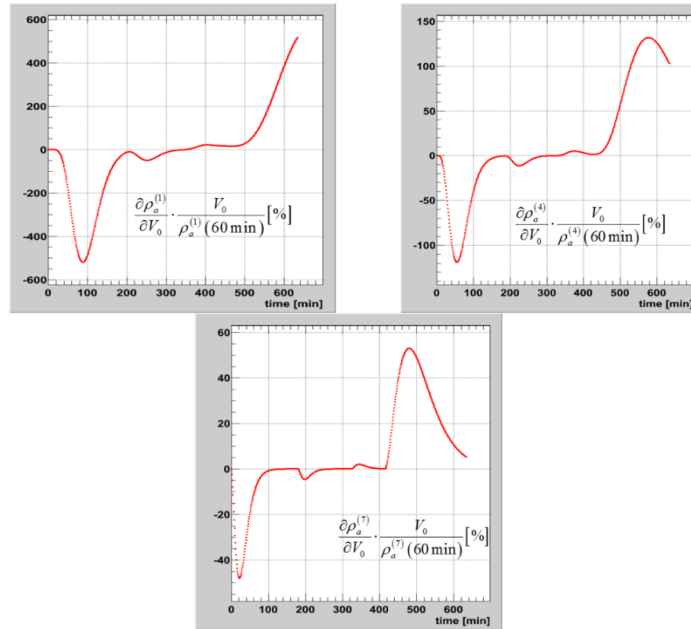
Figure 4.7 Relative sensitivities of $\rho_{a,nom}^{(1)}\left(t_i\right)$, $\rho_{a,nom}^{(4)}\left(t_i\right)$, and $\rho_{a,nom}^{(7)}\left(t_i\right)$, to the scalar parameter V_0.
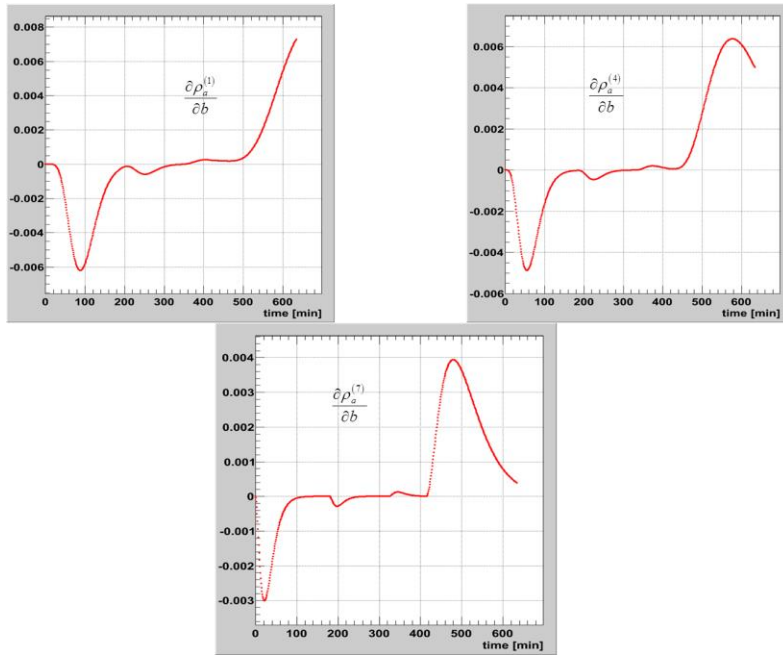
Figure 4.8 Absolute sensitivities, in units of $[\text{mol/g}]$, of $\rho_{a,nom}^{(1)}(t_i)$, $\rho_{a,nom}^{(4)}(t_i)$, and $\rho_{a,nom}^{(7)}(t_i)$, to the scalar parameter b
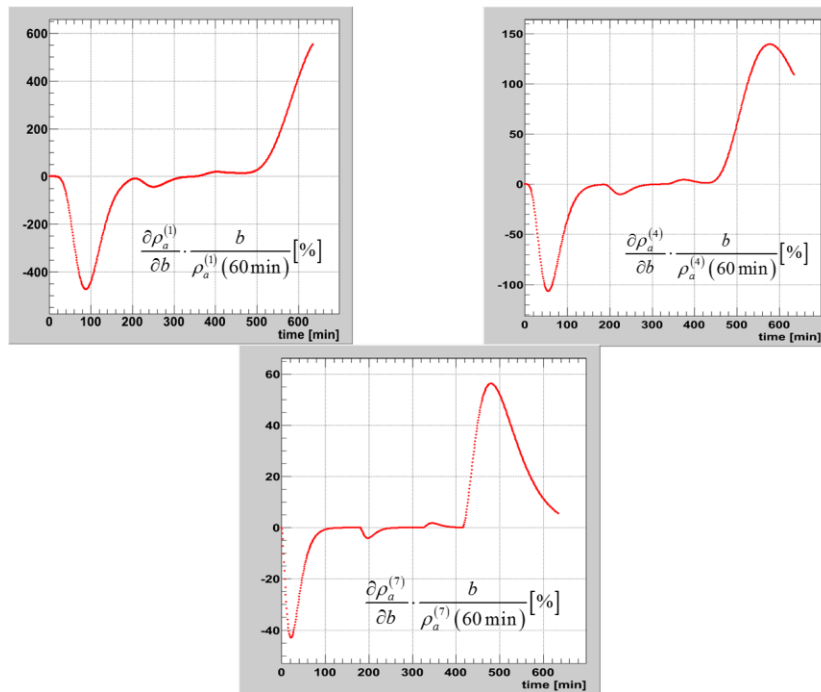
Figure 4.9 Relative sensitivities of $\rho_{a,nom}^{(1)}(t_i)$, $\rho_{a,nom}^{(4)}(t_i)$, and $\rho_{a,nom}^{(7)}(t_i)$, to the scalar parameter b
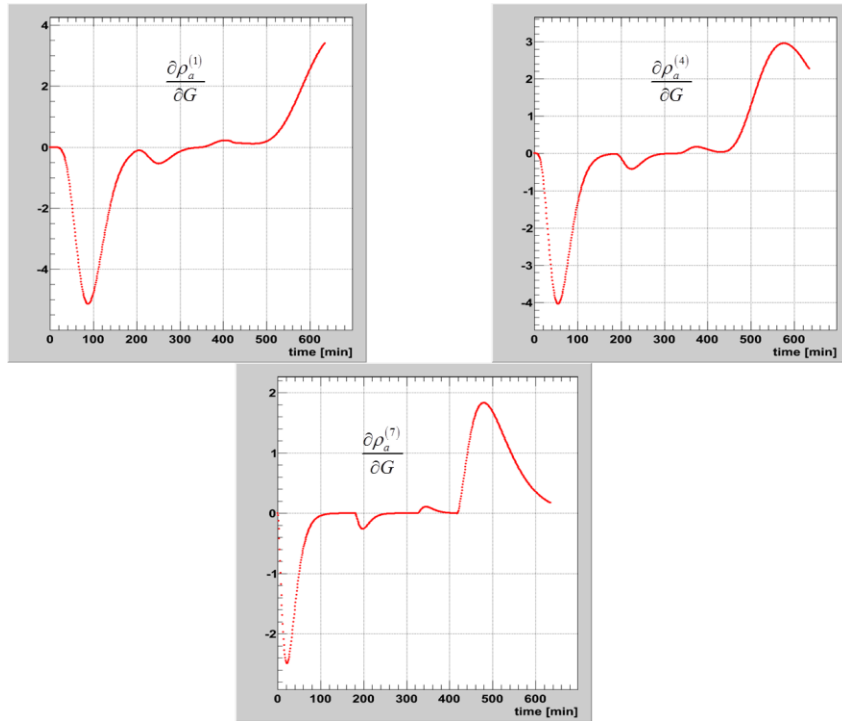
Figure 4.10 Absolute sensitivities, in units of $\left[\text{mol/L}^2\right]$, of $\rho_{a,nom}^{(1)}\left(t_i\right)$, $\rho_{a,nom}^{(4)}\left(t_i\right)$, and $\rho_{a,nom}^{(7)}\left(t_i\right)$ to the scalar parameter G
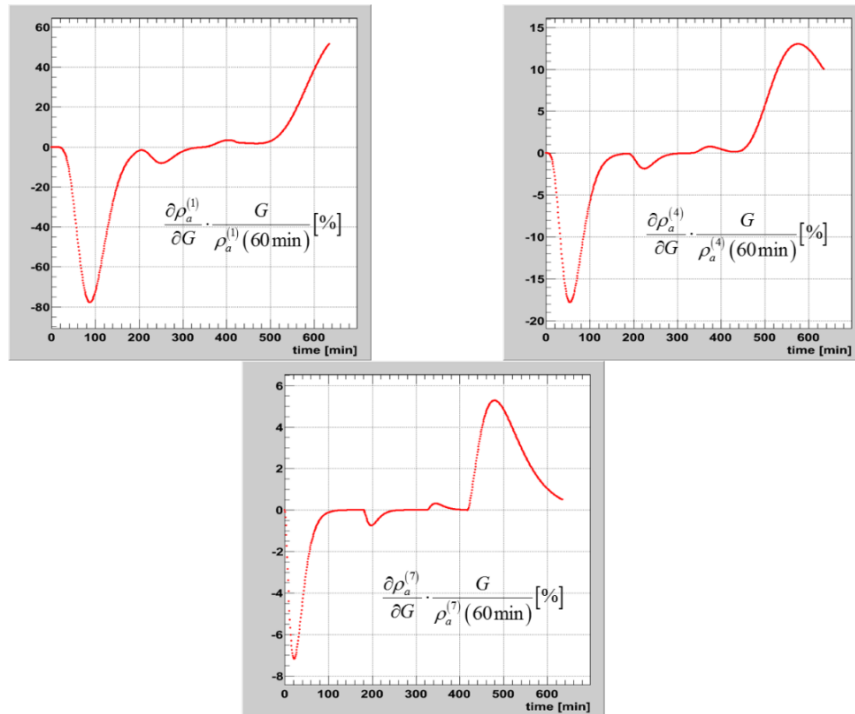
Figure 4.11 Relative sensitivities of $\rho_{a,nom}^{(1)}\left(t_i\right)$, $\rho_{a,nom}^{(4)}\left(t_i\right)$, and $\rho_{a,nom}^{(7)}\left(t_i\right)$ to the scalar parameter G

The sensitivities of $\rho_{a,nom}^{(1)}(t_i)$, $\rho_{a,nom}^{(4)}(t_i)$, and $\rho_{a,nom}^{(7)}(t_i)$ to the scalar parameter p are depicted in Figures 4.12 and 4.13. As these figures indicate these sensitivities behave opposite of the manner to the behavior of the response sensitivities to the parameters V_0, b and G, in that:

(i) Over time, the sensitivities of the responses to each of these parameters is positive and increase to a maximum, plateau around zero, then decrease to minimum negative value; and after increase again toward zero in compartment (#7). However, there is not "sufficient time" for these same characteristics to be play out in compartment (#1), and thus the sensitivities remain negative at the end of the transient;

(ii) The earliest impact of the respective sensitivity is on the compartment (#7) closest to the inlet; and the impact of the sensitivity/disturbance propagates toward the last compartment over time;

(iii) The largest impact, in absolute value, of the each of these sensitivities is on the compartment (#1) furthest from the inlet.
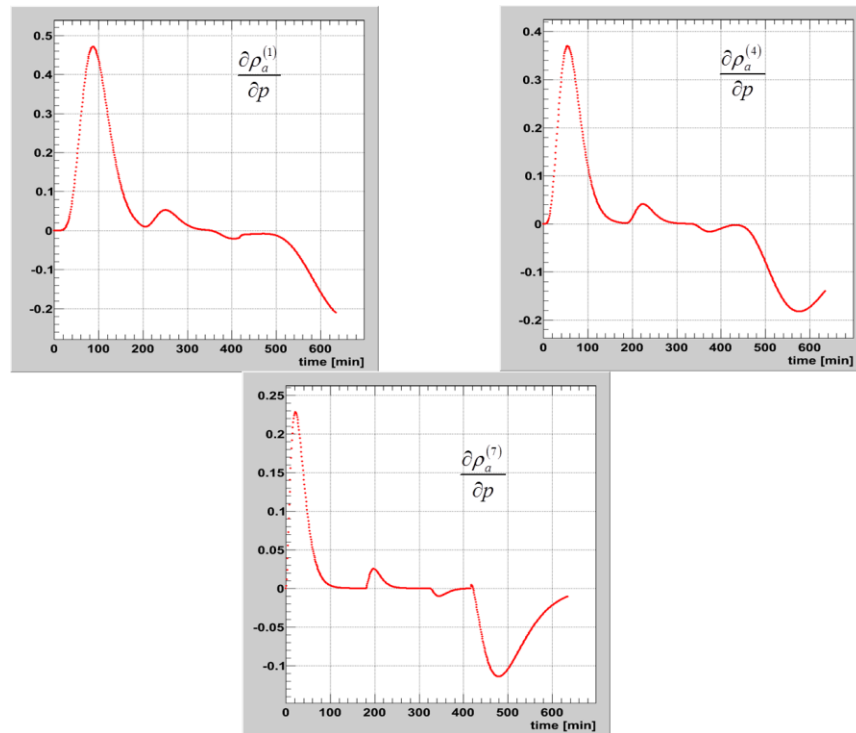
Figure 4.12 Absolute sensitivities, in units of $[\mathrm{mol/L}]$, of $\rho_{a,nom}^{(1)}(t_i)$, $\rho_{a,nom}^{(4)}(t_i)$, and $\rho_{a,nom}^{(7)}(t_i)$ to the scalar parameter p
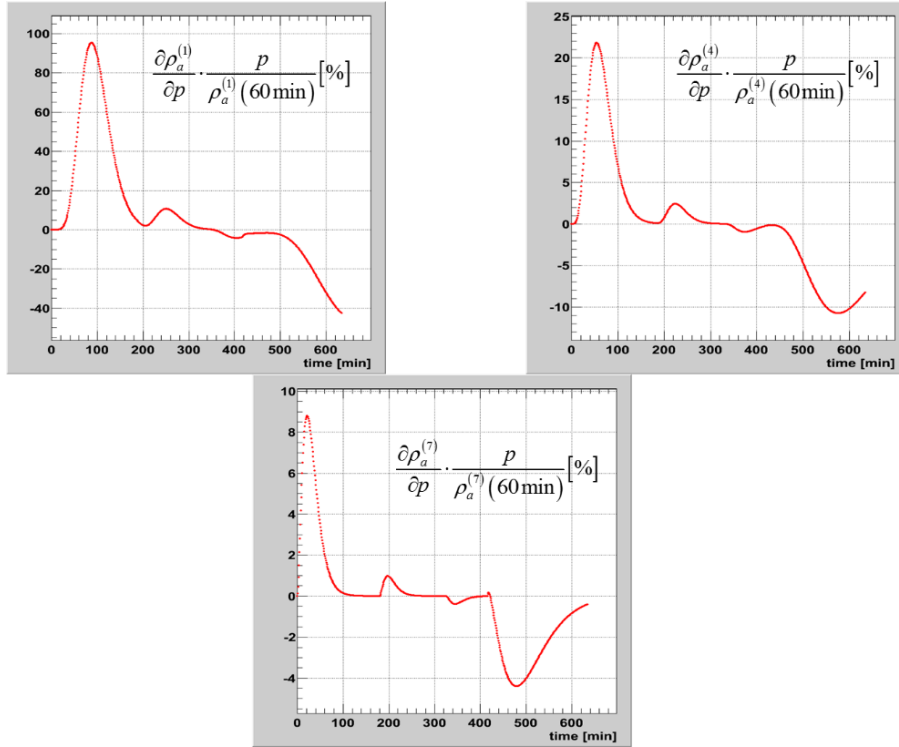
Figure 4.13 Relative sensitivities of $\rho_{a,nom}^{(1)}\left(t_i\right)$, $\rho_{a,nom}^{(4)}\left(t_i\right)$, and $\rho_{a,nom}^{(7)}\left(t_i\right)$ to the scalar parameter p.

All of the sensitivities of $\rho_{a,nom}^{(1)}\left(t_i\right)$, $\rho_{a,nom}^{(4)}\left(t_i\right)$, and $\rho_{a,nom}^{(7)}\left(t_i\right)$ to the scalar parameters $\dot{m}^{(in)}\left(t_i\right)$, $i=1,...,1291$, have been computed using the ASAM for subsequent use in the formulas for combining experimental and computational data to perform "forward and inverse predictive modeling", as will be discussed in Chapters 5 and 6, below. The sensitivities of $\rho_{a,nom}^{(1)}\left(t_i\right)$, $\rho_{a,nom}^{(4)}\left(t_i\right)$, and $\rho_{a,nom}^{(7)}\left(t_i\right)$ to all 1291 model parameters $\dot{m}^{(in)}\left(t_i\right)$ are numerous so only selected Figures 4.14 through 4.19 that illustrated major trends were chosen to display the relative sensitivities of $\rho_{a,nom}^{(1)}\left(t_i\right)$, $\rho_{a,nom}^{(4)}\left(t_i\right)$, and $\rho_{a,nom}^{(7)}\left(t_i\right)$ to the scalar parameters $\dot{m}^{(in)}\left(t_i\right)$. The following features become apparent from Figures 4.14 through 4.16:

(i)   As Figure 4.14 indicates, all of the relative sensitivities of $\rho_{a,nom}^{(1)}\left(t_i\right)$, $\rho_{a,nom}^{(4)}\left(t_i\right)$, and $\rho_{a,nom}^{(7)}\left(t_i\right)$ to $\dot{m}^{(in)}\left(t_i\right)$ at $t_i=31$ minutes are significant having values greater

than 1 (recall that a relative sensitivity of 1 implies that a 1% change in the respective parameter would induce a 1% change in the respective response).

The response furthest from the inlet, namely $\rho_{a,nom}^{(1)}(t_i)$, displays the largest relative sensitivities to the parameter $\dot{m}^{(in)}(t_i)$ at $t_i = 31$ minutes. The closer the compartment is to the inlet, the increasingly smaller the corresponding responses are to responses in the compartment closest to the inlet, namely $\rho_{a,nom}^{(7)}(t_i)$. The response $\rho_{a,nom}^{(7)}(t_i)$, displays the smallest sensitivities, and hence is least affected by uncertainties in $\dot{m}^{(in)}(t_i)$. The compartment (#7) closest to the inlet responds first while the compartment (#1) furthest from the inlet responds last in time, and all of these sensitivities are positive.

(ii)   As Figure 4.15 indicates, the relative sensitivities of $\rho_{a,nom}^{(1)}(t_i)$, $\rho_{a,nom}^{(4)}(t_i)$, and $\rho_{a,nom}^{(7)}(t_i)$ to the parameter $\dot{m}^{(in)}(t_i)$ at $t_i = 240$ minutes continues to display the same trend described above, remaining all positive while decreasing proportionally from the inlet to the outlet. All sensitivities are comparatively smaller than those with respect to $\dot{m}^{(in)}(t_i)$ at $t_i = 31$ minutes.

(iii)   Recall from Figure 3.3 that the inlet mass rate flow, $\dot{m}^{(in)}(t_i)$, of nitric acid decreases at 325 minutes (5.42 hours) from the value of 46.83 to 41.67 $\left[kg/h\right]$. This (negative) change is reflected in Figure 4.16, which shows that the response closest to the change, namely the acid concentration $\rho_{a,nom}^{(7)}(t_i)$ in compartment 7, changes from positive to negative from the influence of the sensitivity $\partial\rho_{a,nom}^{(7)}(t_i)/\partial\dot{m}^{(in)}(t_i)$. This abrupt change causes some very minor Gibbs-like oscillations around zero in $\partial\rho_{a,nom}^{(7)}(t_i)/\partial\dot{m}^{(in)}(t_i)$ which propagate later in time. The negative change in $\dot{m}^{(in)}(t_i)$ affects all compartments "downstream" from the inlet, up to and including compartment #4, as depicted by the graph of

$\partial \rho_{a,nom}^{(4)}\left(t_i\right)\big/\partial \dot{m}^{(in)}\left(t_i\right)$, which at 325 minutes precisely changes signs from positive to negative. The sensitivities of the compartments #3, #2, and #1, furthest away from the disturbance in the inlet mass flow rate, remain positive showing no effect on acid concentrations.

(iv) One time-step (1 minute) later, at 326 minutes, the graphs in Figure 4.17 show the disturbance in the inlet mass flow rate, $\dot{m}^{(in)}\left(t_i\right)$ finally reaching the furthest compartment from the inlet, namely compartment #1, where the sensitivity $\partial \rho_{a,nom}^{(1)}\left(t_i\right)\big/\partial \dot{m}^{(in)}\left(t_i\right)$ changes signs from positive to negative, with the discontinuity in the derivative $\partial \rho_{a,nom}^{(1)}\left(t_i\right)\big/\partial \dot{m}^{(in)}\left(t_i\right)$ occurring at 325 minutes. The corresponding sensitivities in all of the other compartments are negative, reflecting the effect of the disturbance in $\dot{m}^{(in)}\left(t_i\right)$.

(v) Figure 4.18 shows that the relative sensitivities to the parameter $\dot{m}^{(in)}\left(t_i\right)$ at $t_i = 360$ minutes remain negative and is small in absolute value. The largest (albeit small) impact of a change in $\dot{m}^{(in)}\left(t_i\right)$ is on the response furthest from the outlet, while the smallest impact is on the response in the compartment closets to the inlet.

(vi) Figure 4.19 shows that at $t_i = 540$ minutes, the relative sensitivities to the parameter $\dot{m}^{(in)}\left(t_i\right)$ remain negative, but increase in absolute value, becoming significantly larger over time, than those with respect to the parameter $\dot{m}^{(in)}\left(t_i\right)$ at $t_i = 360$ minutes.

(vii) At all times, all of the above sensitivities are sharply localized around the respective instance in time, and are zero otherwise.

123
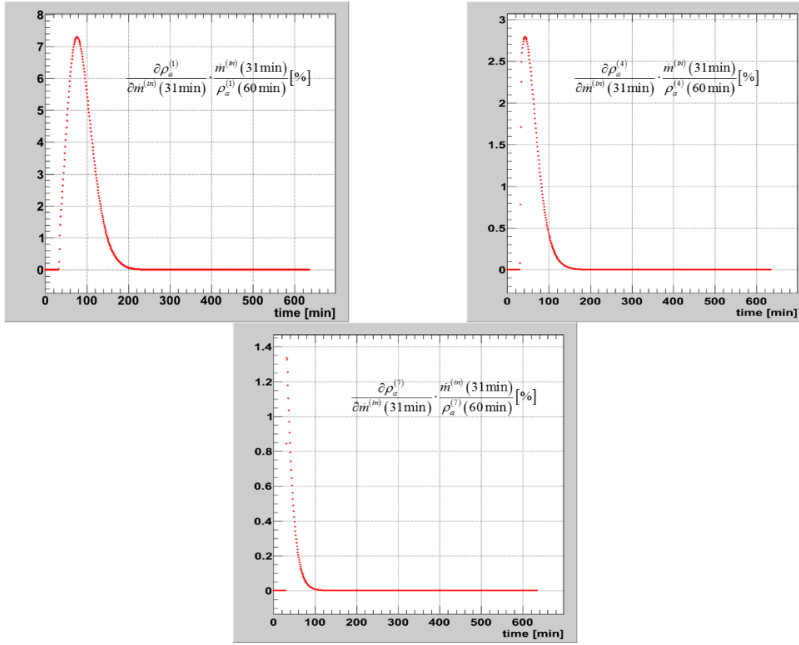
Figure 4.14 Relative sensitivities of $\rho_{a,nom}^{(1)}\left(t_i\right)$, $\rho_{a,nom}^{(4)}\left(t_i\right)$, and $\rho_{a,nom}^{(7)}\left(t_i\right)$ to the scalar parameter $\dot{m}^{(in)}\left(t_i\right)$ at $t_i = 31$ minutes.
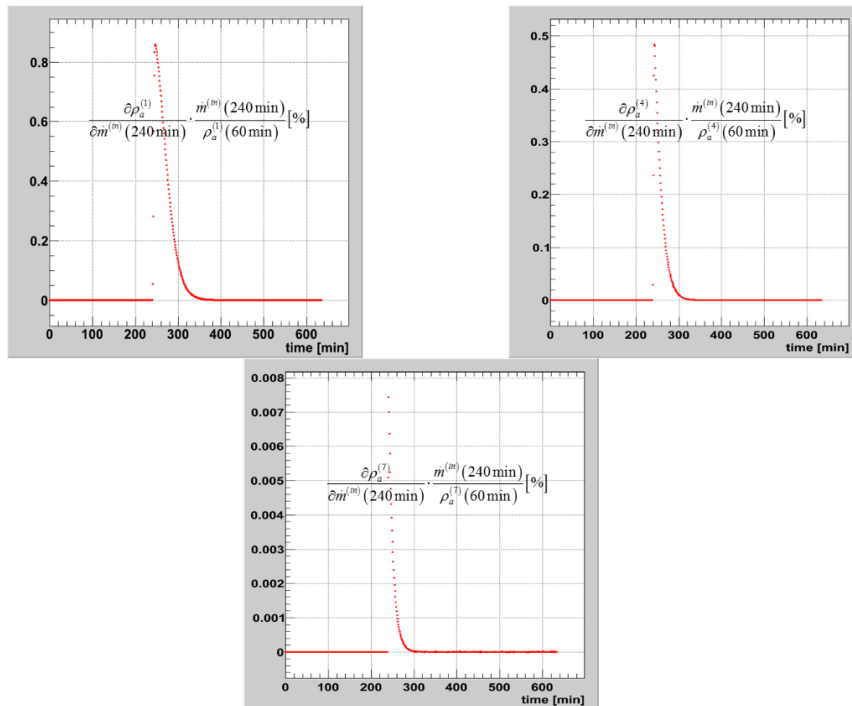
Figure 4.15 Relative sensitivities of $\rho_{a,nom}^{(1)}\left(t_i\right)$, $\rho_{a,nom}^{(4)}\left(t_i\right)$, and $\rho_{a,nom}^{(7)}\left(t_i\right)$ to the scalar parameter $\dot{m}^{(in)}\left(t_i\right)$ at $t_i = 240$ minutes.
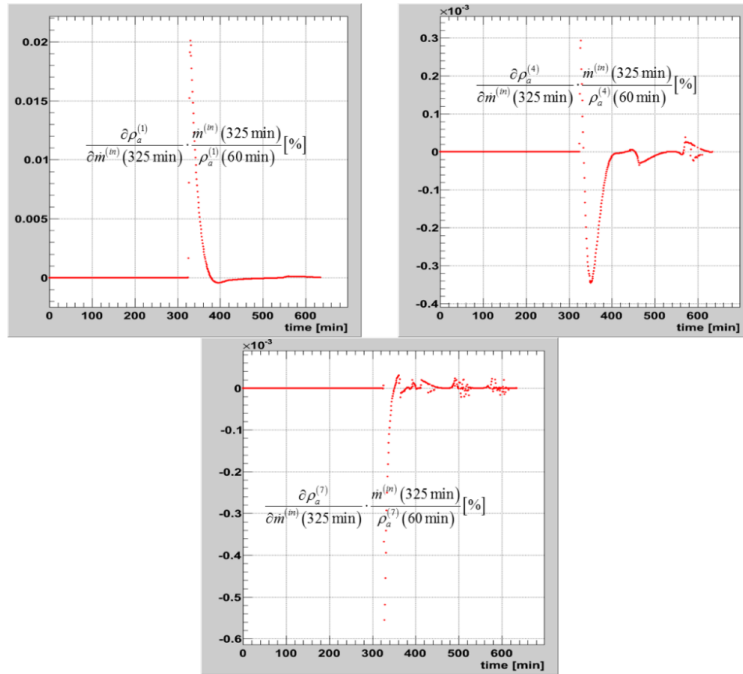
Figure 4.16 Relative sensitivities of $\rho^{(1)}_{a,nom}\left(t_i\right)$, $\rho^{(4)}_{a,nom}\left(t_i\right)$, and $\rho^{(7)}_{a,nom}\left(t_i\right)$ to the scalar parameter $\dot{m}^{(in)}\left(t_i\right)$ at $t_i = 325$ minutes
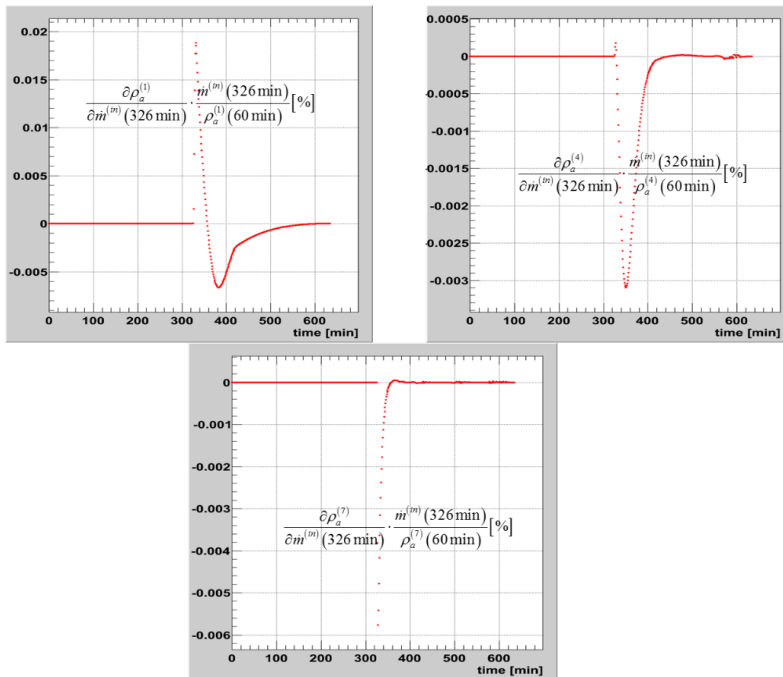
Figure 4.17 Relative sensitivities of $\rho^{(1)}_{a,nom}\left(t_i\right)$, $\rho^{(4)}_{a,nom}\left(t_i\right)$, and $\rho^{(7)}_{a,nom}\left(t_i\right)$ to the scalar parameter $\dot{m}^{(in)}\left(t_i\right)$ at $t_i = 326$ minutes
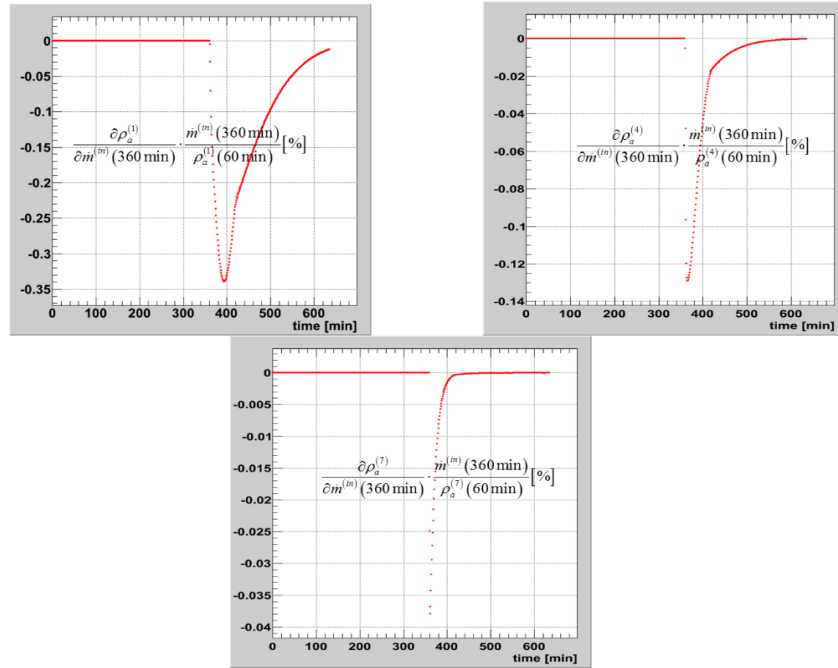
Figure 4.18 Relative sensitivities of $\rho_{a,nom}^{(1)}(t_i)$, $\rho_{a,nom}^{(4)}(t_i)$, and $\rho_{a,nom}^{(7)}(t_i)$ to the scalar parameter $\dot{m}^{(in)}(t_i)$ at $t_i = 360$ minutes
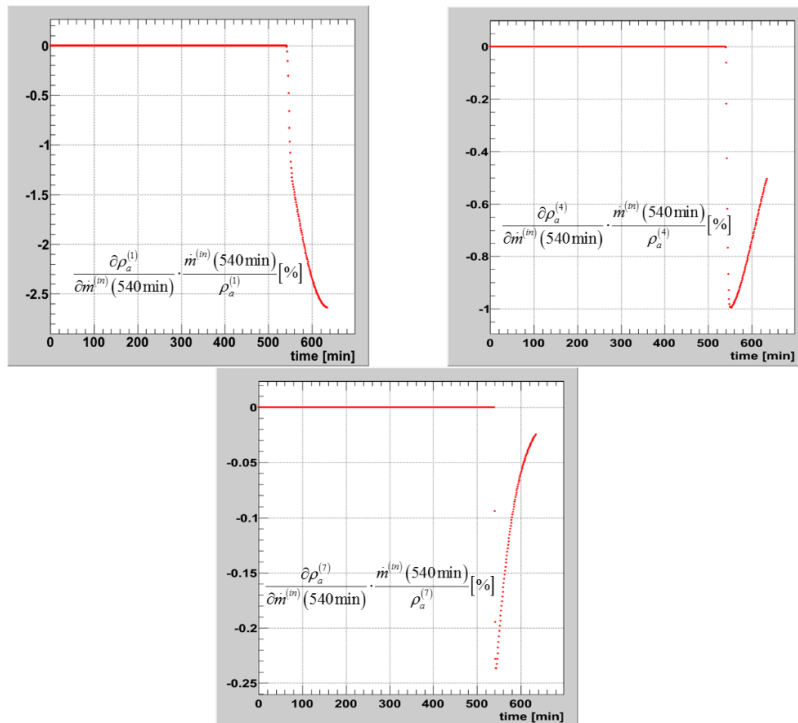
Figure 4.19 Relative sensitivities of $\rho_{a,nom}^{(1)}(t_i)$, $\rho_{a,nom}^{(4)}(t_i)$, and $\rho_{a,nom}^{(7)}(t_i)$ to the scalar parameter $\dot{m}^{(in)}(t_i)$ at $t_i = 540$ minutes

All of the sensitivities of $\rho_{a,nom}^{(1)}(t_i)$, $\rho_{a,nom}^{(4)}(t_i)$, and $\rho_{a,nom}^{(7)}(t_i)$ to the scalar parameters $\rho_a^{(in)}(t_i)$, $i = 1,...,1291$, have also been computed for subsequent use for the "forward and inverse predictive modeling" investigations to be discussed in the following, in Chapters 5 and 6. Nevertheless, the major trends become apparent from Figures 4.20 through 4.23, which display the relative sensitivities of $\rho_{a,nom}^{(1)}(t_i)$, $\rho_{a,nom}^{(4)}(t_i)$, and $\rho_{a,nom}^{(7)}(t_i)$ to the scalar parameters $\rho_a^{(in)}(t_i)$ at $t_i = 31$ minutes, $t_i = 240$ minutes, $t_i = 360$ minutes, and $t_i = 416$ minutes, respectively. Recall from Figure 3.4 that $\rho_a^{(in)}(t_i) = 0$ beyond 6.91 hours (415 minutes). Figures 4.20 through 4.23 show that all of the relative sensitivities of $\rho_{a,nom}^{(1)}(t_i)$, $\rho_{a,nom}^{(4)}(t_i)$, and $\rho_{a,nom}^{(7)}(t_i)$ to the parameters $\rho_a^{(in)}(t_i)$ are significant (i.e., larger than 1) and positive.
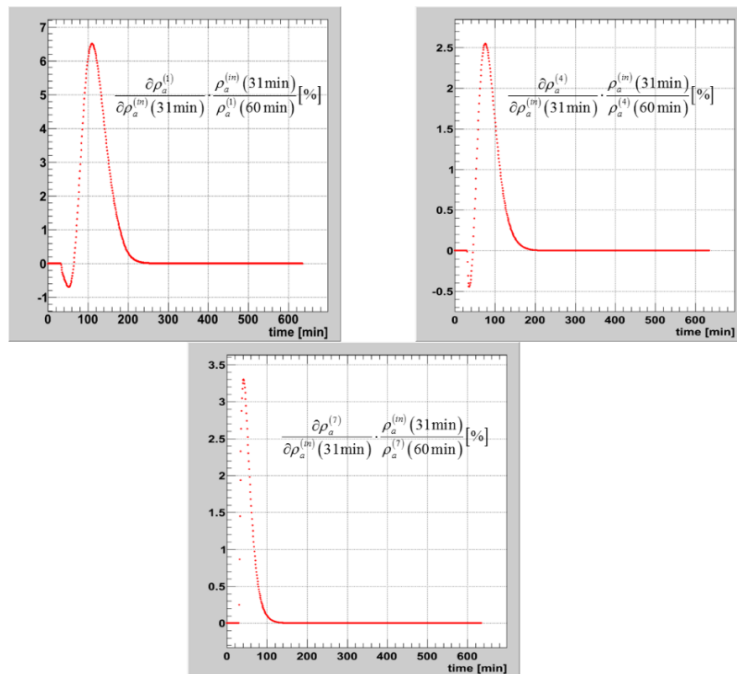
Figure 4.20 Relative sensitivities of $\rho_{a,nom}^{(1)}(t_i)$, $\rho_{a,nom}^{(4)}(t_i)$, and $\rho_{a,nom}^{(7)}(t_i)$ to the scalar parameter $\rho_a^{(in)}(t_i)$ at $t_i = 31$ minutes
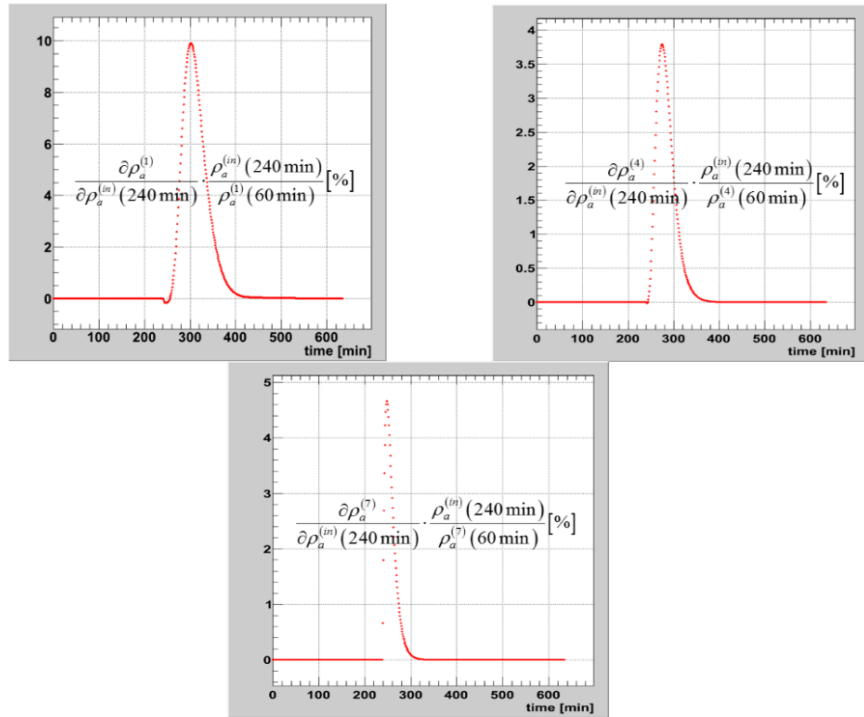
Figure 4.21 Relative sensitivities of $\rho_{a,nom}^{(1)}\left(t_i\right)$, $\rho_{a,nom}^{(4)}\left(t_i\right)$, and $\rho_{a,nom}^{(7)}\left(t_i\right)$ to the scalar parameter $\rho_a^{(in)}\left(t_i\right)$ at $t_i = 240$ minutes
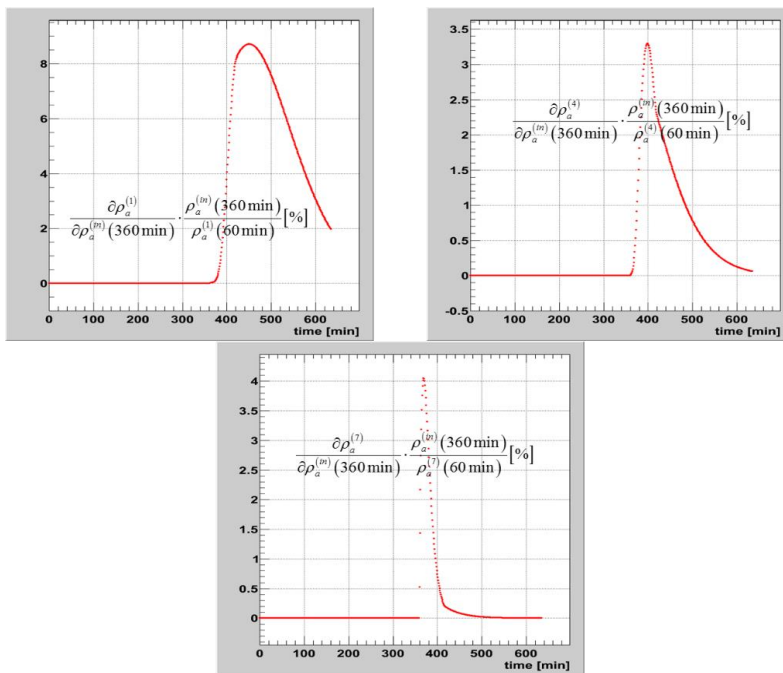
Figure 4.22 Relative sensitivities of $\rho_{a,nom}^{(1)}\left(t_i\right)$, $\rho_{a,nom}^{(4)}\left(t_i\right)$, and $\rho_{a,nom}^{(7)}\left(t_i\right)$ to the scalar parameter $\rho_a^{(in)}\left(t_i\right)$ at $t_i = 360$ minutes
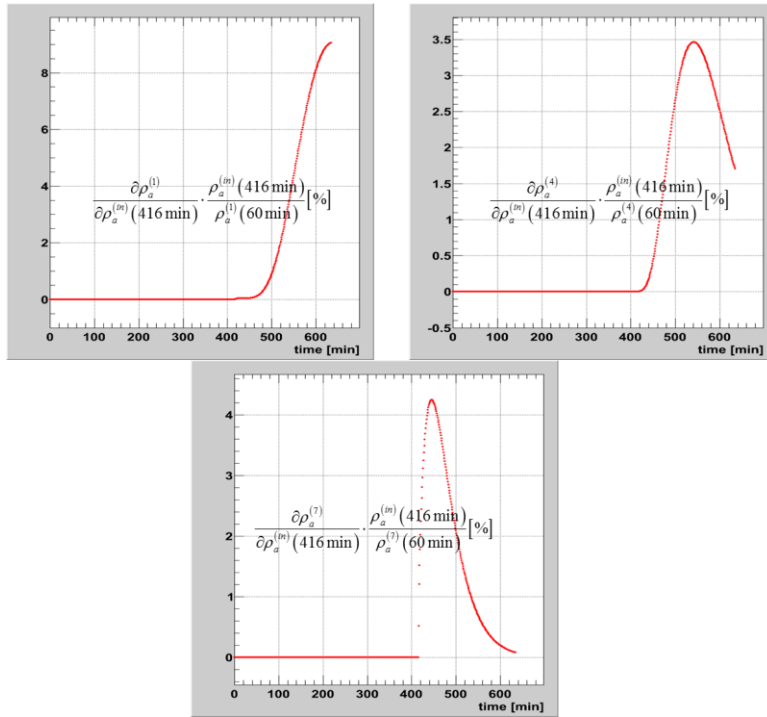
Figure 4.23 Relative sensitivities of $\rho_{a,nom}^{(1)}\left(t_i\right)$, $\rho_{a,nom}^{(4)}\left(t_i\right)$, and $\rho_{a,nom}^{(7)}\left(t_i\right)$ to the scalar parameter $\rho_a^{(in)}\left(t_i\right)$ at $t_i = 416\,\text{minutes}$

5. FORWARD PREDICTIVE MODELING FOR OBTAINING OPTIMAL DISSOLVER MODEL PERFORMANCE WITH REDUCED UNCERTAINTIES

The results presented in this chapter were obtained by applying the general predictive modeling methodology of Cacuci and Ionescu-Bujor (2010b) to the paradigm dissolver model. The application of this methodology will use the sensitivities previously in order to quantify the uncertainties in the computed results, and subsequently reduce them by assimilating the experimental data of Lewis and Weber (1980). For convenient reference, the main results of the predictive modeling methodology of Cacuci and Ionescu-Bujor (2010b) are summarized to better inform how the method will be used to support the subsequent chapters of this work.

Cacuci and Ionescu-Bujor (2010b) consider a general time-dependent physical system comprising N_α^ν model parameters and N_r^ν distinct responses, respectively, at every time node $\nu = 1,...,N_t$. At every time node ν, the (column) vector $\boldsymbol{\alpha}^\nu$ of J_α^ν system parameters, and the (column) vector $\boldsymbol{r}^\nu$ of J_r^ν responses can be represented in component form as

$$\boldsymbol{\alpha}^\nu = \left\{ \alpha_n^\nu \,/ n = 1,\dots N_\alpha^\nu \right\}, \quad \boldsymbol{r}^\nu = \left\{ r_i^\nu \,/ i = 1,\dots,N_r^\nu \right\}, \quad \nu = 1,\dots,N_t. \tag{5.1}$$

at any time node ν, the system parameters are considered to be variates with mean values $\left(\boldsymbol{\alpha}^0 \right)^\nu$. Furthermore, the general form of correlations between two parameters α_i^ν and α_j^μ, at two time nodes μ and ν are denotes as

$$c_{\alpha,ij}^{\nu\mu} \triangleq \left\langle \left[\alpha_i^\nu - \left(\alpha_i^\nu \right)^0 \right] \left[\alpha_j^\mu - \left(\alpha_j^\mu \right)^0 \right] \right\rangle. \tag{5.2}$$

The above covariances constitute the elements of symmetric covariance matrices of the form

$$C_\alpha^{\mu\nu} \triangleq \left\langle (\alpha - \alpha^0)^\mu \left[(\alpha - \alpha^0)^\nu \right]^\dagger \right\rangle = \left(C_\alpha^{\mu\nu} \right)^\dagger = C_\alpha^{\nu\mu} = \left(C_\alpha^{\nu\mu} \right)^\dagger . \tag{5.3}$$

Similarly, the measured responses are characterized by mean values $(r_m)^\nu$ at a time node ν and by symmetric covariance matrices between two time nodes μ and ν defined as

$$C_m^{\mu\nu} \triangleq \left\langle (r - r_m)^\mu \left[(r - r_m)^\nu \right]^\dagger \right\rangle = \left(C_m^{\mu\nu} \right)^\dagger = C_m^{\nu\mu} = \left(C_m^{\nu\mu} \right)^\dagger \tag{5.4}$$

In general, the measured responses may be correlated to the parameters through response-parameter uncertainty matrices of the form

$$C_{r\alpha}^{\mu\nu} \triangleq \left\langle (r - r_m)^\mu \left[(\alpha - \alpha^0)^\nu \right]^\dagger \right\rangle \tag{5.5}$$

By using the maximum entropy principle in conjunction with Bayes' theorem, the methodology of Cacuci and Ionescu-Bujor (2010b) combines the above-mentioned "a priori" information with the "likelihood" provided by the model (as in the case of this work: the dissolver model considered from the previous sections) to yield expressions for the best-estimate predicted values for the model parameters and responses, along with corresponding reduced uncertainties (covariance):

1. Best-estimate predicted nominal values for the calibrated (adjusted) parameters:

$$\alpha^{be} = \alpha^0 + \left(C_{\alpha r} - C_\alpha \left[S(\alpha^0) \right]^T \right) \left[C_d (\alpha^0) \right]^{-1} d . \tag{5.6}$$

In component form, the above expression for the calibrated best-estimate parameter values can be written in the form

$$\left(\alpha^{be} \right)^\nu = \left(\alpha^0 \right)^\nu + \sum_{\mu=1}^{N_t} \left\{ \left[C_{\alpha r}^{\nu\mu} - \sum_{\rho=1}^{\mu} C_\alpha^{\nu\rho} \left(S^T \right)^{\mu\rho} \right] \left[\sum_{\eta=1}^{N_t} K_d^{\mu\eta} d^\eta \right] \right\}, \quad \nu = 1, \ldots, N_t , \tag{5.7}$$

where $K_d^{\nu\eta}$ denotes the corresponding (ν, η)-element of the block-matrix C_d^{-1}, with the block-matrix $C_d(\alpha^0)$ defined as follows:

$$C_d\left(\boldsymbol{\alpha}^0\right) \triangleq \left\langle \boldsymbol{dd}^\dagger \right\rangle = \left\langle \left(\delta\boldsymbol{r} - \boldsymbol{S}\left(\boldsymbol{\alpha}^0\right)\delta\boldsymbol{\alpha}\right)\left(\delta\boldsymbol{r}^T - \delta\boldsymbol{\alpha}^T\left[\boldsymbol{S}\left(\boldsymbol{\alpha}^0\right)\right]^T\right)\right\rangle$$

$$= C_{rc}\left(\boldsymbol{\alpha}^0\right) - C_{r\alpha}\left[\boldsymbol{S}\left(\boldsymbol{\alpha}^0\right)\right]^T - \left[\boldsymbol{S}\left(\boldsymbol{\alpha}^0\right)\right]C_{\alpha r} + C_m. \tag{5.8}$$

In the above (and subsequent) expressions, the superscript "T" denotes "transposition". Furthermore, the block-matrix $\boldsymbol{S}$ that appears in the above expressions is defined as

$$\boldsymbol{S} \triangleq \begin{pmatrix} \boldsymbol{S}^{11} & \cdots & \boldsymbol{0} \\ \vdots & \ddots & \vdots \\ \boldsymbol{S}^{N_t,1} & \cdots & \boldsymbol{S}^{N_t,N_t} \end{pmatrix}, \tag{5.9}$$

comprising $\left(J_r^\nu \times J_\alpha^\mu\right)$-dimensional matrix components $S^{\nu\mu}$, $1 \le \mu \le \nu$, defined as

$$\boldsymbol{S}^{\nu\mu}\left(\boldsymbol{\alpha}^\mu\right) = \begin{pmatrix} s_{11}^{\nu\mu} & \cdots & s_{1N}^{\nu\mu} \\ \vdots & s_{in}^{\nu\mu} & \vdots \\ s_{I1}^{\nu\mu} & \cdots & s_{IN}^{\nu\mu} \end{pmatrix} = \begin{pmatrix} \dfrac{\partial R_1^\nu}{\partial \alpha_1^\mu} & \cdots & \dfrac{\partial R_1^\nu}{\partial \alpha_N^\mu} \\ \vdots & \dfrac{\partial R_i^\nu}{\partial \alpha_n^\mu} & \vdots \\ \dfrac{\partial R_I^\nu}{\partial \alpha_1^\mu} & \cdots & \dfrac{\partial R_I^\nu}{\partial \alpha_N^\mu} \end{pmatrix}, \quad 1 \le \mu \le \nu, \tag{5.10}$$

where the elements $\partial R_i^\nu / \partial \alpha_n^\mu$ represents the sensitivities (Gateaux-derivatives) of a computed response R_i^ν with respect to a model parameter α_n^μ.

The covariance matrix $\boldsymbol{C}_{rc}$ appearing in Eq. (5.8) is a symmetric block-matrix that denotes the covariances of the computed responses, and is defined as follows:

$$\boldsymbol{C}_{rc} \triangleq \begin{pmatrix} \boldsymbol{C}_{rc}^{11} & \cdots & \boldsymbol{C}_{rc}^{1N_t} \\ \vdots & \ddots & \vdots \\ \boldsymbol{C}_{rc}^{N_t,1} & \cdots & \boldsymbol{C}_{rc}^{N_t,N_t} \end{pmatrix} \qquad \boldsymbol{C}_{rc}^{\nu\mu} = \sum_{\eta=1}^{\nu}\sum_{\rho=1}^{\mu} \boldsymbol{S}^{\nu\eta}\boldsymbol{C}_\alpha^{\eta\rho}\left(\boldsymbol{S}^{\mu\rho}\right)^\dagger = \left(\boldsymbol{C}_{rc}^{\mu\nu}\right)^\dagger; \quad \nu,\mu = 1,...,N_t. \tag{5.11}$$

The diagonal elements of the above matrix are the variances (i.e., squared standard deviations) of the computed responses; these arise from the parameter uncertainties, "weighted" by the corresponding sensitivities. Finally, the vector $\boldsymbol{d}$ which appears in

Eq. (5.6) denotes the vector of "deviations" or rather the discrepancies between the nominal computations and the nominal measured responses, and is defined as

$$d \triangleq R(\alpha^0) - r_m \qquad (5.12)$$

2. The best-estimate predicted nominal values for the calibrated (adjusted) responses:

$$r(\alpha^{be}) = r_m + \left(C_m - C_{r\alpha} \left[S(\alpha^0) \right]^T \right) \left[C_d(\alpha^0) \right]^{-1} d \qquad (5.13)$$

At a specific time node ν, each component $(r^{be})^\nu$ of $r(\alpha^{be})$ has the explicit form

$$\left(r^{be} \right)^\nu = \left(r_m \right)^\nu + \sum_{\mu=1}^{N_t} \left\{ \left[C_m^{\nu\mu} - \sum_{\rho=1}^{\mu} C_{r\alpha}^{\nu\rho} \left(S^T \right)^{\mu\rho} \right] \left[\sum_{\eta=1}^{N_t} K_d^{\mu\eta} d^\eta \right] \right\}, \quad \nu = 1,\ldots,N_t. \qquad (5.14)$$

3. The expressions for the best-estimate predicted covariances C_α^{be} and C_r^{be} corresponding to the best-estimate parameters α^{be} and responses $r(\alpha^{be})$, together with the predicted best-estimate parameter-response covariance matrix $C_{\alpha r}^{be}$. The block-matrix components, which correlate two (distinct or not) time-nodes, of these calibrated best-estimate covariance matrices are given below:

$$\left(C_\alpha^{be} \right)^{\nu\mu} = C_\alpha^{\nu\mu} - \sum_{\eta=1}^{N_t} \sum_{\rho=1}^{N_t} \left[C_{\alpha r}^{\nu\rho} - \sum_{\pi=1}^{\rho} C_\alpha^{\nu\pi} \left(S^T \right)^{\rho\pi} \right] K_d^{\rho\eta} \left[C_{r\alpha}^{\eta\mu} - \sum_{\pi=1}^{\eta} S^{\eta\pi} C_\alpha^{\pi\mu} \right], \qquad (5.15)$$

$$\left(C_r^{be} \right)^{\nu\mu} = C_m^{\nu\mu} - \sum_{\eta=1}^{N_t} \sum_{\rho=1}^{N_t} \left[C_m^{\nu\rho} - \sum_{\pi=1}^{\rho} C_{r\alpha}^{\nu\pi} \left(S^T \right)^{\rho\pi} \right] K_d^{\rho\eta} \left[C_m^{\eta\mu} - \sum_{\pi=1}^{\eta} S^{\eta\pi} C_{\alpha r}^{\pi\mu} \right], \qquad (5.16)$$

$$\left(C_{r\alpha}^{be} \right)^{\nu\mu} = C_{r\alpha}^{\nu\mu} - \sum_{\eta=1}^{N_t} \sum_{\rho=1}^{N_t} \left[C_m^{\nu\rho} - \sum_{\pi=1}^{\rho} C_{r\alpha}^{\nu\pi} \left(S^T \right)^{\rho\pi} \right] K_d^{\rho\eta} \left[C_{\alpha r}^{\eta\mu} - \sum_{\pi=1}^{\eta} S^{\eta\pi} C_\alpha^{\pi\mu} \right]. \qquad (5.17)$$

The methodology of Cacuci and Ionescu-Bujor (2010b) also provides the consistency indicator

$$\chi^2 \triangleq d^\dagger \left[C_d(\alpha^0) \right]^{-1} d . \qquad (5.18)$$

As the above expression indicates, χ^2 represents the square of the length of the vector d, measuring (in the corresponding metric) the deviations between the experimental and nominally computed responses. Note that χ^2 is independent of calibrating (or adjusting) the original data and can be evaluated directly from the given data (i.e., given parameters and responses, together with their original uncertainties). Recall that the χ^2 (chi-square) distribution with n degrees of freedom of the continuous variable ($0 \leq x < \infty$) is defined as

$$P\left(x < \chi^2 < x + dx\right) \triangleq k_n\left(x\right)dx = \frac{1}{2^{n/2}\Gamma\left(n/2\right)} x^{n/2-1}e^{-x/2}dx, \; x > 0, \; \left(n = 1, 2, \ldots\right). \;\; (5.19)$$

The χ^2- distribution is a measure of the deviation of a "true distribution" (in this case – the distribution of experimental responses) from the hypothetic one (in this case – a Gaussian). The mean and variance of x are $\langle x \rangle = n$ and $\mathrm{var}\left(x\right) = 2n$. As the dimension of d indicates, the number n, of degrees of freedom characteristic of the calibration under consideration is equal to the number of experimental responses. The value of χ^2 computed using Eq. (5.18) provides a very valuable quantitative indicator of the agreement between the computed and experimental responses, measuring essentially the consistency of the experimental responses with the model parameters.

As Eqs. (5.6) through (5.17) indicate, *the predictive modeling methodology calibrates simultaneously all model parameters and responses, over all spatial locations and over the entire time interval under consideration.* The optimally predicted "best-estimate" nominal values for the model parameters result from applying Eq. (5.7), and the reduced predicted uncertainties accompanying these predicted nominal values are computed using Eq. (5.15). Table 5.1 and Figures 5.1 through 5.4 present the results of these computations for the scalar model parameters involved in the equation of state. As Table 5.1 indicates, the initial uncertainties for these parameters are reduced from 10% to values as low as 4.5%. The uncertainty reduction is proportional to the sensitivity of the responses (i.e., acid

concentrations) and to the respective parameters. The predicted optimal values were also calibrated accordingly, differing from their original nominal values.

Table 5.1 Initial and Predicted Nominal Values and Standard Deviations for the Scalar Model Parameters

Scalar Parameters	Nominal Values	Predicted Values	Nominal Relative Standard Deviation	Predicted Relative Standard Deviation
#1: a	0.48916	0.50621	10%	7.67834%
#2: b	$1001.2\,[\text{g/L}]$	$948.7\,[\text{g/L}]$	10%	4.54535%
#3: V_0	$4.8\,[\text{L}]$	$5.123\,[\text{L}]$	10%	4.97098%
#4: G	$0.20194\,[\text{L}]$	$0.20591\,[\text{L}]$	10%	9.82085%
#5: p	2.7	2.61256	10%	9.44417%

Figure 5.1 displays the initial correlation matrix for the scalar parameters listed in Table 5.1, indicating that these parameters are uncorrelated, having a relative standard deviation of 10%. The numbers on the vertical axis are in units of $(\%)^2$, so note that values shown should be by $10^{-4,}$ while the numbers on the two horizontal axes correspond to the parameter numbering in Table 5.1. The results after having applied Eq. (5.17) are displayed in Figure 5.2, which shows the predicted correlation matrix for the scalar parameters listed in Table 5.1. It is seen that the predictive modeling induces non-zero correlations among several of the parameters notably between parameters #4 and #5 (*G* and *p*) and, to a lesser extent, between parameters #2 and #3 (*b* and V_0). The diagonal values in Figure 5.2 are the predicted variances, i.e., the squares of the values shown in the last column of Table 5.1.
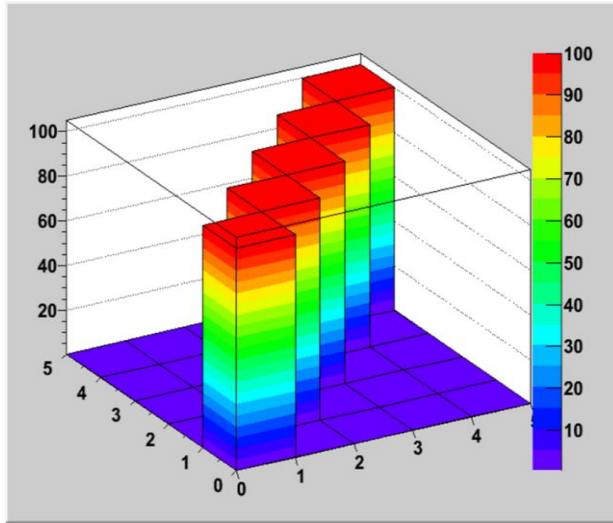
Figure 5.1 Initial correlation matrix for the scalar parameters listed in Table 5.1.
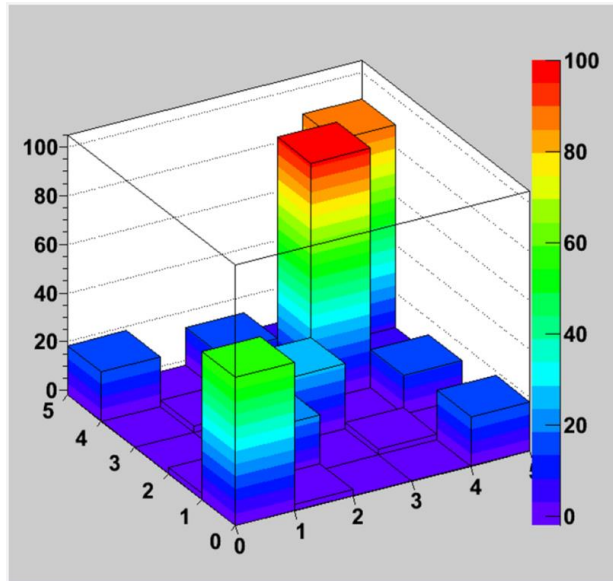
Figure 5.2 Predicted correlation matrix, $\left(C_\alpha^{be} \right)^{\nu\mu}$, for the scalar parameters listed in Table 5.1.

The results of applying Eqs. (5.7) and (5.15) for the time dependent inlet acid concentration, $\rho_a^{(in)}(t)$, are depicted below in Figures 5.3 and 5.4 respectively. The time-dependent calibration of the nominal value $\rho_a^{(in)}(t)$ is relatively small, and so is the reduction in the corresponding time-dependent standard deviation, from the initial value of $\sigma\left[\rho_a^{(in)}(t) \right] = 20\%$. Furthermore, the results of applying Eqs. (5.7) and (5.15) for the time

136

dependent inlet acid concentration, $\dot{m}^{(in)}(t)$, are depicted below in Figures 5.5 and 5.6 respectively is also relatively small, and so is the reduction in the corresponding time-dependent standard deviation, from the initial value of $\sigma\left[\dot{m}^{(in)}(t)\right]=10\%$.
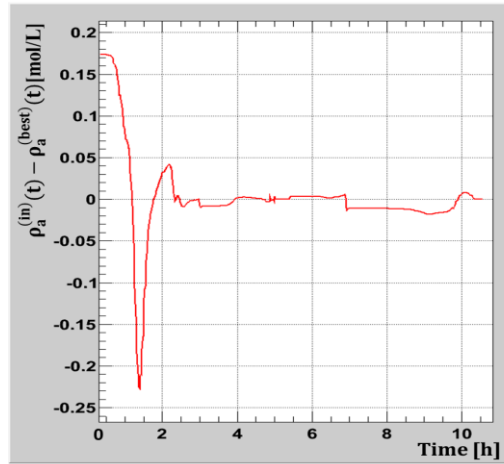
Figure 5.3 Time-dependent behavior of the difference between the nominal value, $\rho_a^{(in)}(t)$, and the optimally predicted "best estimate" value, $\rho_a^{(best)}(t)$, for the inlet acid concentration $\left[\text{mol/L}\right]$.
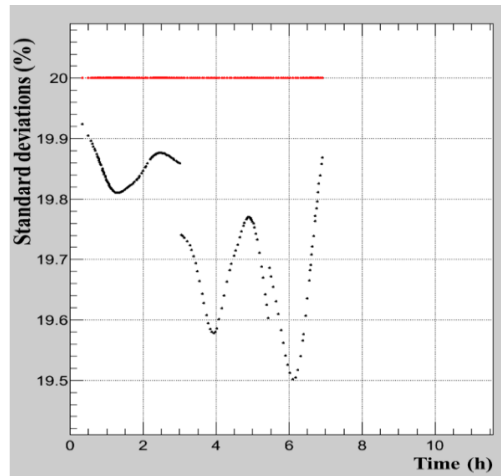
Figure 5.4 Time-dependent behavior of the original relative standard deviation $\sigma\left[\rho_a^{(in)}(t)\right]=20\%$ (in red) and the optimally predicted "best estimate" relative standard deviation $\sigma\left[\rho_a^{(best)}(t)\right]$ (in black), for the inlet acid concentration

137
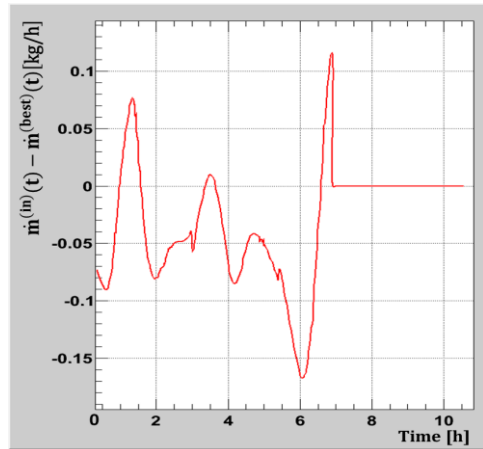
Figure 5.5 Time-dependent behavior of the difference between the nominal value, $\dot{m}^{(in)}(t)$, and the optimally predicted "best estimate" value, $\dot{m}^{(best)}(t)$, for the inlet mass flow rate $[kg/h]$.
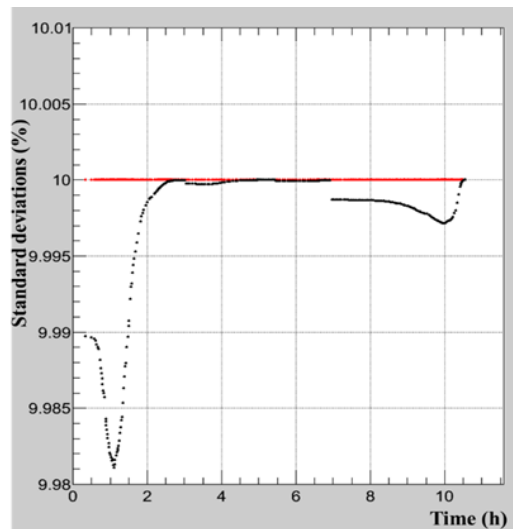
Figure 5.6 Time-dependent behavior of original relative standard deviation, $\sigma\left[\dot{m}^{(in)}(t)\right] = 10\%$ and the optimally predicted "best estimate" $\sigma\left[\dot{m}^{(best)}(t)\right]$, for the inlet mass flow rate.

The predicted best estimate nominal values for the nitric acid concentration responses are obtained using Eq. (5.13). Figure 5.7, below, presents the computed, experimental, and best estimate predicted nominal values for the nitric acid concentration in compartment #1. All of these values are in close agreement with one another. The corresponding (+/-) one-standard deviations are plotted in Figure 5.8, below, which clearly indicates that the predicted best-estimate standard deviations, obtained using Eq. (5.16), are smaller than either the measured

138

(5%) or computed standard deviations [i.e., the diagonal elements of Eq. (5.11)], arising from uncertainties in the model parameters.
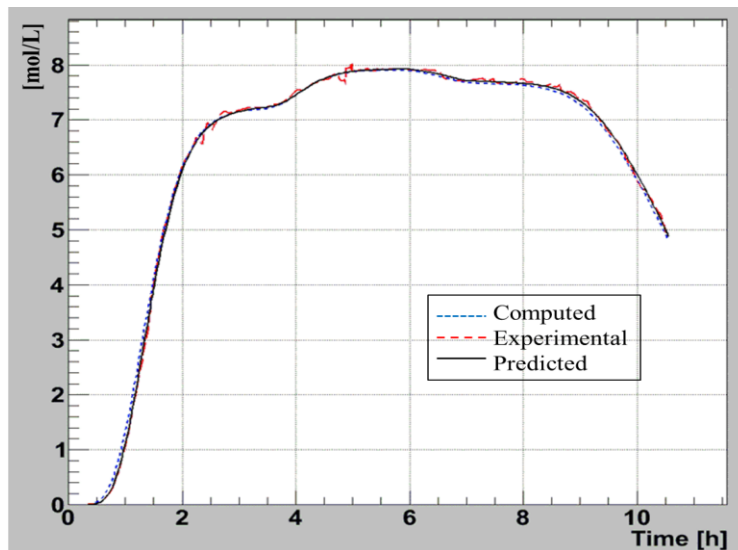
Figure 5.7 Computed, experimental, and best estimate predicted nominal values for the nitric acid concentration in compartment #1 in $[\text{mol/L}]$.
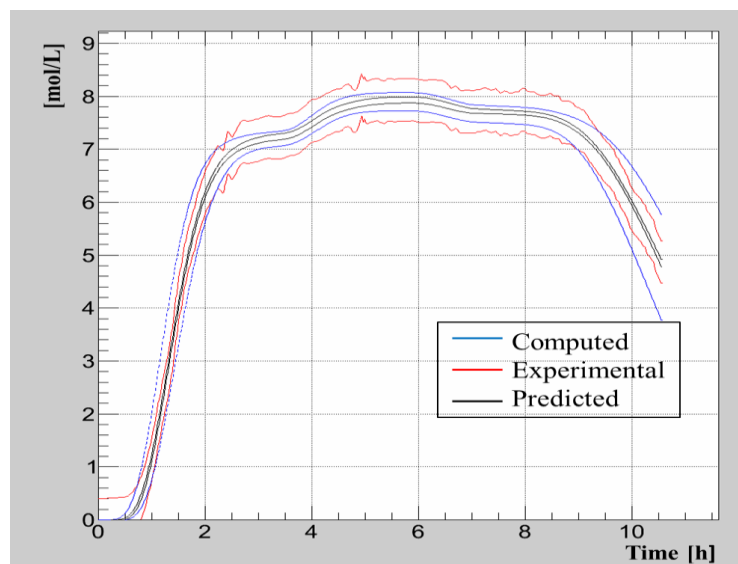
Figure 5.8 Computed, experimental, and best estimate predicted (+/-) standard deviations for the nitric acid concentration in compartment #1 in $[\text{mol/L}]$

For completeness, the full covariance matrix of the computed acid concentration in compartment #1, obtained using Eq. (5.11), is depicted in Figure 5.9, below. This figure shows the computed responses in the early stages of the transient between 1-2 hours into the transient are strongly (up to -0.86 [mol/L]^2) anti-correlated in time with the responses computed towards the end of the transient between hours 9 to 10.5. At other time instances, the responses are weakly correlated, except for the responses between hours 1 to 2, which are strongly (up to 0.86 [mol/L]^2) correlated to each other, and again at the end of the transient, between hours 9 to 10.5, when they again are strongly correlated. Variances of 0.86 [mol/L]^2 correspond to relative standard deviations of about 20% at the end of the transient.
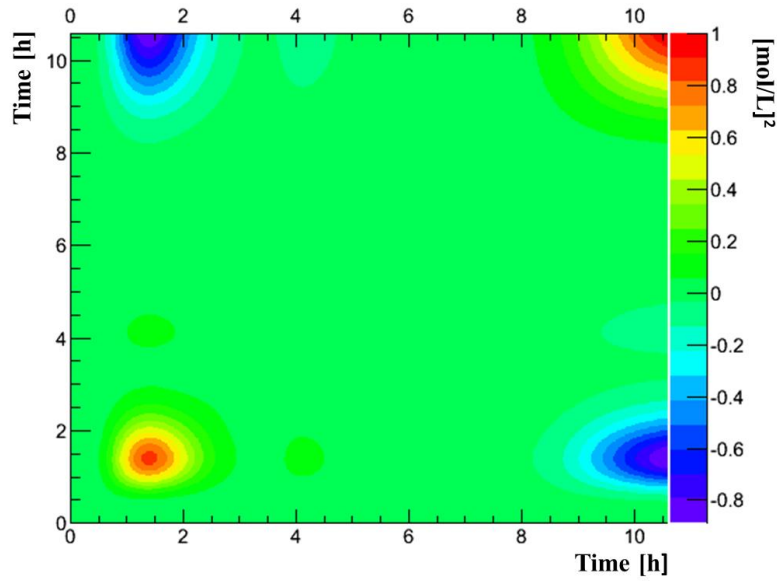
Figure 5.9 Time-dependent *computed* correlation matrix (arising from parameter uncertainties), $C_{rc}^{\nu\mu}$, for the nitric acid concentration in compartment #1

The predicted best estimate response correlations are obtained by using Eq. (5.16) and are depicted in Figure 5.10, below. As indicated in this figure, all best-estimate correlations, including the predicted standard deviations, are significantly reduced and rendered uniform by the predictive modeling procedure of Cacuci and Ionescu-Bujor (2010b). The corresponding (+/-) one-standard deviations are plotted in Figure 5.8, above, which depicts the behavior in time of the measured response standard deviation (5%), the computed response standard deviation [i.e., the diagonal elements of Eq. (5.11) stemming from

uncertainties in the model parameters], and the best-estimate predicted response standard deviation obtained using Eq. (5.16). Figure 5.8, above, shows that the "predicted best-estimate" response standard deviation is smaller than the "measured" standard deviation and the "computed" standard deviation for the entire time-interval under consideration.

After application of the predictive modeling procedure, though, the predicted best estimate correlations (and standard deviations), which are computed using Eq. (5.16), are drastically reduced, as indicated in Figure 5.10.
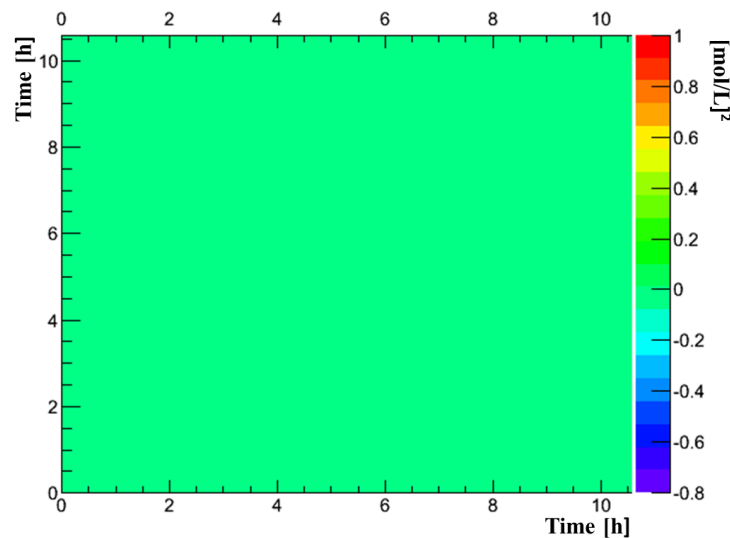
Figure 5.10 Time-dependent *best-estimate predicted* correlation matrix, $\left(C_r^{be}\right)^{\nu\mu}$, for the nitric acid concentration in compartment #1

Even though no measurements were performed in the dissolver compartments 2 through 8, the nominal values of the "best-estimate" responses, $\left(r^{be}\right)^{\nu}$, in these compartments can be computed by using the calibrated best estimate parameter values $\left(\alpha^{be}\right)^{\nu}$. The best-estimate predicted parameter values for all 1291 model parameters (as presented in Table 5.1 and depicted Figures 5.3 and 5.5) together with their reduced predicted uncertainties (as presented in Table 5.1 and depicted Figures 5.4 and 5.6) were used to re-compute the nominal values of the best-estimate responses, $\left(r^{be}\right)^{\nu}$. It turns out that that these best-estimate responses were in good agreement with the originally computed nominal values. In addition, the best-

estimate predicted uncertainties in the best-estimate computed responses can be obtained by using the "propagation of errors" formula given Eq. (5.11), but using the best estimated parameter values and their corresponding best-estimate standard deviations, i.e.,

$$\left(\boldsymbol{C}_r^{be}\right)^{\nu\mu} = \sum_{\eta=1}^{\nu}\sum_{\rho=1}^{\mu}\left[\boldsymbol{S}^{\nu\eta}\right]^{be}\left[\boldsymbol{C}_\alpha^{\eta\rho}\right]^{be}\left[\left(\boldsymbol{S}^{\mu\rho}\right)^\dagger\right]^{be}; \quad \nu,\mu = 1,...,N_t.$$
(5.20)

As will be shown below, the computation of the best-estimate uncertainties using Eq. (5.20) for the compartments in which no measurements were performed indeed experienced reductions in all compartments by comparison to the originally computed uncertainties. Typical results will be presented in the figures below, for compartment #4 (in the middle of the dissolver) and for compartment #7. The uncertainty reductions in the other compartments are not reproduced here because they can be obtained by interpolating linearly between the results presented for compartments #1, #4, and #7.

The original covariance matrix of the computed acid concentration in compartment #4, obtained using Eq. (5.11), is depicted in Figure 5.11, below. This figure shows that the computed responses in the early stages of the transient, between hours 0.5 to 1.5 hours, are anti-correlated in time with the responses computed towards the end of the transient, between hours 8 to 10.5. The anti-correlations for the acid concentration in compartment #4 are similar to the time-dependent response anti-correlations in compartment #1. The acid concentration responses in compartment #4 are less strongly correlated at other time instances, except for the responses between in the initial stages of the transient, between hours 0.5 to 1.5 and hours 8.5 to 10.5, when they are positively correlated, with variances reaching as high as 0.6 [mol/L]^2. This value corresponds to an absolute standard deviation of 0.77 [mol/L], which in turn corresponds to a relative standard deviation of over 50% --which is rather large computed uncertainty in this response (i.e., the acid concentration in compartment #4). Overall, the time-correlations for the acid concentration in compartment #4 are similar to the time-dependent response correlations in compartment #1 but stronger in relative terms.
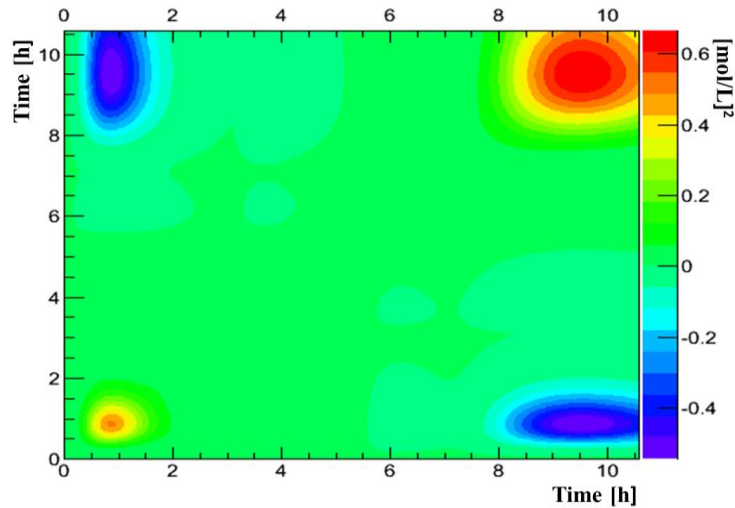
Figure 5.11 Time-dependent *computed* correlation matrix (arising from parameter uncertainties), $C_{rc}^{\nu\mu}$, for the nitric acid concentration in compartment #4

The predicted best estimate response correlations obtained by using Eq. (5.20) are depicted in Figure 5.12, below. As this figure indicates, all best-estimate correlations, including the predicted standard deviations, are drastically reduced and more uniform. The corresponding (+/-) one-standard deviations plotted in Figure 5.13 depict the behavior in time of the computed response standard deviation [i.e., the diagonal elements of Eq. (5.11) stemming from uncertainties in the model parameters] and the best-estimate predicted response standard deviation obtained using Eq. (5.16). It is evident from Figure 5.13 that the "predicted best-estimate" response standard deviation is considerably smaller than that of the "computed" one for the entire time-interval under consideration.
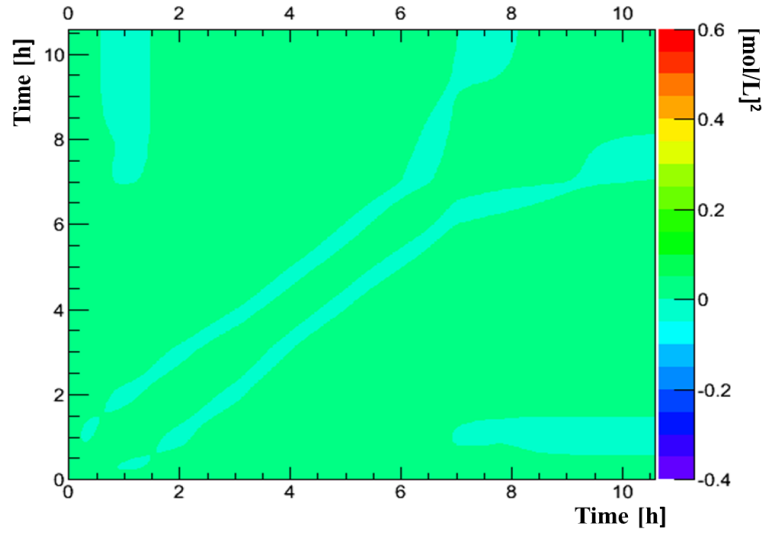
Figure 5.12 Time-dependent *best-estimate predicted* correlation matrix, $\left(C_r^{be}\right)^{v\mu}$, for the nitric acid concentration in compartment #4
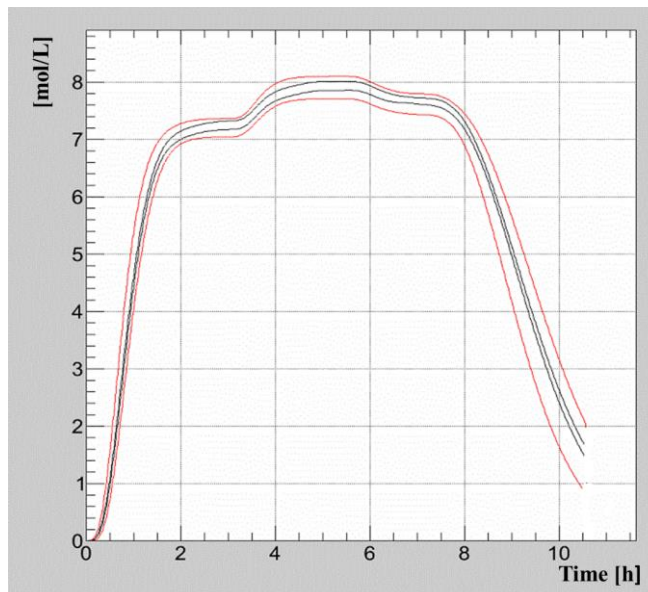
Figure 5.13 Computed (red graph) and best estimate (black graph) predicted *absolute* standard deviations (+/-) for the nitric acid concentration in compartment #4 $\left[\text{mol/L}\right]$

The original covariance matrix of the computed acid concentration in compartment #7, obtained using Eq. (5.11) depicted in Figure 5.14 displays an "island" of anti-correlated responses between hours 0 to 1 and the end of the transient at hours 7 and 10, as well as an

144

"island" of positively correlated acid concentrations during hours 7 to 9. Although the absolute values of the overall uncertainties are smaller in this compartment, by comparison to the other compartments, their relative values are actually larger than those of the other compartments. Depicted in Figure 5.14 is the largest variance of the acid concentration in the compartment at 0.2 [mol/L]^2. This occurs in the interval during hours 7 to 9, and corresponds to a relative standard deviation of 90%. The predicted best estimate response correlations obtained by using Eq. (5.20) are depicted in Figure 5.15, below. As indicated in this figure, all best-estimate correlations, including the predicted standard deviations, are drastically reduced and rendered more uniform. The corresponding (+/-) one-standard deviations are plotted in Figure 5.16 depicts the behavior in time of the computed response standard deviation [i.e., the diagonal elements of Eq. (5.11) stemming from uncertainties in the model parameters] and the best-estimate predicted response standard deviation obtained using Eq. (5.16). It is evident from Figure 5.16 that the "predicted best-estimate" response standard deviation for the acid concentration in compartment #7 is considerably smaller than the "computed" one over the entire time-interval under consideration.
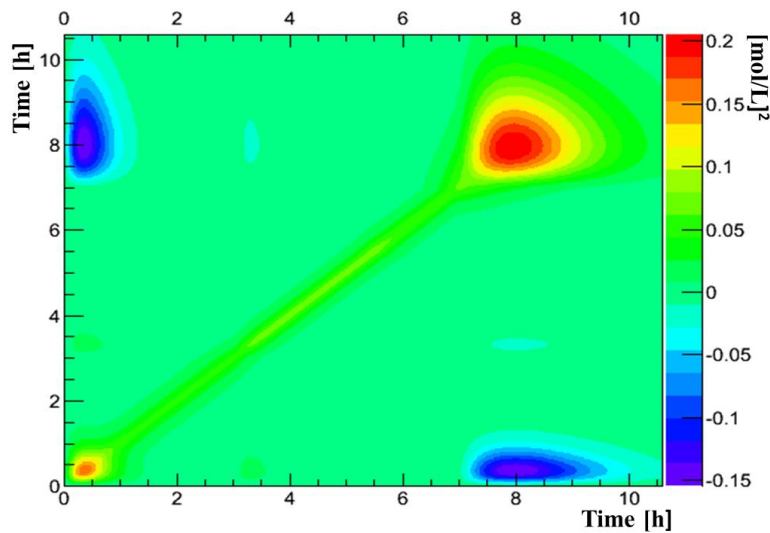
Figure 5.14 Time-dependent *computed* correlation matrix (arising from parameter uncertainties), $C_{rc}^{\nu\mu}$, for the nitric acid concentration in compartment #7
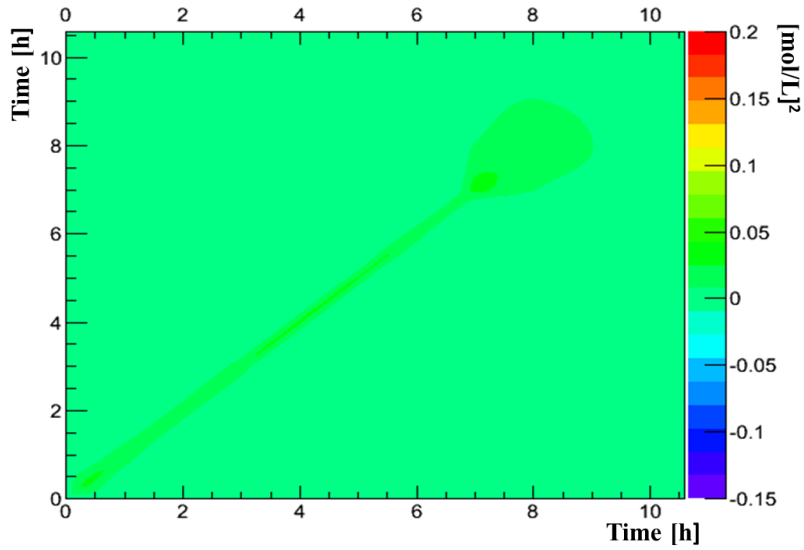
Figure 5.15 Time-dependent *best-estimate predicted* correlation matrix, $\left(C_r^{be}\right)^{v\mu}$, for the nitric acid concentration in compartment #7
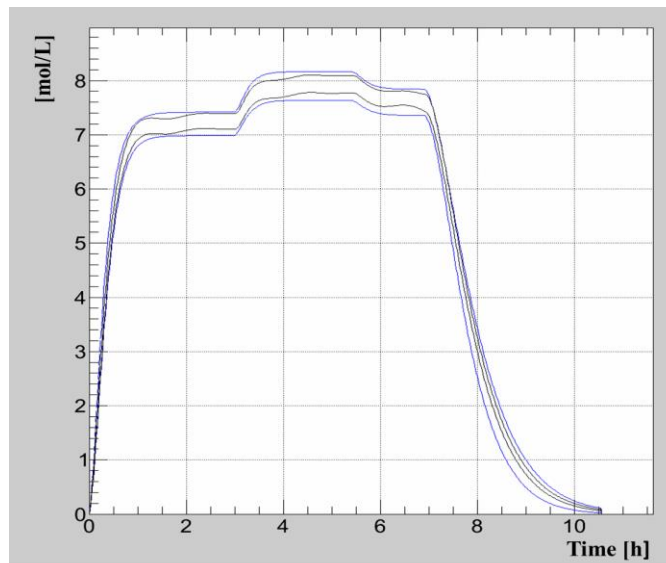
Figure 5.16 Computed (blue graph) and best estimate predicted (black graph) *absolute* standard deviations (+/-) for the nitric acid concentration in compartment #7 $\left[\text{mol/L}\right]$

The results presented in the forgoing highlight the very beneficial effects of the comprehensive framework of the predictive modeling methodology of Cacuci and Ionescu-Bujor (2010b), which considers the entire phase-space of parameters and responses

146

simultaneously over the entire time interval of interest. This unique feature makes it possible to "spread out" the positive effects of having performed measurements in one region of the dissolver (in this case, in compartment #1) and reduce significantly the predicted uncertainties in the acid concentration where measurements were performed, but also for compartments that were not measured. These results show promise in a variety of aspects related to the model itself, its potential impact on coupling this model to other modules in a facility model, and the risk of using the information calculated as a result.

In the next Chapter, the predictive modeling methodology of Cacuci and Ionescu-Bujor (2010b) is applied in the *inverse prediction mode*, demonstrating its usefulness for inferring unknown model parameters (specifically: a time-dependent boundary condition) from measurements. These inverse analyses are characteristic to the mission of proliferation detection since most real world scenarios involve making inferences on a target of interest with statistically low measurements/observations, indirect measurements, and having to rely on measuring surrogate systems/environments.

6. INVERSE PREDICTIVE MODELING OF THE DISSOLVER'S TIME-DEPENDENT INLET ACID CONCENTRATION

Many measurement problems, particularly in nonproliferation activities, are "*inverse*" to the "forward" problem in that they *seek to determine the properties of the medium, and/or the size of the medium on its boundaries, or the properties of the source, from measurements of quantities that depend on the unknown state-variables*. The methods for solving such inverse problems can be categorized as "explicit" or "implicit". The (historically older) explicit methods attempt to manipulate the forward model in conjunction with measurements and result in estimations of the unknown source and/or other unknown characteristics of the medium. The implicit methods rather, combine measurements with repeated solutions of the direct problem which are obtained by varying values of the unknowns and iterating until an "a priori" selected functional is reduced to a value deemed to be "acceptable" by the user. This acceptance is some user-defined "goodness of fit" between measurements and direct computations. All of these methods underscore the fundamental characteristics of inverse problems, namely that inverse problems are ill-posed (admitting non-unique solutions) and/or ill-conditioned, unstable to small errors or perturbations that are inherently affecting both the model parameters and the experimental measurements. Cacuci (2014) highlights the amplification of "noise" on naïve solutions which render these methods rather useless.

In the nuclear engineering literature, the inverse problem seems to be addressed only in the area of *time-independent neutron and radiation transport*. Time-independent inverse radiative transfer problems were reviewed by McCormick (1992), and examples of inverse source problems for time-independent neutron transport by Sanchez and McCormick (2008). More recently, Jarman et al (2011) addressed the "source identification problem" by using a Bayesian approach in conjunction with numerical adjoint transport computations to localize radiological sources, but only accounted for counting statistics while disregarding experimental and modeling uncertainties. Bledsoe et al (2011.a, 2011.b) used the "differential evolution method" and the "Levenberg-Marquardt method" (Levenberg-

Marquardt,1944, 1963), respectively, to solve inverse transport problems by minimizing an "a priori" chosen chi-square-type functional to estimate the "differences between measured and computed quantities of interest", but neglected uncertainties stemming from the underlying cross sections and material properties, which by doing so implies these fundamental data would be perfectly known. Hykes and Azmy (2015) presented a Bayesian approach to solve the inverse problem of mapping the spectral and spatial distributions of radioactive sources using a limited number of detectors when the system's geometry and material composition are known and fixed. The main takeaway is that aforementioned work "regularizes" the solution of the inverse problem in a more or less ad-hoc implicit manner, without clearly showing the effects of the respective implicit regularizations or demonstrating their reproducibility. The fundamental difficulties associated with inverse problems affect profoundly the numerical methods for solving them, particularly in the presence of errors (including numerical ones) since errors in the forward problems are helped by the "smoothing" of integration rather than in the inverse sense where these small errors are amplified as again highlighted by Cacuci (2014). All methods for solving inverse problems do produce different results based on how the user defines their assumptions to "regularize" and solve the problem of interest. This pervasive issue in using error afflicted models and measurements is what makes the results and methods found in this dissertation unique.

Inverse time-dependent problems are yet to be addressed in nuclear engineering activities. This chapter will be the first to the knowledge of the author to address such an inverse problem in the context of the dissolver model analyzed in the previous chapters. The definition used for an inverse problem here considers a time-dependent boundary condition (specifically: the time-dependent inlet acid concentration) to be unknown and is determined from available measurements. The methodology of Cacuci and Ionescu-Bujor (2010b), which was applied in the previous chapter in the "forward predictive modeling" mode will be applied in this chapter in the "*inverse predictive modeling*" mode, and will be shown to predict within an "a priori" chosen error criterion the actual time-dependent boundary condition *without invoking ad-hoc procedures or a need to introduce arbitrary parameters* in order to "regularize" the inverse as the current state of practice does Tichonov (1963), Levenberg-Marquardt (1944, 1963), and/or Tarantola (2005). A careful examination *of the*

(forward and inverse) predictive modeling methodology of Cacuci and Ionescu-Bujor, which were summarized in Eqs. (5.6) through (5.17) shows the results do not contain any arbitrary, user-defined, parameters for controlling the "regularization" of the problem and/or convergence of the respective solution. The reason is that the Cacuci and Ionescu-Bujor (2010b)'s methodology uses the maximum entropy principle to combine the model's uncertainties and sensitivities to construct intrinsically the inverse problem's regularizing metric. The results obtained in this chapter underscore the importance of presenting the *objective resolution* (i.e., resolution in the absence of user-defined subjective "adjustment" of arbitrary "regularization parameters") of a time-dependent inverse "case study" of potential importance to diversion activities associated with proliferation and thus international safeguards since the data themselves regularize the problem rather than any biased individual.

As this "inverse predictive modeling" application illustrates, the time-dependent inlet acid concentration (which is a "time-dependent inlet boundary condition") are unknown. The methodology of Cacuci and Ionescu-Bujor (2010b) as applied in the *inverse predictive mode* predicts time-dependent inlet acid concentration within an "a priori" specified convergence error, by using the measurements of the acid concentration in compartment #1, which were presented in Figure 3.6. Recall that compartment #1 is the furthest from the dissolver's inlet and that the 1291 model parameters from Eq. (3.17) are components of the vector $\boldsymbol{\alpha}$, i.e.,

$$\boldsymbol{\alpha}(t) \triangleq (\alpha_1,...,\alpha_{1291}) \triangleq \left[\rho_a^{(in)}(t_1),...,\rho_a^{(in)}(t_{635}), \dot{m}^{(in)}(t_1),...,\dot{m}^{(in)}(t_{635}), \right.$$
$$\left. \rho_a^{(1)}(0),...,\rho_a^{(8)}(0), V^{(1)}(0),...,V^{(8)}(0), a, b, V_0, p, G \right]. \tag{3.17}$$

Also, the 635 parameters $\rho_a^{(in)}(t_1),...,\rho_a^{(in)}(t_{635})$, which describe the time-evolution of the inlet acid concentration, are considered *"unknown"* and will be determined by using the measurements depicted in Figure 3.6 in conjunction with the inverse predictive modeling application of the methodology of Cacuci and Ionescu-Bujor (2010b). All of *the other model parameters appearing in Eq. (2.17) are considered to be known within negligible errors, as follows*: the model parameters a, b, V_0, G, p have nominal values as provided in Table 3.1 (within negligible errors); the time-dependent inlet mass flow rate $\dot{m}^{(in)}(t)$ behaves (within

negligible errors) as depicted in Figure 3.3; and the initial conditions $\rho_{a0}^{(1)},...,\rho_{a0}^{(8)}, V_0^{(1)},...,V_0^{(8)}$ given in Eq. (3.14) are also considered to be known within negligible errors.

The *inverse predictive modeling* of Cacuci and Ionescu-Bujor (2010b) for the problem definition above iteratively predicts the time-dependent inlet acid concentration as a model parameter using Eq. (5.7), in conjunction with Eqs. (5.8) through (5.17). As were mentioned previously, Eqs. (3.10) through (3.14), are required here as the "base-case" values for the nitric acid concentrations and liquid volumes, $\rho_a^{(k)}(t)$, and $V^{(k)}(t)$, respectively for the dissolver compartments $k=1,...,8$. The nominal values for the base case are to serve as the *"expert opinion"* for the unknown time-dependent inlet acid concentration, $\rho_a^{(in)}(t)$ and the only other "a priori" information that relates the behavior of $\rho_a^{(in)}(t)$ are the measurements $\rho_{a,meas}^{(1)}(t_i)$ from Figure 3.6, and thus, compute the "expert opinion base-case" acid concentrations in compartments #1, 4, and 7 as illustrated by Figure 6.1.
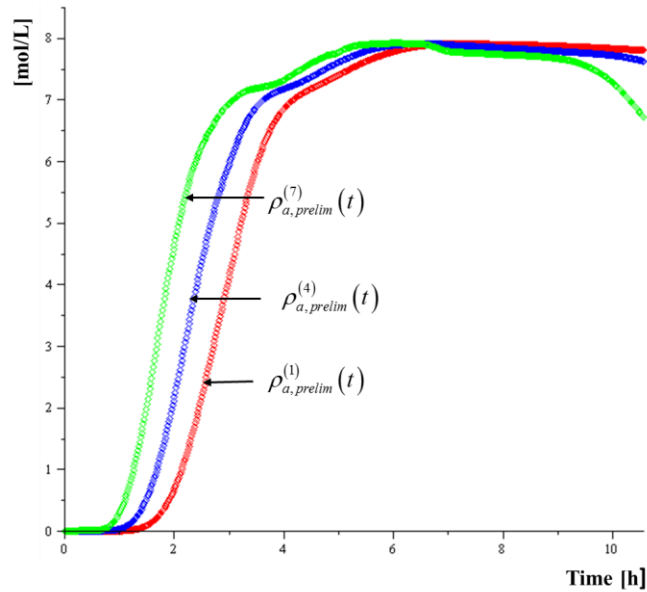
Figure 6.1 Preliminary "expert opinion base-case" computations of the time-dependent nitric acid concentrations [mol/L] $\rho_{a,prelim}^{(1)}(t)$, $\rho_{a,prelim}^{(4)}(t)$, $\rho_{a,prelim}^{(7)}(t)$ in compartments #1, #4, and #7, respectively.

Comparing the experimental measurements, $\rho_{a,meas}^{(1)}(t_i)$, from Figure 3.6 with the preliminary "base-case" computed results for $\rho_{a,prelim}^{(1)}(t)$ obtained from "expert opinion" values for the inlet acid concentration (Figure 6.1) indicates a time-lag of roughly 140 minutes between for phenomena occurring at the dissolver's inlet to propagate" to the compartment furthest away (compartment #1).

Using foregoing 140 minute shift or "lag" for $\rho_{a,prelim}^{(1)}(t)$ the values of the "time-dependent inlet acid concentration" are used for Eqs. (3.10) – (3.14) as the first iterative computation of the forward functions $\left\{\rho_a^{(k)}(t)\right\}^{(1)}$ and $\left\{V^{(k)}(t)\right\}^{(1)}$, $k=1,...,8$; the superscript "(1)" indicates "iteration #1". These forward functions are used in the adjoint dissolver model, cf. Eqs. (4.64) – (4.68) to compute the "1st-iteration values" of the adjoint functions $\left\{\psi_\rho^{(k)}(t)\right\}^{(1)}$ and $\left\{\psi_V^{(k)}(t)\right\}^{(1)}$. Subsequently Eq. (4.19) uses these adjoint functions to compute the "1st-iteration values" of the sensitivities $\left\{\delta\rho_a^{(k)}(t_i)\right\}^{(1)}$ which are used with the measured acid concentrations in compartment #1 (shown in Figure 3.6 and assuming a 1% standard deviation for these measurements) in Eqs. (5.7) – (5.17), to obtain the "*1st-iteration predicted best-estimate values*" for the respective model responses and parameters.

Results denoted in red for the "predicted best-estimate parameter values after the 1st-iteration," $\left\{\left(\alpha^{be}\right)^v\right\}^{(1)}$, from Eq. (5.7) are depicted in Figure 6.2, below, using the label "iteration 1". These results include the predicted nominal values of all 1291 model parameters, but only for the values for the time-dependent inlet acid concentration that are affected; the nominal values for the other parameters will not be calibrated by the inverse predictive modeling methodology of Cacuci and Ionescu-Bujor (2010b) because the nominal values for the remaining model parameters are considered to be known within negligible uncertainties.
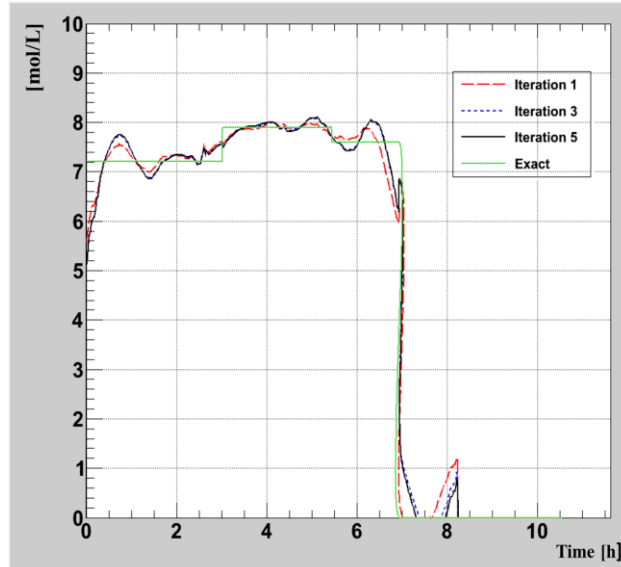
Figure 6.2 Values predicted for the inlet acid concentration, $\left\{\rho_a^{(in)}(t)\right\}^{(1)}$, $\left\{\rho_a^{(in)}(t)\right\}^{(3)}$, $\left\{\rho_a^{(in)}(t)\right\}^{(5)}$ in $[mol/L]$ and after the inverse predictive modeling iterations #1, #3, and #5, respectively, and their comparison to the actual time-dependence of the inlet nitric acid concentration reproduced (in green) from Figure 3.4

The procedure is iterated until the maximum error between the time-dependent predicted inlet acid concentration converges within 0.1%, for the entire time interval, i.e., $\max_t \left| 1 - \left\{\rho_a^{(in)}(t)\right\}^{(J-1)} \Big/ \left\{\rho_a^{(in)}(t)\right\}^{(J)} \right| < 0.1\%$. The convergence criterion of 1%" was selected based on "expert opinion" regarding the accuracy that can be expected of measurements of the time-dependent inlet acid concentration over the duration of 10.5 hours. This inequality is reached after $J=5$ iterations, at which stage the inverse predictive modeling iterations were considered as converged. The results obtained after the 3rd- and 5th-iteration, respectively, are also depicted in Figure 6.2.

To facilitate the comparison between the various iterations and the desired result, Figure 6.2 also presents the actual time-dependency of the inlet acid concentration, which caused the measurements reported in Figure 3.4 but were considered to be unknown for the purposes of this "inverse predictive modeling" "case study". Figure 6.2 illustrates that exact time-dependent inlet acid concentration $\rho_a^{(in)}(t)$ converges reasonably well, except for discontinuities at three time instances, where solutions take on constant values between these

153

respective discontinuities and becoming zero after 7 hours in a manner very similar to a Heaviside step-function. It is known that such step-functions are notoriously difficult to approximate by continuous functions, and these approximations will appear as oscillations around any discontinuities. In particular, the largest point-wise discrepancies between the "inverse predicted values" and the exact values are clustered at the beginning and ends of the transient period, which is not surprising given the step-like time-distribution of the exact inlet acid concentration. These discrepancies are irrelevant, however, for the time-integrated the inlet acid concentration, $\left\{\rho_a^{(in)}(t)\right\}^{(5)}$, predicted after the 5th-iteration, which differs by less than 1% of the time-integral of the exact inlet acid concentration.

Results for compartment #1 for the predicted nominal value of the acid concentration from (5th-) iteration, $\left\{\rho_a^{(1)}(t)\right\}^{(5)}$ and the predicted covariance matrix for this concentration are depicted in Figure 6.3. Nominal values obtained for $\left\{\rho_a^{(1)}(t)\right\}^{(5)}$ are reported with a standard deviation of less than 2% and within 1% for the experimentally measured results, $\rho_{a,meas}^{(1)}(t_i)$ over 10.5 hours.
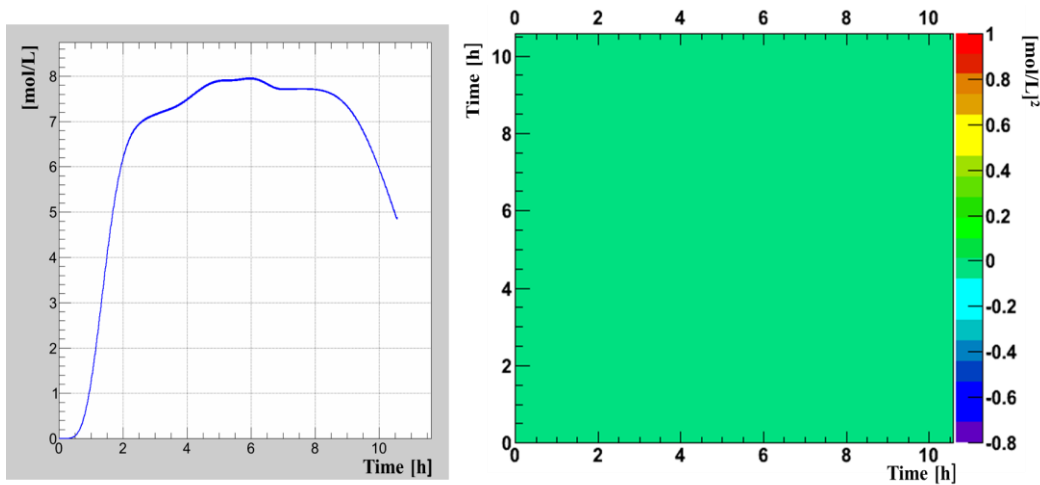
Figure 6.3 Left: predicted nominal time-dependent acid concentration $[\text{mol}/\text{L}]$ in compartment #1 after the 5th iteration, $\left\{\rho_a^{(1)}(t)\right\}^{(5)}$, with one standard deviation error bands; Right: the accompanying predicted covariance matrix for $\left\{\rho_a^{(1)}(t)\right\}^{(5)}$.

The results produced by the 5$^\text{th}$-iteration of the inverse predictive modeling methodology also yield predicted values for the nominal values of the acid concentrations in all of the other dissolver compartments. Furthermore, using the results from this 5$^\text{th}$-iteration in the "sandwich formula" below

$$\left(C_r^{be}\right)^{\nu\mu} = \sum_{\eta=1}^{\nu}\sum_{\rho=1}^{\mu}\left[S^{\nu\eta}\right]^{be}\left[C_\alpha^{\eta\rho}\right]^{be}\left[\left(S^{\mu\rho}\right)^\dagger\right]^{be}; \quad \nu,\mu = 1,...,N_t,$$

(5.20)

will provide the covariance matrix ("uncertainties") for the predicted acid concentration responses in the dissolver's compartments even again where measurements are not available. In particular, the predicted results for the compartment #4 (in the middle of the dissolver) and compartment #7 (closest to the inlet), along with the accompanying covariance matrices, are depicted in Figures 6.4 and 6.5, below.
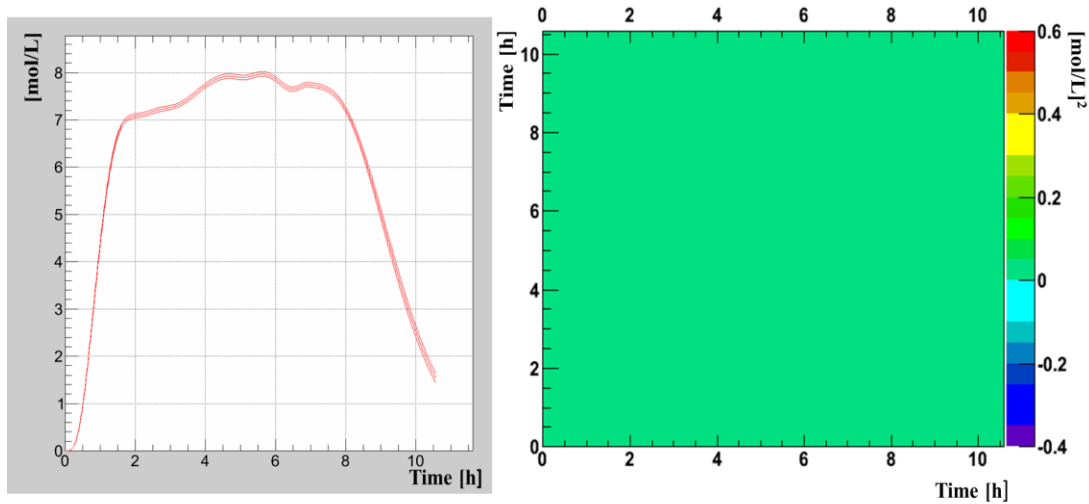
Figure 6.4 Left: predicted nominal time-dependent acid concentration $[\text{mol/L}]$ in compartment #4 after the 5$^\text{th}$ iteration, $\left\{\rho_a^{(4)}(t)\right\}^{(5)}$, with one standard deviation error bands; Right: the accompanying predicted covariance matrix for $\left\{\rho_a^{(4)}(t)\right\}^{(5)}$.
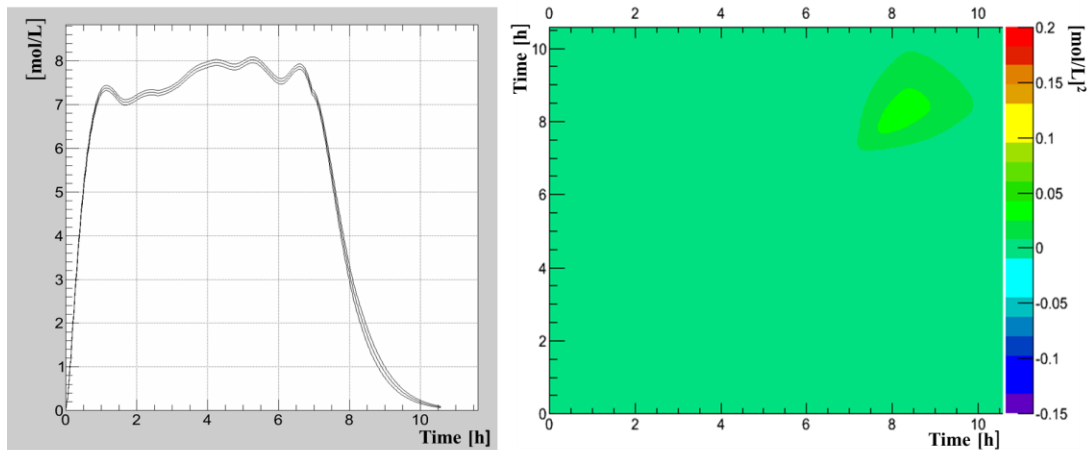
Figure 6.5 Left: predicted nominal time-dependent acid concentration $[\text{mol/L}]$ in compartment #7 after the 5th iteration, $\left\{\rho_a^{(7)}(t)\right\}^{(5)}$, with one standard deviation error bands; Right: the accompanying predicted covariance matrix for $\left\{\rho_a^{(7)}(t)\right\}^{(5)}$.

Figures 6.6 through 6.8, below, compare the exact results for the actual time-dependent distributions of acid concentrations within the dissolver (and, in particular, for compartments #1, #4 and #7) and the inlet acid from Chapter 5 with the results obtained in Figures 6.3 through 6.5. Figures 6.6 through 6.8 illustrate good agreement within their respective standard deviations, for the exact *forward* predictions (i.e., those obtained using the known inlet acid concentration) and the corresponding values for the acid concentrations obtained using the *inverse predictive mode*. This close agreement indicates that the effects of the less-than-perfect inverse prediction of the time-dependent inlet acid concentration (time-dependent boundary condition) have very little effect on predicting the responses of interest, namely the time-dependent acid concentrations in the various compartments, and, in particular, in compartment #1, where the experimental measurements are available. These first-of-a-kind results illustrate the all-encompassing generality and applicability of *the forward and inverse* predictive modeling capabilities embodied in the methodology of Cacuci and Ionescu-Bujor (2010b) and indicate the way for further similar applications.
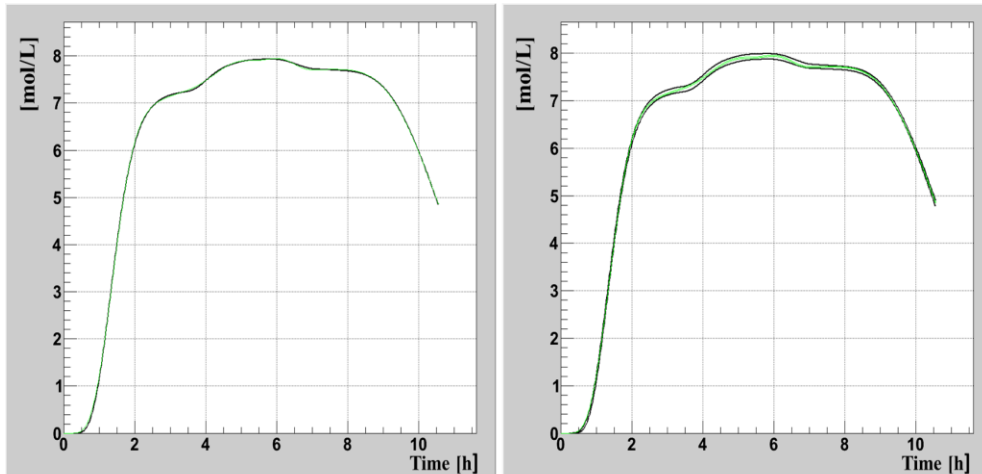
Figure 6.6 **Left:** Black label: forward predicted nominal value of the acid concentration $[\text{mol/L}]$ in compartment #1, from Figure 5.7. Green label: inverse predicted nominal value of the acid concentration in compartment #1, from Figure 6.3. **Right** Black label: forward predicted one standard deviation error bands of the acid concentration in compartment #1, from Figure 5.8. Green label: inverse predicted one standard deviation error bands of the acid concentration in compartment #1, from Figure 6.3.
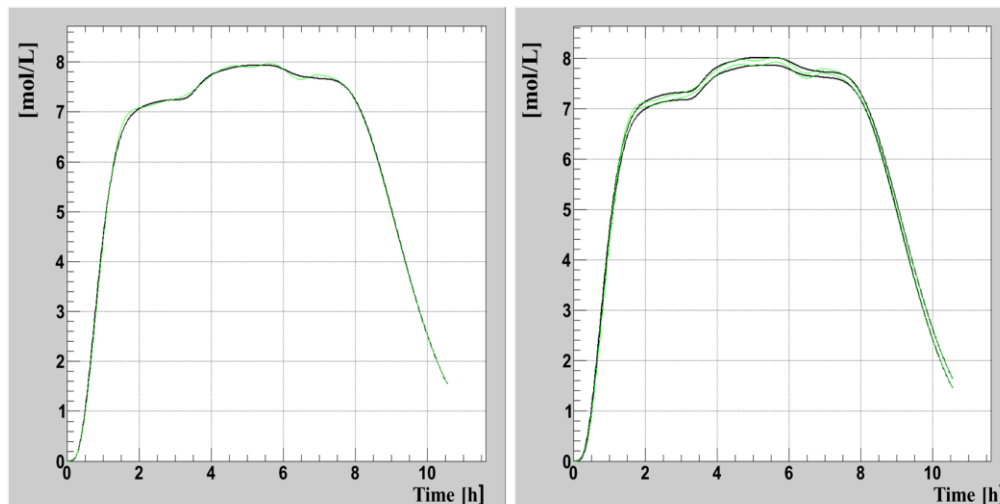
Figure 6.7 **Left:** Black label: forward predicted nominal value of the acid concentration $[\text{mol/L}]$ in compartment #4, from Figure 3.5. Green label: inverse predicted nominal value of the acid concentration in compartment #1, from Figure 6.4. **Right** Black label: forward predicted one standard deviation error bands of the acid concentration in compartment #4, from Figure 5.13. Green label: inverse predicted one standard deviation error bands of the acid concentration in compartment #1, from Figure 6.4.
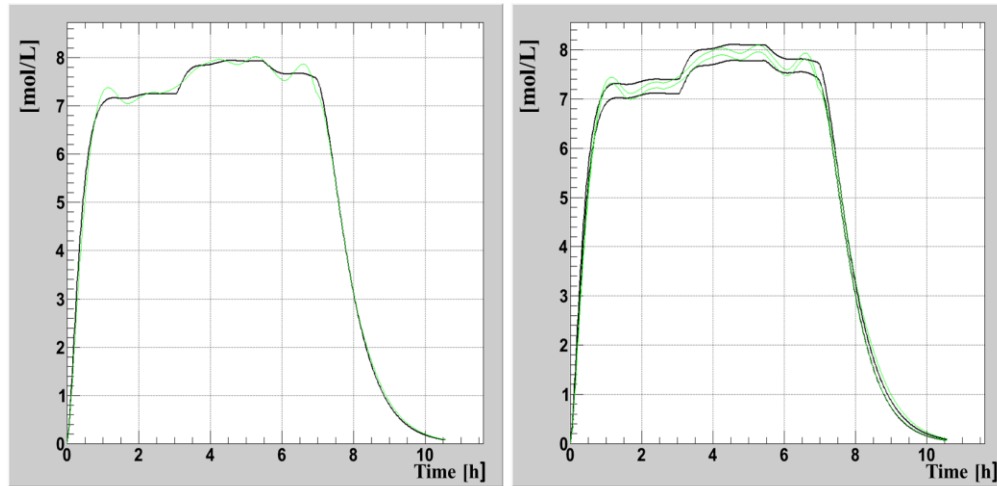
Figure 6.8 **Left:** Black label: forward predicted nominal value of the acid concentration $[\text{mol/L}]$ in compartment #7, from Figure 3.5. Green label: inverse predicted nominal value of the acid concentration in compartment #7, from Figure 6.5.
Right: Black label: forward predicted one standard deviation error bands of the acid concentration in compartment #7, from Figure 5.16. Green label: inverse predicted one standard deviation error bands of the acid concentration in compartment #7, from Figure 6.5.

This chapter presented an application of the (forward and inverse) predictive modeling methodology of Cacuci and Ionescu-Bujor (2010b) *in the inverse mode* and results are shown for an *unknown time-dependent boundary condition*. Moreover, the unknown time-dependent boundary condition described by 635 unknown discrete scalar parameters is accurate throughout the dissolver within a tight "a priori" specified convergence criterion specified by the time-dependent inlet acid concentration as well as by the time-dependent acid concentration for a specified location using measurements of the state function including the compartment furthest from the inlet.

This methodology uses the maximum entropy principle to construct an optimal approximation of the unknown "a priori" distribution by using the "a priori" known mean values and uncertainties characterizing the model parameters, along with the computed and experimentally measured model responses and their covariances. This methodology avoids the need for ad hoc regularizations since "a priori" distributions are subsequently combined using Bayes' theorem and the "likelihood" from the model itself, using the first-order response sensitivities as weighting functions for combining the computational and

experimental information rather than biased subject matter experts or inspectors as in the case of nuclear safeguards. This forward and inverse predictive modeling methodology yields optimally calibrated values for time-dependent acid concentrations in the dissolver's compartments for all model parameters with reduced predicted uncertainties. Notably, even though the experimental data pertains solely to the compartment furthest from the inlet, uncertainties throughout the entire dissolver are reduced because information is combined and transmitted simultaneously through covariance matrices over the entire phase-space at all time steps and all spatial locations.

7. SECOND-ORDER ADJOINT SENSITIVITY ANALYSIS FOR QUANTIFYING NON-GAUSSIAN FEATURES OF TIME-DEPENDENT ACID CONCENTRATIONS

This chapter is dedicated to quantifying the non-Gaussian features of the acid concentration responses within selected compartments of the dissolver. As has been discussed in Chapter 2, the quantification of non-Gaussian features of responses necessitates the computation of the second-order responses sensitivities to the model parameters. Section 7.1 presents a new method, using adjoint operators, for computing most efficiently the exact (as opposed to the approximate) 2nd-order sensitivities of the acid concentration in the surrogate dissolver model. For the full dissolver model, however, only the mean values and the standard deviations are available so all of the model's parameters are then assumed to be *uncorrelated and normally distributed*. Section 7.2 will then show results for the non-Gaussian features of the acid concentrations in the full dissolver model that are quantified.

7.1. A New Adjoint Sensitivity Analysis Method for Computing Efficiently the Second-Order Sensitivities of the Surrogate Dissolver Model

Recall from Chapter 2, which analyzed the surrogate dissolver model, that the expressions of partial sensitivities of the acid concentration response $\rho(t_1)$ with respect to variations in the model parameters β_i and $\rho_{a,A}^{in}$ were as follows:

$$\frac{\partial \rho(t_1)}{\partial \beta_i} = w_i \int_0^{t_1} \psi^{(1)}(t) \left[\rho_{a,A}^{in,0} - \rho^0(t) \right] dt, \quad i = 1,...,N_\alpha,$$

(2.99)

$$\frac{\partial \rho(t_1)}{\partial \rho_{a,A}^{in}} = \left(\sum_{i=1}^{N_\alpha} w_i \beta_i^0 \right) \int_0^{t_1} \psi^{(1)}(t) dt.$$

(2.100)

The adjoint function $\psi^{(1)}(t)$, which appears in the above expressions, is the solution of the 1st-LASS, comprising the following equations:

$$-\frac{d\psi^{(1)}(t)}{dt}+\psi^{(1)}(t)\sum_{i=1}^{N_\alpha}w_i\beta_i^0=\delta(t-t_1),\ \ 0<t\leq t_1, \tag{2.96}$$

$$\psi^{(1)}(t_1)=0, \tag{2.97}$$

The 2nd-order sensitivities of $\rho(t_1)$ with respect to the model parameters will be computed by *devising a novel procedure*, based on computing the first-order G-differentials of Eqs. (2.99) and (2.100). Thus, the G-differential of Eqs. (2.99) is obtained by applying its definition:

$$\delta\left[\frac{\partial\rho(t_1)}{\partial\beta_i}\right]=\frac{\partial^2\rho(t_1)}{\partial\beta_i\partial\rho_{a,A}^{in}}\delta\rho_{a,A}^{in}+\sum_{j=1}^{N_\alpha}\frac{\partial^2\rho(t_1)}{\partial\beta_i\partial\beta_j}\delta\beta_j$$

$$\triangleq\frac{d}{d\varepsilon}\left\{w_i\int_0^{t_1}\left[\psi^{(1)}(t)+\varepsilon\delta\psi^{(1)}(t)\right]\left[\rho_{a,A}^{in}+\varepsilon\delta\rho_{a,A}^{in}-\rho(t)-\rho_{a,A}^{in}\delta\rho(t)\right]dt\right\}_{\varepsilon=0}$$

$$=w_i\int_0^{t_1}\delta\psi^{(1)}(t)\left[\rho_{a,A}^{in}-\rho(t)\right]dt-w_i\int_0^{t_1}\psi^{(1)}(t)\delta\rho(t)dt+w_i\delta\rho_{a,A}^{in}\int_0^{t_1}\psi^{(1)}(t)dt,\ i=1,...,N_\alpha. \tag{7.1}$$

Note that the superscript "zero," which denoted "nominal values", was omitted, for simplicity, in Eqs. (7.1). The last term on the right-side of the above expression can be computed immediately, since the adjoint function $\psi^{(1)}(t)$ is known. However, the first and second terms on the right-side of Eq. (7.1) contain the variation $\delta\psi^{(1)}(t)$ in the adjoint function and, respectively, the variation $\delta\rho(t)$ in the forward function, and the variation $\delta\rho_{a,A}^{in}$ in the respective model parameter. As has been shown in Chapter 2, the variation $\delta\rho(t)$ in the forward function is related to the parameter variations through the 1st-LFSS for the surrogate dissolver model, namely:

$$\frac{d\left[\delta\rho(t)\right]}{dt}+\delta\rho(t)\sum_{i=1}^{N_\alpha}w_i\beta_i=\left[\rho_{a,A}^{in}-\rho(t)\right]\sum_{i=1}^{N_\alpha}w_i\delta\beta_i+\delta\rho_{a,A}^{in}\sum_{i=1}^{N_\alpha}w_i\beta_i,\ \ 0<t\leq t_1, \tag{2.87}$$

$$\delta\rho(0) = 0, \quad t = 0. \tag{2.88}$$

Furthermore, the variation $\delta\psi^{(1)}(t)$ is related to the parameter variations through the G-differential of the 1st-LASS, which is computed, by definition, as follows:

$$\frac{d}{d\varepsilon}\left\{-\frac{d\left[\psi^{(1),0}(t) + \varepsilon\delta\psi^{(1)}(t)\right]}{dt} + \left[\psi^{(1),0}(t) + \varepsilon\delta\psi^{(1)}(t)\right]\sum_{i=1}^{N_\alpha} w_i\left[\beta_i^0 + \varepsilon\delta\beta_i\right]\right\}_{\varepsilon=0},$$

$$= -\frac{d\left[\delta\psi^{(1)}(t)\right]}{dt} + \delta\psi^{(1)}(t)\sum_{i=1}^{N_\alpha} w_i\beta_i^0 + \psi^{(1),0}(t)\sum_{i=1}^{N_\alpha} w_i\delta\beta_i = 0, \quad 0 < t \le t_1, \tag{7.2}$$

$$\delta\psi^{(1)}(t_1) = 0, \tag{7.3}$$

Altogether, Eqs. (2.87), (2.88), (7.2), and (7.3) constitute a well-posed system of equations for computing the variations $\delta\psi^{(1)}(t)$ and $\delta\rho(t)$ in terms of the parameter variations. Omitting, for simplicity, the superscript "zero," which denoted "nominal values", Eqs. (2.87) and (7.2) can be written in matrix form as follows:

$$\begin{pmatrix} -\dfrac{d}{dt} + \sum_{i=1}^{N_\alpha} w_i\beta_i & 0 \\[4mm] 0 & \dfrac{d}{dt} + \sum_{i=1}^{N_\alpha} w_i\beta_i \end{pmatrix}\begin{pmatrix} \delta\psi^{(1)}(t) \\[3mm] \delta\rho(t) \end{pmatrix} = \begin{pmatrix} -\psi^{(1)}(t)\sum_{i=1}^{N_\alpha} w_i\delta\beta_i \\[4mm] \left[\rho_{a,A}^{in} - \rho(t)\right]\sum_{i=1}^{N_\alpha} w_i\delta\beta_i + \delta\rho_{a,A}^{in}\sum_{i=1}^{N_\alpha} w_i\beta_i \end{pmatrix}, \quad 0 < t \le t_1. \tag{7.4}$$

In principle, Eq. (7.4) could be solved, subject to Eqs. (7.3) and (2.88) to obtain the variations $\delta\psi^{(1)}(t)$ and $\delta\rho(t)$, but such a procedure would be just as computationally impractical as solving the 1st-LFSS, cf. Eqs. (2.87) and (2.88). Expressing the first and second terms on the right-side of Eq. (7.1) in alternative ways that eliminate the appearances of $\delta\psi^{(1)}(t)$ and $\delta\rho(t)$, (i.e., in a manner analogous to the way in which the "indirect effect term" was re-expressed in terms of the adjoint function $\psi^{(1)}(t)$ when constructing the 1st-LFSS in Chapter 2) will circumvent the need for solving Eq. (7.4). For this purpose, an inner product is made by multiplying Eq. (7.4) with a two-component vector $\left[\psi_1^{(2)}(t), \psi_2^{(2)}(t)\right]$ and integrating the resulting equation to obtain the following relation:

$$\int_0^{t_1} \left[\psi_1^{(2)}(t), \psi_2^{(2)}(t) \right] \begin{pmatrix} -\dfrac{d}{dt} + \sum_{i=1}^{N_\alpha} w_i \beta_i & 0 \\ 0 & \dfrac{d}{dt} + \sum_{i=1}^{N_\alpha} w_i \beta_i \end{pmatrix} \begin{pmatrix} \delta\psi^{(1)}(t) \\ \delta\rho(t) \end{pmatrix} dt$$

$$= \int_0^{t_1} \left[\psi_1^{(2)}(t), \psi_2^{(2)}(t) \right] \begin{pmatrix} -\psi^{(1)}(t) \sum_{i=1}^{N_\alpha} w_i \delta\beta_i \\ \left[\rho_{a,A}^{in} - \rho(t) \right] \sum_{i=1}^{N_\alpha} w_i \delta\beta_i + \delta\rho_{a,A}^{in} \sum_{i=1}^{N_\alpha} w_i \beta_i \end{pmatrix} dt, \ 0 < t \le t_1.$$

(7.5)

Integration by parts transfers the differential operation from $\delta\psi^{(1)}(t)$ and $\delta\rho(t)$ to the differential operations on $\psi_1^{(2)}(t)$ and $\psi_2^{(2)}(t)$ and yields the term on the left-side of Eq. (7.5) as:

$$\int_0^{t_1} \psi_1^{(2)}(t) \left[-\frac{d}{dt} \delta\psi^{(1)}(t) + \delta\psi^{(1)}(t) \sum_{i=1}^{N_\alpha} w_i \beta_i \right] + \psi_2^{(2)}(t) \left[\frac{d}{dt} \delta\rho(t) + \delta\rho(t) \sum_{i=1}^{N_\alpha} w_i \beta_i \right] dt$$

$$= -\psi_1^{(2)}(t_1) \delta\psi^{(1)}(t_1) + \psi_1^{(2)}(0) \delta\psi^{(1)}(0) + \psi_2^{(2)}(t_1) \delta\rho(t_1) - \psi_2^{(2)}(0) \delta\rho(0)$$

$$+ \int_0^{t_1} \delta\psi^{(1)}(t) \left[\frac{d\psi_1^{(2)}(t)}{dt} + \psi_1^{(2)}(t) \sum_{i=1}^{N_\alpha} w_i \beta_i \right] dt + \int_0^{t_1} \delta\rho(t) \left[-\frac{d\psi_2^{(2)}(t)}{dt} + \psi_2^{(2)}(t) \sum_{i=1}^{N_\alpha} w_i \beta_i \right] dt.$$

(7.6)

The first term on the left-side of Eq. (7.6) will now be replaced by the term on the right-side of Eq. (7.5), and the conditions expressed by Eqs. (2.88) and (7.3) are replaced on the right-side of Eq. (7.6) to reduce the latter to the following expression:

$$\int_0^{t_1} \psi_1^{(2)}(t) \left[-\psi^{(1)}(t) \sum_{i=1}^{N_\alpha} w_i \delta\beta_i \right] dt + \int_0^{t_1} \psi_2^{(2)}(t) \left\{ \left[\rho_{a,A}^{in} - \rho(t) \right] \sum_{i=1}^{N_\alpha} w_i \delta\beta_i + \delta\rho_{a,A}^{in} \sum_{i=1}^{N_\alpha} w_i \beta_i \right\} dt$$

$$= \psi_1^{(2)}(0) \delta\psi^{(1)}(0) + \psi_2^{(2)}(t_1) \delta\rho(t_1)$$

$$+ \int_0^{t_1} \delta\psi^{(1)}(t) \left[\frac{d\psi_1^{(2)}(t)}{dt} + \psi_1^{(2)}(t) \sum_{i=1}^{N_\alpha} w_i \beta_i \right] dt + \int_0^{t_1} \delta\rho(t) \left[-\frac{d\psi_2^{(2)}(t)}{dt} + \psi_2^{(2)}(t) \sum_{i=1}^{N_\alpha} w_i \beta_i \right] dt.$$

(7.7)

The last two terms on the right-side of Eq. (7.7) can now be identified with the first two terms on the right-side of Eq. (7.1) by requiring that

$$\frac{d\psi_1^{(2)}(t)}{dt} + \psi_1^{(2)}(t)\sum_{i=1}^{N_\alpha} w_i\beta_i = w_i\left[\rho_{a,A}^{in} - \rho(t)\right] = w_i\rho_{a,A}^{in}\exp\left(-t\sum_{i=1}^{N_\alpha} w_i\beta_i\right), \tag{7.8}$$

$$-\frac{d\psi_2^{(2)}(t)}{dt} + \psi_2^{(2)}(t)\sum_{i=1}^{N_\alpha} w_i\beta_i = -w_i\psi^{(1)}(t) = -w_i\exp\left[(t-t_1)\sum_{i=1}^{N_\alpha} w_i\beta_i\right]. \tag{7.9}$$

The unknown values $\delta\psi^{(1)}(0)$ and $\delta\rho(t_1)$ can be eliminated from the right-side of Eq. (7.7) by requiring that

$$\psi_2^{(2)}(t_1) = 0, \tag{7.10}$$

$$\psi_1^{(2)}(0) = 0. \tag{7.11}$$

Collecting now the results in Eqs. (7.7) through (7.11) and inserting them into Eq. (7.1) transforms the latter into the form

$$
\begin{aligned}
\delta\left[\frac{\partial\rho(t_1)}{\partial\beta_i}\right] &= \frac{\partial^2\rho(t_1)}{\partial\beta_i\partial\rho_{a,A}^{in}}\delta\rho_{a,A}^{in} + \sum_{j=1}^{N_\alpha}\frac{\partial^2\rho(t_1)}{\partial\beta_i\partial\beta_j}\delta\beta_j = w_i\delta\rho_{a,A}^{in}\int_0^{t_1}\psi^{(1)}(t)dt \\
&\quad + \int_0^{t_1}\psi_2^{(2)}(t)\left\{\left[\rho_{a,A}^{in}-\rho(t)\right]\sum_{i=1}^{N_\alpha} w_i\delta\beta_i + \delta\rho_{a,A}^{in}\sum_{i=1}^{N_\alpha} w_i\beta_i\right\}dt \\
&\quad - \sum_{i=1}^{N_\alpha} w_i\delta\beta_i\int_0^{t_1}\psi_1^{(2)}(t)\psi^{(1)}(t)dt, \quad i=1,...,N_\alpha.
\end{aligned}
\tag{7.12}
$$

Identifying in Eq. (7.12) the respective coefficients of the parameter variations yields the following expressions for the 2nd-order sensitivities

$$\frac{\partial^2\rho(t_1)}{\partial\beta_i\partial\rho_{a,A}^{in}} = w_i\int_0^{t_1}\psi^{(1)}(t)dt + \sum_{i=1}^{N_\alpha} w_i\beta_i\int_0^{t_1}\psi_2^{(2)}(t)dt, \quad i=1,...,N_\alpha, \tag{7.13}$$

$$\frac{\partial^2\rho(t_1)}{\partial\beta_i\partial\beta_j} = w_j\int_0^{t_1}\psi_2^{(2)}(t)\left[\rho_{a,A}^{in}-\rho(t)\right]dt - w_j\int_0^{t_1}\psi_1^{(2)}(t)\psi^{(1)}(t)dt; \quad i,j=1,...,N_\alpha. \tag{7.14}$$

The solution of Eqs. (7.8) and (7.10) can be obtained by using the integrating factor method (see Appendix A) in the form

$$\psi_1^{(2)}(t) = \left(w_i\rho_{a,A}^{in}\right)t\exp\left(-t\sum_{i=1}^{N_\alpha} w_i\beta_i\right). \tag{7.15}$$

The solution of Eqs. (7.9) and (7.11) can be obtained by using the integrating factor method (see Appendix A) in the form

$$\psi_2^{(2)}(t) = w_i(t-t_1)\exp\left[(t-t_1)\sum_{i=1}^{N_\alpha} w_i\beta_i\right].$$

(7.16)

Replacing Eqs. (2.101) and (7.16) in Eq. (7.13) and carrying out the respective integrations yields:

$$\frac{\partial^2\rho(t_1)}{\partial\beta_i\partial\rho_{a,A}^{in}} = w_i\int_0^{t_1}\psi^{(1)}(t)dt + \sum_{i=1}^{N_\alpha} w_i\beta_i\int_0^{t_1}\psi_2^{(2)}(t)dt = \frac{w_i}{\sum_{j=1}^{N_\alpha} w_j\beta_j}\left[1-\exp\left(-t_1\sum_{j=1}^{N_\alpha} w_j\beta_j\right)\right]$$

$$+\left(\sum_{i=1}^{N_\alpha} w_i\beta_i\right)\frac{w_i}{\sum_{j=1}^{N_\alpha} w_j\beta_j}\left\{\left[t_1\exp\left(-t_1\sum_{j=1}^{N_\alpha} w_j\beta_j\right) - \frac{1}{\sum_{j=1}^{N_\alpha} w_j\beta_j}\left[1-\exp\left(-t_1\sum_{j=1}^{N_\alpha} w_j\beta_j\right)\right]\right]\right\}$$

(7.17)

$$= w_it_1\exp\left(-t_1\sum_{j=1}^{N_\alpha} w_j\beta_j\right)_i, \quad i=1,...,N_\alpha.$$

Replacing now Eqs. (2.101), (7.15) and (7.16) in Eq. (7.14) and carrying out the respective integrations yields:

$$\frac{\partial^2\rho(t_1)}{\partial\beta_i\partial\beta_j} = w_j\int_0^{t_1}\psi_2^{(2)}(t)\left[\rho_{a,A}^{in}-\rho(t)\right]dt - w_j\int_0^{t_1}\psi_1^{(2)}(t)\psi^{(1)}(t)dt$$

$$= w_j\left[-\frac{(t_1)^2}{2}\rho_{a,A}^{in,0}w_i\exp\left(-t_1\sum_{k=1}^{N_\alpha} w_k\beta_k\right)\right] - w_j\left[\frac{(t_1)^2}{2}\rho_{a,A}^{in,0}w_i\exp\left(-t_1\sum_{k=1}^{N_\alpha} w_k\beta_k\right)\right]$$

(7.18)

$$= -\rho_{a,A}^{in,0}(t_1)^2 w_iw_j\exp\left(-t_1\sum_{k=1}^{N_\alpha} w_k\beta_k\right); \quad i,j=1,...,N_\alpha.$$

The entire procedure that has been applied to the 1st-order sensitivities represented by Eq. (2.99), which has started by computing the G-derivative in Eq. (7.1) and has ended by deriving the 2nd-order sensitivities obtained in Eqs. (7.17) and (7.18), will now be applied to the 1st-order sensitivities represented by Eq. (2.100). Thus, taking the G-differential of Eq. (2.100) yields

$$\delta\left[\frac{\partial\rho(t_1)}{\partial\rho_{a,A}^{in}}\right] = \frac{\partial^2\rho(t_1)}{\partial\left(\rho_{a,A}^{in}\right)^2}\delta\rho_{a,A}^{in} + \sum_{j=1}^{N_\alpha}\frac{\partial^2\rho(t_1)}{\partial\rho_{a,A}^{in}\partial\beta_j}\delta\beta_j$$

$$= \frac{d}{d\varepsilon}\left\{\sum_{i=1}^{N_\alpha}w_i\left(\beta_i^0+\varepsilon\delta\beta_i\right)\int_0^{t_1}\psi^{(1),0}(t)dt + \left(\sum_{i=1}^{N_\alpha}w_i\beta_i^0\right)\int_0^{t_1}\left[\psi^{(1),0}(t)+\varepsilon\delta\psi^{(1)}(t)\right]dt\right\}_{\varepsilon=0} \qquad (7.19)$$

$$= \left(\sum_{i=1}^{N_\alpha}w_i\beta_i\right)\int_0^{t_1}\delta\psi^{(1)}(t)dt + \sum_{i=1}^{N_\alpha}w_i\delta\beta_i\int_0^{t_1}\psi^{(1)}(t)dt.$$

Note that the superscript "zero," which denoted "nominal values", was omitted, for simplicity, in the expression on the right-side of the last equality in Eq. (7.19). Next, construct an inner product by multiplying Eq. (7.4) with a two-component vector $\left[\psi_3^{(2)}(t),\psi_4^{(2)}(t)\right]$ and integrate the resulting equation to obtain the following relation:

$$\int_0^{t_1}\left[\psi_3^{(2)}(t),\psi_4^{(2)}(t)\right]\begin{pmatrix} -\dfrac{d}{dt}+\sum_{i=1}^{N_\alpha}w_i\beta_i & 0 \\ 0 & \dfrac{d}{dt}+\sum_{i=1}^{N_\alpha}w_i\beta_i \end{pmatrix}\begin{pmatrix}\delta\psi^{(1)}(t) \\ \delta\rho(t)\end{pmatrix}dt$$

$$\qquad (7.20)$$

$$= \int_0^{t_1}\left[\psi_3^{(2)}(t),\psi_4^{(2)}(t)\right]\begin{pmatrix} -\psi^{(1)}(t)\sum_{i=1}^{N_\alpha}w_i\delta\beta_i \\ \left[\rho_{a,A}^{in}-\rho(t)\right]\sum_{i=1}^{N_\alpha}w_i\delta\beta_i+\delta\rho_{a,A}^{in}\sum_{i=1}^{N_\alpha}w_i\beta_i \end{pmatrix}dt, \; 0<t\le t_1.$$

Integrating by parts the term on the left-side of Eq. (7.20) so as to transfer the differential operation from $\delta\psi^{(1)}(t)$ and $\delta\rho(t)$ to differential operations on $\psi_3^{(2)}(t)$ and $\psi_4^{(2)}(t)$ yields:

$$\int_0^{t_1}\psi_3^{(2)}(t)\left[-\frac{d}{dt}\delta\psi^{(1)}(t)+\delta\psi^{(1)}(t)\sum_{i=1}^{N_\alpha}w_i\beta_i\right]+\psi_4^{(2)}(t)\left[\frac{d}{dt}\delta\rho(t)+\delta\rho(t)\sum_{i=1}^{N_\alpha}w_i\beta_i\right]dt$$

$$= -\psi_3^{(2)}(t_1)\delta\psi^{(1)}(t_1)+\psi_3^{(2)}(0)\delta\psi^{(1)}(0)+\psi_4^{(2)}(t_1)\delta\rho(t_1)-\psi_4^{(2)}(0)\delta\rho(0)$$

$$+\int_0^{t_1}\delta\psi^{(1)}(t)\left[\frac{d\psi_3^{(2)}(t)}{dt}+\psi_3^{(2)}(t)\sum_{i=1}^{N_\alpha}w_i\beta_i\right]dt+\int_0^{t_1}\delta\rho(t)\left[-\frac{d\psi_4^{(2)}(t)}{dt}+\psi_4^{(2)}(t)\sum_{i=1}^{N_\alpha}w_i\beta_i\right]dt.$$

$$(7.21)$$

The first term on the left-side of Eq. (7.21) will now be replaced by the term on the right-side of Eq. (7.20), and the conditions expressed by Eqs. (2.88) and (7.3) are replaced on the right-side of Eq. (7.21) to reduce the latter to the following expression:

$$\int_0^{t_1} \psi_3^{(2)}(t)\left[-\psi^{(1)}(t)\sum_{i=1}^{N_\alpha} w_i\delta\beta_i\right]dt + \int_0^{t_1} \psi_4^{(2)}(t)\left\{\left[\rho_{a,A}^{in} - \rho(t)\right]\sum_{i=1}^{N_\alpha} w_i\delta\beta_i + \delta\rho_{a,A}^{in}\sum_{i=1}^{N_\alpha} w_i\beta_i\right\}dt$$

$$= \psi_3^{(2)}(0)\delta\psi^{(1)}(0) + \psi_4^{(2)}(t_1)\delta\rho(t_1)$$

$$+ \int_0^{t_1} \delta\psi^{(1)}(t)\left[\frac{d\psi_3^{(2)}(t)}{dt} + \psi_3^{(2)}(t)\sum_{i=1}^{N_\alpha} w_i\beta_i\right]dt + \int_0^{t_1} \delta\rho(t)\left[-\frac{d\psi_4^{(2)}(t)}{dt} + \psi_4^{(2)}(t)\sum_{i=1}^{N_\alpha} w_i\beta_i\right]dt.$$

(7.22)

The last two terms on the right-side of Eq. (7.22) can now be identified with the first term on the right-side of Eq. (7.19) by requiring that

$$\frac{d\psi_3^{(2)}(t)}{dt} + \psi_3^{(2)}(t)\sum_{i=1}^{N_\alpha} w_i\beta_i = \sum_{i=1}^{N_\alpha} w_i\beta_i ,$$

(7.23)

$$-\frac{d\psi_4^{(2)}(t)}{dt} + \psi_4^{(2)}(t)\sum_{i=1}^{N_\alpha} w_i\beta_i = 0 .$$

(7.24)

The unknown values $\delta\psi^{(1)}(0)$ and $\delta\rho(t_1)$ can be eliminated from the right-side of Eq. (7.22) by requiring that

$$\psi_3^{(2)}(0) = 0,$$

(7.25)

$$\psi_4^{(2)}(t_1) = 0 .$$

(7.26)

Collecting now the results in Eqs. (7.22) through (7.26) and inserting them into Eq. (7.19) transforms the latter into the form

$$\frac{\partial^2\rho(t_1)}{\partial\left(\rho_{a,A}^{in}\right)^2}\delta\rho_{a,A}^{in} + \sum_{j=1}^{N_\alpha}\frac{\partial^2\rho(t_1)}{\partial\rho_{a,A}^{in}\partial\beta_j}\delta\beta_j = \sum_{i=1}^{N_\alpha} w_i\delta\beta_i\int_0^{t_1}\psi^{(1)}(t)dt - \sum_{i=1}^{N_\alpha} w_i\delta\beta_i\int_0^{t_1}\psi_3^{(2)}(t)\psi^{(1)}(t)dt$$

$$+ \int_0^{t_1}\psi_4^{(2)}(t)\left\{\left[\rho_{a,A}^{in} - \rho(t)\right]\sum_{i=1}^{N_\alpha} w_i\delta\beta_i + \delta\rho_{a,A}^{in}\sum_{i=1}^{N_\alpha} w_i\beta_i\right\}dt, \quad i = 1,...,N_\alpha,$$

(7.27)

where the adjoint functions $\psi_3^{(2)}$ and $\psi_4^{(2)}$ are the solutions of Eqs. (7.23) - (7.26). Identifying in Eq. (7.19) the respective coefficients of the parameter variations yields the following expressions for the 2nd-order sensitivities

$$\frac{\partial^2\rho(t_1)}{\partial\left(\rho_{a,A}^{in}\right)^2} = \sum_{i=1}^{N_\alpha} w_i\beta_i\int_0^{t_1}\psi_4^{(2)}(t)dt, \quad i = 1,...,N_\alpha;$$

(7.28)

$$\frac{\partial^2 \rho(t_1)}{\partial \rho_{a,A}^{in} \partial \beta_j} = w_i \int_0^{t_1} \psi^{(1)}(t) dt - w_i \int_0^{t_1} \psi_3^{(2)}(t) \psi^{(1)}(t) dt$$

$$+ w_i \int_0^{t_1} \psi_4^{(2)}(t) \left[\rho_{a,A}^{in} - \rho(t) \right] dt, \quad i,j = 1,...,N_\alpha; \tag{7.29}$$

Applying the integrating factor method (see Appendix A) to Eqs. (7.23) - (7.26) yields the following solutions:

$$\psi_3^{(2)}(t) = 1 - \exp\left(-t \sum_{i=1}^{N_\alpha} w_i \beta_i \right), \tag{7.30}$$

$$\psi_4^{(2)}(t) \equiv 0 \tag{7.31}$$

Replacing now Eqs. (2.101), (7.30) and (7.31) in Eqs. (7.28) and (7.29), and carrying out the respective integrations yields:

$$\frac{\partial^2 \rho(t_1)}{\partial \left(\rho_{a,A}^{in} \right)^2} = 0, \tag{7.32}$$

$$\frac{\partial^2 \rho(t_1)}{\partial \rho_{a,A}^{in} \partial \beta_j} = w_i \int_0^{t_1} \psi^{(1)}(t) dt - w_i \int_0^{t_1} \psi_3^{(2)}(t) \psi^{(1)}(t) dt$$

$$= w_i \frac{\left[1 - \exp\left(-t_1 \sum_{j=1}^{N_\alpha} w_j \beta_j \right) \right]}{\sum_{j=1}^{N_\alpha} w_j \beta_j} - w_i \left\{ \frac{\left[1 - \exp\left(-t_1 \sum_{j=1}^{N_\alpha} w_j \beta_j \right) \right]}{\sum_{j=1}^{N_\alpha} w_j \beta_j} - t_1 \exp\left(-t_1 \sum_{j=1}^{N_\alpha} w_j \beta_j \right) \right\} \tag{7.33}$$

$$= w_i t_1 \exp\left(-t_1 \sum_{j=1}^{N_\alpha} w_j \beta_j \right), \quad i,j = 1,...,N_\alpha.$$

The correctness of the above expressions for the 2$^{\text{nd}}$-order response sensitivities can be readily verified by computing the derivatives of the 1$^{\text{st}}$-order sensitivities expressed by Eqs. (2.103) and (2.104). Thus, taking the partial derivatives of Eq. (2.103) yields:

$$\frac{\partial^2 \rho(t_1)}{\partial \beta_i \partial \rho_{a,A}^{in}} = t_1 w_i \exp\left(-t_1 \sum_{j=1}^{N_\alpha} w_j \beta_j \right), \quad i = 1,...,N_\alpha, \tag{7.17}$$

$$\frac{\partial^2 \rho(t_1)}{\partial \beta_i \partial \beta_j} = -\rho_{a,A}^{in,0}(t_1)^2 w_i w_j \exp\left(-t_1 \sum_{k=1}^{N_\alpha} w_k \beta_k \right); \quad i,j = 1,...,N_\alpha. \tag{7.18}$$

Furthermore, taking the partial derivatives of Eq. (2.104) yields:

$$\frac{\partial^2 \rho(t_1)}{\partial \left(\rho_{a,A}^{in} \right)^2} \equiv 0, \tag{7.32}$$

$$\frac{\partial^2 \rho(t_1)}{\partial \rho_{a,A}^{in} \partial \beta_i} = t_1 w_i \exp\left(-t_1 \sum_{j=1}^{N_\alpha} w_j \beta_j \right) = \frac{\partial^2 \rho(t_1)}{\partial \beta_i \partial \rho_{a,A}^{in}}, \quad i = 1, ..., N_\alpha, \tag{7.33}$$

The following conclusions can be drawn from these results:

1. The 2nd-order response sensitivities to all of the model parameters have been computed by a *new method* which uses adjoint operators for computing these sensitivities efficiently and exactly. This method considers each 1st-order sensitivity as a separate response and develops corresponding 2nd-level adjoint system for computing the respective 2nd-order sensitivities. In particular, for the surrogate dissolver model, the new method first considered as response the 1st-order sensitivity defined in Eq. (2.99), for which the corresponding 2nd-level adjoint system is given by Eqs. (7.8) - (7.11). Solving this 2nd-level adjoint system once only for each 1st-order sensitivity has yielded the adjoint functions $\psi_1^{(2)}$ and $\psi_2^{(2)}$, which are independent of parameter variations, and which were used for computing the respective 2nd-order sensitivities shown in Eqs. (7.17) and (7.18). Subsequently, the new method was similarly applied to the 1st-order sensitivity defined in Eq. (2.100), considered as a "model response." The corresponding 2nd-level adjoint system for this 1st-order sensitivity is given by Eqs. (7.23) - (7.26), which was solved, again only once, to obtain the adjoint functions $\psi_3^{(2)}$ and $\psi_4^{(2)}$. These adjoint functions are also independent of any parameter variations; they were used to compute the respective 2nd-order sensitivities shown in Eqs. (7.32) and (7.33).

2. Note that the *mixed 2nd-order sensitivities* are obtained *twice*, once in terms of the adjoint functions $\psi_1^{(2)}$ and $\psi_2^{(2)}$ [in Eq. (7.17)], and again in terms of the adjoint functions $\psi_3^{(2)}$ and $\psi_4^{(2)}$ [in Eq. (7.33)]. Thus, the new method provides an inherent independent verification of the correctness of the *mixed 2nd-order sensitivities*.

3. The specific 2nd-order sensitivities to be computed can be selected "a priori", based on the magnitude/importance of the 1st-order sensitivities. For the specific case of the surrogate dissolver model, it is obvious from the 1st-order sensitivity provided by Eq. (2.100) that $\partial^2 \rho(t_1) / \partial \left(\rho_{a,A}^{in} \right)^2 \equiv 0$, so that all of the non-zero 2nd-order sensitivities would have been obtained by computing just the adjoint functions $\psi_1^{(2)}$ and $\psi_2^{(2)}$, by solving Eqs. (7.8) - (7.11). Nevertheless, the *mixed 2nd-order sensitivities* were alternatively computed in terms of the adjoint functions $\psi_3^{(2)}$ and $\psi_4^{(2)}$ [in Eq. (7.33)], to demonstrate the full potential of the new adjoint-based methodology here.

4. The *un-mixed 2nd-order sensitivities* of the form $\partial^2 \rho(t_1) / \partial \alpha_i^2$ are obtained only once, so they can be independently verified only by recomputing, e.g., using finite difference formulas of the form

$$\frac{\partial^2 \rho(t_1)}{\partial \alpha_i^2} \cong \frac{\rho\left(t_1; \alpha_i^0 + \delta\alpha_i\right) - 2\rho\left(t_1; \alpha_i^0\right) + \rho\left(t_1; \alpha_i^0 - \delta\alpha_i\right)}{\left|\delta\alpha_i\right|^2}. \tag{7.34}$$

It is important to note that using diference formulas such as in Eq. (7.34) computes *approximate*, rather than exact, *values* for the respective 2nd-order sensitivities.

5. Computing the 2nd-order sensitivities using Eq. (7.34) would require $\left(N_\alpha + 1\right)\left(N_\alpha + 2\right)/2$ forward computations, which would be impractical. In contradistinction, the new method presented in this Chapter would require at most $\left(N_\alpha + 1\right)$ adjoint computations.

6. The availability of the 2nd-order sensitivities obtained in Eqs. (7.17), (7.18), and (7.32) makes it possible to compute the respective 2nd-order terms in the expressions given in Eqs. (2.51) - (2.53) for the first three moments of the response distribution.

7.2. Skewness and Non-Gaussian Features of the Acid Concentrations in the Full Dissolver Model

Recall from Chapters 3 and 4, that the dissolver model comprises $N_\alpha = 1291$ experimentally parameters α_i, for which only the mean values and the standard deviations are available. Having *only this information* available is equivalent to the assumption that these parameters are *uncorrelated and normally distributed*. For such parameters, the expressions given in Eqs. (2.51) - (2.53) simplify to the following forms:

$$\left[E(r_k) \right]^{UG} = r_k\left(\boldsymbol{\alpha}^0\right) + \frac{1}{2}\sum_{i=1}^{N_\alpha} \frac{\partial^2 r_k}{\partial \alpha_i^2} \sigma_i^2 , \tag{7.35}$$

where the superscript "*UG*" indicates "*uncorrelated Gaussian*" parameters. The covariance $\left[cov(r_k, r_\ell) \right]^{UG}$, for such parameters, takes on the form:

$$\left[cov(r_k, r_\ell) \right]^{UG} = \sum_{i=1}^{N_\alpha} \left(\frac{\partial r_k}{\partial \alpha_i} \frac{\partial r_\ell}{\partial \alpha_i} \right) \sigma_i^2 + \frac{1}{2}\sum_{i=1}^{N_\alpha} \left(\frac{\partial^2 r_k}{\partial \alpha_i^2} \right)\left(\frac{\partial^2 r_\ell}{\partial \alpha_i^2} \right) \sigma_i^4 . \tag{7.36}$$

In particular, the variance, $\left[var(r_k) \right]^{UG}$, of a response r_k that depends on *uncorrelated and normally distributed* parameters is obtained by setting $r_k \equiv r_l$ in Eq. (7.36), which yields

$$\left[var(r_k) \right]^{UG} = \sum_{i=1}^{N_\alpha} \left(\frac{\partial r_k}{\partial \alpha_i} \right)^2 \sigma_i^2 + \frac{1}{2}\sum_{i=1}^{N_\alpha} \left(\frac{\partial^2 r_k}{\partial \alpha_i^2} \right)^2 \sigma_i^4 . \tag{7.37}$$

The third-order central moment, $\left[\mu_3(r_k) \right]^{UG}$, of a response r_k that depends on *uncorrelated and normally distributed* is obtained from Eq. (2.53) in the form

$$\left[\mu_3(r_k) \right]^{UG} = 3\sum_{i=1}^{N_\alpha} \left(\frac{\partial r_k}{\partial \alpha_i} \right)^2 \frac{\partial^2 r_k}{\partial \alpha_i^2} \sigma_i^4 . \tag{7.38}$$

As indicated by the expressions in Eqs. (7.35) through (7.38), the 2nd-order sensitivities have the following impacts on the response moments:

(a) They cause the "expected value of the response", $\left[E(r_k) \right]^{UG}$, to differ from the "computed nominal value of the response", $r_k \left(\boldsymbol{\alpha}^0 \right)$;

(b) They contribute to the response variances and covariances; however, since the contributions involving the second-order sensitivities are multiplied by the fourth power of the parameters' standard deviations, the total of these contributions is expected to be relatively smaller than the contributions stemming from the first-order response sensitivities;

(c) On the other hand, as indicated by Eq. (7.38), the 2nd-order sensitivities provide the leading contributions to the third-order moment, $\left[\mu_3 (r_k) \right]^{UG}$, and –hence-- skewness a response that depends on *uncorrelated and normally distributed* parameters.

The above relations are also valid when the parameters and/or responses are implicit functions of time, as is the case for the acid concentration responses $\rho_a^{(k)} (t_i)$, $k = 1,...,8$, which are functions of 1291 scalar parameters, if the inlet mass rate flow $\dot{m}^{(in)} (t_i)$ and the inlet acid concentration $\rho_a^{(in)} (t_i)$ are considered to vary independently at every time node $t_i = 1,...,635$, as has been considered in the previous Chapters of this work. Recall from Chapter 5, Eq. (5.9), that the time-dependent acid concentrations $\rho_a^{(k)} (t_i)$, $k = 1,...,8$, do *not* depend on parameters at time steps "in the future of the current time step", which means that

$$\frac{\partial \rho_a^{(k)} \left(t_i; \boldsymbol{\alpha}^0 \right)}{\partial \rho_a^{(in)} \left(t_j \right)} = 0, \quad \frac{\partial \rho_a^{(k)} \left(t_i; \boldsymbol{\alpha}^0 \right)}{\partial \dot{m}^{(in)} \left(t_j \right)} = 0, \quad j > i, \ i = 1,...,635;$$

$$\frac{\partial^2 \rho_a^{(k)} \left(t_i; \boldsymbol{\alpha}^0 \right)}{\partial \left[\rho_a^{(in)} \left(t_j \right) \right]^2} = 0, \quad \frac{\partial^2 \rho_a^{(k)} \left(t_i; \boldsymbol{\alpha}^0 \right)}{\partial \left[\dot{m}^{(in)} \left(t_j \right) \right]^2} = 0, \quad j > i, \ i = 1,...,635. \tag{7.39}$$

Recall also from Figures 3.3 and 3.4 that the inlet mass flow rate $\dot{m}^{(in)}(t)$ and the inlet acid concentration $\rho_a^{(in)}(t)$ do *not* vary independently at each time step, but are piecewise constant functions of the form

$$\dot{m}^{(in)}(t)=\begin{cases} \dot{m}_A, & t_0 \leq t < t_A \\ \dot{m}_B, & t_A \leq t < t_B \\ \dot{m}_C, & t_C \leq t < t_D \\ \dot{m}_D, & t_D \leq t < t_f \end{cases} \quad ; \quad \rho_a^{(in)}(t)=\begin{cases} \rho_{a,A}^{(in)}, & t_0 \leq t < t_A \\ \rho_{a,B}^{(in)}, & t_A \leq t < t_B \\ \rho_{a,C}^{(in)}, & t_C \leq t < t_D \\ \rho_{a,D}^{(in)}, & t_D \leq t < t_f \end{cases} \quad (7.40)$$

Consequently, Eqs. (7.35), (7.37) and (7.38) take on the following forms for the time-dependent acid concentration, $\rho_a^{(k)}(t_i)$, $k=1,...,8$, in each of the eight compartments:

(i)   The expectation, $E\left[\rho_a^{(k)}(t_i;\boldsymbol{\alpha}^0)\right]$, of $\rho_a^{(k)}(t_i;\boldsymbol{\alpha}^0)$:

$$E\left[\rho_a^{(k)}(t_i;\boldsymbol{\alpha}^0)\right]=\rho_a^{(k)}(t_i;\boldsymbol{\alpha}^0)+E_2\left[\rho_a^{(k)}(t_i;\boldsymbol{\alpha}^0)\right], \quad k=1,...,8; \ i=1,...,635; \quad (7.41)$$

where the quantity $E_2\left[\rho_a^{(k)}(t;\boldsymbol{\alpha}^0)\right]$ comprises the 2nd-order contributions to the expectation $E\left[\rho_a^{(k)}(t;\boldsymbol{\alpha}^0)\right]$ and is defined as

$$\begin{aligned} E_2\left[\rho_a^{(k)}(t_i;\boldsymbol{\alpha}^0)\right] &\triangleq \frac{1}{2}\frac{\partial^2 \rho_a^{(k)}(t_i;\boldsymbol{\alpha}^0)}{\partial a^2}\mathrm{var}(a)+\frac{1}{2}\frac{\partial^2 \rho_a^{(k)}(t_i;\boldsymbol{\alpha}^0)}{\partial b^2}\mathrm{var}(b) \\ &+\frac{1}{2}\frac{\partial^2 \rho_a^{(k)}(t_i;\boldsymbol{\alpha}^0)}{\partial V_0^2}\mathrm{var}(V_0)+\frac{1}{2}\frac{\partial^2 \rho_a^{(k)}(t_i;\boldsymbol{\alpha}^0)}{\partial p^2}\mathrm{var}(p)+\frac{1}{2}\frac{\partial^2 \rho_a^{(k)}(t_i;\boldsymbol{\alpha}^0)}{\partial G^2}\mathrm{var}(G) \\ &+X(k;t_i)+\frac{1}{2}\sum_{j=1}^{8}\left\{\frac{\partial^2 \rho_a^{(k)}(t_i;\boldsymbol{\alpha}^0)}{\partial\left[\rho_a^{(j)}(0)\right]^2}\mathrm{var}\left[\rho_a^{(j)}(0)\right]+\frac{\partial^2 \rho_a^{(k)}(t_i;\boldsymbol{\alpha}^0)}{\partial\left[V^{(j)}(0)\right]^2}\mathrm{var}\left[V^{(j)}(0)\right]\right\}, \end{aligned} \quad (7.42)$$

for $k=1,...,8; \ i=1,...,635;$

where the quantity $X(k;t_i)$ is defined, *for* $k=1,...,8; \ i=1,...,635$, as follows:

$$X(k;t_i)\triangleq\frac{1}{2}\left\{\frac{\partial^2 \rho_a^{(k)}(t_i;\boldsymbol{\alpha}^0)}{\partial\left[\rho_{a,A}^{(in)}\right]^2}\mathrm{var}\left[\rho_{a,A}^{(in)}\right]+\frac{\partial^2 \rho_a^{(k)}(t_i;\boldsymbol{\alpha}^0)}{\partial\left[\dot{m}_A\right]^2}\mathrm{var}\left[\dot{m}_A\right]\right\}, \ for \ t_0 \leq t_i < t_A; (7.43)$$

173

$$X(k;t_i) \triangleq \frac{1}{2} \left\{ \frac{\partial^2 \rho_a^{(k)}(t_i;\boldsymbol{\alpha}^0)}{\partial \left[\rho_{a,A}^{(in)}\right]^2} \text{var}\left[\rho_{a,A}^{(in)}\right] + \frac{\partial^2 \rho_a^{(k)}(t_i;\boldsymbol{\alpha}^0)}{\partial \left[\dot{m}_A\right]^2} \text{var}\left[\dot{m}_A\right] \right\}$$

$$+ \frac{1}{2} \left\{ \frac{\partial^2 \rho_a^{(k)}(t_i;\boldsymbol{\alpha}^0)}{\partial \left[\rho_{a,B}^{(in)}\right]^2} \text{var}\left[\rho_{a,B}^{(in)}\right] + \frac{\partial^2 \rho_a^{(k)}(t_i;\boldsymbol{\alpha}^0)}{\partial \left[\dot{m}_B\right]^2} \text{var}\left[\dot{m}_B\right] \right\}, \; for \;\; t_A \le t_i < t_B; \tag{7.44}$$

$$X(k;t_i) \triangleq \frac{1}{2} \left\{ \frac{\partial^2 \rho_a^{(k)}(t_i;\boldsymbol{\alpha}^0)}{\partial \left[\rho_{a,A}^{(in)}\right]^2} \text{var}\left[\rho_{a,A}^{(in)}\right] + \frac{\partial^2 \rho_a^{(k)}(t_i;\boldsymbol{\alpha}^0)}{\partial \left[\dot{m}_A\right]^2} \text{var}\left[\dot{m}_A\right] \right\}$$

$$+ \frac{1}{2} \left\{ \frac{\partial^2 \rho_a^{(k)}(t_i;\boldsymbol{\alpha}^0)}{\partial \left[\rho_{a,B}^{(in)}\right]^2} \text{var}\left[\rho_{a,B}^{(in)}\right] + \frac{\partial^2 \rho_a^{(k)}(t_i;\boldsymbol{\alpha}^0)}{\partial \left[\dot{m}_B\right]^2} \text{var}\left[\dot{m}_B\right] \right\}$$

$$+ \frac{1}{2} \left\{ \frac{\partial^2 \rho_a^{(k)}(t_i;\boldsymbol{\alpha}^0)}{\partial \left[\rho_{a,C}^{(in)}\right]^2} \text{var}\left[\rho_{a,C}^{(in)}\right] + \frac{\partial^2 \rho_a^{(k)}(t_i;\boldsymbol{\alpha}^0)}{\partial \left[\dot{m}_C\right]^2} \text{var}\left[\dot{m}_C\right] \right\}, \; for \;\; t_B \le t_i < t_C; \tag{7.45}$$

$$X(k;t_i) \triangleq \frac{1}{2} \left\{ \frac{\partial^2 \rho_a^{(k)}(t_i;\boldsymbol{\alpha}^0)}{\partial \left[\rho_{a,A}^{(in)}\right]^2} \text{var}\left[\rho_{a,A}^{(in)}\right] + \frac{\partial^2 \rho_a^{(k)}(t_i;\boldsymbol{\alpha}^0)}{\partial \left[\dot{m}_A\right]^2} \text{var}\left[\dot{m}_A\right] \right\}$$

$$+ \frac{1}{2} \left\{ \frac{\partial^2 \rho_a^{(k)}(t_i;\boldsymbol{\alpha}^0)}{\partial \left[\rho_{a,B}^{(in)}\right]^2} \text{var}\left[\rho_{a,B}^{(in)}\right] + \frac{\partial^2 \rho_a^{(k)}(t_i;\boldsymbol{\alpha}^0)}{\partial \left[\dot{m}_B\right]^2} \text{var}\left[\dot{m}_B\right] \right\}$$

$$+ \frac{1}{2} \left\{ \frac{\partial^2 \rho_a^{(k)}(t_i;\boldsymbol{\alpha}^0)}{\partial \left[\rho_{a,C}^{(in)}\right]^2} \text{var}\left[\rho_{a,C}^{(in)}\right] + \frac{\partial^2 \rho_a^{(k)}(t_i;\boldsymbol{\alpha}^0)}{\partial \left[\dot{m}_C\right]^2} \text{var}\left[\dot{m}_C\right] \right\}$$

$$+ \frac{1}{2} \left\{ \frac{\partial^2 \rho_a^{(k)}(t_i;\boldsymbol{\alpha}^0)}{\partial \left[\rho_{a,D}^{(in)}\right]^2} \text{var}\left[\rho_{a,D}^{(in)}\right] + \frac{\partial^2 \rho_a^{(k)}(t_i;\boldsymbol{\alpha}^0)}{\partial \left[\dot{m}_D\right]^2} \text{var}\left[\dot{m}_D\right] \right\}, \; for \;\; t_C \le t_i < t_D; \tag{7.46}$$

(ii) The variance, $\text{Var}\left[\rho_a^{(k)}(t_i;\boldsymbol{\alpha}^0)\right]$, of $\rho_a^{(k)}(t_i;\boldsymbol{\alpha}^0)$:

$$\text{Var}\left[\rho_a^{(k)}(t_i;\boldsymbol{\alpha}^0)\right] = \text{Var}_1\left[\rho_a^{(k)}(t_i;\boldsymbol{\alpha}^0)\right] + \text{Var}_2\left[\rho_a^{(k)}(t_i;\boldsymbol{\alpha}^0)\right], \;\; k=1,...,8; \; i=1,...,635;$$

$$\tag{7.47}$$

where the quantities $\text{Var}_1\left[\rho_a^{(k)}\left(t_i;\boldsymbol{\alpha}^0\right)\right]$ and $\text{Var}_2\left[\rho_a^{(k)}\left(t_i;\boldsymbol{\alpha}^0\right)\right]$ comprise the 1st-order and, respectively, the 2nd-order contributions to the variance $\text{Var}\left[\rho_a^{(k)}\left(t_i;\boldsymbol{\alpha}^0\right)\right]$, and are defined as follows:

$$\text{Var}_1\left[\rho_a^{(k)}\left(t_i;\boldsymbol{\alpha}^0\right)\right] \triangleq \left[\frac{\partial\rho_a^{(k)}\left(t_i;\boldsymbol{\alpha}^0\right)}{\partial a}\right]^2 \text{var}\left(a\right) + \left[\frac{\partial\rho_a^{(k)}\left(t_i;\boldsymbol{\alpha}^0\right)}{\partial b}\right]^2 \text{var}\left(b\right)$$

$$+ \left[\frac{\partial\rho_a^{(k)}\left(t_i;\boldsymbol{\alpha}^0\right)}{\partial V_0}\right]^2 \text{var}\left(V_0\right) + \left[\frac{\partial\rho_a^{(k)}\left(t_i;\boldsymbol{\alpha}^0\right)}{\partial p}\right]^2 \text{var}\left(p\right) + \left[\frac{\partial\rho_a^{(k)}\left(t_i;\boldsymbol{\alpha}^0\right)}{\partial G}\right]^2 \text{var}\left(G\right)$$

$$+ \sum_{j=1}^{i}\left\{\frac{\partial\rho_a^{(k)}\left(t_i;\boldsymbol{\alpha}^0\right)}{\partial\rho_a^{(in)}\left(t_j\right)}\right\}^2 \text{var}\left[\rho_a^{(in)}\left(t_j\right)\right] + \sum_{i=1}^{i}\left\{\frac{\partial\rho_a^{(k)}\left(t_i;\boldsymbol{\alpha}^0\right)}{\partial\dot{m}^{(in)}\left(t_j\right)}\right\}^2 \text{var}\left[\dot{m}^{(in)}\left(t_j\right)\right] \qquad (7.48)$$

$$+ \sum_{j=1}^{8}\left\{\frac{\partial\rho_a^{(k)}\left(t_i;\boldsymbol{\alpha}^0\right)}{\partial\rho_a^{(j)}\left(0\right)}\right\}^2 \text{var}\left[\rho_a^{(j)}\left(0\right)\right] + \sum_{j=1}^{8}\left\{\frac{\partial\rho_a^{(k)}\left(t_i;\boldsymbol{\alpha}^0\right)}{\partial V^{(j)}\left(0\right)}\right\}^2 \text{var}\left[V^{(j)}\left(0\right)\right],$$

$for \quad k=1,...,8, \quad i=1,...,635;$

$$\text{Var}_2\left[\rho_a^{(k)}\left(t_i;\boldsymbol{\alpha}^0\right)\right] \triangleq \frac{1}{2}\left[\frac{\partial^2\rho_a^{(k)}\left(t_i;\boldsymbol{\alpha}^0\right)}{\partial a^2}\text{var}\left(a\right)\right]^2 + \frac{1}{2}\left[\frac{\partial^2\rho_a^{(k)}\left(t_i;\boldsymbol{\alpha}^0\right)}{\partial b^2}\text{var}\left(b\right)\right]^2$$

$$+ \frac{1}{2}\left[\frac{\partial^2\rho_a^{(k)}\left(t_i;\boldsymbol{\alpha}^0\right)}{\partial V_0^2}\text{var}\left(V_0\right)\right]^2 + \frac{1}{2}\left[\frac{\partial^2\rho_a^{(k)}\left(t_i;\boldsymbol{\alpha}^0\right)}{\partial p^2}\text{var}\left(p\right)\right]^2 + \frac{1}{2}\left[\frac{\partial^2\rho_a^{(k)}\left(t_i;\boldsymbol{\alpha}^0\right)}{\partial G^2}\text{var}\left(G\right)\right]^2$$

$$+ Y\left(k;t_i\right) + \frac{1}{2}\sum_{j=1}^{8}\left\{\frac{\partial^2\rho_a^{(k)}\left(t_i;\boldsymbol{\alpha}^0\right)}{\partial\left[\rho_a^{(j)}\left(0\right)\right]^2}\text{var}\left[\rho_a^{(j)}\left(0\right)\right]\right\}^2 + \frac{1}{2}\sum_{j=1}^{8}\left\{\frac{\partial^2\rho_a^{(k)}\left(t_i;\boldsymbol{\alpha}^0\right)}{\partial\left[V^{(j)}\left(0\right)\right]^2}\text{var}\left[V^{(j)}\left(0\right)\right]\right\}^2,$$

$for \quad k=1,...,8; \quad i=1,...,635;$

$$(7.49)$$

where the quantity $Y\left(k;t_i\right)$ is defined, $for \quad k=1,...,8; \quad i=1,...,635$, as follows:

$$Y\left(k;t_i\right) \triangleq \frac{1}{2}\left\{\frac{\partial^2\rho_a^{(k)}\left(t_i;\boldsymbol{\alpha}^0\right)}{\partial\left[\rho_{a,A}^{(in)}\right]^2}\text{var}\left[\rho_{a,A}^{(in)}\right]\right\}^2 + \frac{1}{2}\left\{\frac{\partial^2\rho_a^{(k)}\left(t_i;\boldsymbol{\alpha}^0\right)}{\partial\left[\dot{m}_A\right]^2}\text{var}\left[\dot{m}_A\right]\right\}^2, \quad for \quad t_0 \le t_i < t_A;$$

$$(7.50)$$

$$
Y\left(k;t_i\right) \triangleq \frac{1}{2}\left\{\frac{\partial^2 \rho_a^{(k)}\left(t_i;\boldsymbol{\alpha}^0\right)}{\partial\left[\rho_{a,A}^{(in)}\right]^2}\operatorname{var}\left[\rho_{a,A}^{(in)}\right]\right\}^2 + \frac{1}{2}\left\{\frac{\partial^2 \rho_a^{(k)}\left(t_i;\boldsymbol{\alpha}^0\right)}{\partial\left[\dot{m}_A\right]^2}\operatorname{var}\left[\dot{m}_A\right]\right\}^2
$$

$$
+ \frac{1}{2}\left\{\frac{\partial^2 \rho_a^{(k)}\left(t_i;\boldsymbol{\alpha}^0\right)}{\partial\left[\rho_{a,B}^{(in)}\right]^2}\operatorname{var}\left[\rho_{a,B}^{(in)}\right]\right\}^2 + \frac{1}{2}\left\{\frac{\partial^2 \rho_a^{(k)}\left(t_i;\boldsymbol{\alpha}^0\right)}{\partial\left[\dot{m}_B\right]^2}\operatorname{var}\left[\dot{m}_B\right]\right\}^2 ,\ for\ \ t_A \le t_i < t_B;
$$

(7.51)

$$
Y\left(k;t_i\right) \triangleq \frac{1}{2}\left\{\frac{\partial^2 \rho_a^{(k)}\left(t_i;\boldsymbol{\alpha}^0\right)}{\partial\left[\rho_{a,A}^{(in)}\right]^2}\operatorname{var}\left[\rho_{a,A}^{(in)}\right]\right\}^2 + \frac{1}{2}\left\{\frac{\partial^2 \rho_a^{(k)}\left(t_i;\boldsymbol{\alpha}^0\right)}{\partial\left[\dot{m}_A\right]^2}\operatorname{var}\left[\dot{m}_A\right]\right\}^2
$$

$$
+ \frac{1}{2}\left\{\frac{\partial^2 \rho_a^{(k)}\left(t_i;\boldsymbol{\alpha}^0\right)}{\partial\left[\rho_{a,B}^{(in)}\right]^2}\operatorname{var}\left[\rho_{a,B}^{(in)}\right]\right\}^2 + \frac{1}{2}\left\{\frac{\partial^2 \rho_a^{(k)}\left(t_i;\boldsymbol{\alpha}^0\right)}{\partial\left[\dot{m}_B\right]^2}\operatorname{var}\left[\dot{m}_B\right]\right\}^2
$$

(7.52)

$$
+ \frac{1}{2}\left\{\frac{\partial^2 \rho_a^{(k)}\left(t_i;\boldsymbol{\alpha}^0\right)}{\partial\left[\rho_{a,C}^{(in)}\right]^2}\operatorname{var}\left[\rho_{a,C}^{(in)}\right]\right\}^2 + \frac{1}{2}\left\{\frac{\partial^2 \rho_a^{(k)}\left(t_i;\boldsymbol{\alpha}^0\right)}{\partial\left[\dot{m}_C\right]^2}\operatorname{var}\left[\dot{m}_C\right]\right\}^2 ,\ for\ \ t_B \le t_i < t_C;
$$

$$
Y\left(k;t_i\right) \triangleq \frac{1}{2}\left\{\frac{\partial^2 \rho_a^{(k)}\left(t_i;\boldsymbol{\alpha}^0\right)}{\partial\left[\rho_{a,A}^{(in)}\right]^2}\operatorname{var}\left[\rho_{a,A}^{(in)}\right]\right\}^2 + \frac{1}{2}\left\{\frac{\partial^2 \rho_a^{(k)}\left(t_i;\boldsymbol{\alpha}^0\right)}{\partial\left[\dot{m}_A\right]^2}\operatorname{var}\left[\dot{m}_A\right]\right\}^2
$$

$$
+ \frac{1}{2}\left\{\frac{\partial^2 \rho_a^{(k)}\left(t_i;\boldsymbol{\alpha}^0\right)}{\partial\left[\rho_{a,B}^{(in)}\right]^2}\operatorname{var}\left[\rho_{a,B}^{(in)}\right]\right\}^2 + \frac{1}{2}\left\{\frac{\partial^2 \rho_a^{(k)}\left(t_i;\boldsymbol{\alpha}^0\right)}{\partial\left[\dot{m}_B\right]^2}\operatorname{var}\left[\dot{m}_B\right]\right\}^2
$$

$$
+ \frac{1}{2}\left\{\frac{\partial^2 \rho_a^{(k)}\left(t_i;\boldsymbol{\alpha}^0\right)}{\partial\left[\rho_{a,C}^{(in)}\right]^2}\operatorname{var}\left[\rho_{a,C}^{(in)}\right]\right\}^2 + \frac{1}{2}\left\{\frac{\partial^2 \rho_a^{(k)}\left(t_i;\boldsymbol{\alpha}^0\right)}{\partial\left[\dot{m}_C\right]^2}\operatorname{var}\left[\dot{m}_C\right]\right\}^2
$$

(7.53)

$$
+ \frac{1}{2}\left\{\frac{\partial^2 \rho_a^{(k)}\left(t_i;\boldsymbol{\alpha}^0\right)}{\partial\left[\rho_{a,D}^{(in)}\right]^2}\operatorname{var}\left[\rho_{a,D}^{(in)}\right]\right\}^2 + \frac{1}{2}\left\{\frac{\partial^2 \rho_a^{(k)}\left(t_i;\boldsymbol{\alpha}^0\right)}{\partial\left[\dot{m}_D\right]^2}\operatorname{var}\left[\dot{m}_D\right]\right\}^2 ,\ for\ \ t_C \le t_i < t_D;
$$

(iii)   The 3$^{\text{rd}}$-order moment, $\mu_3\left[\rho_a^{(k)}\left(t_i;\mathbf{a}^0\right)\right]$, of $\rho_a^{(k)}\left(t_i;\mathbf{a}^0\right)$:

$$\mu_3\left[\rho_a^{(k)}\left(t_i;\mathbf{a}^0\right)\right]=Z\left(k;t_i\right)$$

$$3\left[\frac{\partial\rho_a^{(k)}\left(t_i;\mathbf{a}^0\right)}{\partial a}\right]^2\frac{\partial^2\rho_a^{(k)}\left(t_i;\mathbf{a}^0\right)}{\partial a^2}\left[\operatorname{var}\left(a\right)\right]^2+3\left[\frac{\partial\rho_a^{(k)}\left(t_i;\mathbf{a}^0\right)}{\partial b}\right]^2\frac{\partial^2\rho_a^{(k)}\left(t_i;\mathbf{a}^0\right)}{\partial b^2}\left[\operatorname{var}\left(b\right)\right]^2$$

$$+3\left[\frac{\partial\rho_a^{(k)}\left(t_i;\mathbf{a}^0\right)}{\partial V_0}\right]^2\frac{\partial^2\rho_a^{(k)}\left(t_i;\mathbf{a}^0\right)}{\partial V_0^2}\left[\operatorname{var}\left(V_0\right)\right]^2+3\left[\frac{\partial\rho_a^{(k)}\left(t_i;\mathbf{a}^0\right)}{\partial p}\right]^2\frac{\partial^2\rho_a^{(k)}\left(t_i;\mathbf{a}^0\right)}{\partial p^2}\left[\operatorname{var}\left(p\right)\right]^2$$

$$+3\left[\frac{\partial\rho_a^{(k)}\left(t_i;\mathbf{a}^0\right)}{\partial G}\right]^2\frac{\partial^2\rho_a^{(k)}\left(t_i;\mathbf{a}^0\right)}{\partial G^2}\left[\operatorname{var}\left(G\right)\right]^2+3\sum_{j=1}^{8}\left\{\frac{\partial\rho_a^{(k)}\left(t_i;\mathbf{a}^0\right)}{\partial\rho_a^{(j)}\left(0\right)}\right\}^2\frac{\partial^2\rho_a^{(k)}\left(t_i;\mathbf{a}^0\right)}{\partial\left[\rho_a^{(j)}\left(0\right)\right]^2}\left\{\operatorname{var}\left[\rho_a^{(j)}\left(0\right)\right]\right\}^2$$

$$+3\sum_{i=1}^{8}\left\{\frac{\partial\rho_a^{(k)}\left(t_i;\mathbf{a}^0\right)}{\partial V^{(i)}\left(0\right)}\right\}^2\frac{\partial^2\rho_a^{(k)}\left(t_i;\mathbf{a}^0\right)}{\partial\left[V^{(i)}\left(0\right)\right]^2}\left\{\operatorname{var}\left[V^{(i)}\left(0\right)\right]\right\}^2,$$

for $k=1,...,8;\ i=1,...,635;$

(7.54)

where the quantity $Z\left(k;t_i\right)$ is defined, *for* $k=1,...,8;\ i=1,...,635$, as follows:

$$Z\left(k;t_i\right)\triangleq 3\left\{\frac{\partial\rho_a^{(k)}\left(t_i;\mathbf{a}^0\right)}{\partial\rho_{a,A}^{(in)}}\right\}^2\frac{\partial^2\rho_a^{(k)}\left(t_i;\mathbf{a}^0\right)}{\partial\left[\rho_{a,A}^{(in)}\right]^2}\left\{\operatorname{var}\left[\rho_{a,A}^{(in)}\right]\right\}^2$$

$$+3\left\{\frac{\partial\rho_a^{(k)}\left(t_i;\mathbf{a}^0\right)}{\partial\dot{m}_A^{(in)}}\right\}^2\frac{\partial^2\rho_a^{(k)}\left(t_i;\mathbf{a}^0\right)}{\partial\left[\dot{m}_A\right]^2}\left\{\operatorname{var}\left[\dot{m}_A\right]\right\}^2,\ \textit{for}\ \ t_0\le t_i<t_A;$$

(7.55)

$$Z(k;t_i) \triangleq 3\left\{\frac{\partial \rho_a^{(k)}(t_i;\boldsymbol{\alpha}^0)}{\partial \rho_{a,A}^{(in)}}\right\}^2 \frac{\partial^2 \rho_a^{(k)}(t_i;\boldsymbol{\alpha}^0)}{\partial\left[\rho_{a,A}^{(in)}\right]^2}\left\{\mathrm{var}\left[\rho_{a,A}^{(in)}\right]\right\}^2$$

$$+3\left\{\frac{\partial \rho_a^{(k)}(t_i;\boldsymbol{\alpha}^0)}{\partial \dot{m}_A^{(in)}}\right\}^2 \frac{\partial^2 \rho_a^{(k)}(t_i;\boldsymbol{\alpha}^0)}{\partial\left[\dot{m}_A\right]^2}\left\{\mathrm{var}\left[\dot{m}_A\right]\right\}^2$$

$$+3\left\{\frac{\partial \rho_a^{(k)}(t_i;\boldsymbol{\alpha}^0)}{\partial \rho_{a,B}^{(in)}}\right\}^2 \frac{\partial^2 \rho_a^{(k)}(t_i;\boldsymbol{\alpha}^0)}{\partial\left[\rho_{a,B}^{(in)}\right]^2}\left\{\mathrm{var}\left[\rho_{a,B}^{(in)}\right]\right\}^2$$

$$+3\left\{\frac{\partial \rho_a^{(k)}(t_i;\boldsymbol{\alpha}^0)}{\partial \dot{m}_B^{(in)}}\right\}^2 \frac{\partial^2 \rho_a^{(k)}(t_i;\boldsymbol{\alpha}^0)}{\partial\left[\dot{m}_B\right]^2}\left\{\mathrm{var}\left[\dot{m}_B\right]\right\}^2, \;\; for \;\; t_A \le t_i < t_B;$$

$$\text{(7.56)}$$

$$Z(k;t_i) \triangleq 3\left\{\frac{\partial \rho_a^{(k)}(t_i;\boldsymbol{\alpha}^0)}{\partial \rho_{a,A}^{(in)}}\right\}^2 \frac{\partial^2 \rho_a^{(k)}(t_i;\boldsymbol{\alpha}^0)}{\partial\left[\rho_{a,A}^{(in)}\right]^2}\left\{\mathrm{var}\left[\rho_{a,A}^{(in)}\right]\right\}^2$$

$$+3\left\{\frac{\partial \rho_a^{(k)}(t_i;\boldsymbol{\alpha}^0)}{\partial \dot{m}_A^{(in)}}\right\}^2 \frac{\partial^2 \rho_a^{(k)}(t_i;\boldsymbol{\alpha}^0)}{\partial\left[\dot{m}_A\right]^2}\left\{\mathrm{var}\left[\dot{m}_A\right]\right\}^2$$

$$+3\left\{\frac{\partial \rho_a^{(k)}(t_i;\boldsymbol{\alpha}^0)}{\partial \rho_{a,B}^{(in)}}\right\}^2 \frac{\partial^2 \rho_a^{(k)}(t_i;\boldsymbol{\alpha}^0)}{\partial\left[\rho_{a,B}^{(in)}\right]^2}\left\{\mathrm{var}\left[\rho_{a,B}^{(in)}\right]\right\}^2$$

$$+3\left\{\frac{\partial \rho_a^{(k)}(t_i;\boldsymbol{\alpha}^0)}{\partial \dot{m}_B^{(in)}}\right\}^2 \frac{\partial^2 \rho_a^{(k)}(t_i;\boldsymbol{\alpha}^0)}{\partial\left[\dot{m}_B\right]^2}\left\{\mathrm{var}\left[\dot{m}_B\right]\right\}^2$$

$$+3\left\{\frac{\partial \rho_a^{(k)}(t_i;\boldsymbol{\alpha}^0)}{\partial \rho_{a,C}^{(in)}}\right\}^2 \frac{\partial^2 \rho_a^{(k)}(t_i;\boldsymbol{\alpha}^0)}{\partial\left[\rho_{a,C}^{(in)}\right]^2}\left\{\mathrm{var}\left[\rho_{a,C}^{(in)}\right]\right\}^2$$

$$+3\left\{\frac{\partial \rho_a^{(k)}(t_i;\boldsymbol{\alpha}^0)}{\partial \dot{m}_C^{(in)}}\right\}^2 \frac{\partial^2 \rho_a^{(k)}(t_i;\boldsymbol{\alpha}^0)}{\partial\left[\dot{m}_C\right]^2}\left\{\mathrm{var}\left[\dot{m}_C\right]\right\}^2, \;\; for \;\; t_B \le t_i < t_C; \quad \text{(7.57)}$$

$$Z(k;t_i) \triangleq 3 \left\{ \frac{\partial \rho_a^{(k)}(t_i;\boldsymbol{\alpha}^0)}{\partial \rho_{a,A}^{(in)}} \right\}^2 \frac{\partial^2 \rho_a^{(k)}(t_i;\boldsymbol{\alpha}^0)}{\partial \left[\rho_{a,A}^{(in)}\right]^2} \left\{ \text{var}\left[\rho_{a,A}^{(in)}\right] \right\}^2$$

$$+ 3 \left\{ \frac{\partial \rho_a^{(k)}(t_i;\boldsymbol{\alpha}^0)}{\partial \dot{m}_A^{(in)}} \right\}^2 \frac{\partial^2 \rho_a^{(k)}(t_i;\boldsymbol{\alpha}^0)}{\partial \left[\dot{m}_A\right]^2} \left\{ \text{var}\left[\dot{m}_A\right] \right\}^2$$

$$+ 3 \left\{ \frac{\partial \rho_a^{(k)}(t_i;\boldsymbol{\alpha}^0)}{\partial \rho_{a,B}^{(in)}} \right\}^2 \frac{\partial^2 \rho_a^{(k)}(t_i;\boldsymbol{\alpha}^0)}{\partial \left[\rho_{a,B}^{(in)}\right]^2} \left\{ \text{var}\left[\rho_{a,B}^{(in)}\right] \right\}^2$$

$$+ 3 \left\{ \frac{\partial \rho_a^{(k)}(t_i;\boldsymbol{\alpha}^0)}{\partial \dot{m}_B^{(in)}} \right\}^2 \frac{\partial^2 \rho_a^{(k)}(t_i;\boldsymbol{\alpha}^0)}{\partial \left[\dot{m}_B\right]^2} \left\{ \text{var}\left[\dot{m}_B\right] \right\}^2$$

$$+ 3 \left\{ \frac{\partial \rho_a^{(k)}(t_i;\boldsymbol{\alpha}^0)}{\partial \rho_{a,C}^{(in)}} \right\}^2 \frac{\partial^2 \rho_a^{(k)}(t_i;\boldsymbol{\alpha}^0)}{\partial \left[\rho_{a,C}^{(in)}\right]^2} \left\{ \text{var}\left[\rho_{a,C}^{(in)}\right] \right\}^2$$

$$+ 3 \left\{ \frac{\partial \rho_a^{(k)}(t_i;\boldsymbol{\alpha}^0)}{\partial \dot{m}_C^{(in)}} \right\}^2 \frac{\partial^2 \rho_a^{(k)}(t_i;\boldsymbol{\alpha}^0)}{\partial \left[\dot{m}_C\right]^2} \left\{ \text{var}\left[\dot{m}_C\right] \right\}^2$$

$$+ 3 \left\{ \frac{\partial \rho_a^{(k)}(t_i;\boldsymbol{\alpha}^0)}{\partial \rho_{a,D}^{(in)}} \right\}^2 \frac{\partial^2 \rho_a^{(k)}(t_i;\boldsymbol{\alpha}^0)}{\partial \left[\rho_{a,D}^{(in)}\right]^2} \left\{ \text{var}\left[\rho_{a,D}^{(in)}\right] \right\}^2 \tag{7.58}$$

$$+ 3 \left\{ \frac{\partial \rho_a^{(k)}(t_i;\boldsymbol{\alpha}^0)}{\partial \dot{m}_D^{(in)}} \right\}^2 \frac{\partial^2 \rho_a^{(k)}(t_i;\boldsymbol{\alpha}^0)}{\partial \left[\dot{m}_D\right]^2} \left\{ \text{var}\left[\dot{m}_D\right] \right\}^2, \; for \;\; t_C \leq t_i < t_D;$$

(iv)   The skewness, $\gamma_1 \left[\rho_a^{(k)}(t_i;\boldsymbol{\alpha}^0) \right]$, of $\rho_a^{(k)}(t_i;\boldsymbol{\alpha}^0)$:

$$\gamma_1 \left[\rho_a^{(k)}(t_i;\boldsymbol{\alpha}^0) \right] \triangleq \mu_3 \left[\rho_a^{(k)}(t_i;\boldsymbol{\alpha}^0) \right] \Big/ \left\{ \text{Var}\left[\rho_a^{(k)}(t_i;\boldsymbol{\alpha}^0) \right] \right\}^{3/2}, \quad k=1,...,8; \; i=1,...,635.$$

$$\tag{7.59}$$

Recall that the 1ˢᵗ-order contributions comprised in the quantity $\text{Var}_1 \left[\rho_a^{(1)}(t_i;\boldsymbol{\alpha}^0) \right]$ were already computed in Figure 5.8; similarly, the quantities $\text{Var}_1 \left[\rho_a^{(4)}(t_i;\boldsymbol{\alpha}^0) \right]$ and $\text{Var}_1 \left[\rho_a^{(7)}(t_i;\boldsymbol{\alpha}^0) \right]$ were computed in Figure 5.13 and Figure 5.16, respectively, using the 1ˢᵗ-order sensitivities that were computed exactly using the *ASAM*.

Since only a relatively few number of non-mixed 2nd-order response sensitivities are needed to compute the respective terms in the above expressions, it is not efficient to apply the new 2nd-order adjoint method developed in Section 7.1 to the full dissolver model. Rather, it is more expedient to compute the respective non-mixed 2nd-order response sensitivities by using forward computations in conjunction with finite difference formulas, at every time step t_i, $i = 1,...,635$, of the type shown below:

$$
\frac{\partial^2 \rho_a^{(k)}\left(t_i;\boldsymbol{\alpha}^0\right)}{\partial\left[\rho_a^{(in)}\left(t_i\right)\right]^2} \cong \frac{1}{\left[\Delta\rho_a^{(in)}\left(t_i\right)\right]^2}\left\{\rho_a^{(k)}\left[t_i;\rho_a^{(in)}\left(t_i\right)+\Delta\rho_a^{(in)}\left(t_i\right)\right]\right.
$$
$$
\left. -2\rho_a^{(k)}\left[t_i;\rho_a^{(in)}\left(t_i\right)\right]+\rho_a^{(k)}\left[t_i;\rho_a^{(in)}\left(t_i\right)-\Delta\rho_a^{(in)}\left(t_i\right)\right]\right\}, \quad k=1,...,8. \tag{7.60}
$$

The above formula is exact for a quadratic test function of the form $\rho_{a,test}^{(k)}\left(t\right) = f_2\left(t\right)\left[\rho_a^{(in)}\left(t\right)\right]^2 + f_1\left(t\right)\rho_a^{(in)}\left(t\right) + f_0\left(t\right)$. The other 2nd-order derivatives appearing in the expressions of $E\left[\rho_a^{(k)}\left(t_i;\boldsymbol{\alpha}^0\right)\right]$, $\mathrm{Var}\left[\rho_a^{(k)}\left(t_i;\boldsymbol{\alpha}^0\right)\right]$, and $\mu_3\left[\rho_a^{(k)}\left(t_i;\boldsymbol{\alpha}^0\right)\right]$ can be computed by using forward computations in conjunction with finite-difference formulas similar to the one provided in Eq. (7.64). As illustrative examples, the relative and absolute 2nd-order sensitivities of the time-dependent acid concentrations $\rho_a^{(1)}\left(t_i;\boldsymbol{\alpha}^0\right)$ in compartment #1 (furthest from the inlet) and, respectively, $\rho_a^{(7)}\left(t_i;\boldsymbol{\alpha}^0\right)$ in compartment #7 (closest to the inlet) are depicted in Figures 7.1 through 7.12, below. These figures indicate that the relative 2nd-order sensitivities are much smaller than the corresponding 1st-order ones; the largest are the relative 2nd-order sensitivity of $\rho_a^{(1)}\left(t_i;\boldsymbol{\alpha}^0\right)$ with respect to the model parameters $\dot{m}_A^{(in)}$, V_0 and b, at early times into the transient, as well as to the model parameter $\dot{m}_D^{(in)}$, towards the end of the transient. The other general trend is that the 2nd-order sensitivities of the acid concentration in compartment #1 (furthest from the inlet) are all larger than the corresponding 2nd-order sensitivities of the acid concentration in compartment #7 (closest to the inlet).
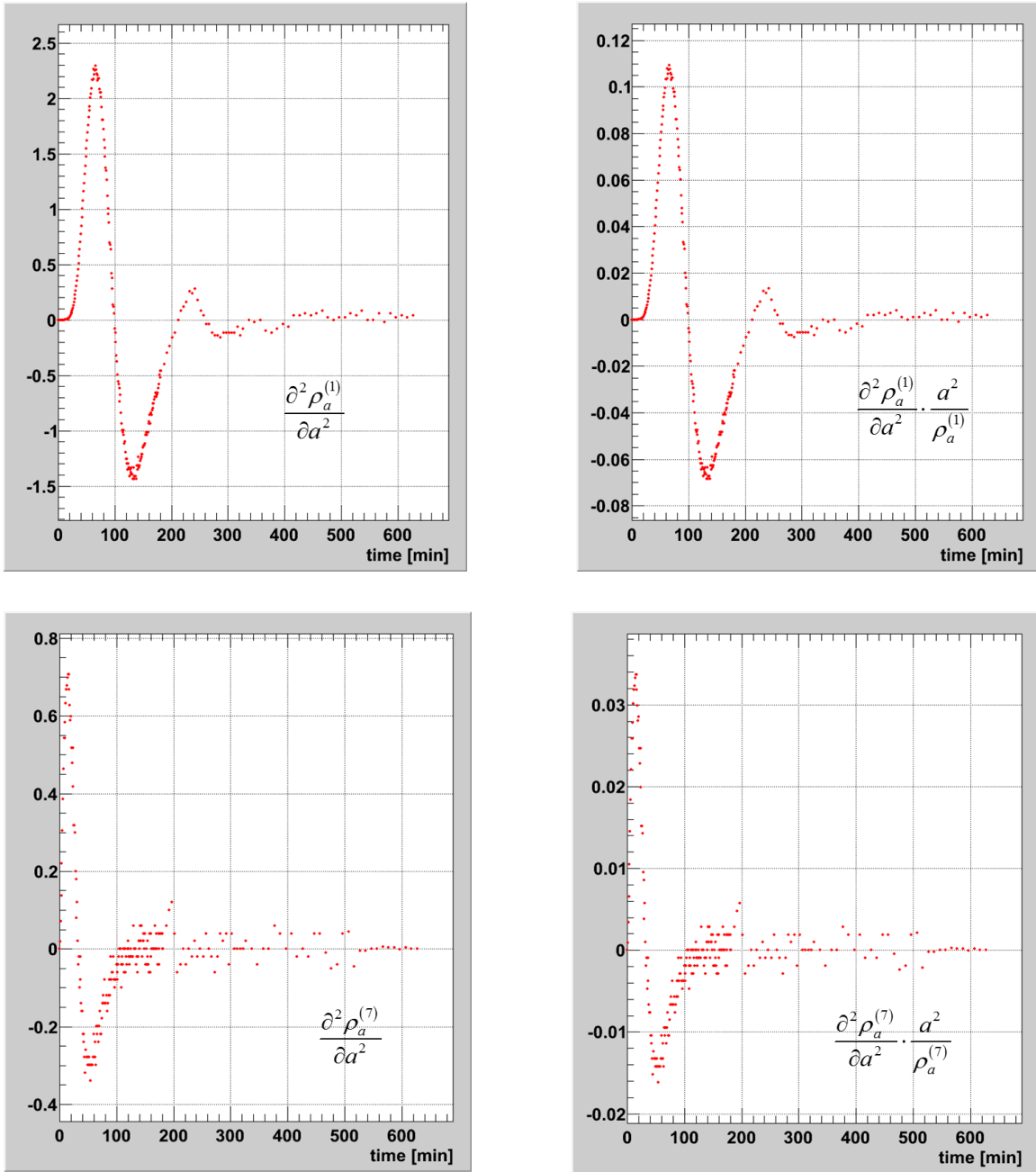
Figure 7.1 Absolute and relative 2$^{\text{nd}}$-order sensitivities of $\rho_a^{(1)}\left(t_i;\boldsymbol{\alpha}^0\right)$ and $\rho_a^{(7)}\left(t_i;\boldsymbol{\alpha}^0\right)$ with respect to a, for t_i, $i=1,...,635$

181
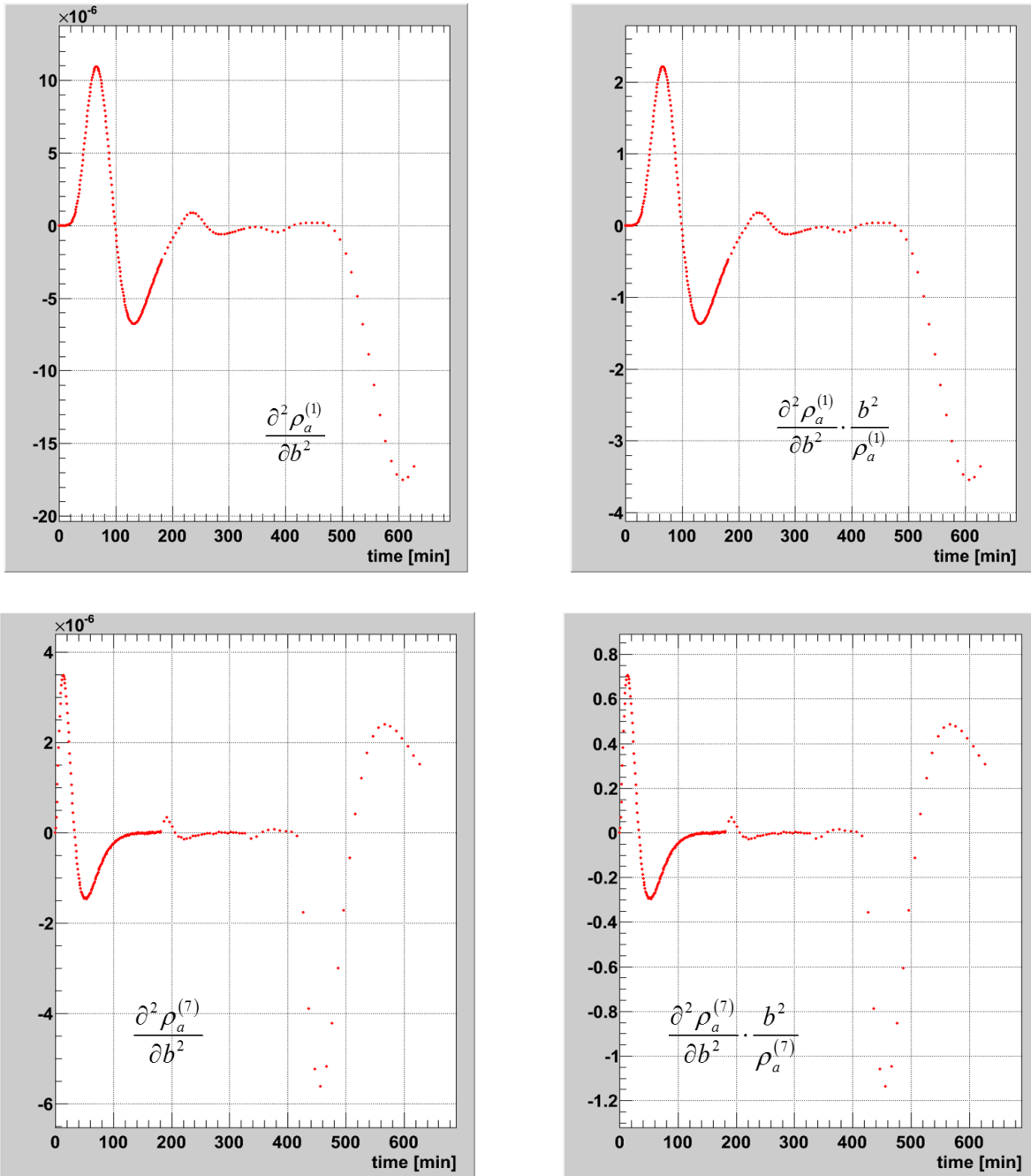
Figure 7.2 Absolute and relative 2$^{\text{nd}}$-order sensitivities of $\rho_a^{(1)}\left(t_i; \boldsymbol{\alpha}^0\right)$ and $\rho_a^{(7)}\left(t_i; \boldsymbol{\alpha}^0\right)$ with respect to b, for t_i, $i = 1, ..., 635$
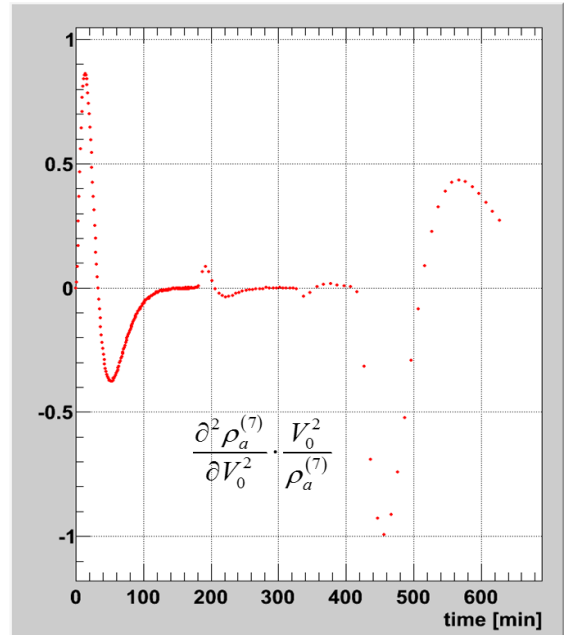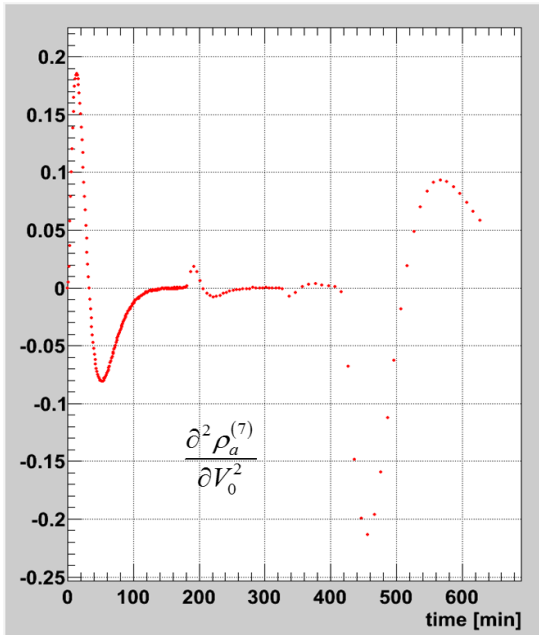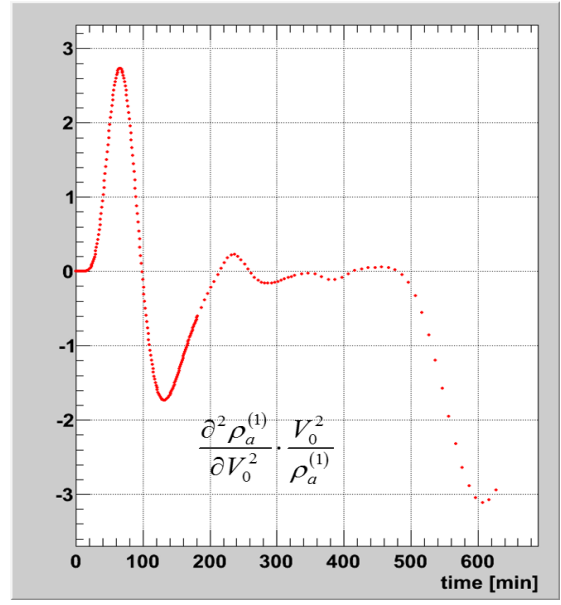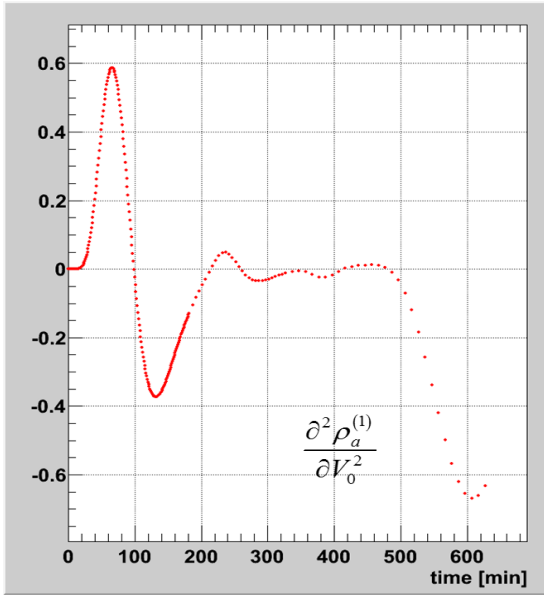
Figure 7.3 Absolute and relative 2nd-order sensitivities of $\rho_a^{(1)}\left(t_i; \boldsymbol{\alpha}^0\right)$ and $\rho_a^{(7)}\left(t_i; \boldsymbol{\alpha}^0\right)$ with respect to V_0, for t_i, $i = 1, ..., 635$
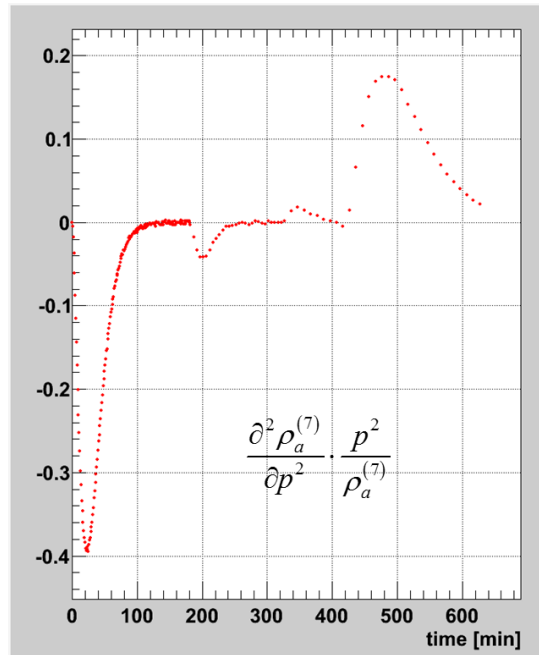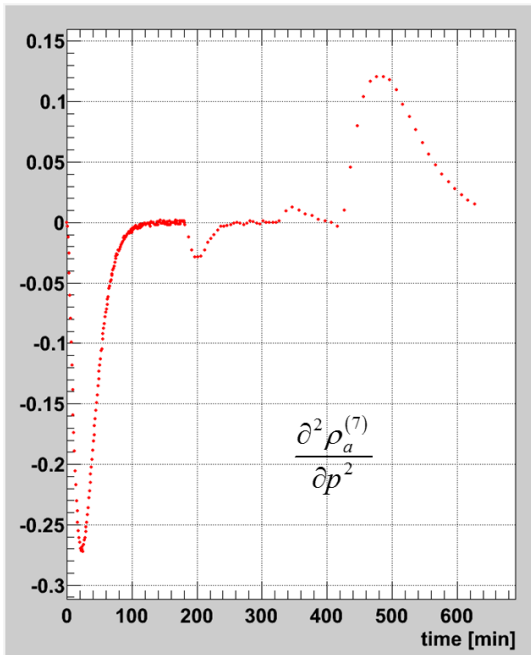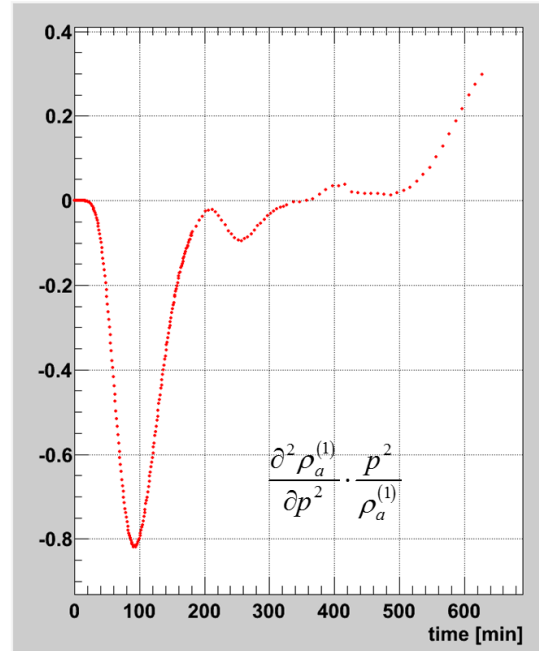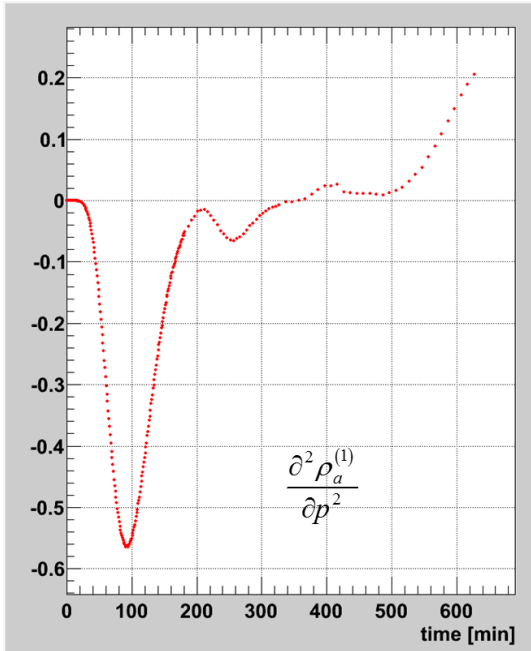
Figure 7.4 Absolute and relative 2nd-order sensitivities of $\rho_a^{(1)}\left(t_i;\boldsymbol{\alpha}^0\right)$ and $\rho_a^{(7)}\left(t_i;\boldsymbol{\alpha}^0\right)$ with respect to p, for t_i, $i=1,...,635$
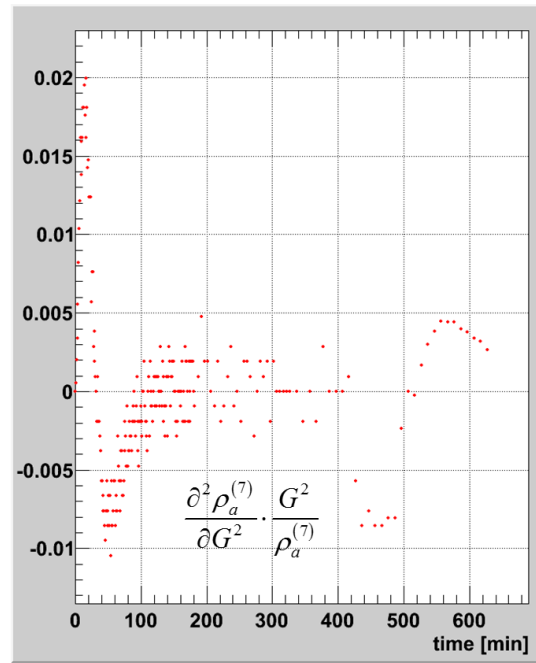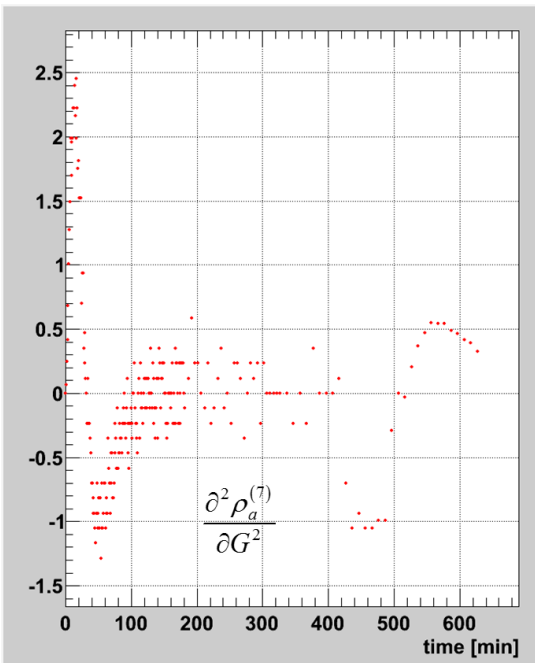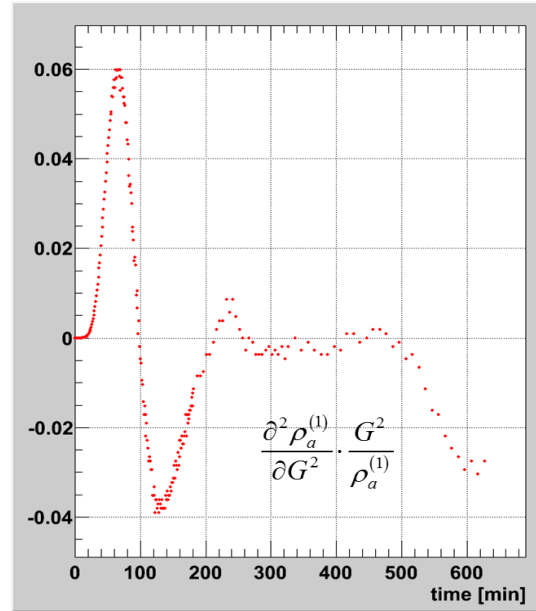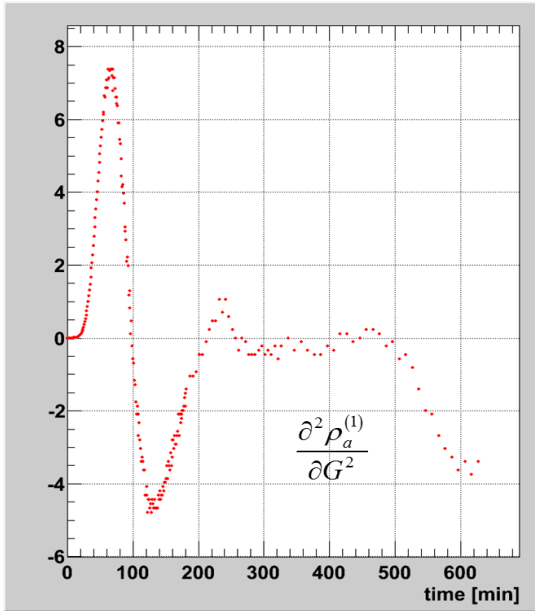
Figure 7.5 Absolute and relative 2$^{\text{nd}}$-order sensitivities of $\rho_a^{(1)}\left(t_i; \boldsymbol{\alpha}^0\right)$ and $\rho_a^{(7)}\left(t_i; \boldsymbol{\alpha}^0\right)$ with respect to G, for t_i, $i=1,...,635$
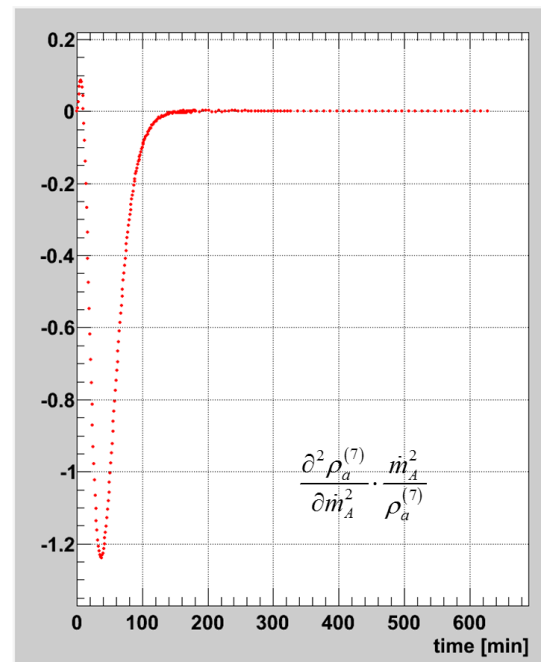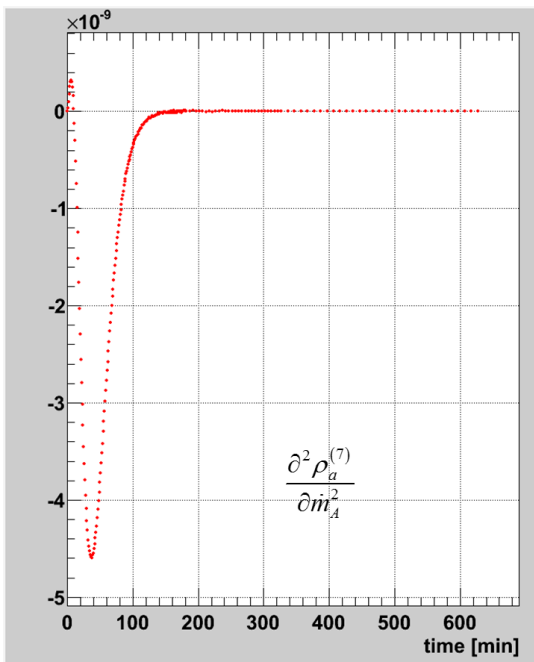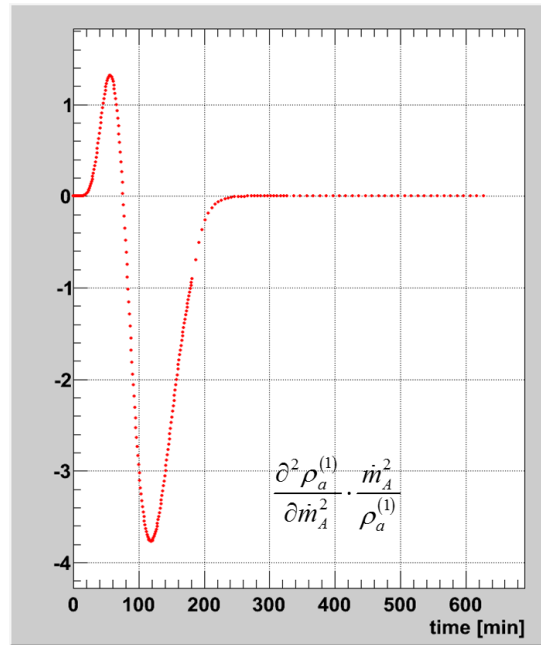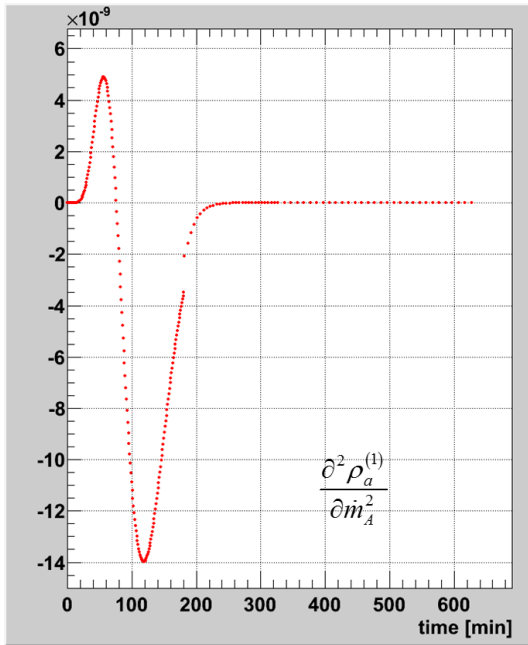
Figure 7.6 Absolute and relative 2nd-order sensitivities of $\rho_a^{(1)}\left(t_i;\boldsymbol{\alpha}^0\right)$ and $\rho_a^{(7)}\left(t_i;\boldsymbol{\alpha}^0\right)$ with respect to $\dot{m}_A$, for t_i, $i=1,...,635$
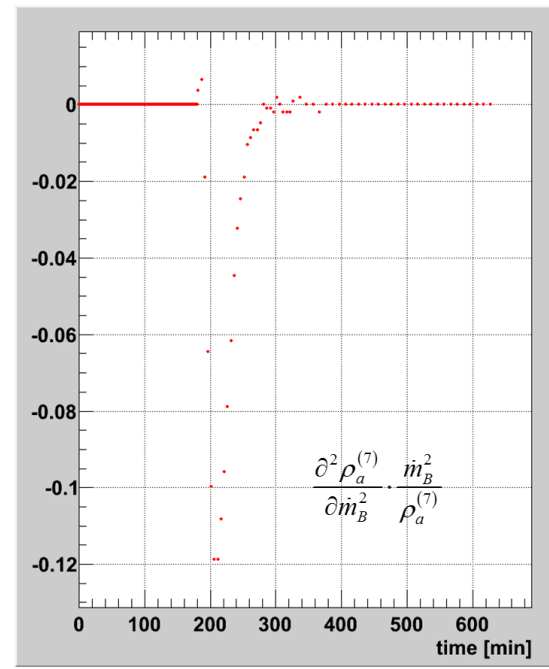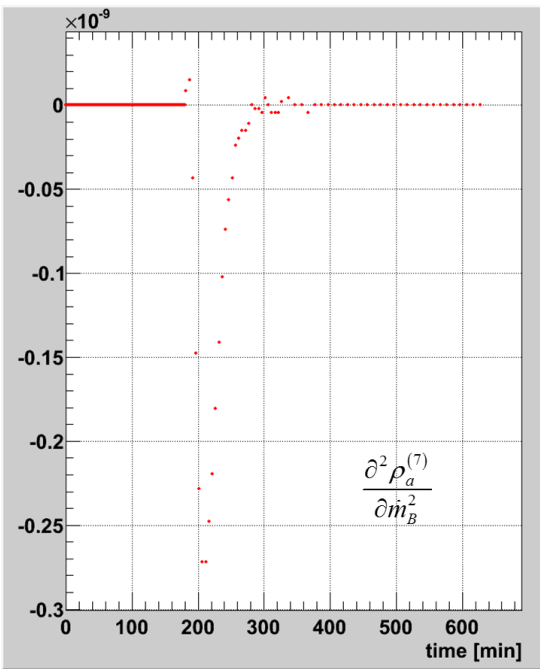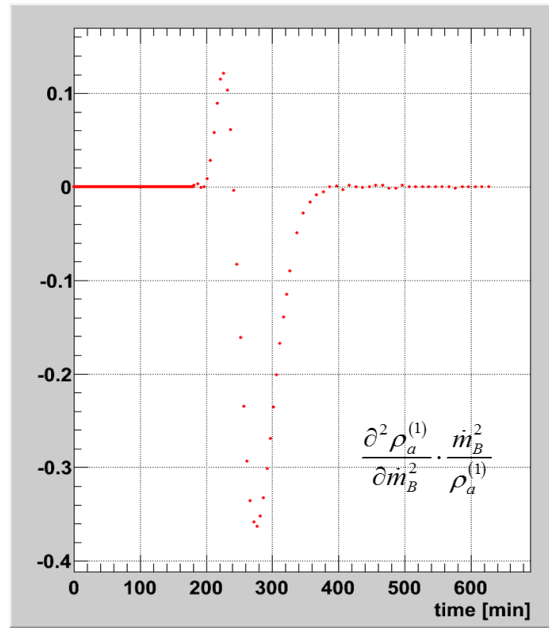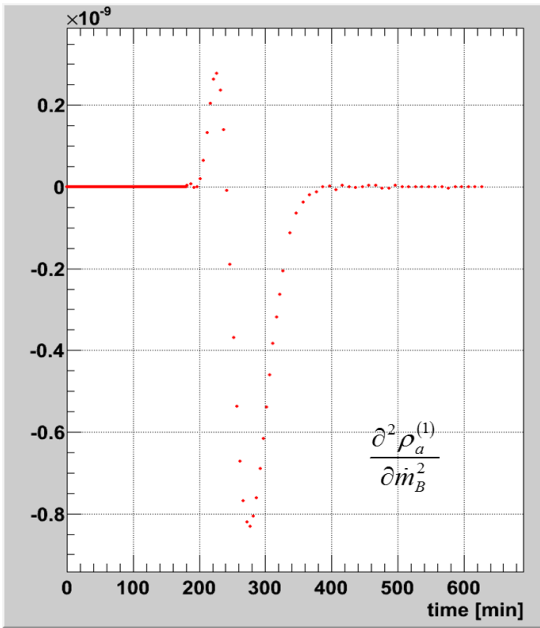
Figure 7.7 Absolute and relative 2nd-order sensitivities $\dot{m}_B^{(in)}$ and, respectively, for $\dot{m}_B$ t_i, $i = 1, ..., 635$.

187
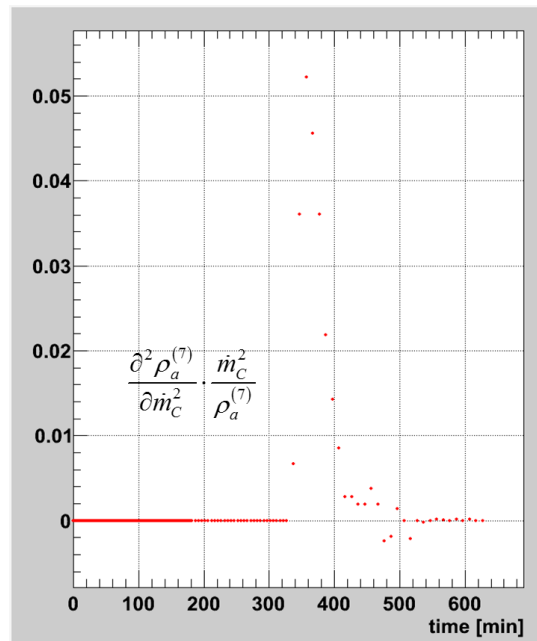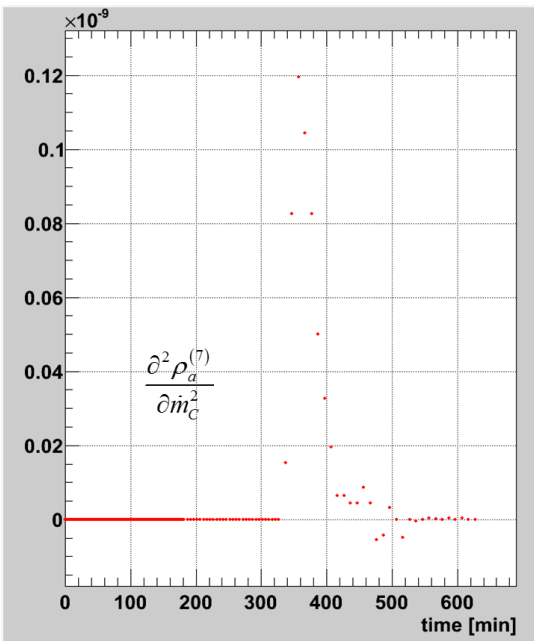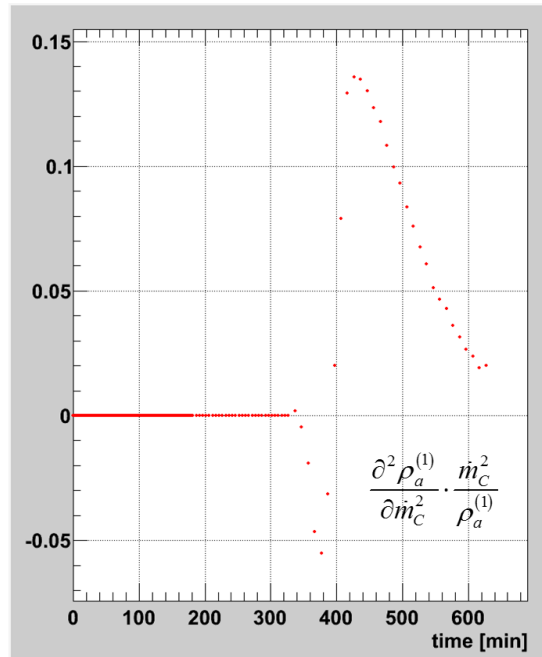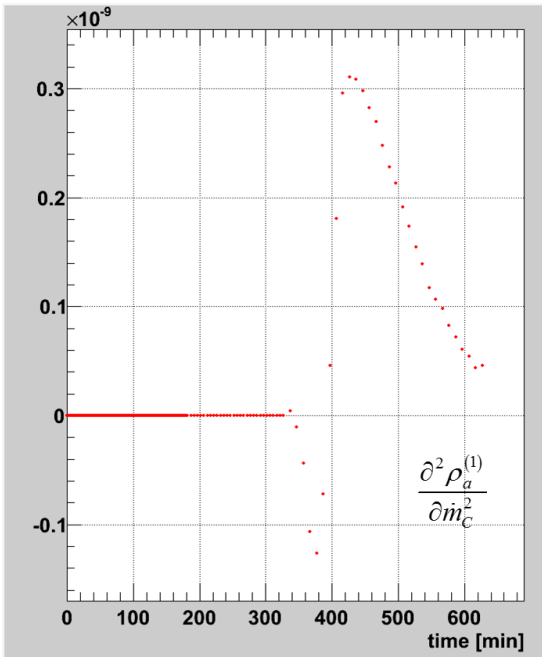
Figure 7.8 Absolute and relative 2$^{\text{nd}}$-order sensitivities of $\rho_a^{(1)}\left(t_i;\boldsymbol{\alpha}^0\right)$ and $\rho_a^{(7)}\left(t_i;\boldsymbol{\alpha}^0\right)$ with respect to $\dot{m}_C$, for t_i, $i=1,...,635$

188
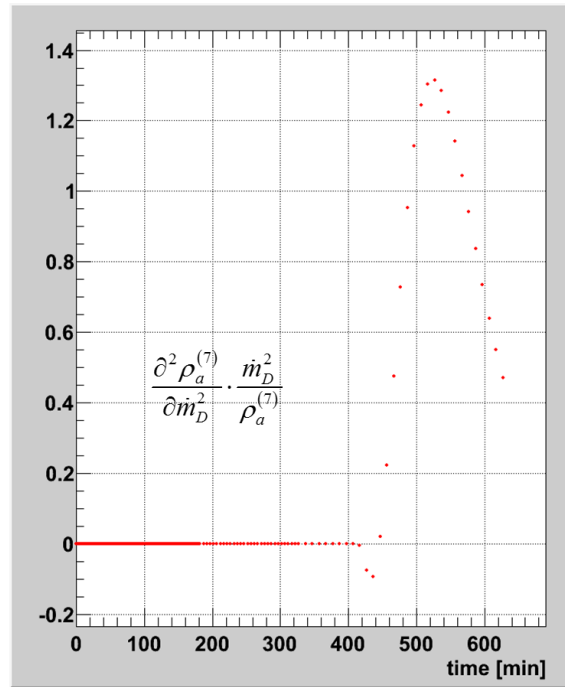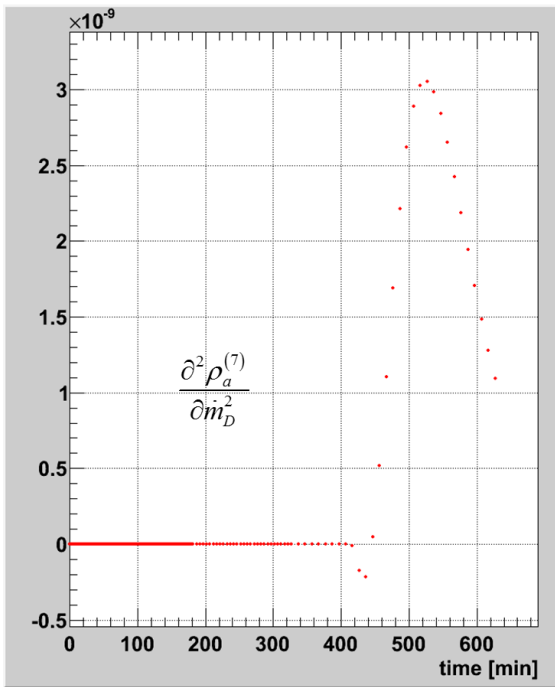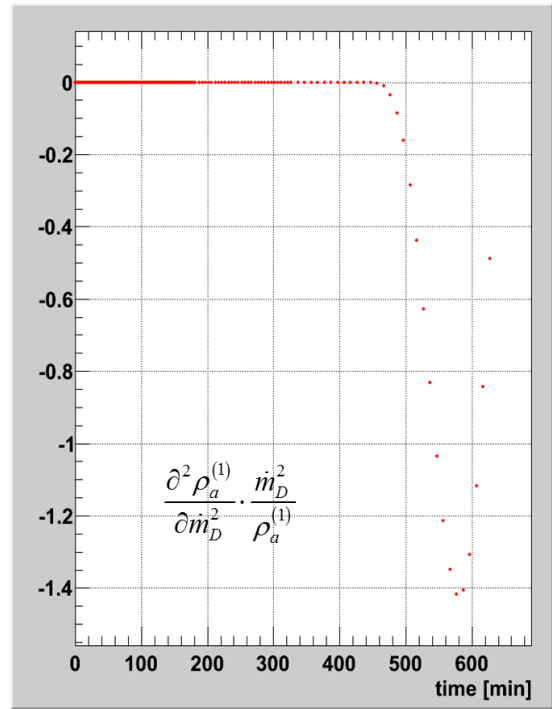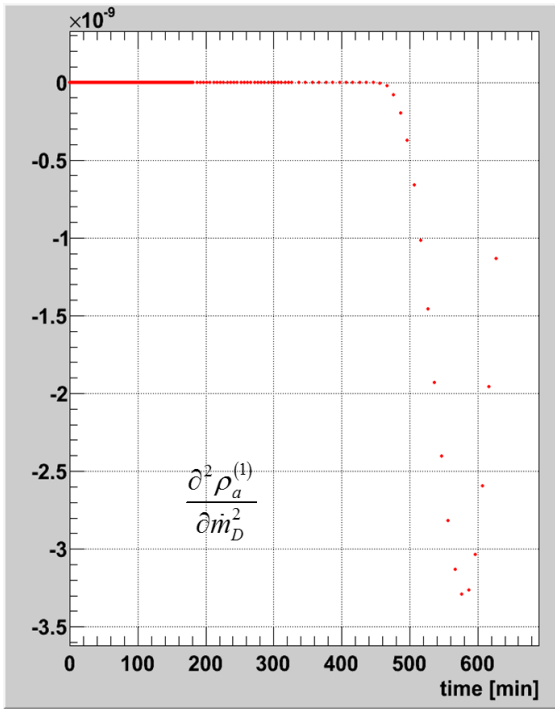
Figure 7.9 Absolute and relative 2nd-order sensitivities of $\rho_a^{(1)}\left(t_i;\boldsymbol{\alpha}^0\right)$ and $\rho_a^{(7)}\left(t_i;\boldsymbol{\alpha}^0\right)$ with respect to $\dot{m}_D$, for t_i, $i=1,...,635$
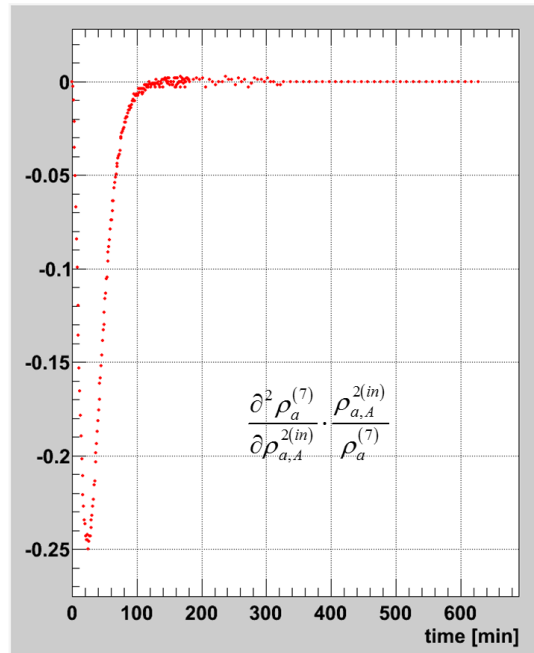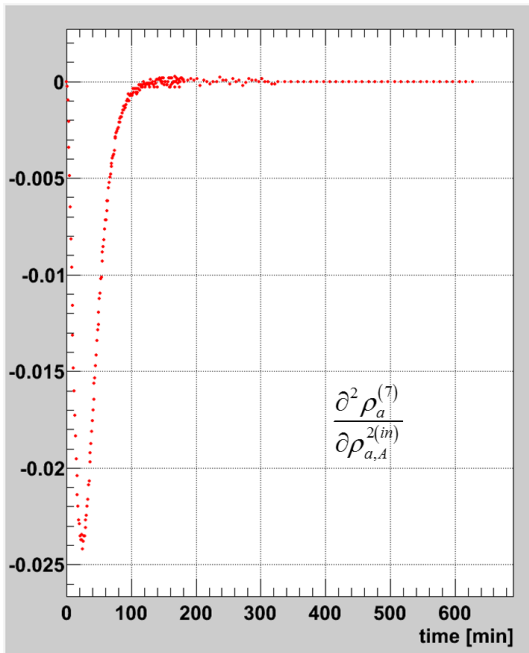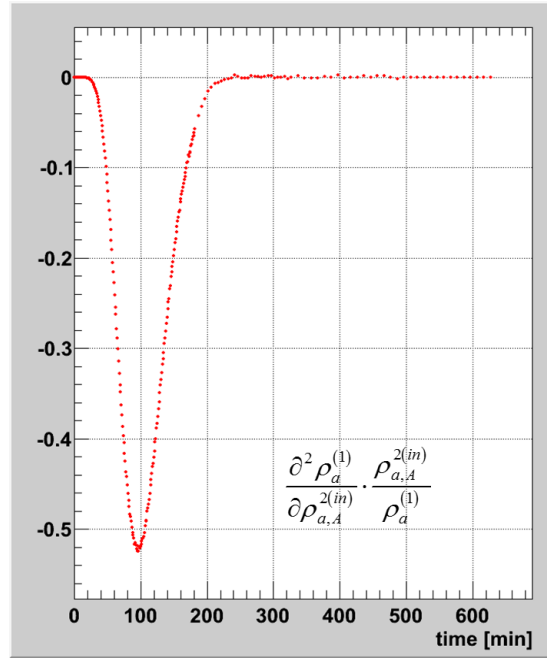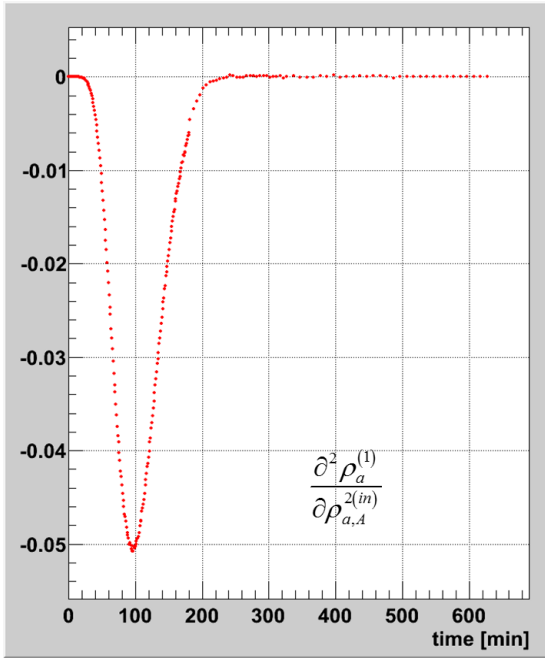
Figure 7.10 Absolute and relative 2nd-order sensitivities of $\rho_a^{(1)}\left(t_i;\boldsymbol{\alpha}^0\right)$ and $\rho_a^{(7)}\left(t_i;\boldsymbol{\alpha}^0\right)$ with respect to $\rho_{a,A}^{(in)}$, for t_i, $i=1,...,635$.

190
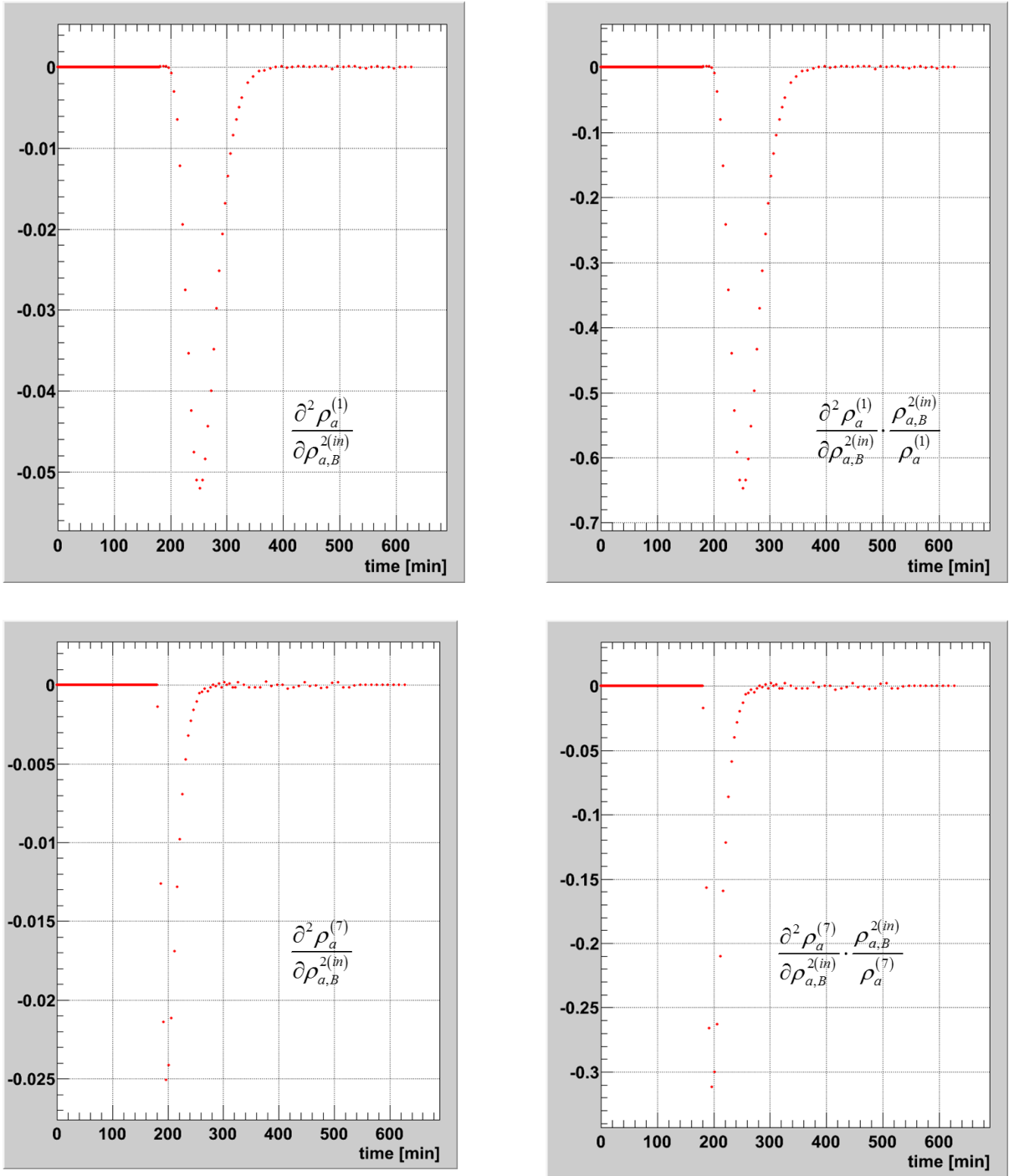
Figure 7.11 Absolute and relative 2$^{\text{nd}}$-order sensitivities of $\rho_a^{(1)}\left(t_i;\boldsymbol{\alpha}^0\right)$ and $\rho_a^{(7)}\left(t_i;\boldsymbol{\alpha}^0\right)$ with respect to $\rho_{a,B}^{(in)}$, for t_i, $i=1,...,635$.
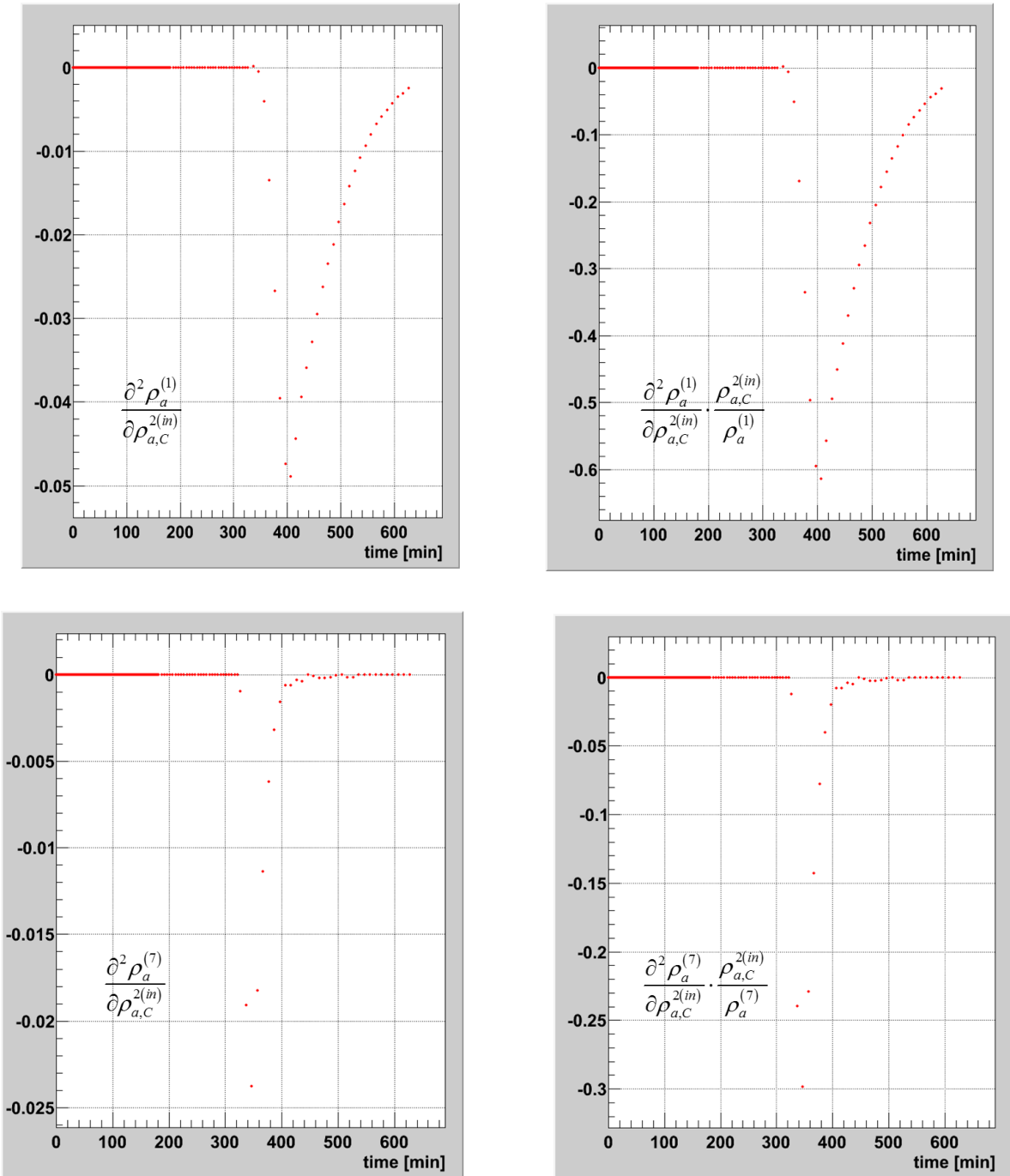
Figure 7.12 Absolute and relative 2nd-order sensitivities of $\rho_a^{(1)}\left(t_i; \boldsymbol{\alpha}^0\right)$ and $\rho_a^{(7)}\left(t_i; \boldsymbol{\alpha}^0\right)$ with respect to $\rho_{a,C}^{(in)}$, for t_i, $i=1,...,635$.

The effects of the 2nd-order sensitivities on the expectation values, $E\left[\rho_a^{(1)}\left(t_i;\boldsymbol{\alpha}^0\right)\right]$, of the acid concentration responses in the dissolver's compartments have been computed using Eq. (7.41) and were found to be very small as depicted by Figure 7.13. The largest effects are on the expected value of the acid concentration in compartment #1.
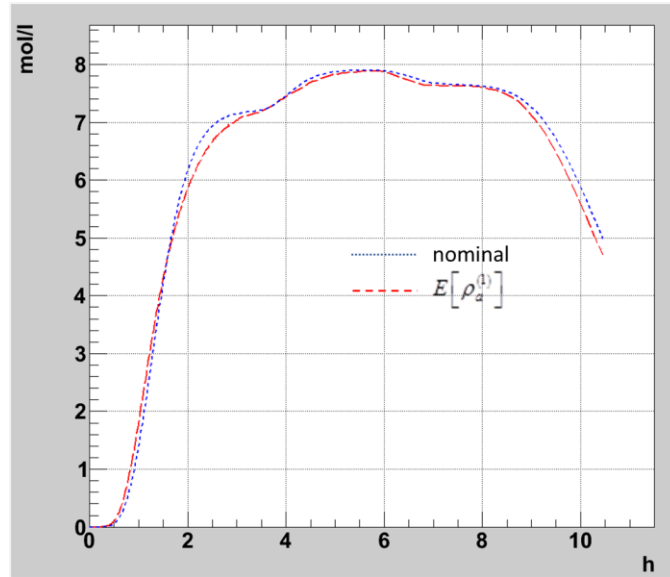
Figure 7.13 Comparison of the nominal values $\rho_a^{(1)}\left(t_i;\boldsymbol{\alpha}^0\right)$ and $E\left[\rho_a^{(1)}\left(t_i;\boldsymbol{\alpha}^0\right)\right]$ for $t_i,\ i=1,...,635$

The effects of the 2nd-order sensitivities on the variance, $\mathrm{Var}\left[\rho_a^{(k)}\left(t_i;\boldsymbol{\alpha}^0\right)\right]$, of the acid concentration responses in the dissolver's compartments $\rho_a^{(k)}\left(t_i;\boldsymbol{\alpha}^0\right)$ computed from Eq. (7.47) were minimal. Figure 7.14 illustrates these effects by depicting the contributions of the 2nd-order sensitivities, contained in the quantity $\mathrm{Var}_2\left[\rho_a^{(1)}\left(t_i;\boldsymbol{\alpha}^0\right)\right]$, to the variance of the acid concentration, $\rho_a^{(1)}\left(t_i;\boldsymbol{\alpha}^0\right)$, in compartment #1. This figure also depicts the minute influence of the 2nd-order sensitivities on the standard deviation of the acid concentration, $\rho_a^{(1)}\left(t_i;\boldsymbol{\alpha}^0\right)$, in compartment #1.
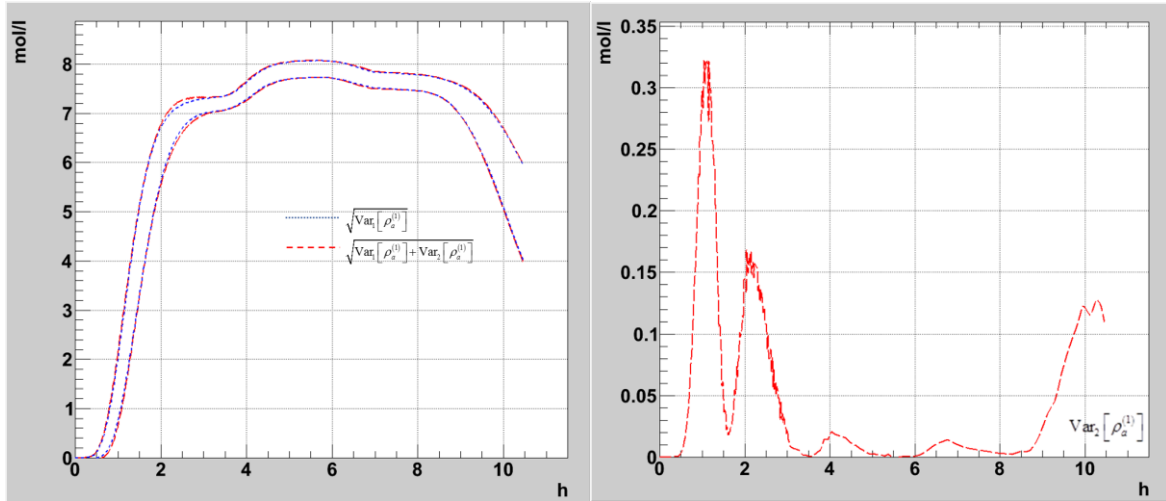
Figure 7.14 **Left:** Comparison of the standard deviation of $\rho_a^{(1)}\left(t_i;\boldsymbol{\alpha}^0\right)$ computed with 1st-order sensitivities vs. both 1st- and 2nd-order sensitivities, for t_i, $i=1,...,635$ **Right:** Time-dependent variation of $\text{Var}_2\left[\rho_a^{(1)}\left(t_i;\boldsymbol{\alpha}^0\right)\right]$, cf. Eq. (7.47), for t_i, $i=1,...,635$.

The individual contributions of the 2nd-order sensitivities to the most important model parameters and the *skewness* of the acid concentration responses $\rho_a^{(1)}\left(t_i;\boldsymbol{\alpha}^0\right)$ and $\rho_a^{(7)}\left(t_i;\boldsymbol{\alpha}^0\right)$ in compartments #1 and #7, furthest and closest to the inlet, respectively are depicted Figures 7.15 – 7.18. Recall, all parameters are assumed to be uncorrelated and normally distributed. Figures 7.15 and 7.16 depict notably large negative values for skewness in the distributions that occur in the middle of the transient for $\rho_a^{(1)}\left(t_i;\boldsymbol{\alpha}^0\right)$ and $\rho_a^{(7)}\left(t_i;\boldsymbol{\alpha}^0\right)$, induced by the parameters $\rho_{a,B}^{(in)}$ and $\rho_{a,C}^{(in)}$, respectively. These highly negative values would imply that the distributions of the responses $\rho_a^{(1)}\left(t_i;\boldsymbol{\alpha}^0\right)$ and $\rho_a^{(7)}\left(t_i;\boldsymbol{\alpha}^0\right)$ become heavily skewed toward smaller values than what would be calculated for the expected values. This behavior continues and increases by a factor of about 5 for the distribution of $\rho_a^{(1)}\left(t_i;\boldsymbol{\alpha}^0\right)$ in the compartment furthest from the inlet which again would imply smaller values than expected values. The skewness in the response distributions caused by the 2nd-order sensitivities and variances due to the model parameter $\rho_{a,B}^{(in)}$ occurs earlier in time than the skewness caused by the parameter $\rho_{a,C}^{(in)}$ and "skews" the distribution for $\rho_a^{(7)}\left(t_i;\boldsymbol{\alpha}^0\right)$ earlier in time than the distribution of $\rho_a^{(1)}\left(t_i;\boldsymbol{\alpha}^0\right)$ furthest from the inlet.

194
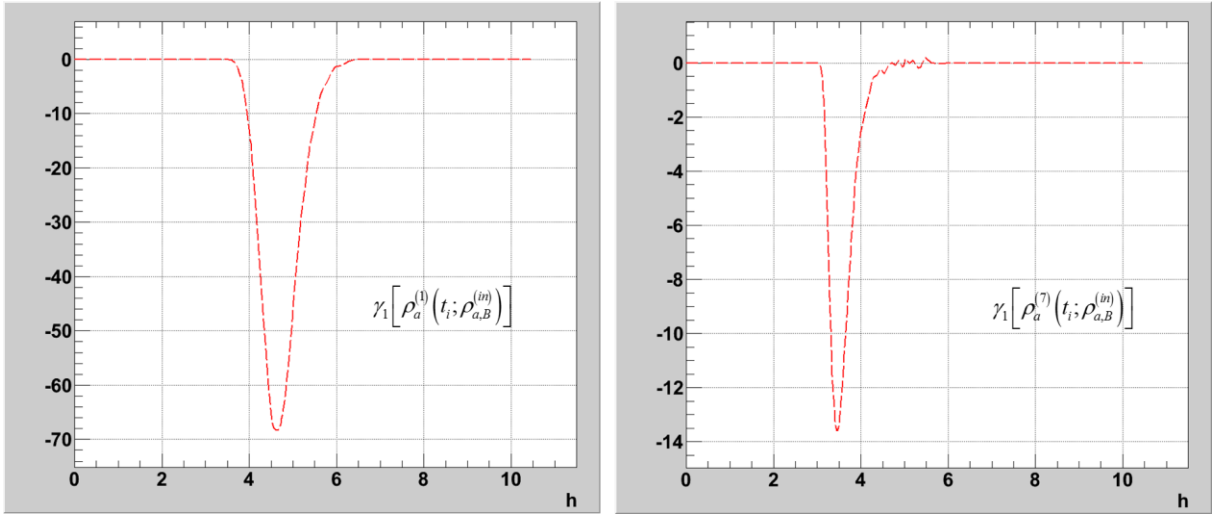
Figure 7.15 Skewness in the distribution of $\rho_a^{(1)}\left(t_i;\boldsymbol{\alpha}^0\right)$ (left) and, respectively, $\rho_a^{(7)}\left(t_i;\boldsymbol{\alpha}^0\right)$ (right) due to the uncertainties in the (assumed) normally-distributed model parameter $\rho_{a,B}^{(in)}$
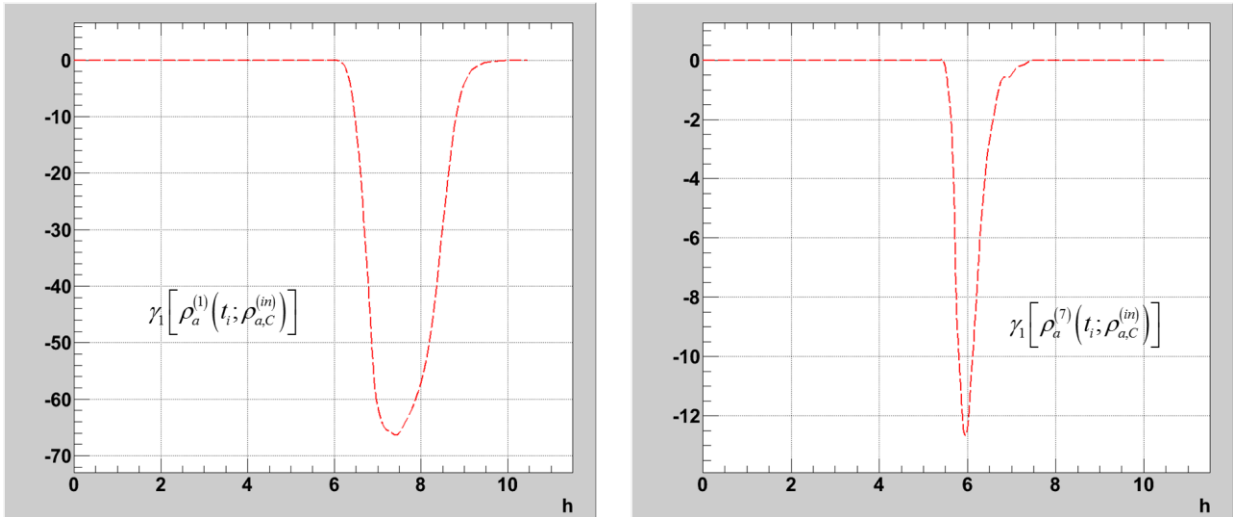
Figure 7.16 Skewness in the distribution of $\rho_a^{(1)}\left(t_i;\boldsymbol{\alpha}^0\right)$ (left) and, respectively, $\rho_a^{(7)}\left(t_i;\boldsymbol{\alpha}^0\right)$ (right) due to the uncertainties in the (assumed) normally-distributed model parameter $\rho_{a,C}^{(in)}$

Figure 7.17 depicts the skewness in the distributions of $\rho_a^{(1)}\left(t_i;\boldsymbol{\alpha}^0\right)$ and $\rho_a^{(7)}\left(t_i;\boldsymbol{\alpha}^0\right)$, respectively, induced by the parameter $\rho_{a,A}^{(in)}$. The respective skewness is also negative but occurs earlier in time and is less negative than the skewness induced by either $\rho_{a,B}^{(in)}$ or $\rho_{a,C}^{(in)}$. The skewness is first induced in the distribution of $\rho_a^{(7)}\left(t_i;\boldsymbol{\alpha}^0\right)$ by the parameters $\rho_{a,A}^{(in)}$, $\rho_{a,B}^{(in)}$

195

and $\rho_{a,C}^{(in)}$, sequentially in this order over time. The skewness in the distribution of $\rho_a^{(1)}\left(t_i;\boldsymbol{\alpha}^0\right)$ in induced in the same sequential order by the same parameters, albeit with a delay, and much stronger toward the inlet. Notably, the skewness induced by $\rho_{a,A}^{(in)}$ in the distribution of $\rho_a^{(7)}\left(t_i;\boldsymbol{\alpha}^0\right)$ is minimal suggesting uncertainties in $\rho_{a,A}^{(in)}$ affect the skewness of the acid distributions increasingly for compartments further from the inlet.
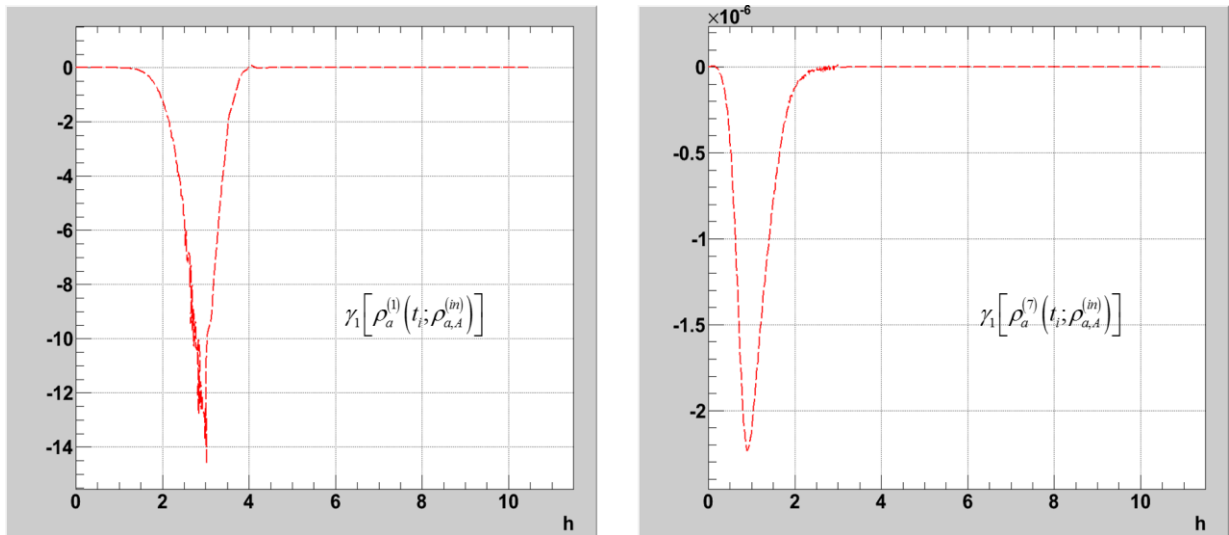
Figure 7.17 Skewness in the distribution of $\rho_a^{(1)}\left(t_i;\boldsymbol{\alpha}^0\right)$ (left) and, respectively, $\rho_a^{(7)}\left(t_i;\boldsymbol{\alpha}^0\right)$ (right) due the uncertainties in the (assumed) normally-distributed model parameter $\rho_{a,A}^{(in)}$

The skewness in the distribution of $\rho_a^{(1)}\left(t_i;\boldsymbol{\alpha}^0\right)$ is next in importance and stems from the uncertainties in the model parameter a, as depicted in Figure 7.18. Note the uncertainties in this parameter affects the skewness in the distribution of $\rho_a^{(1)}\left(t_i;\boldsymbol{\alpha}^0\right)$ positively starting around 3.5 hours then oscillates; from negative to zero from 4 to 8 hours, and then from positive to zero toward the latter part of the of the transient. Contrary to the behavior of the previous skewness in response distributions, the uncertainties in the model parameter a barely affect the skewness in the distribution of $\rho_a^{(7)}\left(t_i;\boldsymbol{\alpha}^0\right)$ and do it quite early. This skewness induced in the distribution of $\rho_a^{(7)}\left(t_i;\boldsymbol{\alpha}^0\right)$ is slightly positive, rather than negative which would imply larger than expected values for these time periods.
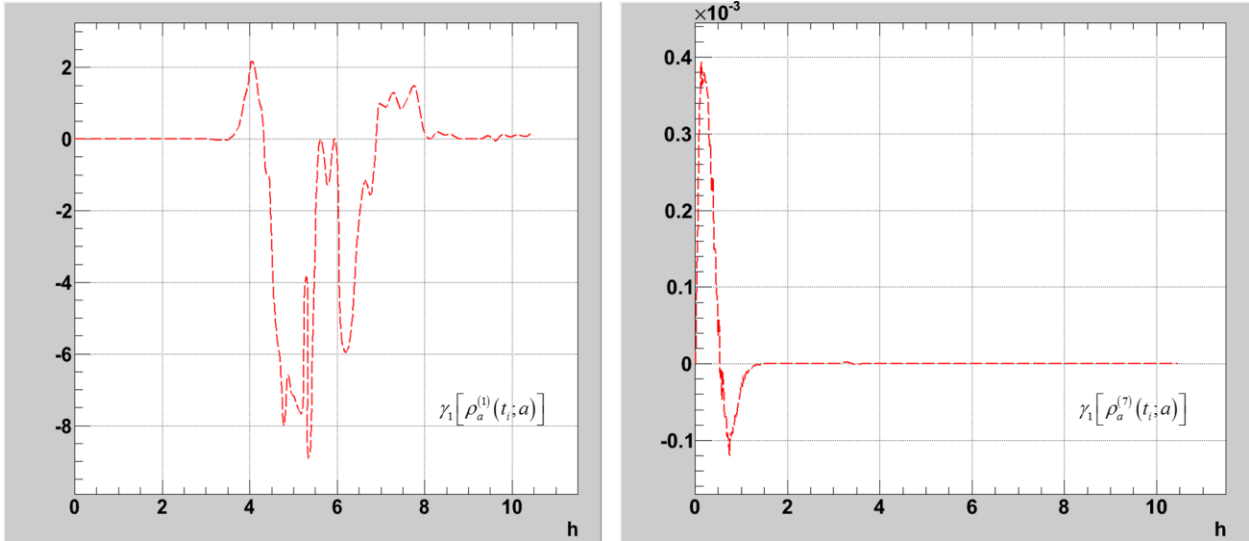
Figure 7.18 Skewness in the distribution of $\rho_a^{(1)}\left(t_i;\boldsymbol{\alpha}^0\right)$ (left) and, respectively, $\rho_a^{(7)}\left(t_i;\boldsymbol{\alpha}^0\right)$ (right) due to the uncertainties in the (assumed) normally-distributed model parameter a.

The uncertainties in the remaining model parameters barely affect the skewness in the distribution of $\rho_a^{(1)}\left(t_i;\boldsymbol{\alpha}^0\right)$ and do not practically affect the skewness in the distribution of $\rho_a^{(7)}\left(t_i;\boldsymbol{\alpha}^0\right)$ so Figures 7.19 – 7.22 are only included for $\rho_a^{(1)}\left(t_i;\boldsymbol{\alpha}^0\right)$. The skewness is impacted both positively and negatively in time, but again the impact is minor as shown with values close to zero throughout the transient. Zero-skewness means that the respective distribution is symmetric with respect to its mean and thus more or less Gaussian.
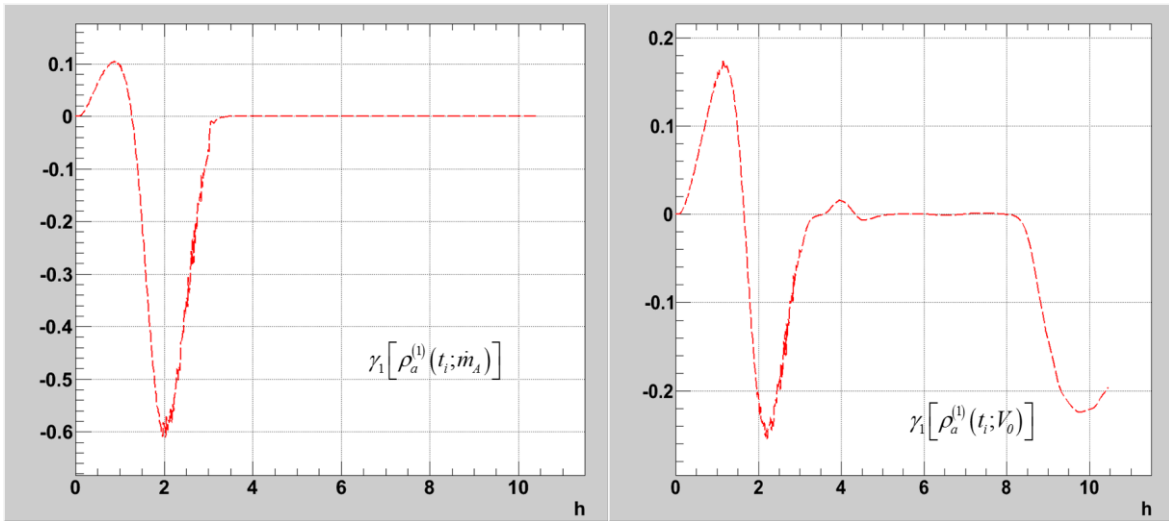
Figure 7.19 Skewness in the distribution of $\rho_a^{(1)}\left(t_i;\boldsymbol{\alpha}^0\right)$ due to the uncertainties in the (assumed) normally-distributed model parameters $\dot{m}_A$ and V_0.
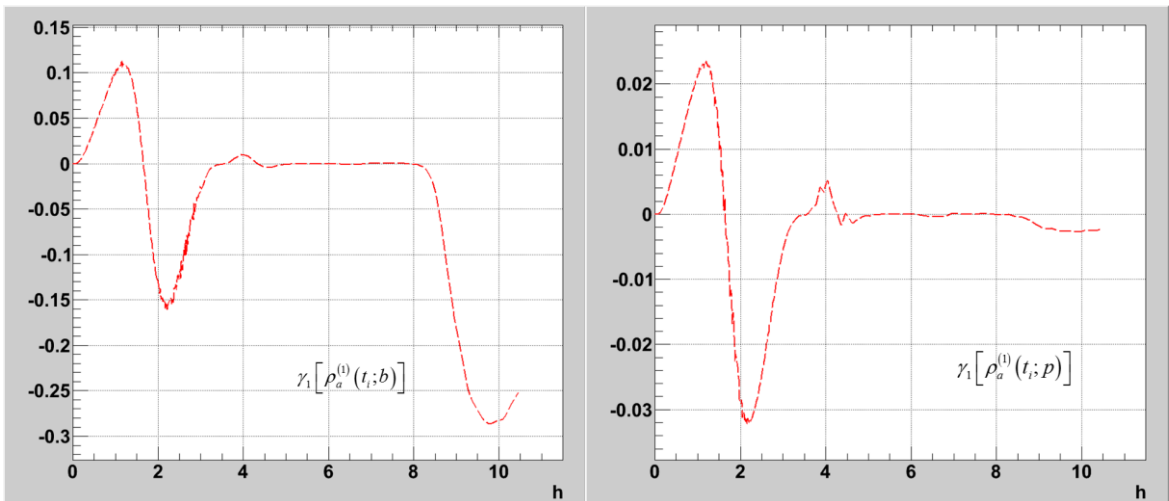
Figure 7.20 Skewness in the distribution of $\rho_a^{(1)}\left(t_i;\boldsymbol{\alpha}^0\right)$ due to the uncertainties in the (assumed) normally-distributed model parameters b and p.

198
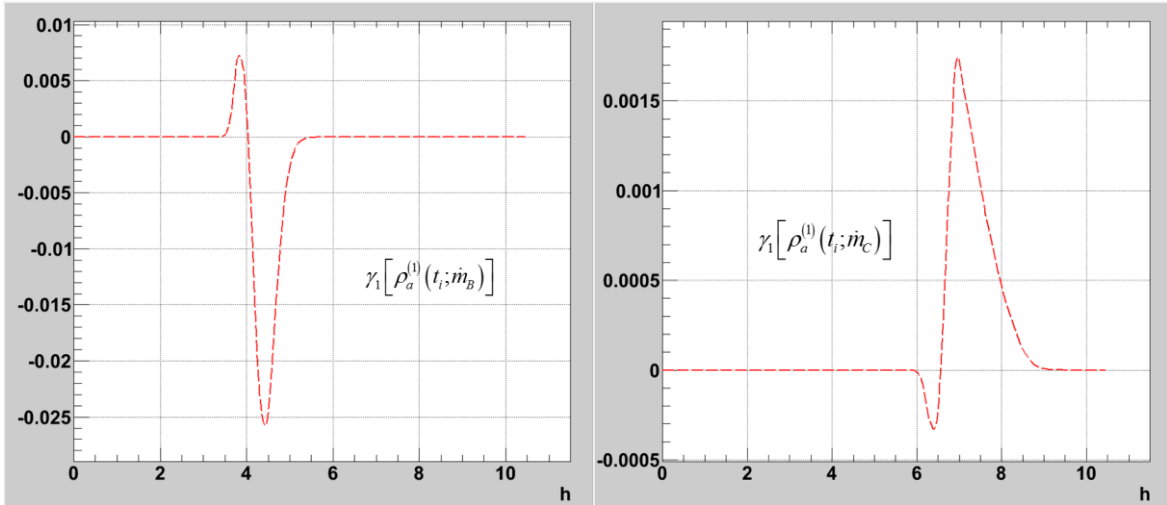
Figure 7.21 Skewness in the distribution of $\rho_a^{(1)}\left(t_i;\boldsymbol{\alpha}^0\right)$ due to the uncertainties in the (assumed) normally-distributed the model parameters $\dot{m}_B$ and $\dot{m}_C$.
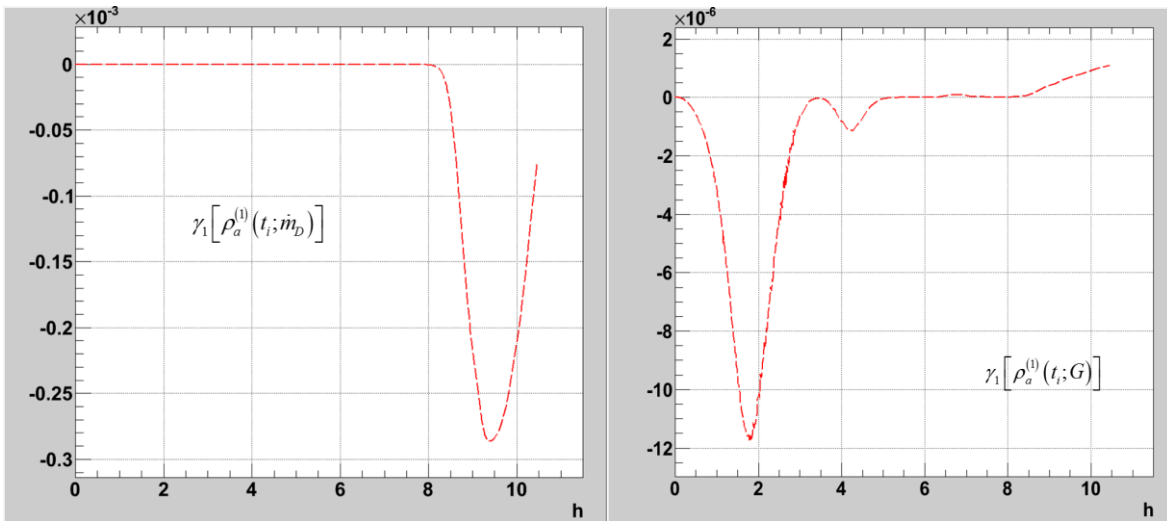
Figure 7.22 Skewness in the distribution of $\rho_a^{(1)}\left(t_i;\boldsymbol{\alpha}^0\right)$ due to the uncertainties in the (assumed) normally-distributed the model parameters $\dot{m}_D$ and G.

The cumulative impact of the uncertainties in the parameter distributions (assumed to be normal) on the skewness in the distributions of $\rho_a^{(1)}\left(t_i;\boldsymbol{\alpha}^0\right)$ and $\rho_a^{(7)}\left(t_i;\boldsymbol{\alpha}^0\right)$, respectively, are depicted in Figure 7.23. As the plot on the right-side in this figure indicates, the largest negative skewness in the distribution of $\rho_a^{(1)}\left(t_i;\boldsymbol{\alpha}^0\right)$ occurs at ca. 4.5 hours into the transient, and this negative skewness can be attributed overwhelmingly to the uncertainties stemming

from the parameter $\rho_{a,B}^{(in)}$ (see Figure 7.15) and, much less, to the uncertainties stemming from the model parameter a (see Figure 7.18). The second-largest negative skewness in the distribution of $\rho_a^{(1)}\left(t_i;\boldsymbol{\alpha}^0\right)$ occurs at ca. 7-7.5 hours into the transient, and this negative skewness can be attributed overwhelmingly to the uncertainties stemming from the parameter $\rho_{a,C}^{(in)}$ (see Figure 7.16). The third-largest negative "dip" in the skewness in the distribution of $\rho_a^{(1)}\left(t_i;\boldsymbol{\alpha}^0\right)$ occurs earlier in the transient, at ca. 3 hours into the transient; this negative "dip" stems from the uncertainties in the (assumed) normally-distributed model parameter $\rho_{a,A}^{(in)}$ (see Figure 7.17). The same features are evident in the plot of the skewness in the distribution of $\rho_a^{(7)}\left(t_i;\boldsymbol{\alpha}^0\right)$, depicted on the left-side of Figure 7.23. The three negative "dips" of varying magnitudes are similar to, but are much smaller and occur earlier in time than the negative "dips" in the distribution of $\rho_a^{(1)}\left(t_i;\boldsymbol{\alpha}^0\right)$. The three "dips" in the skewness of the distribution of $\rho_a^{(7)}\left(t_i;\boldsymbol{\alpha}^0\right)$, are caused by the uncertainties in the same parameters (sequentially in time) $\rho_{a,A}^{(in)}$, $\rho_{a,B}^{(in)}$, and $\rho_{a,C}^{(in)}$. In conclusion, the combination of 2nd-order sensitivities and uncertainties in $\rho_{a,B}^{(in)}$, $\rho_{a,C}^{(in)}$, and $\rho_{a,A}^{(in)}$ are the most important, in this order, in contributing to the marked negative dips in the skewness of the acid concentration response distributions. The effects of the combination of 2nd-order sensitivities and uncertainties in $\rho_{a,B}^{(in)}$, $\rho_{a,C}^{(in)}$, and $\rho_{a,A}^{(in)}$ increase in strength for the acid concentrations in the compartments furthest away from the inlet.
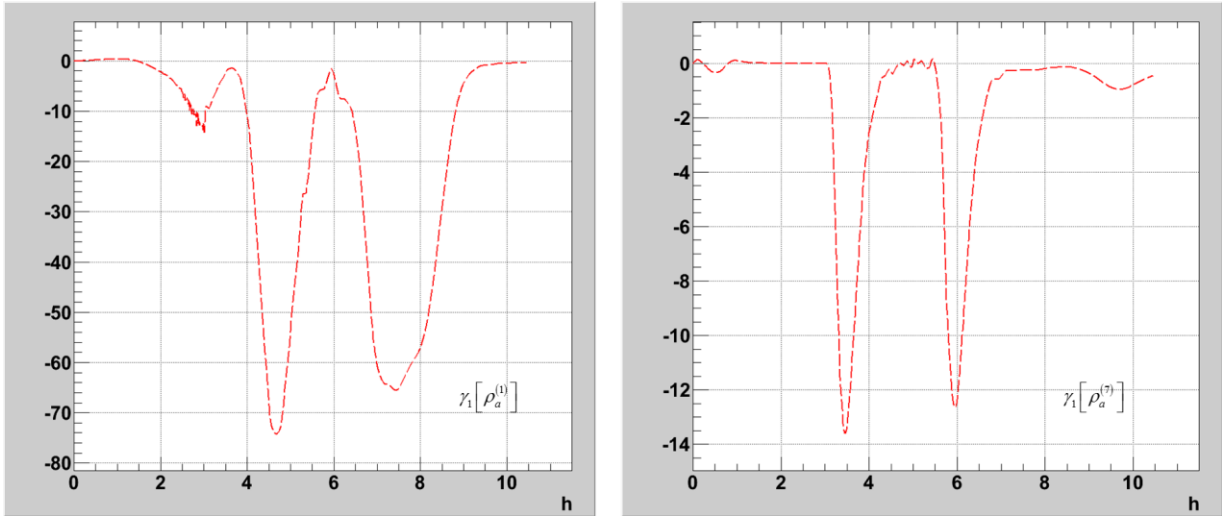
Figure 7.23 **Left:** time-dependence of the total skewness, $\gamma_1\left[\rho_a^{(1)}\left(t_i;\boldsymbol{\alpha}^0\right)\right]$, in the distribution of $\rho_a^{(1)}\left(t_i;\boldsymbol{\alpha}^0\right)$; **Right:** time-dependence of the total skewness, $\gamma_1\left[\rho_a^{(1)}\left(t_i;\boldsymbol{\alpha}^0\right)\right]$, in the distribution of $\rho_a^{(7)}\left(t_i;\boldsymbol{\alpha}^0\right)$.

Non-zero skewness implies asymmetric distribution of responses; in the cases of the acid concentration responses, the respective asymmetries are negative, meaning that the respective distributions favor values lower than the mean values. These results imply that using these calculations to support decisions regarding dissolver/model performance, or for coupling other physico-mechanical models or adding sophistication such as equations for accounting for fission materials and gasses, or using measurements to "inversely" verify declarations with these calculations would be misled. Asymmetries are extremely important to consider when establishing confidence intervals for decision-making goals since Gaussian-based intervals, valid for symmetric distributions, would become non-conservative for asymmetric distributions. In the case of the model developed and analyzed in this work, Gaussian-based confidence intervals would be very misleading for the times into the transient behavior of the acid concentration in the dissolver, particularly around the middle of the transient (around 3.5 to 4.5 hours after the initiation of the transient) and towards the last third of the transient (after 6 to 7.5 hours) that lasts for 10.5 hours. To accurately account for these asymmetries, different procedures, e.g., based on chi-squared (with few degrees of freedom) or other asymmetric distributions would be needed. The results presented in this chapter highlight the importance of quantifying, as exactly as possible, not only the 1st-order,

but also the 2nd-order sensitivities of responses with respect to all of the model parameters. In the absence of the 2nd-order sensitivities, non-linear features, such as asymmetries, would not be identifiable in the response distributions.

8. CONCLUSIONS AND OUTLOOK

The results of this work establish and document the dissolver model's performance and accuracy for simulating nitric acid concentrations needed to dissolve spent nuclear fuel which in turn suggest accuracy in generating the source terms for key reprocessing facility components downstream. Thinking holistically about nuclear fuel reprocessing these source terms could include actinide concentrations, fission gases, material inventories, etc., which either would be used to understand operational performance or for activities such as material accountability for nuclear safeguards. Accuracy would be key to having the confidence to use these data beyond a paper study regardless of the application. In particular, ongoing work is aimed at extending and coupling the dissolver model analyzed here to other key reprocessing facility components, including condenser, solvent extractor, and evaporator, which will, in turn, will be coupled to a cooling tower and atmospheric transport models for a full component capability to model aqueous nuclear fuel reprocessing. Future work will extend the application of the forward and inverse predictive modeling methodology of Cacuci and Ionescu-Bujor (2010b) and its applications to multiple components of nuclear facilities more comprehensive nuclear safeguard applications.

The dissolver was selected as a "case study" to demonstrate a useful analysis to support international nuclear safeguards in its ability to produce chemical feed stock within an aqueous nuclear fuel separations facility and thus its source for material diversion activities. A full description of quantified discrepancies allows one to better understand the physics captured by model, the potential impact on coupling this model to other models, and the risk of using the information calculated and assumed to be Gaussian. This model's analysis is complete as evidenced by the calibration, model extrapolation, and estimation of the validation domain both inverse and forward as well as the characterized asymmetries addressed here.

Notably, the predictive modeling methodology by Cacuci and Ionescu-Bujor (2010b) generalizes and significantly extends the "data adjustment" methods customarily used in nuclear engineering, as well as those underlying the 4D-VAR data assimilation procedures in the geophysical sciences (see, e.g., Lahoz et al, 2010, and Cacuci et al., 2014) which

combines experimental and computational information and results in best-estimate values for model responses and parameters, along with reduced predicted uncertainties. This method's unique feature is that it also provides a quantitative indicator, constructed from sensitivity and covariance matrices for determining the consistency (agreement or disagreement) among the "a priori" computational and experimental parameters and responses. Therefore, the deviations between the experimental and nominally computed responses are used as weights for determining consistency rather than ad hoc regularization measures defined by biased subject matter experts or inspectors.

The most important response for the dissolver model is the computed nitric acid in the compartment furthest away from the inlet, because this is the location where measurements (unique in the open literature) were performed over a period of 10.5 hours by Lewis and Weber (1980). The first order sensitivities to *all model parameters* of the acid concentrations at each of these instances in time were computed exactly and efficiently using the *adjoint sensitivity analysis method for nonlinear systems* conceived by Cacuci (1981a), and the relative importance of each sensitivity in contributing to the uncertainties in the computed model responses was quantified numerically, and used to analyze the physics captured by the dissolver model. These sensitivities are the center of all the other results from the subsequent chapters and so their importance, and the methods used to compute them should be recognized as nontrivial.

Clearly, if non-Gaussian features of responses are to be captured and characterized then the computation of the 2nd-order responses sensitivities to the model parameters is also needed. A new method which extends the 1st-order ASAM using adjoint operators, for computing most efficiently the exact 2nd-order sensitivities of the acid concentration in the surrogate dissolver model is presented and enables the computations of all of the 2nd-order response sensitivities exactly and efficiently, requiring at most $(N_\alpha + 1)$ adjoint computations, as opposed to $(N_\alpha + 1)(N_\alpha + 2)/2$ forward computations that are require if the 2nd-order sensitivities are computed using finite-difference formulas. The 2nd-order sensitivities impact the moments of the response distribution causing the "expected value of the response" to differ from the "computed nominal value of the response, albeit generally less than 1st order

sensitivities, and are the leading contributions to the third-order moment, or skewness of response distributions from uncorrelated and normally distributed parameters.

In the case of the full dissolver model developed and analyzed in this work, Gaussian-based confidence intervals would be very misleading for the times into the transient behavior of the acid concentration in the dissolver, particularly around the middle of the transient (around 3.5 to 4.5 hours after the initiation of the transient) and towards the last third of the transient (after 6 to 7.5 hours) that lasts for 10.5 hours, since the response skewness becomes large and negative over these times. Different procedures, based on chi-squared (with few degrees of freedom) or other asymmetric distributions would need to be used for establishing confidence intervals at these particularly important times.

Also, the predictive modeling methodology of Cacuci and Ionescu-Bujor (2010b) was applied in the inverse prediction mode, demonstrating its usefulness for inferring unknown model parameters (specifically: a time-dependent boundary condition) from measurements. Such inverse "problems" are of fundamental importance for the mission of proliferation detection since most scenarios in safeguards and treaty verification involve making inferences on targets of interest based on statistically low measurements/observations, indirect measurements, and a reliance on measurements from surrogate systems/environments. The results obtained for the paradigm inverse dissolver model presented in this work provide enabling capabilities for similar future applications on a broader set of models for studying a full facility.

Finally, it should be mentioned that the accuracy of the adjoint functions computed using the ASAM for the full dissolver model has been verified by forward computations; the results of these "solution verification" computations are presented in Appendix A. Finally, Appendix B presents the description of the forward and inverse predictive modeling software module that was developed to obtain all of the numerical results presented in this work.

9. APPENDIX A: Verification of the Computed Adjoint Functions

The accuracy of the computed solution of the adjoint system, i.e., Eqs. (3.64) - (3.68) has been verified for several model parameters α_i^0 by direct re-computations in conjunction with the finite-difference formula

$$\frac{\partial \rho_a^{(k)}\left(t_j\right)}{\partial \alpha_i} \cong \frac{\rho_a^{(k)}\left(t_j, 1.01 \times \alpha_i^0\right) - \rho_a^{(k)}\left(t_j, \alpha_i^0\right)}{0.01 \times \alpha_i^0}, \tag{A.1}$$

Typical results for such "adjoint solution verification" are presented in Figures A.1 through A.11. The close agreement between the respective sensitivities, computed by the *ASAM* (on the one hand) and direct re-computations (on the other hand) provides additional confidence in verifying the accuracy of the computed (adjoint function) solutions to of Eqs. (3.64) - (3.68).
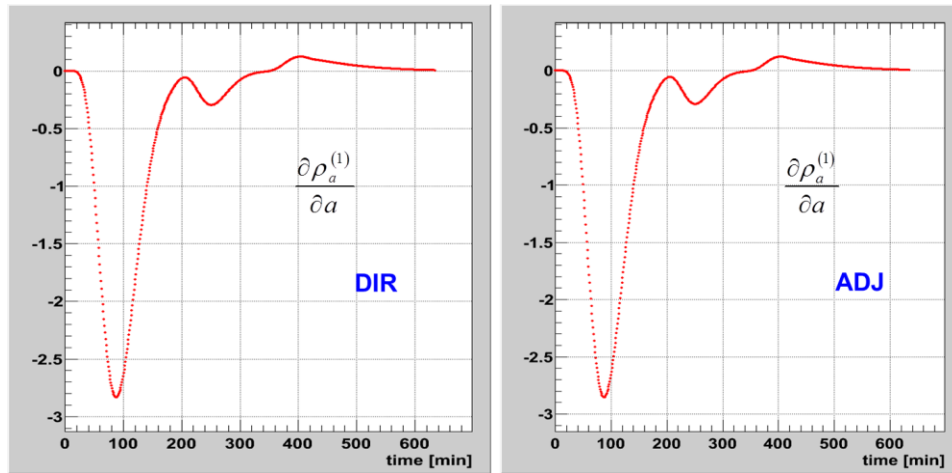
Figure A. 1 Time-evolution of the sensitivity of the nitric acid concentration in compartment 1, $\left[\partial \rho_a^{(1)}(t)/\partial a\right]$ [mol/L], to the model parameter a. Left: computed by finite-differences using direct re-calculations; Right: computed using the *ASAM*
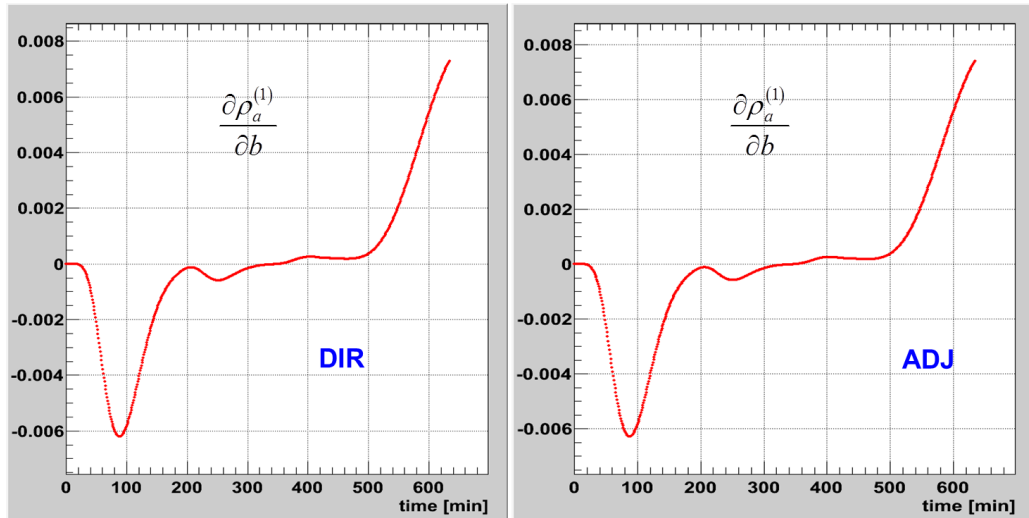
Figure A. 2 Time-evolution of the sensitivity of the nitric acid concentration in compartment 1, $\left[\partial\rho_a^{(1)}(t)/\partial b\right][\mathrm{mol/g}]$, to the model parameter b. Left: computed by finite-differences using direct re-calculations; Right: computed using the *ASAM*.
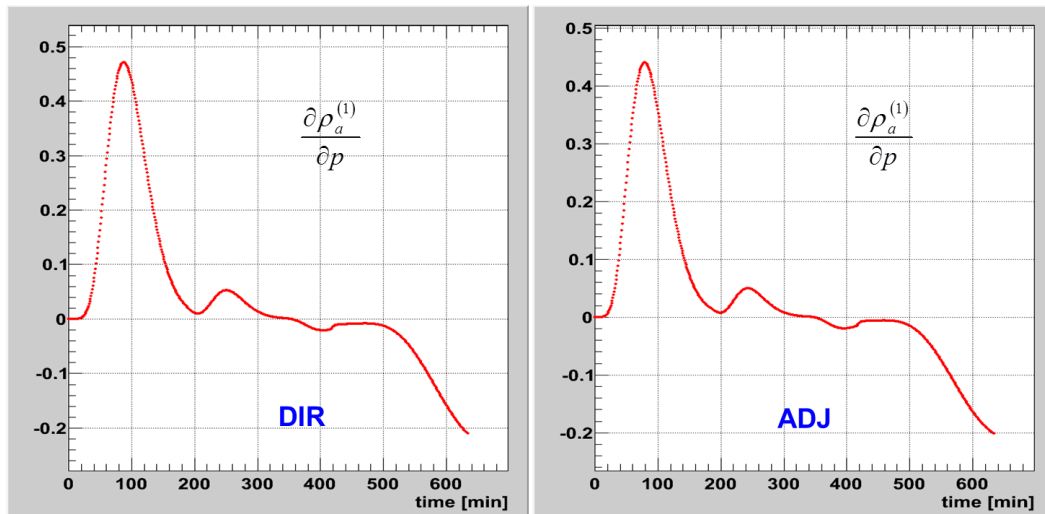
Figure A. 3 Time-evolution of the sensitivity of the nitric acid concentration in compartment 1, $\left[\partial\rho_a^{(1)}(t)/\partial p\right][\mathrm{mol/L}]$, to the model parameter p. Left: computed by finite-differences using direct re-calculations; Right: computed using the *ASAM*.
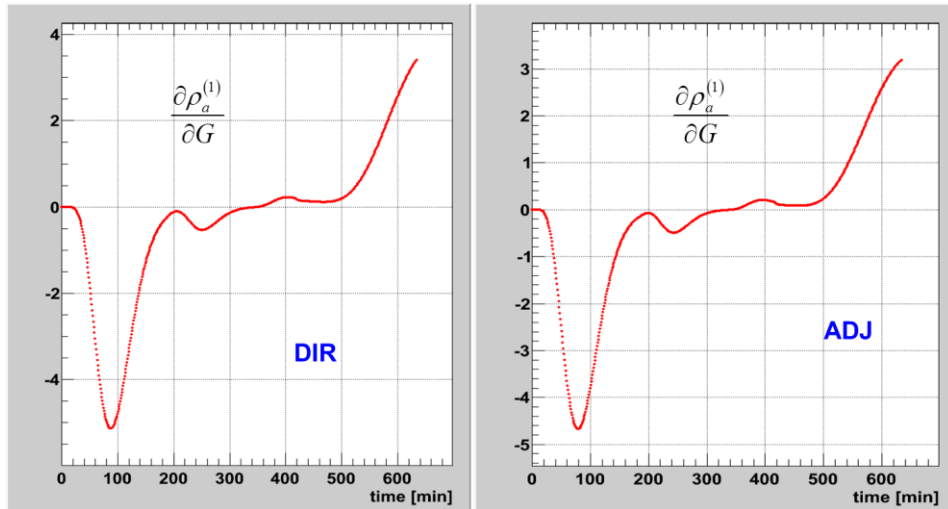
Figure A. 4 Time-evolution of the sensitivity of the nitric acid concentration in compartment 1, $\left[\partial\rho_a^{(1)}(t)\big/\partial G\right]\left[\text{mol}/\text{L}^2\right]$, to the model parameter G. Left: computed by finite-differences using direct re-calculations; Right: computed using the *ASAM*.
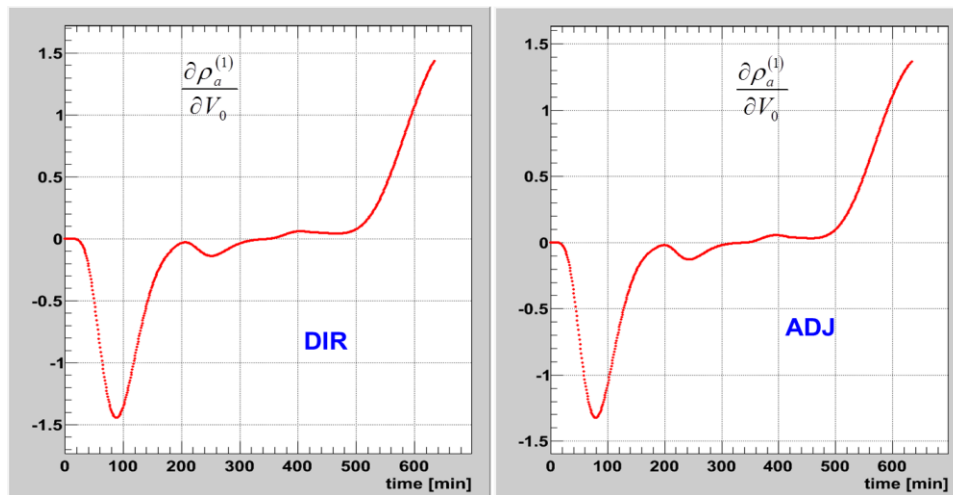
Figure A. 5 Time-evolution of the sensitivity of the nitric acid concentration in compartment 1, $\left[\partial\rho_a^{(1)}(t)\big/\partial V_0\right]\left[\text{mol}/\text{L}^2\right]$, to the model parameter V_0. Left: computed by finite-differences using direct re-calculations; Right: computed using the *ASAM*.
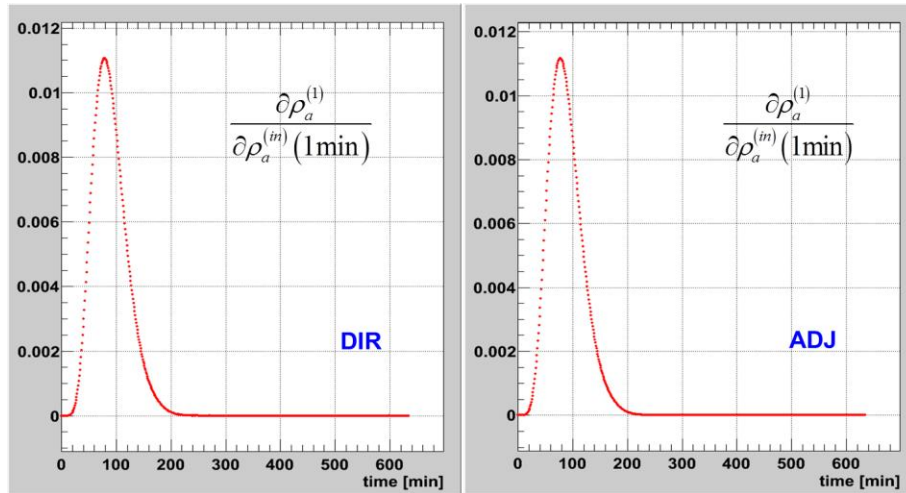
Figure A. 6 Time-evolution of the sensitivity of the nitric acid concentration in compartment 1, $\left[\partial \rho_a^{(1)}(t) / \partial \rho_a^{(in)}(1 \text{ minute}) \right]$, to the inlet nitric acid concentration at 1 minute into the transient, $\partial \rho_a^{(in)}(1 \text{ minute})$. Left: computed by finite-differences using direct re-calculations; Right: computed using the *ASAM*.
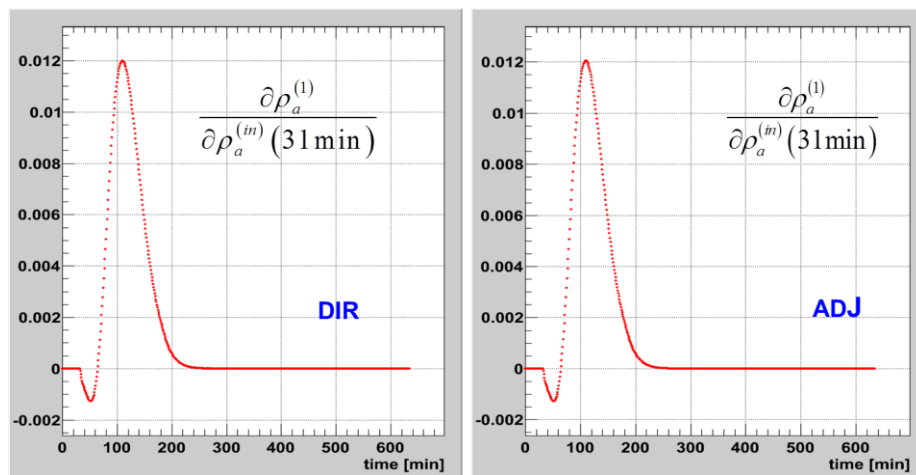
Figure A. 7 Time-evolution of the sensitivity of the nitric acid concentration in compartment 1, $\left[\partial \rho_a^{(1)}(t) / \partial \rho_a^{(in)}(31 \text{ minutes}) \right]$, to the inlet nitric acid concentration at 31 minutes into the transient, $\partial \rho_a^{(in)}(31 \text{ minutes})$. Left: computed by finite-differences using direct re-calculations; Right: computed using the *ASAM*
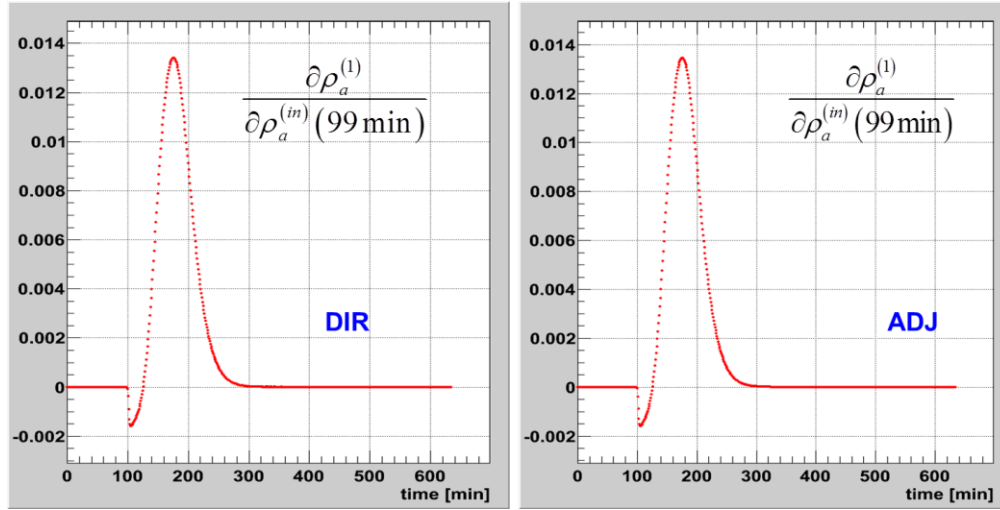
Figure A. 8 Time-evolution of the sensitivity of the nitric acid concentration in compartment 1, $\left[\partial \rho_a^{(1)}(t)/\partial \rho_a^{(in)}(99 \text{ minutes}) \right]$, to the inlet nitric acid concentration at 99 minutes into the transient, $\partial \rho_a^{(in)}(99 \text{ minutes})$. Left: computed by finite-differences using direct re-calculations; Right: computed using the *ASAM*

Many linear ordinary differential equations have appeared in conjunction with the development and sensitivity analysis of the "surrogate dissolver model" used in Chapters 2 and 7. The solutions of all of these equations were obtained by applying the "integrating factor method". For convenient reference, therefore, the general solution of a general first-order linear ordinary differential equation is provided below. The standard form of a general first-order linear ordinary differential equation is:

$$\frac{d\rho(t)}{dt} + a(t)\rho(t) = a(t), \ t_0 < t \le t_1,$$

$$\rho(t_0) = \rho_0.$$

(A.2)

The "integrating factor" for Eq. (A.2) is

$$P(t) = \exp\left(\int^t a(\tau)d\tau \right)$$

(A.3)

In terms of the above integrating factor, the general solution of Eq. (A.2) is given by the expression

$$\rho(t) = \frac{1}{P(t)} \int^t P(\tau)b(\tau)d\tau + \frac{C}{P(t)}, \tag{A.4}$$

where C is an arbitrary constant. In particular, the solution for which $\rho(t_0) = \rho_0$ can be expressed in the form

$$\rho(t) = \frac{1}{P(t)} \int_{t_o}^t P(\tau)b(\tau)d\tau + \rho_0 \frac{P(t_0)}{P(t)}. \tag{A.5}$$

10. APPENDIX B: Description of the Forward and Inverse Predictive Modeling Software Module (FIPRED)

The software module FIPRED implements the time-dependent forward and inverse predictive modelling mathematical formalism of Cacuci and Ionescu-Bujor (2010b), described in Chapters 4 and 5. All routines are written as C++ scripts running under the CERN Platform ROOT (https://root.cern.ch/) compatible with both Linux/Unix and Windows operating systems. The developed software has the following tree-structure of the directories:

1) BESTPRED/**example**/**KERNEL** is a *directory* containing the ***kernel*** of the FIPRED module, for both time-*independent* or time-*dependent* uses.

2) BESTPRED/**example**/**INPfiles** is a *directory* containing the (ASCII format) initial/raw *input files.*

3) BESTPRED/**example** /**vorKERNEL** is a *directory* containing the script vorbestpred.C, which transforms the initial/raw input files into compatible format for the FIPRED kernel.

4) BESTPRED/**example** /**nachKERNEL** is a *directory* containing the scripts for extracting and displaying the results of the FIPRED module; "**example**" refers to the specifc application, such as "**dissolver**".

10.1. Kernel

The following relations from Section 5 [see Eqs. (5.6) - (5.18)] have been implemented in the KERNEL of the FIPRED module.

(i)   Covariances of the computed responses:

$$C_{rc}\left(\boldsymbol{\alpha}^0\right) \triangleq \left\langle \delta \boldsymbol{r} \delta \boldsymbol{r}^\dagger \right\rangle = \left[\boldsymbol{S}\left(\boldsymbol{\alpha}^0\right) \right]\left\langle \delta \boldsymbol{\alpha} \delta \boldsymbol{\alpha}^\dagger \right\rangle \left[\boldsymbol{S}\left(\boldsymbol{\alpha}^0\right) \right]^\dagger =$$
$$\left[\boldsymbol{S}\left(\boldsymbol{\alpha}^0\right) \right] C_\alpha \left[\boldsymbol{S}\left(\boldsymbol{\alpha}^0\right) \right]^\dagger \tag{B.1}$$

(ii)   Discrepancy between the nominal computations and the nominally measured responses:

$$\boldsymbol{d} \triangleq \boldsymbol{R}\left(\boldsymbol{\alpha}^0\right) - \boldsymbol{r}_m \tag{B.2}$$

(iii)   The calibrated best-estimate parameter values:

$$\boldsymbol{\alpha}^{be} = \boldsymbol{\alpha}^0 + \left(C_{\alpha r} - C_\alpha \left[\boldsymbol{S}\left(\boldsymbol{\alpha}^0\right) \right]^\dagger \right)\left[C_d\left(\boldsymbol{\alpha}^0\right) \right]^{-1} \boldsymbol{d} \tag{B.3}$$

with:

$$C_d\left(\boldsymbol{\alpha}^0\right) \triangleq \left\langle \boldsymbol{d}\boldsymbol{d}^\dagger \right\rangle = \left\langle \left(\delta \boldsymbol{r} - \boldsymbol{S}\left(\boldsymbol{\alpha}^0\right)\delta\boldsymbol{\alpha} \right)\left(\delta \boldsymbol{r}^\dagger - \delta\boldsymbol{\alpha}^\dagger \left[\boldsymbol{S}\left(\boldsymbol{\alpha}^0\right) \right]^\dagger \right) \right\rangle$$
$$= C_{rc}\left(\boldsymbol{\alpha}^0\right) - C_{r\alpha}\left[\boldsymbol{S}\left(\boldsymbol{\alpha}^0\right) \right]^\dagger - \left[\boldsymbol{S}\left(\boldsymbol{\alpha}^0\right) \right]C_{\alpha r} + C_m. \tag{B.4}$$

(iv)   The best-estimate predicted nominal values for the calibrated (adjusted) responses:

$$\boldsymbol{r}\left(\boldsymbol{\alpha}^{be}\right) = \boldsymbol{r}_m + \left(C_m - C_{r\alpha}\left[\boldsymbol{S}\left(\boldsymbol{\alpha}^0\right) \right]^\dagger \right)\left[C_d\left(\boldsymbol{\alpha}^0\right) \right]^{-1} \boldsymbol{d}. \tag{B.5}$$

(v)   Best-estimate predicted covariances corresponding to the best-estimate parameters:

$$C_\alpha^{be} \triangleq \left\langle \left(\boldsymbol{\alpha} - \boldsymbol{\alpha}^{be} \right)\left(\boldsymbol{\alpha} - \boldsymbol{\alpha}^{be} \right)^\dagger \right\rangle$$
$$= C_\alpha - \left[C_{\alpha d}\left(\boldsymbol{\alpha}^0\right) \right]\left[C_d\left(\boldsymbol{\alpha}^0\right) \right]^{-1}\left[C_{\alpha d}\left(\boldsymbol{\alpha}^0\right) \right]^\dagger, \tag{B.6}$$

(vi)   Best-estimate predicted covariances corresponding to the best-estimate responses:

$$C_r^{be} \triangleq \left\langle \left(\boldsymbol{r} - \boldsymbol{r}\left(\boldsymbol{\alpha}^{be}\right) \right)\left(\boldsymbol{r} - \boldsymbol{r}\left(\boldsymbol{\alpha}^{be}\right) \right)^\dagger \right\rangle$$
$$= C_m - \left[C_{rd}\left(\boldsymbol{\alpha}^0\right) \right]\left[C_d\left(\boldsymbol{\alpha}^0\right) \right]^{-1}\left[C_{rd}\left(\boldsymbol{\alpha}^0\right) \right]^\dagger, \tag{B.7}$$

(vii)   Predicted best-estimate parameter-response covariances:

$$C_{r\alpha}^{be} = C_{r\alpha} - \left[C_{rd}\left(\alpha^0\right)\right]\left[C_d\left(\alpha^0\right)\right]^{-1}\left[C_{\alpha d}\left(\alpha^0\right)\right]^\dagger,$$ (B.8)

where

$$C_{rd}\left(\alpha^0\right) \triangleq \left\langle (r - r_m)d^\dagger \right\rangle = \left(C_m - C_{r\alpha}\left[S\left(\alpha^0\right)\right]^\dagger\right),$$ (B.9)

and

$$C_{\alpha d}\left(\alpha^0\right) \triangleq \left\langle (\alpha - \alpha^0)d^\dagger \right\rangle = \left(C_{\alpha r} - C_\alpha\left[S\left(\alpha^0\right)\right]^\dagger\right).$$ (B.10)

For computational reasons, the above expressions have been organized as follows:

Notations:

$$A \triangleq C_M - C_{r\alpha}S^T$$ (B.11)

$$B \triangleq -C_{r\alpha}^T + C_\alpha S^T$$ (B.12)

$$d = r - m$$ (B.13)

$$C_r = SC_\alpha S^T$$ (B.14)

$$C_d = A + SB$$ (B.15)

$$\alpha^{BE} = \alpha - BC_d^{-1}d$$ (B.16)

$$C_\alpha^{BE} = C_\alpha - BC_d^{-1}B^T$$ (B.17)

$$r^{BE} = m + AC_d^{-1}d$$ (B.18)

$$C_r^{BE} = C_m - AC_d^{-1}A^T$$ (B.19)

$$C_{r\alpha}^{BE} = C_{r\alpha} - AC_d^{-1}B^T$$ (B.20)

$$\chi^2 = d^T C_d^{-1}d$$ (B.21)

The block-matrix structures of the **basic input** elements $\alpha, r, m, C_\alpha, C_m, C_{r\alpha}, S$ are as follows:

i) Nominal system parameters, computed responses, and measured responses:

$$\alpha = \begin{pmatrix} \alpha_1^1 \\ \alpha_2^1 \\ . \\ \alpha_{N_\alpha}^1 \\ . \\ . \\ \alpha_1^\mu \\ \alpha_2^\mu \\ . \\ \alpha_{N_\alpha}^\mu \\ . \\ . \\ \alpha_1^{N_t} \\ \alpha_2^{N_t} \\ . \\ \alpha_{N_\alpha}^{N_t} \end{pmatrix} \qquad r = \begin{pmatrix} r_1^1 \\ r_2^1 \\ . \\ r_{N_r}^1 \\ . \\ . \\ r_1^\mu \\ r_2^\mu \\ . \\ r_{N_r}^\mu \\ . \\ . \\ r_1^{N_t} \\ r_2^{N_t} \\ . \\ r_{N_r}^{N_t} \end{pmatrix} \qquad m = \begin{pmatrix} m_1^1 \\ m_2^1 \\ . \\ m_{N_r}^1 \\ . \\ . \\ m_1^\mu \\ m_2^\mu \\ . \\ m_{N_r}^\mu \\ . \\ . \\ m_1^{N_t} \\ m_2^{N_t} \\ . \\ m_{N_r}^{N_t} \end{pmatrix} \qquad \begin{array}{l} N_t = number\ of\ time\ nodes \\ N_\alpha = number\ of\ sistem\ parameters \\ N_r = number\ of\ sistem\ responses \end{array} \qquad (B.22)$$

Observation: α^{BE} has the same structure as α; r^{BE} has the same structure as r.

ii) Nominal correlations between system parameters:

$$C_\alpha = \begin{pmatrix} C_\alpha^{11} & C_\alpha^{12} & . & . & C_\alpha^{1\nu} & . & . & C_\alpha^{1N_t} \\ C_\alpha^{21} & C_\alpha^{22} & . & . & C_\alpha^{2\nu} & . & . & C_\alpha^{2N_t} \\ . & . & . & . & . & . & . & . \\ . & . & . & . & . & . & . & . \\ C_\alpha^{\mu 1} & C_\alpha^{\mu 2} & . & . & C_\alpha^{\mu\nu} & . & . & C_\alpha^{\mu N_t} \\ . & . & . & . & . & . & . & . \\ . & . & . & . & . & . & . & . \\ C_\alpha^{N_t 1} & C_\alpha^{N_t 2} & . & . & C_\alpha^{N_t \nu} & . & . & C_\alpha^{N_t N_t} \end{pmatrix} \qquad (B.23)$$

The structure of a matrix of the type $\mathbf{C}_\alpha^{\mu\nu}$ is as follows:

$$C_\alpha^{\mu\nu} = \begin{pmatrix} C_{\alpha,11}^{\mu\nu} & C_{\alpha,12}^{\mu\nu} & . & . & C_{\alpha,1j}^{\mu\nu} & . & . & C_{\alpha,1N_\alpha}^{\mu\nu} \\ C_{\alpha,21}^{\mu\nu} & C_{\alpha,22}^{\mu\nu} & . & . & C_{\alpha,2j}^{\mu\nu} & . & . & C_{\alpha,2N_\alpha}^{\mu\nu} \\ . & . & . & . & . & . & . & . \\ . & . & . & . & . & . & . & . \\ C_{\alpha,i1}^{\mu\nu} & C_{\alpha,i2}^{\mu\nu} & . & . & C_{\alpha,ij}^{\mu\nu} & . & . & C_{\alpha,iN_\alpha}^{\mu\nu} \\ . & . & . & . & . & . & . & . \\ . & . & . & . & . & . & . & . \\ C_{\alpha,N_\alpha 1}^{\mu\nu} & C_{\alpha,N_\alpha 2}^{\mu\nu} & . & . & C_{\alpha,N_\alpha j}^{\mu\nu} & . & . & C_{\alpha,N_\alpha N_\alpha}^{\mu\nu} \end{pmatrix} \qquad (B.24)$$

where N_α is the number of system parameters. The correlation between response i at time node μ and the response j at time node ν is the following scalar:

$$C_{\alpha,ij}^{\mu\nu} = \left\langle \Delta\alpha_i^\mu \Delta\alpha_j^\nu \right\rangle = \left\langle \Delta\alpha_j^\nu \Delta\alpha_i^\mu \right\rangle = C_{\alpha,ji}^{\nu\mu} \qquad (B.25)$$

Therefore:

$$\mathbf{C}_\alpha^{\mu\nu} = \left(\mathbf{C}_\alpha^{\nu\mu} \right)^T, \ \forall \mu,\nu \leq N_t \qquad (B.26)$$

Observation: C_α^{BE} has the same structure as C_α.

iii) correlations of the measured responses:

$$C_m = \begin{pmatrix} C_m^{11} & C_m^{12} & . & . & C_m^{1\nu} & . & . & C_m^{1N_t} \\ C_m^{21} & C_m^{22} & . & . & C_m^{2\nu} & . & . & C_m^{2N_t} \\ . & . & . & . & . & . & . & . \\ . & . & . & . & . & . & . & . \\ C_m^{\mu 1} & C_m^{\mu 2} & . & . & C_m^{\mu\nu} & . & . & C_m^{\mu N_t} \\ . & . & . & . & . & . & . & . \\ . & . & . & . & . & . & . & . \\ C_m^{N_t 1} & C_m^{N_t 2} & . & . & C_m^{N_t \nu} & . & . & C_m^{N_t N_t} \end{pmatrix} \qquad (B.27)$$

The matrices on the diagonal ($\mathbf{C}_m^{11}, \mathbf{C}_m^{22}, ..., \mathbf{C}_m^{N_t N_t}$) contain the correlations between measured responses at the *same* time node ($1, 2, ..., N_t$). The off-diagonal matrices contain correlations between measured responses at *different* time nodes. The structure of a matrix of the type $\mathbf{C}_m^{\mu\nu}$ in the block matrix $\mathbf{C}_m$ is as follows:

$$
C_m^{\mu\nu} = \begin{pmatrix}
C_{m,11}^{\mu\nu} & C_{m,12}^{\mu\nu} & \cdot & \cdot & C_{m,1j}^{\mu\nu} & \cdot & \cdot & C_{m,1N_r}^{\mu\nu} \\
C_{m,21}^{\mu\nu} & C_{m,22}^{\mu\nu} & \cdot & \cdot & C_{m,2j}^{\mu\nu} & \cdot & \cdot & C_{m,2N_r}^{\mu\nu} \\
\cdot & \cdot & \cdot & \cdot & \cdot & \cdot & \cdot & \cdot \\
\cdot & \cdot & \cdot & \cdot & \cdot & \cdot & \cdot & \cdot \\
C_{m,i1}^{\mu\nu} & C_{m,i2}^{\mu\nu} & \cdot & \cdot & C_{m,ij}^{\mu\nu} & \cdot & \cdot & C_{m,iN_r}^{\mu\nu} \\
\cdot & \cdot & \cdot & \cdot & \cdot & \cdot & \cdot & \cdot \\
\cdot & \cdot & \cdot & \cdot & \cdot & \cdot & \cdot & \cdot \\
C_{m,N_r 1}^{\mu\nu} & C_{m,N_r 2}^{\mu\nu} & \cdot & \cdot & C_{m,N_r j}^{\mu\nu} & \cdot & \cdot & C_{m,N_r N_r}^{\mu\nu}
\end{pmatrix}
\tag{B.28}
$$

where N_r is the number of responses. The elements in the matrix above are scalars. The correlation between response i at time node μ and the response j at time node ν. For example:

$$
C_{m,ij}^{\mu\nu} = \left\langle \Delta m_i^\mu \Delta m_j^\nu \right\rangle = \left\langle \Delta m_j^\nu \Delta m_i^\mu \right\rangle = C_{m,ji}^{\nu\mu}
\tag{B.29}
$$

Therefore:

$$
\mathbf{C}_m^{\mu\nu} = \left(\mathbf{C}_m^{\nu\mu} \right)^T, \ \forall \mu, \nu \leq N_t
\tag{B.30}
$$

Observation: C_r and C_r^{BE} have the same structure as C_m.

iv) correlations of the measured responses with system parameters

$$
\mathbf{C}_{r\alpha} = \begin{pmatrix}
\mathbf{C}_{r\alpha}^{11} & \mathbf{C}_{r\alpha}^{12} & \cdot & \cdot & \mathbf{C}_{r\alpha}^{1\nu} & \cdot & \cdot & \mathbf{C}_{r\alpha}^{1N_t} \\
\mathbf{C}_{r\alpha}^{21} & \mathbf{C}_{r\alpha}^{22} & \cdot & \cdot & \mathbf{C}_{r\alpha}^{2\nu} & \cdot & \cdot & \mathbf{C}_{r\alpha}^{2N_t} \\
\cdot & \cdot & \cdot & \cdot & \cdot & \cdot & \cdot & \cdot \\
\cdot & \cdot & \cdot & \cdot & \cdot & \cdot & \cdot & \cdot \\
\mathbf{C}_{r\alpha}^{\mu 1} & \mathbf{C}_{r\alpha}^{\mu 2} & \cdot & \cdot & \mathbf{C}_{r\alpha}^{\mu\nu} & \cdot & \cdot & \mathbf{C}_{r\alpha}^{\mu N_t} \\
\cdot & \cdot & \cdot & \cdot & \cdot & \cdot & \cdot & \cdot \\
\cdot & \cdot & \cdot & \cdot & \cdot & \cdot & \cdot & \cdot \\
\mathbf{C}_{r\alpha}^{N_t 1} & \mathbf{C}_{r\alpha}^{N_t 2} & \cdot & \cdot & \mathbf{C}_{r\alpha}^{N_t \nu} & \cdot & \cdot & \mathbf{C}_{r\alpha}^{N_t N_t}
\end{pmatrix}
\tag{B.31}
$$

The matrices on the diagonal ($\mathbf{C}_{r\alpha}^{11}, \mathbf{C}_{r\alpha}^{22}, ..., \mathbf{C}_{r\alpha}^{N_t N_t}$) contain the correlations between measured responses and system parameters at the *same* time node ($1, 2, ..., N_t$). The off-diagonal matrices contain correlations between measured responses and system parameters at *different* time nodes. The structure of a matrix of the type $\mathbf{C}_{r\alpha}^{\mu\nu}$ is as follows:

$$C_{r\alpha}^{\mu\nu} = \begin{pmatrix} C_{r\alpha,11}^{\mu\nu} & C_{r\alpha,12}^{\mu\nu} & . & . & C_{r\alpha,1j}^{\mu\nu} & . & . & C_{r\alpha,1N_\alpha}^{\mu\nu} \\ C_{r\alpha,21}^{\mu\nu} & C_{r\alpha,22}^{\mu\nu} & . & . & C_{r\alpha,2j}^{\mu\nu} & . & . & C_{r\alpha,2N_\alpha}^{\mu\nu} \\ . & . & . & . & . & . & . & . \\ . & . & . & . & . & . & . & . \\ C_{r\alpha,i1}^{\mu\nu} & C_{r\alpha,i2}^{\mu\nu} & . & . & C_{r\alpha,ij}^{\mu\nu} & . & . & C_{r\alpha,iN_\alpha}^{\mu\nu} \\ . & . & . & . & . & . & . & . \\ . & . & . & . & . & . & . & . \\ C_{r\alpha,N_r 1}^{\mu\nu} & C_{r\alpha,N_r 2}^{\mu\nu} & . & . & C_{r\alpha,N_r j}^{\mu\nu} & . & . & C_{r\alpha,N_r N_\alpha}^{\mu\nu} \end{pmatrix} \tag{B.32}$$

Where N_α is the number of system parameters (static and transient) and N_r is the number of system responses. The elements in the matrix above are scalars. For example:

$$C_{r\alpha,ij}^{\mu\nu} = \left\langle \Delta m_i^\mu \Delta \alpha_j^\nu \right\rangle = \left\langle \Delta \alpha_j^\nu \Delta m_i^\mu \right\rangle = C_{r\alpha,ji}^{\nu\mu} \tag{B.33}$$

is the correlation between the measured response i at time node μ and the parameter j at time node ν.

<u>Observation</u>: $\mathbf{C}_{r\alpha}^{BE}$ has the same structure as $C_{r\alpha}$.

v) sensitivities of the system responses to the system parameters

$$\mathbf{S} = \begin{pmatrix} \mathbf{S}^{11} & \mathbf{0} & . & . & \mathbf{0} & . & . & \mathbf{0} \\ \mathbf{S}^{21} & \mathbf{S}^{22} & \mathbf{0} & . & \mathbf{0} & . & . & \mathbf{0} \\ . & . & . & . & . & . & . & . \\ . & . & . & . & . & . & . & . \\ \mathbf{S}^{\mu1} & \mathbf{S}^{\mu2} & . & . & \mathbf{S}^{\mu\nu} & . & \mathbf{S}^{\mu\mu}. & . & \mathbf{0} \\ . & . & . & . & . & . & . & . \\ . & . & . & . & . & . & . & . \\ \mathbf{S}^{N_t 1} & \mathbf{S}^{N_t 2} & . & . & \mathbf{S}^{N_t \nu} & . & \mathbf{S}^{N_t \mu}. & . & \mathbf{S}^{N_t N_t} \end{pmatrix}, \quad \nu \le \mu \le N_t \tag{B.34}$$

The structure of a matrix of the type $\mathbf{S}^{\mu\nu}$ is as follows:

$$S^{\mu\nu} = \begin{pmatrix} \dfrac{\partial r_1^\mu}{\partial \alpha_1^\nu} & \dfrac{\partial r_1^\mu}{\partial \alpha_2^\nu} & . & \dfrac{\partial r_1^\mu}{\partial \alpha_{N_\alpha}^\nu} \\[3mm] \dfrac{\partial r_2^\mu}{\partial \alpha_1^\nu} & \dfrac{\partial r_2^\mu}{\partial \alpha_2^\nu} & . & \dfrac{\partial r_2^\mu}{\partial \alpha_{N_\alpha}^\nu} \\[3mm] . & . & \dfrac{\partial r_i^\mu}{\partial \alpha_j^\nu} & . \\[3mm] \dfrac{\partial r_{N_r}^\mu}{\partial \alpha_1^\nu} & \dfrac{\partial r_{N_r}^\mu}{\partial \alpha_2^\nu} & . & \dfrac{\partial r_{N_r}^\mu}{\partial \alpha_{N_\alpha}^\nu} \end{pmatrix} \tag{B.35}$$

where N_r is the number of responses and N_α the number of system parameters. An element of the above matrix has the general form:

$$S_{ij}^{\mu\nu} = \frac{\partial r_i^\mu}{\partial \alpha_j^\nu} \tag{B.36}$$

and represented is the sensitivity of response i at time node μ to the parameter j at time node ν.

The FIPRED KERNEL computation can be launched with the following ROOT command:

root -l bestpred.C

in the directory:

BESTPRED/**example**/**KERNEL**

under Linux/Unix operating systems.

In Windows, the script **bestpred.C** is launched by a simple **double click** (the first launch may need an explicit "Open With" ROOT preinstalled software).

Table B. 1 Input and output files (matrices) for the BEST-PRED kernel

Input matrix	Input file	Output matrix	Output file
α	a.abs	α^{BE}	aBE.out
C_α	ca.abs	C_α^{BE}	caBE.out
r	r.abs	r^{BE}	rBE.out
m	m.abs		
C_m	cm.abs	C_m^{BE}	cmBE.out
$C_{r\alpha}$	car.abs	$C_{r\alpha}^{BE}$	carBE.out
S	s.abs	C_r	CR.out
		χ^2	chi2.out

The *prerequisite* input files (**a.abs, ca.abs, …, s.abs**) for the FIPRED kernel are listed on the left (yellow) side of **Table B.1**, and are as follows:

a.abs	nominal parameters
c**a.abs**	nominal parameter correlations
m.abs	measured response(s)
r.abs	nominal computed response(s)
cm.abs	correlations for measured response(s)
s.abs	sensitivities of the response(s) to all parameters (static and transient)
car.abs	initial correlations between parameters and response(s)

They *must* exist in the directory BESTPRED/**example**/**vorKERNEL** (see also the Paragraph 3.2) before launching the FIPRED kernel. The prerequisite input files (**a.abs, ca.abs, …, s.abs**) contain the corresponding block-matrices from the first column of Table B.1 written in **sparse format** as follows:

1) first row:

    nr nc nz

where:

nr (integer) – number of rows

nc (integer) – number of columns

nz (integer) – number of non-zero elements / number of following lines in the file

2) nz rows of the type:

    ir ic w

where:

ir (integer) – global row coordinate in the corresponding block-matrix

ic (integer) – global column coordinate in the corresponding block-matrix

w (float) – numerical value of the element with the global coordinates (ir,ic) in the block-matrix

Remark: The prerequisite input files (**a.abs, ca.abs, …, s.abs**) **are created semi-automatically** (see next Paragraph!).

10.2. *Input Data Preparation*

The raw input data have to be delivered by the user, respecting some simple formatting. The following steps (**1-3**) must be *strictly* followed by the user:

STEP 1) Edit and fill the TXT file:

BESTPRED/**example**/**vorKERNEL**/**dimensions.txt**

which is a header file (to contain the *steering data* of the chosen <u>model</u>) for the C++ script:

BESTPRED/**example**/**vorKERNEL**/**vorbestpred.C (to be NEVER changed!)**

<u>EXAMPLE:</u> **dimension.txt**-file in the case of the "**Dissolver Model**"

****

//number of responses

1

//number of time nodes

635

//number of static parameters

5

//number of transient parameters

2

//Only standard deviations for nominal sistem parameters? **0-NO**; 1-YES absolut; 2-YES relativ

2

//Only standard deviations for measured responses? **0-NO**; 1-YES absolut; 2-YES relativ

1

//Initial correlations between parameters and responses? 0-NO; **1-YES**

0

▪▪

<u>IMPORTANT</u>:

The file **vorbestest.C** will create the sparse matrices:

        a.abs   nominal parameters

m.abs	measured response
r.abs	nominal computed response
s.abs	sensitivities of the response to all parameters (static and

transient)

directly (according to the steering data), making use of the raw input data (already) existing in the directory BESTPRED/**example**/**INPfiles**.

Any of the next 3 files (sparse matrices with structures according to Eqs. B.23, B.27 and B.31) must be provided by the user (and automatically no more touched by **vorbestpred.C**) in the case that the steering file **dimensions.txt** is asking for ("**green**" options in the "dissolver" example above):

ca.abs	nominal parameter correlations
cm.abs	correlations for measured response
car.abs	initial correlations between parameters and responses

As an example, let us consider the following logical ramifications in the (final part of) steering file **dimensions.txt**:

```
*************************************************************************
```

//Only standard deviations for nominal sistem parameters? **0-NO**; 1-YES absolut; 2-YES relativ

0

//Only standard deviations for measured responses? **0-NO**; 1-YES absolut; 2-YES relativ

0

//Initial correlations between parameters and responses? 0-NO; **1-YES**

0

```
*************************************************************************
```

This logical configuration will lead to:

the sparse matrix **car.abs** (initial correlations between responses and parameters) will be still automatically provided by the script **vorbestpred.C**; it will contain in fact only one line of 3 integers:

nr nc 0, i.e.:

nr – number of rows

nc – number of columns

0 non-zero elements (in sparse format).

ca.abs and **cm.abs** have to be provided by the user.

STEP 2) The user must create the following ASCII format input files (containing the raw input data) in the directory BESTPRED/**example**/**INPfiles**:

experimental.txt	the experimental response(s)
NOM.txt	the nominal response(s)
paramSTAT.txt	the nominal values of the *static* system parameters
paramTRANSI.txt	the nominal values of the *transient* system parameters
sensiSTAT.txt	sensitivities to the *static* parameters
sensiTRANSI.txt	sensitivities to the *transient* parameters
respSIGMA.txt	standard deviations for experimental response(s)
paramSIGMA.txt	nominal standard deviations for parameters

The structures of these files are as follows:

experimental.txt

It contains two columns:

1st column - time nodes (but it may contain only a time node counter);

2nd column – the experimental values of the response(s)

The iteration tree looks like:

LOOP for the number of responses (dissolver: 1)

LOOP for time nodes (dissolver: 635)

Dissolver Model: 635 x 1 lines.

NOM.txt

It has the *same* structure as experimental.txt!

paramSTAT.txt

It contains only one column with the nominal values of the static parameters.

The iteration tree is as follows:

LOOP for the number of static parameters (Dissolver: 5): 5 lines.

paramTRANSI.txt

Contains two columns:

1st column - time nodes (but it may contain only a time node counter);

2nd column – the nominal values of the transient parameters

The iteration tree is as follows:

LOOP for the number of transient parameters (Dissolver: 2)

    LOOP for time nodes (Dissolver: 635)

sensiSTAT.txt

It contains two columns:

1st column: time nodes (but it may contain only a time node counter);

2nd column: sensitivity values

The iterations are:

LOOP for the number of responses (dissolver: 1)

    LOOP for the number of static parameters (dissolver: 5)

        LOOP for time nodes (dissolver: 635)

Dissolver model: 1 x 5 x 635 lines.

sensiTRANSI.txt

Contains two columns:

1st column: time nodes (but it may contain only a time node counter);

2nd column: sensitivity values

The iterations are:

LOOP for the number of responses (dissolver: 1)

   LOOP for the number of transient boundary conditions (dissolver: 2)

      LOOP for perturbation nodes (dissolver: 635)

         LOOP for time nodes (dissolver: 635)

Dissolver Model: 1 x 2 x 635 x 635 lines!

The zeros before perturbation nodes (because of causality reasons) are formally kept in the file structure for safety reasons. Anyhow, these zeros will be not transferred towards the sparse matrices as they will contain only the non-zero elements and their matrix coordinates (row number and column number).

respSIGMA.txt

It contains one column with standard deviations (absolute or relative, according to the logical option in the steering file **dimensions.txt**) of the response(s).

The iteration tree looks like:

LOOP for the number of responses (dissolver: 1)

   LOOP for time nodes (dissolver: 635)

Dissolver Model: 635 lines.

paramSIGMA.txt

It contains one column with standard deviations (absolute or relative, according to the logical option in the steering file **dimensions.txt**) of the system parameters

The iterations are:

LOOP for the number of all parameters (static and transient) (dissolver: 7)

Dissolver Model: 7 lines.

STEP 3) The user must run the C++ script

BESTPRED/**example**/**vorKERNEL**/**vorbestpred.C**   C++ script for reading the input files from BESTPRED/**example**/**INPfiles** and generating the sparse matrices a.abs, ca.abs, m.abs, r.abs, cm.abs, s.abs, car.abs (ASCII files containing in sparse matrix format the required data structure for the BEST-EST module). Remark: Do not modify the file **vorbestpred.C**!

10.3.   *Output Data*

The output data obtained by running the FIPRED procedure are contained in the directory:

BESTPRED/**example**/**KERNEL.** All files to be found in this directory are explained in the Table B.2, below:

Table B. 2 Output files (matrices) for the BEST-PRED kernel

Matrix	File	Output matrix	Output file
α	a.inp	α^{BE}	aBE.out
C_α	ca.inp	C_α^{BE}	caBE.out
r	r.inp	r^{BE}	rBE.out
m	m.inp		
C_m	cm.inp	C_m^{BE}	cmBE.out
$C_{r\alpha}$	car.inp	$C_{r\alpha}^{BE}$	carBE.out
S	s.inp	C_r	CR.out
		χ^2	chi2.out

The *prerequisite* input files (**a.abs, ca.abs, …, s.abs**) for the BESTPRED kernel are listed on the left (yellow) side of the **Table B.1**. The same information with the same format is formally written/practically cloned (as safety measure) by the kernel in the files (**a.inp, ca.inp, …, s.inp**), see the left (yellow) side of the **Table B.2**. Let us recall their contents:

      a.inp   nominal parameters (same as a.abs)

      ca.inp   nominal parameter correlations (same as ca.abs)

m.inp	measured response(s) (same as m.abs)
r.inp	nominal computed response(s) (same as r.abs)
cm.inp	correlations for measured response(s) (same as cm.abs)
s.inp	sensitivities of the response(s) to all parameters (static and transient) (same as s.abs)
car.inp	initial correlations between parameters and response(s) (same as car.abs)

The (real) output of the kernel is written in the files on the right (blue) side of the **Table B.2**.

Here are their contents:

aBE.out	best-estimate parameters (same structure as a.abs)
caBE.out	best-estimate parameter correlations (same structure as ca.abs)
rBE.out	best-estimate response(s) (same structure as r.abs)
cmBE.out	best estimate correlations for response(s) (same structure as cm.abs)
carBE.out	best-estimate correlations between parameters and response(s) (same structure as car.abs)
CR.out	initial correlations between computed response(s) (same structure as cm.abs)
chi2.out	value of the consistency indicator χ^2

The data contained in these files from Table B.2 (***.inp** and ***.out)** plus the steering data from the file (already existing, used for the data preparation)

BESTPRED/**example**/**vorKERNEL**/**dimensions.txt**

are sufficient for displaying the results of the BEST-PRED procedure.

10.4.   Display Results

The results of the FIPRED procedure, as well as their comparison with the a-priori data, are displayed by semi-automatic C++ scripts. The scripts are described below.

Script and Figure	Function
paramMOnom.C (see Fig. **B.1**)	- plot nominal correlations of the static parameters - create the file paramMOnomBest.out (it contains a one-to-one comparison of the nominal an best-estimate static parameters with their relative standard deviations)
paramMObest.C (see Fig. **B.2**)	- plot best-estimate correlations of the static parameters - create the file paramMOnomBest.out (the same content as above)
corRESPnom.C (see Fig. **B.3**)	plot initial correlations between computed responses
corRESPbest.C (see Fig. **B.4**)	plot best-estimate correlations between responses
RESPsimexpbest.C (see Fig. **B.5**)	plot computed, experimental and best-estimate responses
sigonlyRESPsimexpbest.C (see Fig. **B.6**)	plot (±) one standard deviation bands for computed, experimental and best-estimate responses
paramBCexpbest.C (see Fig. **B.7**)	plot experimental and best-estimate transient boundary conditions
sigrelparamBCexpbest.C (see Fig. **B.8**)	plot experimental and best-estimate relative standard deviations (in percent) of the transient boundary conditions

The above scripts are semi-automatic: after launching, they ask the user for preferred options. The interactions possible with these scripts are presented next.

Dissolver Model

root -l paramMOnom.C

root [0]

Processing paramMOnom.C...

Number of responses: 1

Number of time nodes: 635

Number of model parameters: 5

Number of transient parameters: 2

What kind of best-estimate relative standard deviations?

1 = relative to nominal values

2 = relative to best-estimate values

1

Set a minimum and a maximum for the histogram?

1 = Yes!

2 = No!

2

root [1]
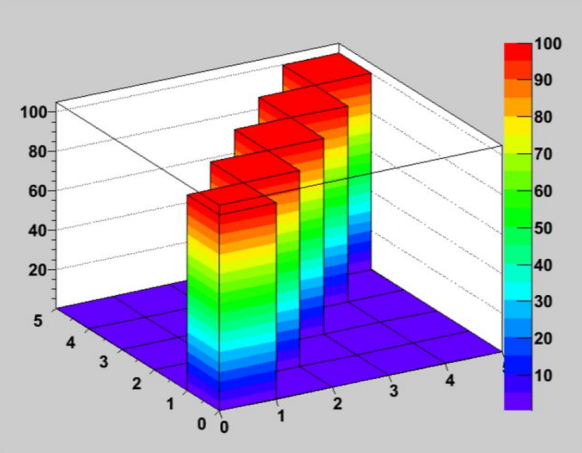
Figure B.1: Nominal static parameters correlations for the dissolver model (cf. Fig. 5.1).

Some observations:

1) All scripts are applicable to time-independent or time-dependent results; some user feedback may be required during running.

2) The user (required) feedback is displayed in red in all panels.

3) Sometimes it appears the question:

What kind of best-estimate relative standard deviations?

1 = relative to nominal values

2 = relative to best-estimate values

Because the best-estimate nominal values can be sometimes smaller than the a-priori values, the a-priori values may be chosen as normalizations for the best-estimate relative standard deviations (option 1); in such a case the best-estimate relative standard deviations will be always smaller than the a-priori relative standard deviations.

4) By selecting on the tool-bar of any plot the option **File->Save** the following picture format may be selected: ps, eps, pdf, gif, jpg, png. The corresponding file will keep the name of the script producing it, with the extension ps, eps and so on.

5) The scripts of the type **paramMOnom.C** and **paramMObest.C** are delivering also a text file **paramMOnomBest.out** which contains a one-to-one comparison of the nominal and best-estimate static parameters with their relative standard deviations.

6) Under Windows operating system the launching command for all scripts is **Double Click**.

Dissolver Model root -l paramMObest.C root [0] Processing paramMObest.C... Number of responses: 1 Number of time nodes: 635 Number of model parameters: 5 Number of transient parameters: 2 What kind of best-estimate relative standard deviations? 1 = relative to nominal values 2 = relative to best-estimate values 2 Set a minimum and a maximum for the histogram? 1 = Yes! 2 = No! 2 root [1]	 **Figure B.2:** Predicted (best-estimate) correlation matrix for the dissolver's scalar parameters (cf., Figure 5.2).
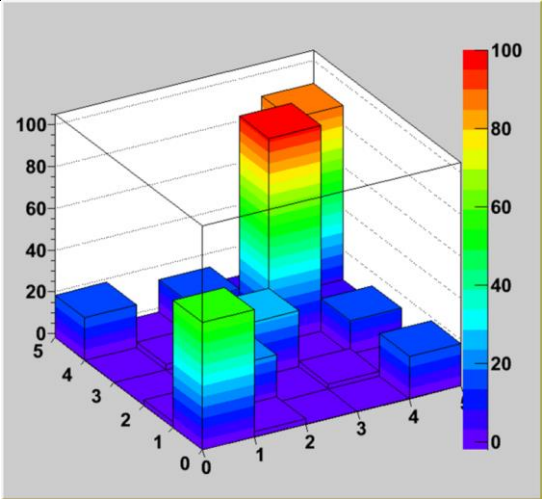
Dissolver Model	
root -l corRESPnom.C	
root [0]	
Processing corRESPnom.C...	
Number of responses: 1	
Number of time nodes: 635	
Number of model parameters: 5	
Number of transient parameters: 2	
What kind of response?	
1 = static	
2 = transient	**Figure B.3:** Initial (i.e., *computed*) correlation matrix for the dissolver (cf., Figure 5.9).
2	
Which response to be plotted?	
Enter an integer between 1 and 1.	
1	
Set a minimum and a maximum for the histogram?	
1 = Yes!	
2 = No!	
2	
root [1]	
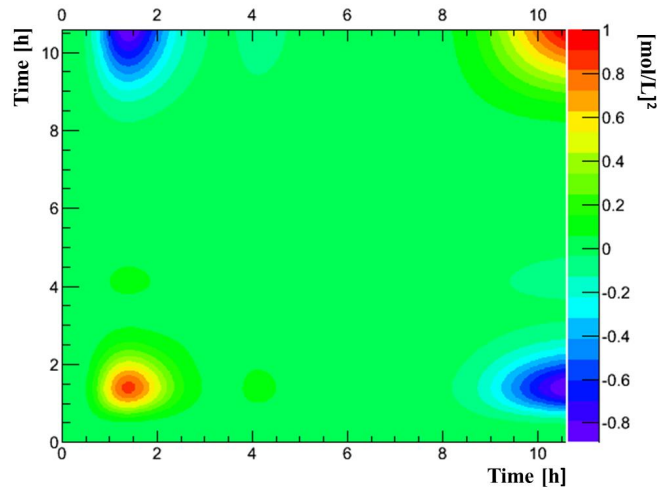
Dissolver Model	
root -l corRESPbest.C	
root [0]	
Processing corRESPbest.C...	
Number of responses: 1	
Number of time nodes: 635	
Number of model parameters: 5	
Number of transient parameters: 2	
What kind of response?	
1 = static	
2 = transient	**Figure B.4:** P*redicted best-estimate* correlation matrix for the nitric acid concentration in compartment #1of the responses for the dissolver model (cf., Figure 5.10).
2	
Which response to be plotted?	
Enter an integer between 1 and 1.	
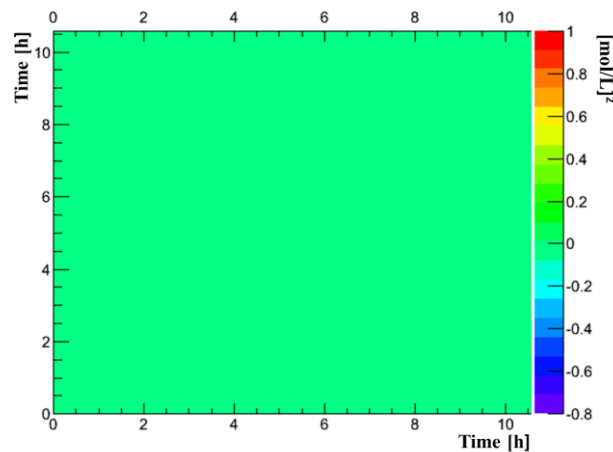
232

Dissolver Model

root -l RESPsimexpbest.C

root [0]

Processing RESPsimexpbest.C...

Number of responses: 1

Number of time nodes: 635

Number of model parameters: 5

Number of transient parameters: 2

transient response

Which response to be plotted?

 Enter an integer between 1 and 1.

1

Set a minimum and a maximum for the histogram?

1 = Yes!

2 = No!

2
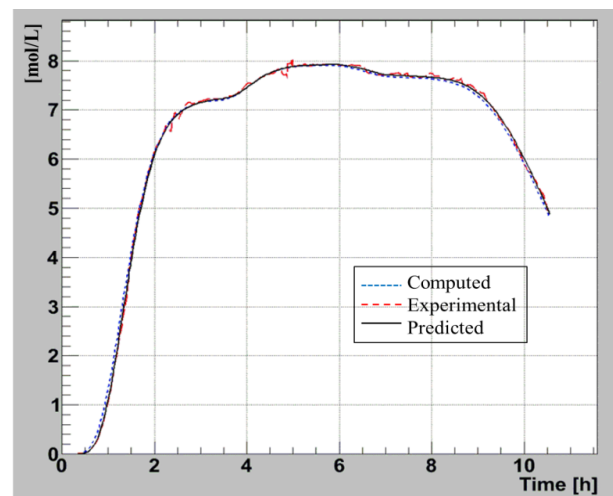
Figure B.5: Computed, experimental, and best estimate predicted nominal values for the nitric acid concentration in compartment #1 (cf., Figure 5.7).

Dissolver Model

root -l paramBCexpbest.C

root [0]

Processing paramBCexpbest.C...

Number of responses: 1

Number of time nodes: 635

Number of model parameters: 5

Number of transient parameters: 2

Which boundary conditions have to be plotted?

Integer allowed between 1 and 2.

1

Set a minimum and a maximum for the histogram?

1 = Yes!

2 = No!

2
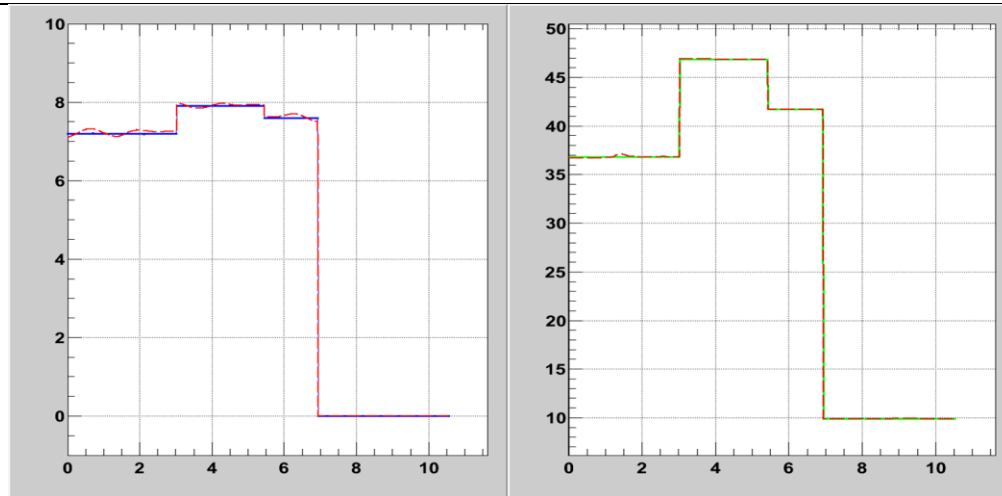
root [1]

Figure B.7: Experimental (red) and best-estimate (black) transient boundary conditions for dissolver model. Left: inlet nitric acid mass concentration. Right: inlet mass flow rate.

Dissolver Model

root -l sigrelparamBCexpbest.C

root [0]

Processing sigrelparamBCexpbest.C...

Number of responses: 1

Number of time nodes: 635

Number of model parameters: 5

Number of transient parameters: 2

What kind of best-estimate relative standard deviations?

1 = relative to nominal values

2 = relative to best-estimate values

1

Which boundary conditions have to be plotted?

Integer allowed between 1 and 5.

1

Set a minimum and a maximum for the histogram?

1 = Yes!

2 = No!

1

Provide the minimum 9.98

Provide the maximum 10.01

root [1]
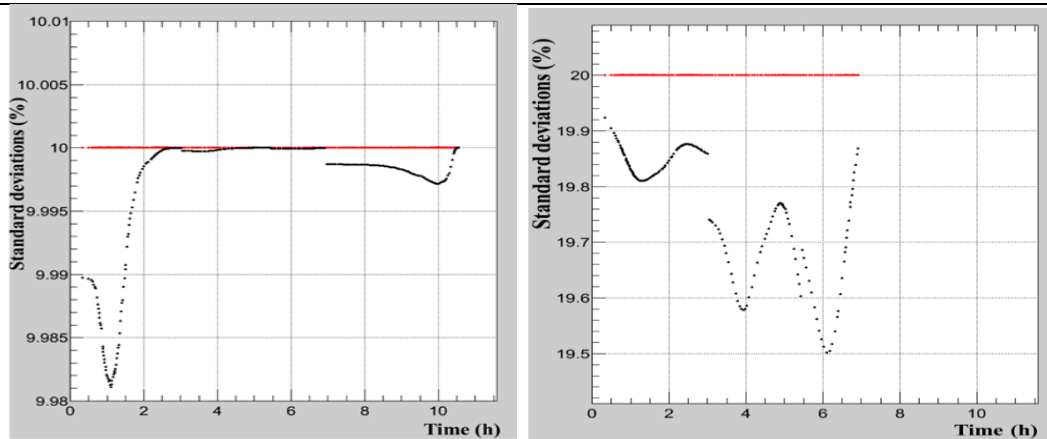
Figure B.8: Experimental (red) and best-estimate (black) relative standard deviations (in percent) of the transient boundary conditions for the dissolver model. Left: inlet mass flow rate (see Figure 5.6). Right: inlet nitric acid mass concentration (see Figure 5.4).

11. REFERENCES

Archer, G., Saltelli, A. and Sobol', I.M., "Sensitivity measures, ANOVA like techniques and the use of bootstrap," *J. Statist. Comput. Simul.,* **58**, 99, 1997.

Arslan, E., and Cacuci, D. G., "Predictive Modeling of Liquid-Sodium Thermal-Hydraulics Experiments and Computations", *Annals of Nucl. Energy*, **63C**, 355-370, 2014.

Badea, M. C., Cacuci, D. G., and Badea, A. F., "Best-Estimate Predictions and Model Calibration for Reactor Thermal-Hydraulics", *Nucl. Sci. Eng*., **172**, 1-19, 2012.

Berger, J., *Statistical Decision Theory and Bayesian Analysis*, 2nd ed., Springer Verlag, New York, 1985.

Bledsoe, K. C., Favorite, J. A., and Aldemir, T., "Application of the Differential Evolution Method for Solving Inverse Transport Problems", *Nucl. Sci. Eng*., **169**, 208, 2011a.

Bledsoe, K. C., Favorite, J. A., and Aldemir, T., "Using the Levenberg-Marquardt Method for Solutions of Inverse Transport Problems in One- and Two-Dimensional Geometries," *Nucl. Techn.*, **176**, 106-126, 2011b.

Bonano, E.J. and Apostolakis, G.E., "Theoretical foundations and practical issues for using expert judgments in uncertainty analysis of high-level radioactive waste disposal," *Radioactive Waste Manag. and Nucl. Fuel Cycle*, **16**, 137, 1991.

Box, G.E.P. and Draper, N.R., *Empirical Model-Building and Response Surfaces*, Wiley, New York, 1987.

Burr, M. H. T., "TR LA-UR-13-24737 International versus Domestic Diversion Scenarios in the Context of Process Monitoring," U.S. Department of Energy, Los Alamos National Laboratory, 2013.

Cacuci, D. G., "Sensitivity theory for nonlinear systems: I. Nonlinear functional analysis approach". *J., Math. Phys*. **22**, 2794–2802. 1981a.

Cacuci, D. G., "Sensitivity theory for nonlinear systems: II. Extensions to additional classes of responses". *J., Math. Phys*. **22**, 2803–2812, 1981b.

Cacuci, D. G., *Sensitivity and Uncertainty Analysis*: *Theory*, Vol. 1, Chapman & Hall/CRC, Boca Raton, 2003.

Cacuci, D. G., "Predictive Modeling of Coupled Multi-Physics Systems: I. Theory", *Annals of Nucl. Energy*, **70,** 266–278, 2014.

Cacuci, D. G., and Arslan, E., "Reducing Uncertainties via Predictive Modeling: FLICA4 Calibration Using BFBT Benchmarks", *Nucl. Sci. Eng.*, **176**, 339–349, 2014.

Cacuci, D. G., and Ionescu-Bujor, M., "On the Evaluation of Discrepant Scientific Data with Unrecognized Errors," *Nucl. Sci. Eng*., **165**, 1–17, 2010a.

Cacuci, D. G., and Ionescu-Bujor, M., "Best-Estimate Model Calibration and Prediction," *Nucl. Sci. Eng*., **165**, pp. 18-44, 2010b.

Cacuci, D. G., Navon, M. I., and Ionescu-Bujor, M., *Computational Methods for Data Evaluation and Assimilation*, Chapman & Hall/CRC, Boca Raton, 2014.

Cacuci, D. G., "On the Ill-Posed Nature of Inverse Problems: An Exactly Solvable Paradigm Inverse Neutron Diffusion Problem Illustrating the Solution's Non-Computability," ANS RPSD 2014 - 18th Topical Meeting of the Radiation Protection & Shielding Division of ANS Knoxville, TN, September 14 – 18, 2014, on CD-ROM, American Nuclear Society, LaGrange Park, IL, 2014.

Cipiti, B. B., and McDaniel, M. D., "SANDIA REPORT SAND2012-7779 Reprocessing Plant Scale Model Integration," U.S. Department of Energy, Sandia National Laboratories, 2012.

Clement, R.T. and Winkler, R.L., Combining probability distributions from experts in risk analysis, *Risk Anal.*, **19**, 187, 1999.

Cowan, G., *Statistical Data Analysis*, Clarendon Press, Oxford, 1998.

Cukier, R.I. et al., "Study of the sensitivity of coupled reaction systems to uncertainties in rate coefficients. I : Theory," *J. Chem. Phys.*, **59**, 3873, 1973.

Eslami, M., *Theory of Sensitivity in Dynamic Systems*, Springer-Verlag, Heidelberg, 1994.

Faragó, I., Havasi, Á., and Zlatev, Z., Editors, *Advanced Numerical Methods for Complex Environmental Models: Needs and Availability*, Bentham Science Publishers, 2014.

Ganapol, B.D., *Analytical Benchmarks for Nuclear Engineering Applications, Case Studies in Neutron Transport Theory*, NEA/DB(2008)1, ISBN 978-92-64-99056-2, NEA No. 6292 OECD, 2008.

Garcia, H. E., et al, "Integration of facility modeling capabilities for nuclear," *Progress in Nuclear Energy,* vol. **54**, no. 1, pp. 96-111, 2011.

Hora, S.C. and Iman, R.L., "Expert opinion in risk analysis: The NUREG-1150 methodology," *Nucl. Sci. Eng*., **102**, 323, 1989.

Hu, Z., Smith, R. C., Willert, J., and Kelley, C. T., "High-Dimensional Model Representations for the Neutron Transport Equation", *Nucl. Sci. Eng*., **177**, 350–360, 2014.

Jarman, K. D., Miller, E. A., Wittman, R. S., and Gesh, C., "Bayesian Radiation Source Localization", *Nucl. Technol*., **175**, 326, 2011.

Jubin, R., "Nuclear Chemistry Course," CRESP, 2009. [Online]. Available: http://www.cresp.org/NuclearChemCourse/monographs/07_Jubin_Introduction%20to%20 Nuclear%20Fuel%20Cycle%20Separations%20-%20Final%20rev%202_3_2_09.pdf . [Accessed 01 April 2015].

Kleijnen, J.P.C. and Helton, J.C., "Statistical analyses of scatterplots to identify important factors in large-scale simulations. 1. Review and comparison of techniques," *Reliab. Eng., Syst. Safety*, **65**, 147, 1999.

Kleijnen, J.P.C. and Helton, J.C., "Statistical analyses of scatterplots to identify important factors in large-scale simulations. 2. Robustness of techniques," Reliab. Eng., Syst. Safety, 65, 187, 1999.

Kleijnen, J.P.C. and Helton, J.C., "Statistical analyses of scatterplots to identify important factors in large-scale simulations," SAND98-2202, Sandia National Laboratories, Albuquerque, NM, 1999.

Lahoz, W., Khattatov, B., and Ménard, R., (Editors), *Data Assimilation: Making Sense of Observations*, Springer Verlag, 2010.

Le Maître, O.P., and Knio, O.M., Spectral Methods for Uncertainty Quantification with Applications to Computational Fluid Dynamics, ISBN 978-90-481-3519-6 e-ISBN 978-90-481-3520-2, DOI 10.1007/978-90-481-3520-2, Springer Dordrecht Heidelberg London New York, 2010.

Levenberg-Marquard; The so-called *Levenberg–Marquardt methods* are due to Levenberg and Marquardt. See: K. Levenberg, "A method for the solution of certain nonlinear problems in least squares," *Quart. Appl. Math.*, **2**, 164–168, 1944.; and D. W. Marquardt, "An algorithm for least-squares estimation of nonlinear parameters," *J. Soc. Indust. Appl. Math.*, **11**, 431–441, 1963.

Lewis B. E., and Weber, F. E., "A Mathematical Model for Liquid Flow Transients in a Rotary Dissolver", ORNL/TM-7490, Oak Ridge National Laboratory, 1980.

Maple (16). Maplesoft, a division of Waterloo Maple Inc., Waterloo, Ontario. 2016

McCormick, N. J., "Inverse Radiative Transfer Problems: A Review", *Nucl. Sci. Eng*., **112***, 185, 1992.

McKay, M.D., Evaluating prediction uncertainty, Technical Report NUREG/CR-6311, US Nuclear Regulatory Commission and Los Alamos National Laboratories, 1995.

Morris, M.D., "Factorial sampling plans for preliminary computational experiments," Technometrics, 33, 161, 1991.

National Research Council., Assessing the Reliability of Complex Models: Mathematical and Statistical Foundations of Verfication, Validation, and Uncertainty Quantification. Washington, DC: The National Academies Press, 2012a.

National Research Council. The Comprehensive Nuclear Test Ban Treaty: Technical Issues for the United States. Washington, DC: The National Academies Press, 2012b.

Nelson, R., Stewart, J., Williams B., and Unal, C., "Technical Report LA-UR-10-06125," U.S. Department of Energy, Los Alamos National Laboratory, 2010.

Oberkampf, W., "Sandia Technical Report SAND2002-0529 Verficaiton and Validation in Computational Fluid Dynamics," U.S. Department of Energy, Sandia National Laboratories, 2002.

Oberkampf, W., and Smith, B., "Assessment Criteria for Computational Fluid Dynamics Validation Benchmark Experiments", 52nd Aerospace Sciences Meeting, AIAA SciTech, (AIAA 2014-0205), 2014.

Paulenova, A., "Modeling of distribution and speciation of plutonium in the Urex extraction system.," United States: Canadian Institute of Mining, Metallurgy and Petroleum, Montreal, Quebec (Canada)., 2008.

Petruzzi, A., Cacuci, D.G., and F., D'Auria., "Best-Estimate Model Calibration and Prediction through Experimental Data Assimilation - II: Application to a Blowdown Benchmark Experiment." *Nucl. Sci. Eng*., **165**, pp. 45-100, 2010.

Rabitz, H., and Alis, O. F., ''General Foundation of High Dimensional Model Representations,'' J. Math. Chem., 25, 197, 1999.

[ROOT]   https://root.cern.ch

Sadasivan, P., and DePaoli, D. W., "Technical Report LA-UR-11-00531 NEAMS Safeguards and Separations IPSC," U.S. Department of Energy, Los Alamos National Laboratory, 2011.

Saltelli, A., Chan, K., Scott, E.M., Editors, Sensitivity Analysis, John Wiley & Sons, Ltd., West Sussex, UK, 2000.

Sanchez, R., and McCormick, N. J., "On the Uniqueness on the Inverse Source Problem for Linear Particle Transport Theory", *TTSP*, **37**, 236, 2008.

Sobol', I.M., "Sensitivity analysis for non-linear mathematical models," Math. Model. Comput. Exp., 1, 407, 1993.

Tarantola, A., *Inverse Problem Theory and Methods for Model Parameter Estimation*, Society for Industrial and Applied Mathematics, 2005.

Tichonov, A. N., "Regularization of Non-Linear Ill-Posed Problems", Doklady Akademii Nauk, **49**(4), 1963. See also: Tichonov, "Solution of Incorrectly Formulated Problems and the Regularization Method", Soviet Math. Doklady **4**, 1035, 1963.

US NRC (Nuclear Regulatory Commission), Severe accident risks: An assessment for five U.S. nuclear power plants, NUREG-1150, US Nuclear Regulatory Commission, Washington, DC, 1990-1991.

US DOE (US Department of Energy), Title 40 CFR Part 191 Compliance Certification Application for the Waste Isolation Pilot Plant, DOE/CAO-1996-2184, US Department of Energy, Carlsbad Area Office, Carlsbad, NM, 1996.

Woolf, A., Kerr, P.K., Nikitin, M., *Arms Control and Nonproliferation: A Catalog of Treaties and Agreements* (CRS Report No. RL33865). Washington, DC, 2014